Dissertation
submitted to the
Combined Faculties for the Natural Sciences and for Mathematics
of the Ruperto-Carola University of Heidelberg, Germany
for the degree of
Doctor of Natural Science

presented by

Diplom-Biologin Lisa Weber
Born in: Erlangen
Oral-examination: ……..

Characterization of *Schizosachharomyces pombe* Sup11p, a protein involved in β-1,6-glucan biosynthesis

Referees: Prof. Dr. Sabine Strahl

Prof. Dr. Thomas Söllner

1. Zusammenfassung

Extensiv *O*-mannosylierte Proteine stellen einen wesentlichen Bestandteil der pilzlichen Zellwand dar. Mit Zellwand-Polysacchariden verknüpft formen sie eine ausgeprägte Mannanschicht. Verschiedenste Mannoproteine sind über einen Glykosylphosphatidylinositol (GPI) Ankerrest kovalent mit dem β-1,6-Glukan der Zellwand verbunden.

In einem Multicopy-Suppressor Screening, welches mit einer konditional letalen *O*-Mannosyltransferase Mutante (nmt81-*oma2*) aus *Schizosaccharomyces pombe* durchgeführt wurde, wurde *sup11*$^{+}$ identifiziert. Sup11p weist eine erhebliche Homologie zu *Saccharomyces cerevisiae* Kre9 auf, welches an der β-1,6-Glukan Synthese beteiligt ist. Die genaue Funktion von Kre9 ist allerdings noch ungeklärt.

Es konnte hier gezeigt werden, dass *sup11*$^{+}$ ein essentielles Gen ist, welches für die β-1,6-Glukan Bildung notwendig ist. Bei einer Mutante mit reduzierter *sup11*$^{+}$ Expression konnte kein β-1,6-Glukan in der Zellwand detektiert werden. Des Weiteren ist Sup11p unentbehrlich für die korrekte Zellwandausbildung. Eine konditional letale nmt81-*sup11* Mutante zeigt schwerwiegende morphologische Defekte sowie ein missgestaltetes Septum. In dessen Zentrum finden sich massive Anreicherungen an Zellwandmaterial. Die Einlagerungen bestehen zum Teil aus β-1,3-Glukan, welches normalerweise ausschließlich im primären Septum vorkommt. Die Zellwandanalyse der nmt81-*sup11* Mutante zeigt, dass Gas2p eine bedeutende Rolle bei der Ausbildung des Septum-Phänotyps einnimmt. Gas2p gehört der β-1,3-Glukanosyltransferase GH72 Familie an und ist an der Umstrukturierung von Septum-Material beteiligt. Darüber hinaus zeigt eine nmt81-*sup11* Transkriptomanalyse, dass auffällig viele Zellwand-Glukan modifizierenden Enzyme reguliert werden.

Des Weiteren ist Sup11p:HA stark unterglykosyliert, wenn es in einem *oma4*Δ Stammhintergrund expremiert wird. Unter diesen Umständen kann es vom *N*-Glykosylierungs Komplex an einem ungewöhnlichem N-X-A Sequon modifiziert werden. Dieses Sequon befindet sich in einer S/T-reichen Region und ist daher im Wildtyp durch *O*-Mannosylierung maskiert. In *S. cerevisiae* konnte bereits gezeigt werden, dass *N*- und *O*-Glykosylierung in Konkurrenz zueinander stehen. Diese Arbeit legt nun einen generellen Mechanismus nahe, da zum ersten Mal ein Beispiel dieser Konkurrenz in *S. pombe* gezeigt werden konnte.

2. Summary

Proteins that are extensively *O*-mannosylated constitute crucial components of the fungal cell wall. They are linked to cell wall polysaccharides forming a distinct mannan layer. Various mannoproteins are covalently attached to the cell wall β-1,6-glucan via remnants of their glycosylphosphatidylinositol (GPI) -anchor.

A multicopy-suppressor screen of a conditionally lethal *Schizosaccharomyces pombe* protein *O*-mannosyl transferase mutant (nmt81-*oma2*) identified *sup11*$^{+}$. Sup11p shows significant homology to *Saccharomyces cerevisiae* Kre9 which is involved in β-1,6-glucan synthesis although its exact function remains uncertain.

This study gives evidence that *sup11*$^{+}$ is an essential gene that is required for β-1,6-glucan formation. In a mutant with reduced *sup11*$^{+}$ expression, β-1,6-glucan was absent from the cell wall. Further, it is demonstrated that Sup11p is indispensable for proper septum assembly. A conditionally lethal nmt81-*sup11* knock-down mutant shows severe morphological defects and malformation of the septum with massive accumulation of cell wall material at the centre of the closing septum. These depositions consist partially of β-1,3-glucan which ought to be restricted to the primary septum. Analysis of the nmt81-*sup11* mutant cell wall brought evidence that Gas2p, a member of the β-1,3-glucanosyl-transferases GH72 family, plays a crucial role in accumulating the observed septum material depositions. Moreover, a transcriptome analysis performed on the nmt81-sup11 mutant identified significant regulation of several cell wall glucan modifying enzymes.

Moreover, it is shown that Sup11p:HA is hypo-mannosylated when expressed in an *O*-mannosylation mutant background. The hypo-mannosylated Sup11p can be *N*-glycosylated on an unusual N-X-A sequon in the *oma4*Δ background. This unusual sequon is located inside a S/T-rich region which is prone to be highly *O*-mannosylated in wild type yeast, masking the N-X-A sequon for *N*-glycosylation. Competition between *N*- and *O*-glycosylation has been shown in *S. cerevisiae*, but this study presents the first example for *S. pombe* demonstrating that such competition is a general mechanism.

3. Introduction

3.1. Fungal Cell Wall

Single cell organisms are usually exposed to various hazards provided by the diverse environments they live in. For fungi, the cell wall is the outer protective layer that defends the protoplast from abiotic and biotic threats like extreme pH, osmotic stress, toxins, and attacks of immune defense systems (Latgé, 2007). Additionally, the cell wall also determines cell shape and provides mechanical protection. This rigid exoskeletal structure is indispensible for growth and survival of fungi but it is absent in mammalian cells (Klis *et al.*, 2006). Hence, the fungal cell wall is an attractive target for developing new antifungal drugs for medical applications or crop protection in agriculture (Georgopapadakou and Tkacz, 1995; Georgopapadakou and Walsh, 1996). For that reason it is of major importance to know how the wall matrix is synthesized and to elucidate the mechanisms how cell wall synthesis is synchronized by different molecules.

3.2. Ultra-structure and composition of fission yeast cell wall

The fungal model organism used in this study is fission yeast, *Schizosaccharomyces pombe.* The cell wall of *S. pombe* is mainly composed of glucose polysaccharides and some glycoproteins (Bush et al., 1974). Electron microscopy (EM) studies revealed that the cell wall of the fission yeast is build up in a three layered structure. An electron transparent layer consisting of a diverse mixture of β-glucans separates two electron dense layers containing glycoproteins, which are referred to as α-galactomannans (Fig. 3.1) (Humbel *et al.*, 2001). The α-galactomannan layer which is close to the plasma membrane (PM) is a mixture of glycoproteins and α-glucan. The outer layer which is facing the outside environment consists mainly of galactomannoproteins (Humbel *et al.*, 2001). The portion of glycoproteins that are present in the wall matrix varies between 9 to 14% of all wall matrix components. Polysaccharides are the main constituent of the fission yeast cell wall and are classified in α-glucans (28%) and β-glucans (46 to 54%) (Bush *et al.*, 1974; Manners and Meyer, 1977). The latter are further subdivided in linear β-1,3-glucan, β-1,6-branched-β-1,3-glucan and a minor portion of β-1,3-branched-β-1,6-glucan (now referred to as β-1,6-glucan) (Kopecká *et al.*, 1995).

Structural studies revealed that the β-1,6-glucan backbone is a highly branched polymer in *S. pombe*. In this species 75% of the β-1,6-glucan residues are β-1,3 linked whereas the β-1,6-glucan backbone is only moderately β-1,3-branched in *S. cerevisiae* (7%) and *C. albicans* (15%) (Magnelli *et al.*, 2005). Immunogold labeling of fission yeast cells revealed that the β-1,6-glucan is located directly underneath the outer electron dense layer linking the α-galactomanan to the glucan matrix (Horisberger and Rouvet-Vauthey, 1985; Humbel *et al.*, 2001).

The morphology and mechanical strength of the fungal wall matrix depends on the flexible, wire spring like structure of β-1,3-glucan. The β-1,3-glucan is synthesized in linear chains of diverse extension sizes. Since the mature β-1,3-glucan structure of the wall matrix is a branched molecule the polymer is further modified by introduction of intrachain β-1,6-linkages (reviewed in Klis *et al.*, 2002).

A major fraction of 28% of the fission yeast cell wall is built of α-1,3-glucan which locates close to the PM (Bush *et al.*, 1974; Manners and Meyer, 1977; Humbel *et al.*, 2001). An α-1,3-glucan synthase mutant exhibits thick, loose cell walls compared to the wild type, demonstrating that α-1,3-glucan plays an important role in the normal construction of the fission yeast cell wall by maintaining its rigidity and rod like shape (Hochstenbach *et al.*, 1998; Konomi *et al.*, 2003). An α-1,3-glucan synthase mutant *mok1*$^{-}$ also formed a thick secondary septum, but formation of the primary septum appeared to be unaffected (Konomi *et al.*, 2003).

Due to its complex architecture, a plurality of glucan-synthases, glucanases, glucan-transferases, and many more enzymes are involved in establishing, maintaining and degrading individual components of the cell matrix to ensure functionality of this exoskeletal structure.

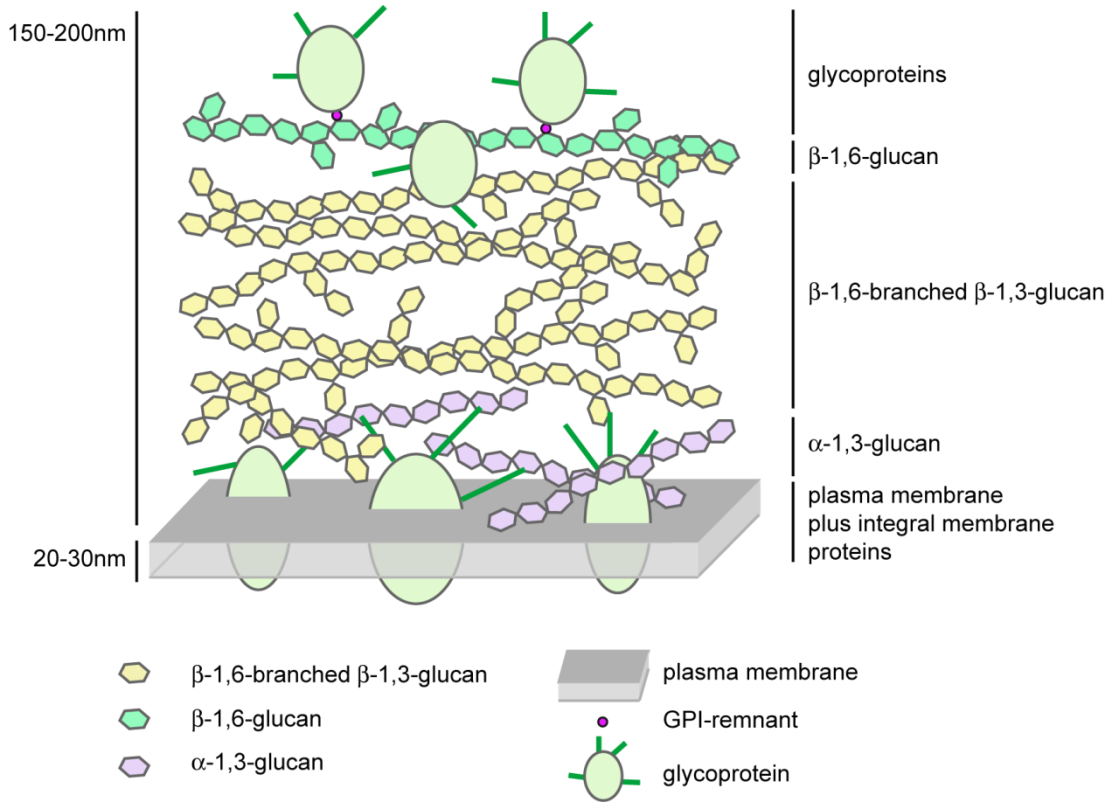

Fig. 3.1: Schematic illustration of the cell wall structure of *S. pombe*:
The fission yeast cell wall is mainly composed of glucose polysaccharides and a small portion of glycoproteins. The wall matrix components are forming three layers. Next to the PM and the integral membrane proteins is a layer of α-1,3-glucan. Seated on top of this is a thick layer of β-1,6-branched β-1,3-glucan. Mannoproteins are the top coat of the extracellular matrix of fission yeast, facing the outer environment. These glycoproteins can be associated to the wall matrix due to ionic bounds or covalently linked via the remnant of a cleaved GPI-anchor and β-1,6-glucan.

3.3. Biosynthesis of cell wall components

3.3.1. Role and biosynthesis of α-1,3-glucan

The α-1,3-glucan accounts for a major fraction of the fission yeast cell wall. This polysaccharide consists of a short chain structure of approximately 260 linear α-1,3-glucose residues with some α-1,4-residues in the center. It is synthesized by Ags1p which interconnects of two linear chains of ~120 α-1,3-glucose residues each (Grün *et al.*, 2005). Ags1p is an integral membrane protein. Its extracellular domain is speculated to function in a transglycosylase reaction and its intracellular domain performs the glucan synthesis (Hochstenbach *et al.*, 1998; Katayama *et al.*, 1999; Grün *et al.*, 2005). The proposed model is that the intracellular domain of Ags1p contributes to the synthesis of a first glucan chain which is then transported across the PM, perhaps via the multipass transmembrane domain of Ags1p. The first chain retains at the Ags1

protein and a second round of α-1,3-glucan synthesis and transport to the extracellular space takes place. Finally the extracellular domain catalyses the connection of the two α-glucan chains to the mature ~260 residue polysaccharide which is then released the cell wall (Grün *et al.*, 2005). Mutant cells of *ags1*$^-$ exhibit a temperature sensitive morphology causing lysis at restrictive temperature (Hochstenbach *et al.*, 1998).

A second α-1,3-glucan synthase, Mok1p, was described by Konomi and co-workers (2003). A *mok1*$^-$ shows an irregular, round or pear-like shape and the cells were swollen at the site of the septum or cell tip demonstrating the vital role of α-1,3-glucan to maintain the structural integrity of fission yeast cells (Konomi *et al.*, 2003). Mok1p locates to the sites of cellular growth (cell tips) and at the medial region during septum formation where it is indispensable for correct secondary septum formation (Konomi *et al.*, 2003).

3.3.2. Biosynthesis of β-1,3-glucan

Four genes (*bgs1*$^+$, *bgs2*$^+$, *bgs3*$^+$ and *bgs4*$^+$) have been identified in *S. pombe*. The corresponding gene products share homology with *S. cerevisiae* β-1,3-glucan synthase catalytic subunits (Fks1 and Fks2) (Parent *et al.*, 1993; Ishiguro *et al.*, 1997; Liu *et al.*, 2000; Martín *et al.*, 2003; Cortés *et al.*, 2005).

Although the sites of operation within the cell partially overlap, each Bgs protein is also specialized for unique assignments. The integral membrane protein Bgs1p localizes to the cell division site late in anaphase (Liu *et al.*, 2002). β-1,3-glucan synthase activity for this enzyme was demonstrated during polarized growth and sporulation. Moreover, Bgs1p is indispensable for correct septum formation (Liu *et al.*, 1999; Cortés *et al.*, 2002). Although Bgs1p seems to be crucial for primary septum assembly and Bgs2p is needed for sporulation, it is feasible that these two isoforms execute overlapping roles in cell wall synthesis (Martín *et al.*, 2003). Bgs2p and Bgs3p are both needed for cell elongation and spore formation (Martín *et al.*, 2000; Martín *et al.*, 2003). Bgs3p localization corresponds to regions at which the wall matrix is growing or being actively remodelled. Intracellular localization also varies at different stages of the cell cycle and thus localization regulates its function (Martín *et al.*, 2000; Martín *et al.*, 2003). During interphase Bgs3p localizes to the growing poles and during cytokinesis it is found at the septum (Martín *et al.*, 2003). Bgs4p is synthesized periodically during cell cycle and is

indispensable during cytokinesis and polarized growth (Cortés *et al.*, 2005). In contrast, *bgs1*$^{+}$, *bgs2*$^{+}$ and *bgs3*$^{+}$ expression levels do not change significantly during cell cycle.
Since the wall matrix is of highly interwoven construction, the nascent β-1,3-glucan needs to be cross-linked to other components of the cell wall. It has been postulated that this is achieved by the action of glycoside hydrolases and transglycosidases (Lesage and Bussey, 2006; Latgé, 2007). Four genes encoding β-1,3-glucanosyl transferases of the GH72 family (*gas1*$^{+}$, *gas2*$^{+}$, *gas4*$^{+}$ and *gas5*$^{+}$) have been identified by de Medina-Redondo and colleges (2010). Gas1p and Gas2p were detected at the poles of bipolar cells and at the septum of dividing cells. These localizations overlap with the sites of active cell wall growth, where long polymers of β-1,3-glucan are needed. More general, Gas1p is crucial for cell integrity and viability during vegetative growth while Gas2p and Gas5p play a minor role in cell wall construction (de Medina-Redondo *et al.*, 2010). Gas4p is crucial for spore wall assembly and spore viability and this glucanosyl-transferase catalyzes a transfer reaction with similar specificity to that found for Gas1p (De Medina-Redondo *et al.*, 2008).

3.3.3. Synthesis of β-1,6-glucan polymers

In contrast to the detailed knowledge how β-1,3-glucans are synthesized and which enzymes are involved in remodeling of this polymer, biosynthesis of β-1,6-glucan is less understood. Even though β-1,6-glucan accounts only for a minor fraction of the cell wall glucan, this polysaccharide plays a key role in maintaining cell wall integrity (Kollár *et al.*, 1997). Genes involved in β-1,6-glucan synthesis of fission yeast have not been characterized so far. To elucidate synthesis of β-1,6-glucan *S. cerevisiae* has been studied as model organism. Although a set of genes involved in β-1,6-glucan synthesis have been identified in *S. cerevisiae* and characterized in the past decades, neither synthase activity nor the underlying mechanism or site of synthesis has been described (Lesage and Bussey, 2006). Genes involved in β-1,6-glucan production were initially identified in yeast *K*1 toxin *re*sistant (*KRE*) strains. The K1 toxin is one of the most studied variants of killer toxins in *S. cerevisiae*. It is a protein which is secreted by killer yeast strains and kills sensitive (non-killer) strains (Wickner, 1986). The K1 toxin is a pore-forming protein that binds to a β-1,6-glucan-associated component of the yeast cell wall and subsequently induces lethality by forming pores in the plasma membrane which discharge the transmembrane (TM) proton gradient (Magliani *et al.*, 1997). Due

to a reduced amount of β-1,6-glucan polymer in the cell wall the *KRE*-mutants showed a higher degree of resistance to the toxin (Bussey, 1991; Shahinian and Bussey, 2000).

Kre1, Kre5, Kre6, and Kre9 (plus the Kre6 homologue Skn1 and Kre9 homologue Knh1) have been shown to be involved in β-1,6-glucan synthesis in *S. cerevisiae* (Boone *et al.*, 1990; Brown and Bussey, 1993; Roemer *et al.*, 1993; Dijkgraaf *et al.*, 1996; Lesage and Bussey, 2006). Most of the Kre-family gene products involved in β-1,6-glucan synthesis localize in secretory pathway compartments from the endoplasmic reticulum (ER) to the plasma membrane (PM) (Shahinian and Bussey, 2000).

For example, Kre5 and Kre6 which are candidates to be involved in biogenesis of core polymer reactions localize both in the ER (Meaden *et al.*, 1990). Kre5 shows homology to UDP-glucose glucosyl transferases and Kre6 shares features of the glycoside hydrolase family 16 (GH16) (Levinson *et al.*, 2002; Nakamata *et al.*, 2007). The localization of Kre6 is still debated controversially and has not been finally elucidated yet. Previous studies of Kre6 indicated that this protein is resident in the Golgi apparatus (Li *et al.*, 2002). However, recent results indicated that the majority of Kre6 locates to the ER (Kurita *et al.*, 2011). It was reported that also a minor Kre6-fraction was detected in secretory vesicle-like compartments and the PM. The PM-localized Kre6 signals accumulate at the sites of polarized growth. The authors argue that the ER may be the major reservoir of Kre6. From there it may be transported to the sites of polarized growth whenever needed (Kurita *et al.*, 2011).

Kre1 is a GPI-anchored protein on the outer surface of the PM, and is suggested to extend the linear β-1,6-glucan chains by adding β-1,6-glucan onto a acceptor glucan (Boone *et al.*, 1990; Lesage and Bussey, 2006). *KRE9* contains an *N*-terminal signal peptide and likely encodes an secreted or cell surface *O*-mannosylated protein (Brown and Bussey, 1993). However, secretion of Kre9 to the medium could only be demonstrated by Kre9 overexpression which can cause mislocalization (Brown and Bussey, 1993). In a global localization study of a genomically GPF-tagged budding yeast proteome, Kre9:GFP could not be visualized in order to determine its subcellular localization when expressed under its endogenous promoter (Huh *et al.*, 2003). Thus the actual localization of Kre9 is still under debate.

A likely role for the Kre9 protein includes attachment or cross-linking of the newly synthesized β-1,6-glucan to the wall matrix. Another possibility is, that Kre9 might also

be an extracellular component of a β-1,6-glucan synthase complex (reviewed in Lesage and Bussey, 2006).

However, among all of the above mentioned *KRE*-genes, the ones that seem to play a major role for β-1,6-glucan synthetic are *KRE5* and *KRE9*. The single disruption of each gene lead to significant reduction (100 and 80%, respectively, relative to wild type) in the content of cell wall β-1,6-glucan (Meaden *et al.*, 1990; Brown and Bussey, 1993; Roemer *et al.*, 1994; Aimanianda *et al.*, 2009).

The site of β-1,6-glucan synthesis has not been elucidated yet. The localization of the proteins involved in β-1,6-glucan synthesis along the secretory pathway can be interpreted in various ways: (1) One possibility is that the synthesis of β-1,6-glucan is a gradual process starting in the ER and following the secretory pathway to the extracellular space. (2) Another option is that β-1,6-glucan biogenesis occurs at the PM but requires a primer which is prior synthesized in the secretory pathway (Klis *et al.*, 2002). In order to visualize the site of β-1,6-glucan assembly Montijn and co-workers (Montijn *et al.*, 1999) presented a immunogold labeling study to detect intracellular β-1,6 glucan. However, they could not detect any of this polysaccharide inside the cell but an extensive extracellular cell matrix labeling. Interpretation of this data suggested that the synthesis of β-1,6-glucan takes place mainly at the cell surface (Montijn *et al.*, 1999).

However, these β-1,6-glucan synthesis studies were carried out in *S. cerevisiae* and the components involved in β-1,6-glucan production remain to be elucidated in the fission yeast. So far, homologue genes of the *S. cerevisiae* Kre-family have been identified during *S. pombe* genome sequencing but these genes have not been characterized yet.

3.3.4. Cell wall proteins

Besides the network of various polysaccharides, the yeast cell wall consists of a dense layer of glycoproteins and the glucan serves as a scaffold to retain them to the wall matrix (reviewed in De Groot et al., 2005). The covalently-bound yeast cell wall proteins are divided into two groups depending on their type of linkage to the cell wall: (1) GPI-anchored proteins and (2) proteins which are bound via alkali sensitive linkage, called Pir proteins. Both types have been extensively studied in *S. cerevisiae* (reviewed in De Groot et al., 2005).

In silico analysis of the *S. pombe* genome for cell wall proteins identified 33 candidates for GPI-anchored proteins among 4950 ORFs analyzed (De Groot *et al.*, 2003). However, genome screening indicated that there are no genes encoding for Pir proteins in *S. pombe* (de Groot *et al.*, 2007).

3.3.5. Covalent linkage of GPI-anchored proteins to the wall matrix

The attachment of GPI-anchors to proteins is a common modification in all eukaryotic cells. The purpose of this modification is to anchor cell surface glycoproteins to the PM. In fungi some of these GPI-anchored proteins are processed further. Some of the GPI-anchored proteins contain specific peptide sequences at their C-terminus which allow the proteins to be linked via a so far unknown transglycosylation reaction between the remaining phosphoethanolamine and several mannosyl residues to the β-1,6-glucan of the cell wall matrix (Frieman and Cormack, 2003). Cell wall analysis gave evidence that the interconnecting component for the GPI-anchor with the cell wall matrix is β-1,6-glucan (Kopecká *et al.*, 1974).

The GPI-anchor is a complex structure consisting of a phosphoethanolamine linker, a glycan core, and a phospholipid tail (Ferguson *et al.*, 1988). In order to transglycosylate a GPI-anchored protein to the cell matrix, a covalent linkage with a the non-reducing end of the β-1,6 glucan and the glycan of the GPI-remnant is formed (Fig. 3.2) (de Nobel and Lipke, 1994). By undergoing transglycosylation, only a remnant of the original full length GPI-anchor remains with the mature protein which links it to the cell wall β-1,6-glucan (reviewed in de Nobel and Lipke, 1994; Lu *et al.*, 1995; Van Der Vaart *et al.*, 1996; Kollár *et al.*, 1997; De Groot *et al.*, 2005).

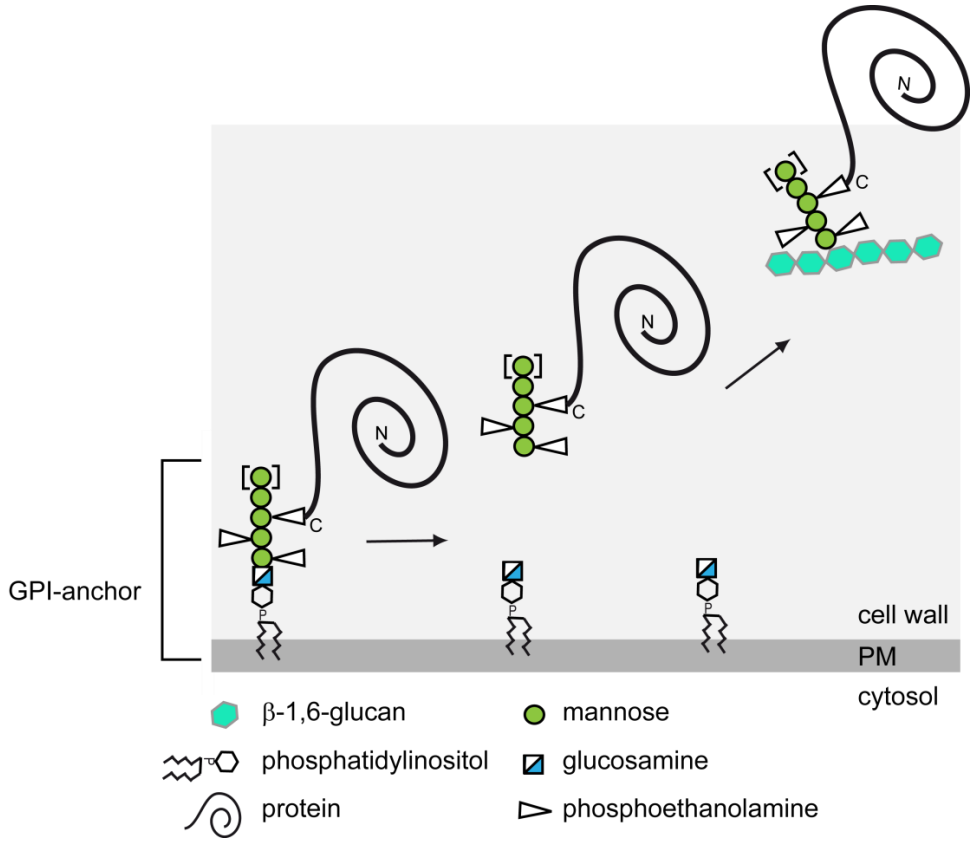

Fig. 3.2: Transglycosylation of GPI-anchored proteins to cell wall β-1,6-glucan (adapted from Gonzalez *et al.*, 2009):
Proteins are attached to a GPI-anchor if containing a C-terminal GPI-anchor signal. GPI-anchored proteins can either stick to the PM due to their anchor or be released to the wall matrix by cleavage of GPI-anchor. These proteins can be covalently attached via their remaining GPI-remnant to the cell wall β-1,6-glucan.

3.3.6. Protein glycosylation in fission yeast

The yeast cell wall is largely composed of glucan polysaccharides and glycoproteins. The rigidity of the cell wall is achieved by the glucan network and the interconnected cell wall glycoproteins fulfill a variety of different tasks. For example the heavily glycoslyated chains of the proteins contribute to water retention (De Groot et al., 2005).
In addition to the modification with a GPI-anchor, two more protein glycosylation types are found in yeasts which are *N*- and *O*-glycosylation (reviewed in Gonzalez *et al.*, 2009). Both modifications are essential for vitality and growth of the yeast cell. Protein glycosylation can change the chemical and physical characteristics of the glycoproteins as well as their cellular localization, protein quality control and solubility (Lehle *et al.*, 2006; Solá and Griebenow, 2009).
Protein *N*-glycosylation describes the transfer of a lipid-linked oligosaccharide onto an asparagine residue of the sequon N-X-S/T (asparagine-X-serine/ threonine), where X

can be every amino acid (aa) except proline, on a nascent protein chain in the lumen of the ER (Kornfeld and Kornfeld, 1985). The early steps of the synthesis of *N*-linked glycans are highly conserved from yeast to higher eukaryotes. However, there are species specific differences in later carbohydrate chain modifications which are happening in the Golgi apparatus. The initial steps of synthesizing the core oligosaccharide are performed at the ER membrane where the sugars of the core oligosaccharide are attached stepwise to the acceptor dolicholphosphate (Dol-P) (reviewed in Kukuruzinskai *et al.*, 1987) (reviewed in Helenius and Aebi, 2004). Dol-P serves not only as pre-precursor for *N*-glycosylation but is also a crucial component for the synthesis of the mannose donor for protein *O*-mannosylation, namely dolicholphosphate mannose (Dol-P-Man), and needed for GPI anchors synthesis (Sharma *et al.*, 1974; Herscovics and Orlean, 1993; reviewed in Lehle et al., 2006).

For assembly of the core oligosaccharide the first seven sugars are attached to Dol-P on the cytosolic side to the intermediate product Dol-P-P-$GlcNAc_2Man_5$ (dolichol diphosphate *N*-Acetylglucosamin$_2$-Mannose$_5$). This precursor is then flipped through the membrane which requires Rtf1 *in vivo*. In yeast cells, this protein is indispensable for flipping of the $GlcNAc_2Man_5$ in an ATP-independent, bi-directional manner from the cytosolic side into the ER lumen where the remaining sugars are added (reviewed in Hirschberg and Snider, 1987; Helenius and Aebi, 2004). However, *in vitro* experiments showed that Rtf1-depleted microsomes are still able to flip Dol-P-P-$GlcNAc_2Man_5$. This indicates that Rtf1 is not the flippase itself but may play a vital accessory role in translocating the Dol-P-P-$GlcNAc_2Man_5$ (Frank *et al.*, 2008).

The completely assembled core oligosaccharide consists of 14 monosaccharides, $GlcNAc_2Man_9Glc_3$. The oligosaccharyl transferase complex (OST) then transfers the lipid-linked oligosaccharide *en block* to the acceptor peptide, which is the conserved N-X-S/T sequon (Fig. 3.3) (Bause and Legler, 1981) (reviewed in Helenius and Aebi, 2004). Subsequently the peptide attached core oligosaccharide undergoes a series of processing steps by being partially trimmed. These glycan modifications which take place in the ER lumen are necessary to ensure proper protein folding and quality control (reviewed in Helenius and Aebi, 2004). This kind of modification can also determine intracellular transportation and targeting. *N*-glycans may undergo extensive elongation in the Golgi apparatus and the functions of the mature proteins are as diverse as the glycan structures themselves (Helenius and Aebi, 2004).

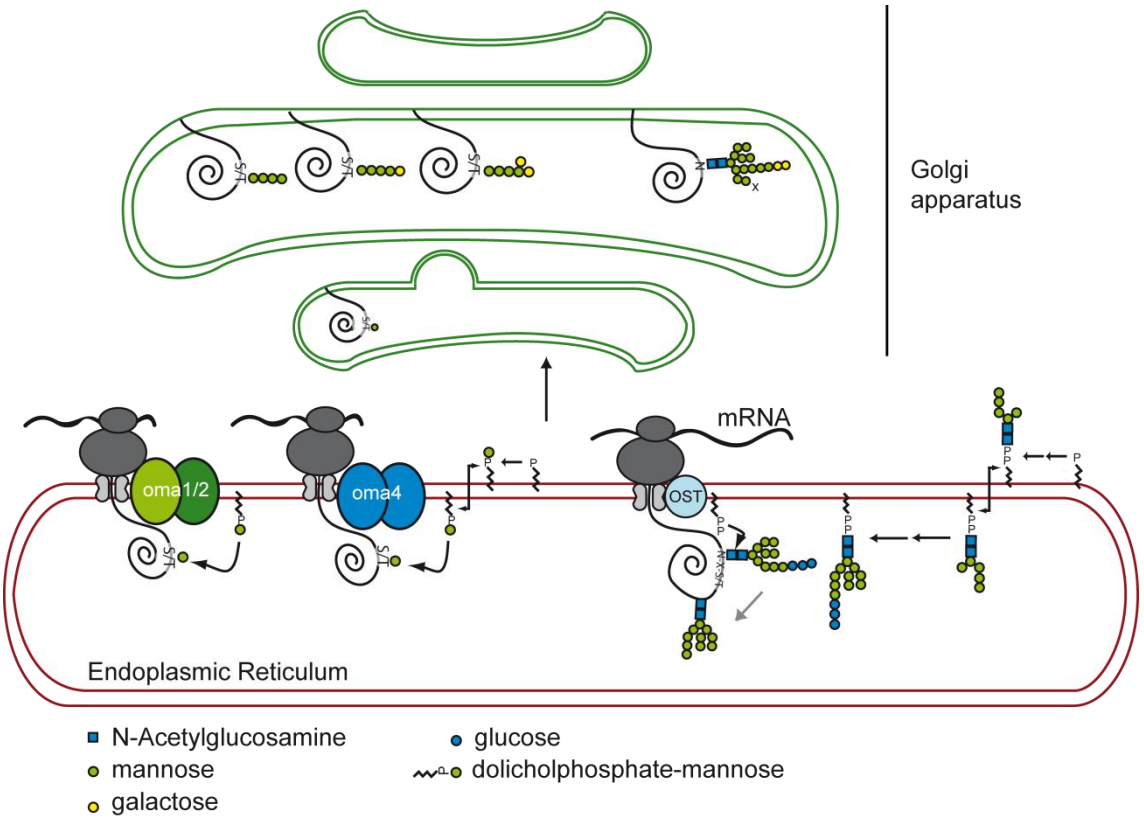

Fig. 3.3: Simplified scheme of protein *N*-glycosylation and *O*-mannosylation in fission yeast:
The initial steps of both modifications take place in the ER and are catalyzed by different enzyme complexes. For *N*-glycosylation a pre-assembled core oligosaccharide gets transferred *en block* to the asparagine of the sequon N-X-S/T. This reaction is catalyzed by the oligosaccharyl transferase (OST) complex. *N*-glycans are trimmed in the ER and remodeled in the Golgi apparatus. *O*-mannosylation is catalyzed by either heteromeric Oma1p/Oma2p or homomeric Oma4p complexes transferring the mannose residue from the Dol-P-Man donor to the S/T of the target protein. This initial mannose can be further elongated in the Golgi apparatus with additional mannoses or galactoses.

Protein *O*-mannosylation is highly conserved among higher eukaryotes and represents the only form of protein *O*-glycosylation in yeasts and fungi (Strahl-Bolsinger *et al.*, 1999). *O*-linked mannosylation describes a protein modification which attaches mannose from activated Dol-P-Man to the hydroxyl group of serine or threonine (S/T) residues in S/T-rich stretches of secretory proteins (reviewed in Lehle et al., 2006). The mannose donor Dol-P-Man is synthesized on the cytosolic side of the ER membrane in *S. pombe* by the essential Dol-P-Man synthase *dpm1*$^{+}$ which is transferring mannose from the mannosyl donor GDP-mannose to the polyisoprenoid Dol-P (Colussi *et al.*, 1997). The Dol-P-Man is then flipped by a yet unidentified mechanism to the luminal side of the ER.

In *S. pombe*, the initial reaction of protein *O*-mannosylation is catalyzed in the ER lumen by the three members of the protein *O*-mannosyl transferase (PMT-family) Oma1p, Oma2p and Oma4p (Fig. 3.3) (Willer *et al.*, 2005). There are viable *S. pombe*

single deletion mutants of *oma1*Δ (SBY90) and *oma4*Δ (SBY88) which exhibit diverse defects caused by protein *O*-mannosylation deficiency.

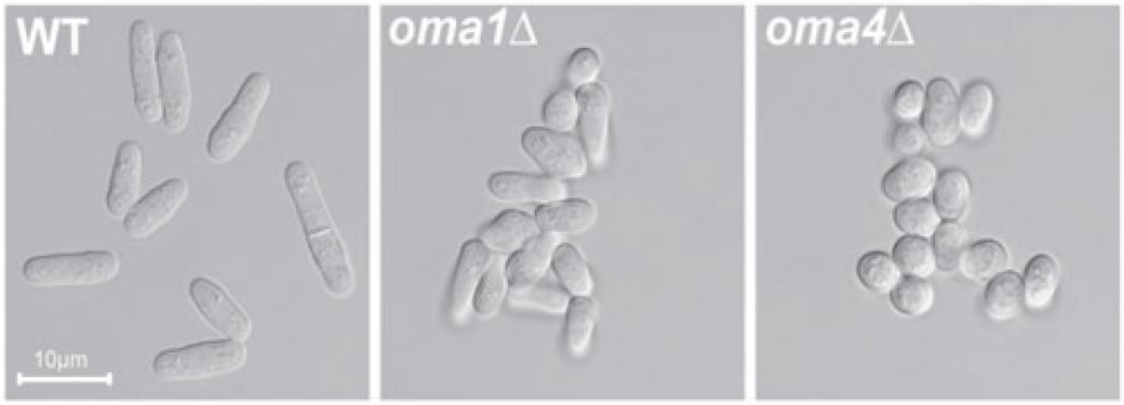

Fig. 3.4: Morphological defects of *S. pombe O*-mannosyl transferase mutants compared to WT (original picture taken from Willer *et al.*, 2005):
Normarski microscopic images show that compared to the rod like shape of WT cells, deletion mutants of *O*-mannosyl transferase *oma1*$^+$ or *oma4*$^+$ are more round and pear shaped.

The *oma4*Δ mutant shows impaired growth on medium containing the cell wall stressor caffeine and *oma1*Δ is sensitive to heat stress. Furthermore it could be demonstrated, that these mutants have morphologically abnormalities like spherical or irregularly shaped cells which form aggregates. The single mutants also exhibit defective septum formation by assembly of irregularly shaped, misplaced or misoriented, double or even branched septa (Willer *et al.*, 2005). The double-mutant *oma1*Δ/*oma4*Δ as well as the single *oma2*Δ mutant were non-viable demonstrating the importance of protein *O*-mannosylation.

A conditional lethal triple-*oma* mutant was created to characterize the consequences caused by a complete block of protein *O*-mannosylation (Fabian, 2009). In this mutant the *oma1*$^+$ gene is disrupted and *oma2*$^+$ and *oma4*$^+$ are under the control of the thiamine repressible nmt81-promoter (no message in thiamine) (Forsburg, 1993; Willer *et al.*, 2005). Transcriptional shut-down of the nmt81-controlled single mutants which were used for creation of the triple-*oma* mutant was demonstrated on mRNA level via Northern Blot. After 12h of repression no *oma2*$^+$ and *oma4*$^+$ transcript could be detected anymore in these mutants (Fabian, 2009). Preliminary analysis of the triple-*oma* mutant indicated multiple cell wall abnormalities including pear-like shape, large β-1,3-glucan depositions in the cell wall and increased lethality.

After attachment of the initial mannose residue by the *O*-mannosyl transferase complex, the mannoprotein proceeds through the secretory pathway. Omh1p is a α-1,2-mannosyl transferase and member of the *KTR*-family (*K*re-*T*wo-*R*elated). Omh1p elongates the *O*-linked mannose in the Golgi apparatus by adding further mannoses from GDP-activated mannose to the initial residue (Lussier *et al.*, 1999; Ikeda *et al.*, 2009). Unlike in *S. cerevisiae* where only mannoses are added to extend the initial *O*-mannosyl glycan, in fission yeast also galactoses are attached in α-1,2- or α-1,3-linkage to the *O*-glycan. *S. pombe* produces diverse *O*-glycans forms of a Galactose$_{0-2}$-Mannose$_{1-3}$ structure (Fig. 3.5) (reviewed in Gemmill and Trimble, 1999; Lommel and Strahl, 2009).

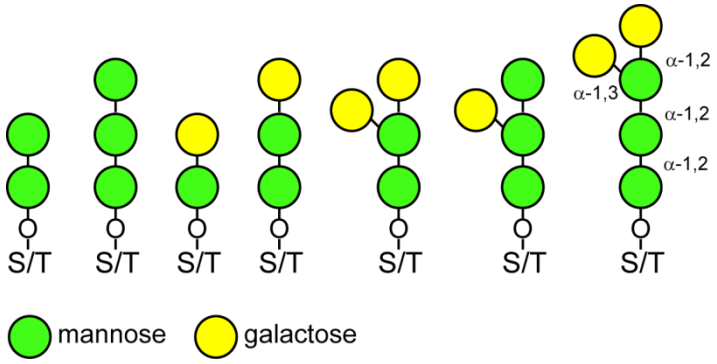

Fig. 3.5: Schematic structure of fission yeast *O*-glycans (adapted from Goto, 2007):
Diverse *O*-glycans are present in *S. pombe*. Stepwise synthesized of the *O*-glycans starts from the side of S/T residue.

The Golgi resident enzyme Gma12p is able to transfer galactose from the donor UDP-galactose in α-1,2-linkage to *O*-mannosyl-S/T to generate Gal-Man$_x$-S/T structures (Chappell *et al.*, 1994; Kainuma *et al.*, 1999). The α-galactosyl transferase genes *gmh1*$^+$ - *gmh6*$^+$ were identified as homologues of *gma12*$^+$ in the fission yeast genome sequence (Yoko-o *et al.*, 1998; Ohashi *et al.*, 2010). However, a strain in which *gma12*$^+$ and *gmh1*$^+$-*gmh6*$^+$ were deleted still contained oligosaccharides consisting of α-1,3-linked galactose residues, suggesting the presence of at least one more α-1,3-galactosyl transferase (Ohashi *et al.*, 2010). Recently, a novel gene-family (*otg1*$^+$-*otg3*$^+$) was identified in the *S. pombe* genome. Some of the *ogt*$^+$-gene products are involved in α-1,3-galactosylation of both *O*- and *N*-linked glycans (Ohashi *et al.*, 2012).

3.4. *Cell cycle, septum assembly and septum separation*

3.4.1. *S. pombe* Cell cycle

In yeast, cell wall assembly and degradation is a vital process that influences several factors including vegetative growth. While running through a complete cell cycle, the cell wall has to expand and a division septum has to be assembled and split.

In all eukaryotes the cell cycle is separated into distinct phases: interphase and mitosis. Interphase consists of G1-phase, S- (DNA replication) and G2-phase (Howard and Pelc, 1953; Tyson *et al.*, 2002). After interphase the cell can initiate mitosis and cytokinesis in order to divide. In *S. pombe* the approximate lengths of Gl/M, S and G2 can be defined by 20%, 10%, and 70% of the cycle (Fig. 3.6) (Mitchison and Creanor, 1971; Forsburg and Rhind, 2006).

Accuracy during the replication process is crucial for survival of the cell and thus controlled very precisely on numerous checkpoints. Failure of DNA repair, initiation of mitosis with incompletely replicated DNA, or initiation of anaphase prior to correct chromosome alignment on the spindle pole bodies, promote cell death, aneuploid or mutant cells (Murray, 1994).

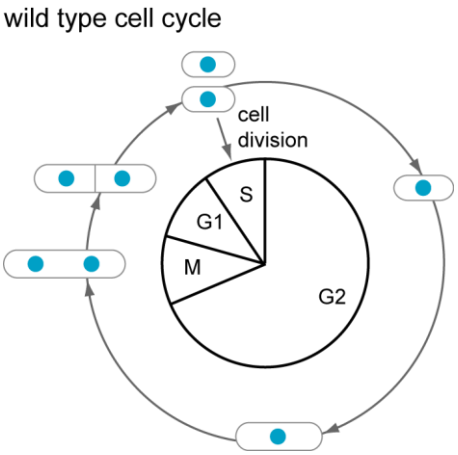

Fig. 3.6: Fission yeast cell cycle under optimal conditions (adapted from Novak *et al.*, 1998): Schematic illustration of the cell cycle of an exponentially growing *S. pombe* culture. 70% of the cell cycle time the cells are in G2-phase. M-, G1- and S-phase share 10% to the cell cycle time each. Fission yeast is known to have a prolonged G2 and very short G1. Cell division takes place while S-phase already started.

3.4.2. Structure and assembly of the fission yeast septum

In fission yeast, a cell cycle is completed when the mother cell has separated into two daughter cells. In order to divide, a cross wall - the septum - needs to be assembled

during cytokinesis. During vegetative growth, the fission yeast cell expands by elongation at its two poles and divides by medial fission, generating two daughter cells of approximately equal size. The division site in *S. pombe* is chosen based on two indicators: a positive signal provided by the pre-mitotic nucleus positioned at the cell center and a negative signal from both cell ends which is regulated by protein kinase Pom1p (Tran *et al.*, 2001; Moseley *et al.*, 2009).

Onset of septum assembly requires positioning of the actomyosin ring at the middle of the mother cell. The actomyosin ring defines the site of septum formation and for correct ring positioning action of the genes products of *mid1*$^+$, *plo1*$^+$ and *pom1*$^+$ is essential (Ohkura *et al.*, 1995; Sohrmann *et al.*, 1996; Bähler and Pringle, 1998; Moseley *et al.*, 2009). Mid1p is localized nuclear through interphase and becomes a component of the actomyosin ring during mitosis and cytokinesis. The phosphatase Plo1p phosphorylates Mid1p during mitosis and is thus causing the nuclear export and recruitment of Mid1p to the division site, where it stabilizes the position of the actomyosin ring (Sohrmann *et al.*, 1996; Bähler and Pringle, 1998). Mid1p itself recruits components of the cortical actomyosin ring to the nodes, where they maturate into the contractile ring (Wu *et al.*, 2006; Pollard and Wu, 2010). Mutants analysis has shown that diverse components are involved in medial ring assembly like Myo2p that is responsible for contraction (Kitayama *et al.*, 1997).

The septum material itself is assembled in a centripetal manner, dependent on the actomyosin ring constriction. The fission yeast septum is composed of a three layered structure (Johnson *et al.*, 1973). The inner primary septum is composed of linear β-1,3-glucan, a polymer which is exclusively present in this structure. On both sides, the primary septum is covered with the secondary septum which consists of, like the regular cell wall, α-1,3-glucan, β-1,6-branched-β-1,3-glucan, β-1,6-glucan, and galactomannans (Horisberger and Rouvet-Vauthey, 1985; Humbel *et al.*, 2001; Sugawara *et al.*, 2003).

The first septum material which is synthesized upon septum assembly is the linear β-1,3-glucan of the primary septum. Responsible for the primary septum β-1,3-glucan assembly is glucan synthase Bgs1p (Le Goff *et al.*, 1999; Liu *et al.*, 1999; Liu *et al.*, 2000; Cortés *et al.*, 2007). Bgs1p is an integral PM protein that is located at the contractile actomyosin ring during septum assembly where it catalyses the β-1,3-glucan elongation using UDP-glucose as substrate (Shematek *et al.*, 1980; Cortés *et al.*, 2002).

To regulate the septum assembly process, β-glucan synthesis itself is tightly controlled. It was demonstrated that the Rho-family GTPases are involved in controlling the activity of β-glucan synthase (Arellano *et al.*, 1996).

Moreover, β-1,3-glucan modifying enzymes are also participating in primary septum formation. De Medina-Redondo and co-workers (de Medina-Redondo *et al.*, 2010) presented evidence that the GH72 family proteins Gas1p, Gas2p and Gas5p display β-1,3-glucanosyl transferase activity. They showed that these proteins elongate β-1,3-glucan chains in a two-step reaction. In the first step, an internal glycosidic linkage of a β-1,3-glucan donor is cleaved creating a new reducing end. In the following step this reducing end is used to elongate an acceptor β-1,3-glucan chain creating a β-1,3-linkage (de Medina-Redondo *et al.*, 2010).

It could be demonstrated that the assembly of cell wall polymers provide the driving force for cytokinesis rather than the force applied from the contractile ring that is largely dispensable (Fig. 3.7) (Proctor *et al.*, 2012).

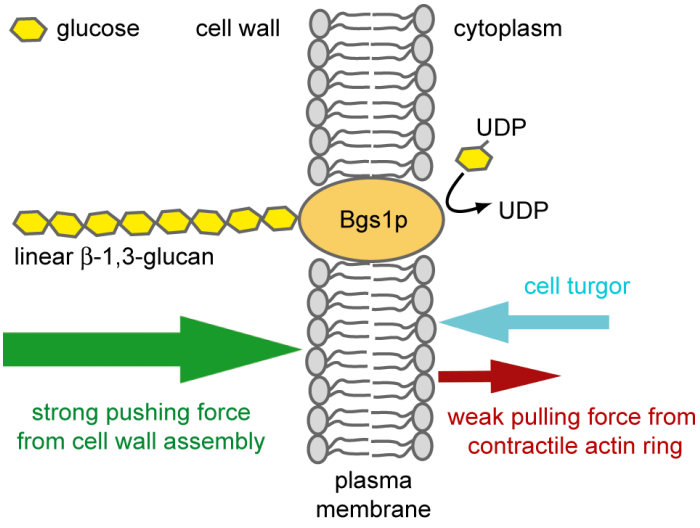

Fig. 3.7: Primary septum synthesis (adapted from Proctor *et al.*, 2012):
Ingression of the primary septum is subject of different forces. The contracting actin ring is applying a weak force pulling towards cell center (red arrow). This is counteracted by the stronger cell turgor (blue arrow). The main force driving the septum formation, is the powerful pushing force from the Bgs1p synthesized linear β-1,3-glucan (green arrow).

Although linear β-1,3-glucan is required for primary septum formation this polysaccharide alone is not sufficient for correct septum assembly (Cortés *et al.*, 2007). It was shown that mutants of α-1,3-glucan synthase Mok1p formed a thick secondary septum compared to wild type (Konomi *et al.*, 2003). Recently, Cortés and co-workers

provided evidence that Ags1p-synthesised α-1,3-glucan is essential for both, correct primary and secondary septum formation. Ags1p provides the rigidity which is necessary to counteract the cell turgor pressure during cell separation secondary septum formation and the primary septum rigidity (Cortés *et al.*, 2012; Proctor *et al.*, 2012). In the absence of Ags1p a twisted primary septum is generated which is highly vulnerable to the cell turgor during the separation process. Moreover, Ags1p depleted cells are unable to assemble a flanking secondary septum. Only after extended time a new remedial cell wall layer appeared to substitute the secondary septum (Cortés *et al.*, 2012). These observations suggested that (1) Ags1p is responsible for the correct primary septum assembly; and (2) for the secondary septum assembly which ought to flank the newly synthesised primary septum (Cortés *et al.*, 2012). It was shown that α-1,3-glucan synthase Ags1p tightly co-localizes with β-1,3-glucan synthase Bgs1p during primary septum formation (Cortés *et al.*, 2012).

Soon after onset of primary septum synthesis the production of the secondary septum starts, flanking the primary septum on both sides. The secondary septum consists of the regular cell wall components (Horisberger and Rouvet-Vauthey, 1985; Humbel *et al.*, 2001; Sugawara *et al.*, 2003).

3.4.3. Splitting of the septum

After the septum assembly is completed the daughter cells have to be separated. In order to accomplish that, the established septum has to be splitted by degradation of the primary septum. To prevent cell lysis during this critical process, the formation and subsequent degradation of cell wall material has to be securely coordinated and controlled.

For separation, the linear β-1,3-glucan of the primary septum is degraded by designated endo-glucanases without compromising the integrity of the daughter cells during division (Fig. 3.6) (reviewed in Sipiczki, 2007). The flanking secondary septum consisting of regular wall material will become the actual cell wall after successful division. In electron microscopic (EM) images there are two electron-dense, triangle-shaped structures visible at the connection between the lateral cell wall and the septum named material triangulaire dense. This junction area is also referred to as septum edging (Dekker *et al.*, 2004). The exact function and composition of these electron-dense structures still needs to be elucidated. However, it is proposed that they form two

rings which are not degraded during cell separation but remain at the daughter cells. After separation, these electron-dense structures are referred to as fuscannels which are visible as division scars (Johnson *et al.*, 1973).

Expression of many genes involved in the complex separation process is regulated by the Sep1p-Ace2p transcription-factor cascade. Target genes of the periodically expressed Ace2p transcription factor encode the key enzymes of septum cleavage, namely Eng1p and Agn1p (Bähler, 2005). Erosion of the septum starts with the degradation of the cell wall surrounding the outer rim of the primary septum by the periodically produced α-1,3-glucanase Agn1p (Dekker *et al.*, 2004; García *et al.*, 2005). After initial disruption of the septum edging, the cell turgor pressure starts rounding the secondary septa. The applied physical force of this process induces the splitting of the primary septum (Sipiczki and Bozsik, 2000). The endo-β-1,3-glucanase Eng1p facilitates the degradation process of the primary septum (Martín-Cuadrado *et al.*, 2003) (Fig. 3.8). Additional Ace2p targets are Adg1p, Adg2p, Adg3p and Cfh4p, but their function in cell separation is still uncertain (Martín-Cuadrado *et al.*, 2003; Dekker *et al.*, 2004; Alonso-Nunez *et al.*, 2005; Bähler, 2005). Although its important role in cell separation, the Sep1p-Ace2p cascade is not the only regulator involved in this process (Sipiczki *et al.*, 1993).

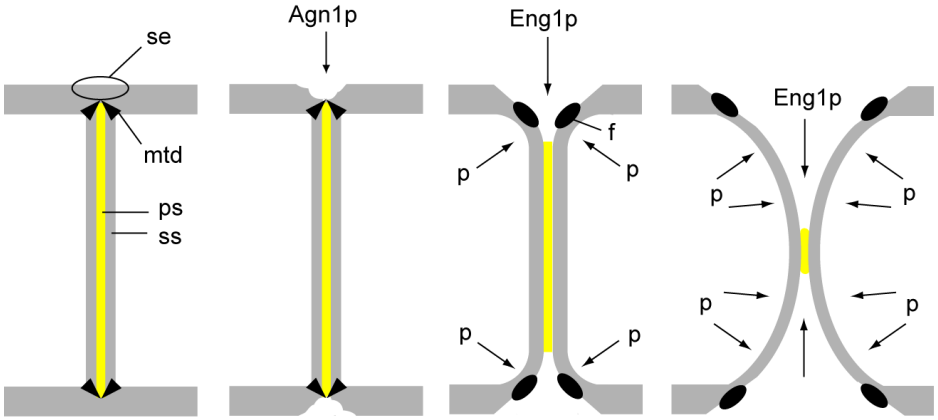

Fig. 3.8: Splitting of the septum (adapted from Cortés *et al.*, 2012):
Septum separation starts with degradation of the region of the septum edging (se) by endo-α-1,3-glucosidase Agn1p. The material triangulaire dense (mtd) is then opening and remaining as fuscannels (f) in the cell wall that will become the division scar. Now the primary septum is accessible for degradation by endo-β-1,3-glucanase Eng1p. The cell turgor (p) immediately rounds the edges of the new ends.

3.5. sup11^{+} *is a multicopy-suppressor of a conditionally lethal* O*-mannosylation mutant*

Both, the fungal cell wall matrix as well as the septum are complex structures as pointed out in previous chapters. A secure regulation of the construction, assembly, modification and even degradation of their multilayered composition is crucial for viability of the yeast cell. Every component fulfills different tasks for example, glucans being mainly responsible for cell wall rigidity. Since loss of protein *O*-mannosylation causes cell death, it is obvious that also various *O*-mannosylated proteins play crucial roles as they are part of the galactomannan layer. But it is not that simple to pin down the role of the various *O*-mannosylated proteins that are present in the cell wall as their function reaches beyond structurally purposes for example being able to work as cell wall stress sensor proteins, like Wsc1p (Willer *et al.*, 2005). But, *O*-mannosylated proteins are not only part of the cell wall but are also secreted or located intracellularly along the secretory pathway.

In order to clarify why protein *O*-mannosylation is an essential modification a multicopy-suppressor screen in a conditionally lethal *S. pombe O*-mannosylation mutant was performed (Willer *et al.*, 2005; Hutzler, 2009). In this mutant strain the *oma2*$^{+}$ gene is expressed under the control of a repressible nmt81-promoter (Forsburg, 1993; Willer *et al.*, 2005). This screen identified 31 genes which were able to suppress lethality of the restricted nmt81-*oma2*$^{+}$-knock-down mutant. Amongst others, genes involved in cell wall formation were identified. Since *oma*$^{+}$-deficient strains reveal cell wall defects such as deformed cell shape, accumulation of cell wall material and septum malformations (Willer *et al.*, 2005), cell wall related genes were further analyzed. Overexpression of genes involved in cell wall polysaccharide biogenesis might counteract the compromised cell wall integrity caused by hypo-mannosylation of cell wall proteins.

In this screening the gene loci SPAC23H3.11c and SPBC11C11.05 were identified which are the *S. pombe* homologue genes encoding for cell wall β-1,6-glucan biogenesis related genes *Sc*Kre6 and *Sc*Kre9 (Brown *et al.*, 1993). SPAC23H3.11c is the fission yeast homologue of the *S. cerevisiae KRE6*-family (*KRE6*, *SKN1*) (Boone *et al.*, 1990). SPBC11C11.05 was identified several times on independent plasmids and is the only homologue of the *KRE9*-family (*KRE9*, *KNH1*) in fission yeast. As mentioned before, the exact function of *ScKRE9* remains uncertain (Brown *et al.*, 1993).

Hutzler (2009) showed that *Sp*Sup11p is an integral membrane protein. A conditional lethal *sup11*$^{+}$ knock-down mutant in which the gene is under control of the thiamine-repressible nmt81-promoter was created and initial analysis revealed a distinct septum malformation phenotype (Hutzler, 2009).

Preliminary characterization of nmt81-*sup11* showed that under restrictive conditions the mutant exhibits an increased sensitivity towards the detergent SDS (Hutzler, 2009). This anionic detergent is known to inflict damage to cell wall mutants because it compromises membrane integrity and therefore impairs growth of strains with disturbed cell walls (Klis *et al.*, 2002). Sup11p depleted cells showed increased resistance towards treatment with Zymolyase has β-1,3-glucanase activity. Chemical cell wall analysis revealed clear abnormalities in cell wall glucan composition (Hutzler, 2009). The cell wall of wild type fission yeast consists of a roughly 15% mannan, 30% α-glucans and 55% β-glucans (Bush *et al.*, 1974; Manners and Meyer, 1977), which resembled the observed glucan and mannan distribution in of a genomically HA-tagged Sup11p strain used as control in this experiment. The depleted nmt81-*sup11* mutant exhibited no divergence in the mannan content compared to the control. However, the ratio of α-glucan and β-glucan differed significantly. Ratiometric measurements showed a strong increase of α-glucan (43%) to β-glucan (42%), demonstrating that the α-glucan and β-glucan in the control ratio is 2:5, but shifts to 1:1 in the restricted nmt81-*sup11*$^{+}$ mutant. These findings suggest an altered wall matrix composition in the restricted nmt81-*sup11* mutant.

Aim of this work is to present an extensive characterization of Sup11p. A detailed phenotypic characterization of a *sup11*$^{+}$ depleted mutant ought to reveal the contribution of Sup11p in cell wall/ septum polysaccharide organization and/or biogenesis, and interactions of Sup11p with other cell wall glucan modifying enzymes.

In addition, important protein features like its subcellular localization and the topology were addressed in this study. Moreover, the effects of hypo-mannosylation of Sup11p in different *O*-mannosyl transferase mutant backgrounds were investigated in order to gain a better understanding about the role of Sup11p to function as a multicopy-suppressor for a conditional lethal *O*-mannosylation mutant.

4. Material and Methods

Material and Methods were taken and/ or adapted on basis of previous dissertations handed in by members of the AG Strahl.

4.1. Material

4.1.1. Chemicals, enzymes and consumables

Babco (Berkeley, USA):
Anti-HA antibody (16B12)

BioRad (München):
Precision Prestained Dual Colour Protein Marker, Precision Prestained Unstained Protein Marker, Proteinbestimmungs-Kit, Quantum Midi Prep Kit,TEMED

Calbiochem (La Jolla, USA)
DAPI

Difco Laboratories (Detroit, USA):
Agar, Bakto-Yeastextract

Fuji (Tokyo, Japan):
X-ray films (Fuji Super RX 18x24)

GE Healthcare (Buckinghamshire, Great Britain):
ECL Western blotting detection reagents, Glutathione sepharose 4B, Hybond ECL nitrocellulose membrane, Streptavidin-horseradish peroxidase conjugate (RPN1231-100µl)

Invitrogen (Karlsruhe):
Anti-GFP (rabbit antiserum, A-6455), anti-mouse AlexaFluor488 antibody (A11001), UltraPure Agarose, pENTR/D-TOPO Cloning Kit

MatTek (Ashland, USA):
Glass Bottom Microwell dishes (P35GC-1.5-14-C)

Merck (Darmstadt):
All not otherwise listed chemicals

Millipore (Eschborn):
Sterile filter

New England BioLabs (Ipswich, USA):
EndoH (P0702S)

Pierce (New York, USA):
EZ-Link Sulfo-NHS-LC-Biotin (21335)

Qiagen (Hilden):
RNeasy Mini Kit, RNeasy Midi Kit

Roth (Karlsruhe):
Acrylamid solution for SDS-PAGE, Ammonium persulfate, cover slips, glycerine, glasbeads 0.45 mm diameter, glasbeads 3.0 mm diameter, glas slides, Roti-Phenol, TEMED, Tris, Tween 20

Santa Cruz (Heidelberg)
Anti-GST antibody (BIP (aC-19): sc-15897)

Sigma Aldrich (Hamburg):
Amino acids, ampicillin, aniline blue (former FLUKA company), anti-Rabbit IgG peroxidase conjugate, anti-Mouse IgG peroxidase conjugate, DMSO, DTT, formamid, isoamylalkohol, lithium acetate, Lysozym, Lyticase (L2524)**,** Lysing Enzymes (L1412), PMSF, Polyethylenglykol 4000, Ponceau S, RNase, salmon sperm-DNA, Triton-X-100

Thermo Fischer (Waltham, USA):
5-Fluoroorotic acid, DNA-Standard (kb ladder), β-glucanase (G8548), dNTPs, Dream-Taq, Fast AP (alkaline phosphatase), GeneJET PCR Purification Kit, GeneJET Gel Extraction Kit, GeneJET Plasmid Miniprep Kit, IPTG, Maxima SYBR Green qPCR Master Mix, Phusion High-Fidelity DNA Polymerase, restriction endonucleases, RevertAid H Minus First Strand cDNA Synthese Kit, T4 DNA Ligase, T4 DNA Polymerase

4.1.2. Antibodies

Primary antibodies

Name	Binding	Source
anti-HA	HA	Sigma
anti-GFP	GFP	Invitrogen
anti-RFP	RFP	Gift from Holger Lorenz, ZMBH University of Heidelberg
anti-Kin1p	Kin1p	Gift from Xavier LeGoff, University of Lausanne,

		Switzerland
anti-β-1,6-glucan	β-1,6-glucan	Gift from Frans Klis, University of Amsterdam, The Netherlands
anti-β-1,3-glucan	β-1,3-glucan	Gift from Frans Klis, University of Amsterdam, The Netherlands

Secondary antibodies

Name	**Source**
anti-mouse	Sigma
anti-rabbit	Sigma
anti-mouse AlexaFluor488	Invitrogen

4.1.3. Media

4.1.3.1. Media for Escherichia coli

LB Medium (Bertani, 1951):

1% Trypton
0.5% Yeast extract
1% NaCl
For plates adding 2% agar (w/v).
For selection ampicillin (Amp) is added 0.1 % (w/v) or kanamycin (Kan) to 0.05% final concentration.

4.1.3.2. Media for *Schizosaccharomyces pombe*

Protocols from (Forsburg and Rhind, 2006)

YES rich medium:
1% Yeast extract
3% D-glucose 16.6 mM
In addition: 0,000225% adenine, histidine, leucine, uracil and lysine (w/v).
For selection G418 is added to 0.0002% (w/v) final concentration
(sterile filtrated) added after autoclaving.

EMM (Edinburgh Minimal Medium)
3 g/l potassium hydrogen phthalate 14.7 mM
2.2 g/l Na_2HPO4 15.5 mM
5 g/l NH_4Cl 93.5 mM
20 g/l glucose 11.1 mM
0.02% salt stock solution (50 x)
1 ml/l vitamin stock solution (1000 x)
0.1 ml/l mineral stock solution (10000 x)

EMM + 5-FOA
EMM with additional 0.1 % 5-fluoroorotic acid (5-FOA) and 225 mg uracil (Forsburg and Rhind, 2006).
Sterile filtrated 5-FOA added after autoclaving.

EMM-N (nitrogen free)
EMM without (w/o) NH_4Cl.

Salt stock solution (50 x)
Contains final concentrations of:
52.5 g/l $MgCl_2$ 6 H_20 (0.26 M)
0.735 g/l $CaCl_2$ $2H_20$ (5 mM)
50 g/l KCl (0.67 M)
2 g/l Na_2SO_4 (14.l mM)
(Can be autoclaved for sterilization)

Vitamin stock solution (1000 x)
Contains final concentrations of:
1 g/l pantothenic acid (4.2 mM)
10 g/l nicotine acid (8l.2 mM)
10 g/l meso-inositol (55.5 mM)
10 mg/l biotin (40.8 μM)

Mineral stock solution (10000 x)
Contains final concentrations of:
5 g/l boric acid (80.9 mM)
4 g/l $MnSO_4$ (23.7 mM)
4 g/l $ZnSO_4 \cdot 7\ H_2O$ (13.9 mM)
2 g/l $FeCl_2 \cdot 6H_2O$ (7.40 mM)
0.4 g/l molybdic acid (2.47 mM)
1 g/l KI (6.02 mM)
0.4 g/l $CuSO_4 \cdot 5H_2O$ (1.60 mM)
10 g/l citric acid (47.6 mM)
Vitamin and mineral stock solutions are sterile filtrated and stored at 4°C.

Sporulation medium (SPO)
1% D-glucose
0.1% monopotassium phosphate
1:5000 vitamin stock solution (100 μg/ml)
In addition: 45 mg/l adenine, histidine, leucine, uracil and lysine (w/v).

EMM /SPO: additional aa if needed for auxotrophy marker: 0.000225% adenine, histidine, leucine, uracil each.
Restrictive conditions of nmt81-promoter: final concentration of thiamine 0.000025% (w/v) (75 μM) from filter sterilized stock at 10 mg/ml stored at 4°C (Moreno *et al.*, 1991).

YES, EMM and SPO plates:
Addition of 2% agar to the liquid medium.

4.1.3.3. Media for *Saccharomyces cerevisiae*

YPD rich medium:

1 % Yeast extract
2 % peptone
2 % D-glucose

SD minimal medium:
0.67 % Yeast nitrogen base w/o aa
2 % D-glucose
1.6 g/l aa dropout
If needed histidine (20 mg/l), leucine (60 mg/l), lysine (30 mg/l), tryptophan (40 mg/l), uracil (19 mg/l) added.

Aa dropout:

nutrient	Amount in dropout powder (g)	Final concentration in prepared media (µg/ml)
adenine	2.5	40
arginine	1.2	20
aspartic acid	6.0	100
glutamic acid	6.0	100
methionine	1.2	20
phenylalanine	3.0	50
serine	22.5	375
threonine	12.0	200
tyrosine	1.8	30
valine	9.0	150

4.1.4. Buffer and Solutions

Molecularbiological methods

5x TBE
445 mM boric acid
5 mM EDTA pH 8.0
445 mM Tris/HCl pH 8.0

10x DNA loading dye
100 mM EDTA pH 8.0
60% glycerine
0.25% bromophenol blue (w/v)
0.25% xylencyanol (w/v)

TE
10 mM Tris/HCl pH 7.5
1 mM EDTA pH 8.0

Isolation of genomic DNA from yeast cells
Resuspension buffer
2% Triton X-100
1% SDS
100 mM NaCl
10 mM Tris/HCl pH 8.0
1 mM EDTA pH 8.0

Isolation of plasmid DNA from bacterial cells

STET buffer
50 mM Tris/HCl pH 8.0
50 mM EDTA
8% sucrose
5% Triton X-100

Yeast transformation

TE/LiAc buffer
100 mM lithium acetate in TE

TE/LiAc/PEG
100 mM lithium acetate in TE
40% PEG 4000 (w/v)

Antibody affinity purification

Glycine buffer pH 2,2
5 mM glycine pH 2,2
0.5 M NaCl

Glycine buffer pH 2,8
5 mM glycine pH 2,8
0.5 M NaCl

Membrane and microsome preparation

Membrane buffer
50 mM Tris/HCl pH 7.5
0.3 mM $MgCl_2$
+ Protinase inhibitor
PMSF : 1 :100
Benzaminide : 1 :100
TLCK : 1 :100
TPCK : 1 :100

Protinase inhibitor stocks
100 mM PMSF in isopropanol (100 x stock)
100 mM benzamidine in ddH_2O (100 x stock)
5 mg/ml TPCK in ethanol (100 x stock)
10 mg/ml TLCK (100 x stock)

sucrose-ficoll-cushion
0.8 M sucrose
1.5% (w/v) Ficoll-400
20 mM HEPES/KOH ph 7.4

spheroblasting buffer
20 mM Tris/HCl pH 7.5
0.8 M sorbitol
25 µM TLCK
50 µM TPCK

sucrose-cushion
1 M sucrose
20 mM HEPES/KOH pH 7.4

spheroblast lysis buffer
0.1 M sorbitol
20 mM Tirs/HCl pH 7.5
10 mM $CaCl_2$

SDS-PAGE and Western blotting

SDS running buffer
25 mM Tris
0.1% SDS
192 mM Glycin

Stacking gel buffer
0.14 M Tris/HCl pH 6.8
0.11 M SDS

Separation gel buffer
0.14 M Tris/HCl pH 8.8
0.3% SDS

SDS sample buffer (4x)
250 mM Tris/HCl pH 6.8
20% glycerin
20% ß-Mercaptoethanol
8% SDS
0.4% bromophenolblau

TBS
50 mM Tris/HCl pH 7.5
140 mM NaCl

TBST
TBS
0.05% Tween20

Transfer buffer
20 mM Tris
150 mM glycine
20% methanol
0.02% SDS

Blocking buffer
TBST
4% dry milk powder

Blocking buffer for biotinylation assay
TBS
0.1% Triton X-100
2% bovine serum albumin (BSA) (w/v)

Buffer for microscopy

PEM
100 mM Pipes
1 mM EGTA
1 mM $MgSO_4$ pH6.9

PEMS
PEM
1.2 M sorbitol

PEMBAL
PEM
1% BSA (essentially FA + globulin free Sigma)
0.1% NaN_3
100 mM lysine-hydrochlorid

4.1.5. Internet sources

NCBI:	http://www.ncbi.nlm.nih.gov/
Google Scholar:	http://scholar.google.de
S. pombe GeneDB:	http://www.genedb.org/genedb/pombe/
	http://www.pombase.org/
SGD:	http://www.yeastgenome.org/
Transmembrane predictions:	
TMHMM:	http://www.cbs.dtu.dk/services/TMHMM-2.0 (CBS; Denmark)
TopPred:	http://mobyle.pasteur.fr/cgi-bin/portal.py?#forms::toppred (Institut Pasteur, France)
TMpred:	http://www.ch.embnet.org/software/TMPRED_form.html (EMBnet-CH, Switzerland)
SOSUI:	http://bp.nuap.nagoya-u.ac.jp/sosui/ (Nagoya University, Japan).
Expasy:	http://www.expasy.org/tools/
PRALINE:	http://www.ibi.vu.nl/programs/pralinewww/
PubMed:	http://www.ncbi.nlm.nih.gov/pubmed/
Forsburg Labor:	http://www-bcf.usc.edu/~forsburg/index.html

Genecodis:	http://genecodis.cnb.csic.es/
ClustalW2:	http://www.ebi.ac.uk/Tools/msa/clustalw2/
Protein blast:	http://blast.ncbi.nlm.nih.gov/Blast.cgi/ (Altschul *et al.*, 1997)
Cyclebase:	http://cyclebase.org/index.action (Gauthier *et al.*, 2008; Gauthier *et al.*, 2010)

4.1.6. Software

DNA Sequence analysis: Vector NTI 9(Invitrogen)

Image processing: Photoshop, Illustrator (Adobe)
Reference list: EndNoteX2 (Thomson)
Quantification of Western Blot signal intensities: Fiji (Madison)
Image processing of CLSM pictures: LSM image browser (Carl-Zeiss)
Image processing of Nikon Total Internal Reflection Fluorescence (TIRF): Fiji (Madison)
Image analysis of confocal Nikon TE2000 inverted microscope: Volocity (PerkinElmer)
Mass spectrometry data analysis: Mascot (Matrix Science, London, UK; version 2.2.04)

4.1.7. External services

Oligo synthesis:	Sigma Aldrich (Hamburg)
Sequencing:	MWG Eurofins (Ebersberg)
Gene synthesis:	Geneart (Regensburg)
Imaging facility:	Nikon imaging center (Heidelberg)
S.cerevisiae mutant library:	Euroscarf (Frankfurt)
FACS analysis:	Cell sorting facility, ZMBH (Heidelberg)
Polyclonal antibody production:	Pineda Antikörper-Service (Berlin)

4.1.8. Growth conditions and genetic manipulations

The *S. pombe* strains used in this study are listed in 4.1.8.2.2. Yeast cells were grown on YES (yeast extract with supplements) medium or Edinburgh minimal medium (EMM) with appropriate supplements (Moreno *et al.*, 1991). For shutoff experiments using the nmt81 promoter cells were grown up to logarithmic phase in liquid culture (EMM), inoculated in EMM with thiamine (20 mg/l) to a density of OD_{600} 0.05 and grown for 16 hours (h) at 32°C or spotted on EMM plates with thiamine (20 mg/l) at 32°C. For plasmid loss experiments cells were grown on EMM plates containing 0.1% 5-FOA (Fermentas, #R0812) and 0.0225% uracil. SDS sensitivity was tested with spotted cells on YES plates without and 0.005% and 0.01% SDS and incubation for 3 days at 32°C.

DNA transformation has been carried out as reviewed in Forsburg and Rhind (2006). Standard procedures described in Sambrook (Sambrook and Russel, 2001) were used for all DNA manipulations. *Escherichia coli* DH5α was used for cloning and transformation.

4.1.9. Plasmids

4.1.9.1. Plasmid construction

pLW65 was constructed for constitutive gene expression in *S. pombe*. The constructed plasmid derived from pREP3-adh (Willer *et al.*, 2005) in which the adh1 promoter was exchanged with the *act1*$^+$ promoter. The -1000bp to +1 promoter region of the *act1*$^+$ were amplified with oligos 1433 and 1434 and inserted to pREP3-adh by *Pst*I and *Not*I restriction sites.

pLW55 was constructed by amplification of the *sup11*$^+$ ORF (bp 1-849) plus *Not*I/*Xho*I overlaps from genomic DNA was done with olgios 1257 and 1258. *Not*I/*Xho*I fragment was inserted in pREP3-adh (*Not*I/*Xho*I).

pLW109 was constructed by amplification of the *sup11*$^+$ ORF (bp 1-849) plus *Not*I/*Xho*I overlaps from pLW55 was done with olgios 1257 and 1258. *Not*I/*Xho*I fragment was inserted inserted into pLW65 (*Not*I/*Xho*I).

pLW106 was created by released of oma1:HA from pTW20 via *Xho*I/*Sal*I digestion. The tagged gene was and inserted via same restriction enzymes into pLW65.

pLW113 was constructed by amplifying *S. cerevisiae KRE9* (start-stop) with oligos 1679/1681, sub-cloned to cloneJET and inserted via *Not*I/*Sal*I into pLW65.

pLW103 was created for cloning a N-terminal SS:eYFP:Sup11 reporter construct. An artificial *Bam*HI restriction site was introduce to the *sup11*$^+$ gene right behind the signal sequence (bp 1-63). Amplification of a act1p:Sup11SS fragment with *Pst*I/*Bam*HI adapter was performed by using oligos 1625 and 1434 and pLW109 as template. The act1p:Sup11SS cassette was inserted via *Pst*I/*Bam*HI to pLW65. For subsequent cloning of Sup11 without signal sequence (bp 63-849) with *Bam*HI/*Sal*I adapter was amplified using oligos 1627 and 1628 (pLW109 template for amplification) and inserted. A Sup11p expression plasmid with *Bam*HI restriction site at bp position 63 was obtained.

pLW104 is the N-terminal SS:eYFP:Sup11 reporter construct. eYFP with *Bam*HI adapters was amplified from pML-PMT:eYFP with oligos 1631 and 1632 and inserted to pLW103 via *Bam*HI overlaps. Correct orientation was confirmed by sequencing and yielded in.

pLW153 was used as disruption construct for *Dis*:*gas2*$^+$:*LEU2*. It was created by amplifying the 1380bp long *gas2*$^+$ gene from genomic DNA (gDNA) with oligos 1933/1934 and blunt-end cloned into cloneJET obtaining pLW152. The gene was disrupted by a *LEU2* cassette cut from pLW65 with *Hind*III and blunted by T4 DNA polymerase. Plasmid pLW152 was opened in *gas2*$^+$ gene with *Nhe*I digestion, blunted with T4 DNA polymerase and inserted the prepared *LEU2* from pLW152 at bp position 333 to obtain pLW153. Digestion with *Bgl*II released disruption cassette from the vector which can be used to introduce disruption in *gas2*$^+$ gene.

pLW51 and **pLW52** were created for rising an antibody against Sup11p. Two GST-fusion proteins for *E. coli* expression were constructed. Sup11 region between putative TM 2 and 3 (aa 170-210) was amplified from gDNA with oligos 1208/1210 and blunt-end inserted in pGEX-6P-1 to obtain pLW51. The second expression construct was designed with the C-terminal Sup11 region behind the putative third TM (aa 232-284). The 169bp region was amplified from gDNA with oligos 1211/1209 and blunt inserted in pGEX-6P-1 which yielded in pLW52.

pLW117 was constructed to overexpress the *exg2*$^+$ gene form plasmid. Therefore the 1713bp ORF (bp 1-1710) was amplified from gDNA with oligopair 1673/1674 (*Not*I/*Xho*I adapter) and cloned via *Not*I/*Xho*I into pLW109.

pLW147 was designed as truncated *sup11*$^+$ (bp 1-73) with C-terminal eGFP fusion. eGFP was amplified with oligos 1780/1781 from pAG426GPD-ccdB-eGFP (Invitrogen) and cloned via *Not*I/*Xho*I into pLW109. *sup11*$^+$ signal anchor sequence (bp 1-73) was amplified by oligos 1257/1912 and ligated via *Not*I to obtain with SAS:Sup11:eGFP under the control of *act1*-promoter. Correct orientation was confirmed via sequencing.

pLW78 was cloned by exchanging the Sup11p:HA to Sup11:GFP from pLW56 via *Not*I/*Sal*I. pLW56 was cloned by cutting the GFP cassette from pFA6a-KanMX-GFP with *Xho*I/*Sal*I (blunt), and inserted it via *Bgl*II (blunt)/*Sac*I.

Plasmids for *N*-glycosylation site scanning

Plasmids were constructed with pLW65 background.

pLW143/ pLW144: To integrate the N239Q mutation two mutagenesis PCRs with oligos 1909/1258 and 1910/1257 were performed. The amplified products were combined for amplification of the mutated full length *sup11*$^{+}$ ORF with oligos 1257/1258. PCR fragment was cloned via *Not*I/*Xho*I to the destination vector pLW65 yielding in pLW144. Mutations N47Q was carried out analogue with mutagenesis oligos 1907/1320 and 1908/1434 to obtain pLW144.

To introduce new artificial sequons to Sup11p followed oligos were used in the same manner as described above: For L181N oligos 1889/1320 and 1890/1434 were used (**pLW140**); P190T was mutated by PCR with 1891/1320 and 1892/1434 (**pLW141**); I250N was created by mutagenesis PCR with oligopairs 1893/1320 and 1894/1434 (**pLW142**).

4.1.9.2. Table of plasmids used in this study

4.1.9.2.1. *E. coli* plasmids

name	**specification**	**reference**
CloneJET	Bacterial expression, Ampicilin^{R}, MCS	Michelsen, 1995, Thermo Fischer
pGEX-6P-1	Bacterial expression, tac promoter with GST-tag, *lacI*^{q}, PreScission Protease cleavage site	Kaelin *et al.*, 1992, GE Healthcare
pENTR/D-TOPO	Gateway® System for blunt-end PCR cloning, Kanamycin^{R}	Invitrogen
pAG426-ccdB	Chloramphenicol ^{R}, MCS, *URA3*	Invitrogen
pLW51	Sup11p soluble domain from AS 170-210 fused to GST tag in pGEX-6P-1	This study
pLW52	Sup11p soluble domain from AS 232-284 fused to GST tag in pGEX-6P-1	This study

4.1.9.2.2. Yeast plasmids

name	**specification**	**reference**
pFA6a-3HA-KanMX	HA-tag cassette and $KanMX^R$	Bähler and Pringle, 1998
pFA6a-KanMX6-P81nmt1	nmt81-promoter cassette with $KanMX^R$	Bähler and Pringle, 1998
pFA6a-KanMX-GFP	GFP-tag cassette and $KanMX^R$	Bähler and Pringle, 1998
pRS416FLAG4-promoter-ro2-C-term	pRS416-FLAG4 and roGFP2	Gift from A. Meyer
pTW20	pREP3X, *oma1*$^+$:HA under nmt81-promoter, *ura4*$^+$	Willer, 2003
pTW23	pREP3X, *oma4*$^+$:HA under nmt81-promoter, *LEU2*	Willer, 2003
pTW28	pREP3X, *oma1*$^+$:HA under nmt81-promoter, *LEU2*	Willer, 2003
pTW51-1	Expression vector with *oma2*$^+$ and *ura4*$^+$, $Ampicillin^R$	Willer et al, 2005
pREP3-adh	pREP3x with *S.pombe adh1* promoter and HA-tag	Willer *et al.*, 2005
pAU-gms1:CFP	*gms1*$^+$:CFP in pAU-KS+	Iwaki *et al.*, 2006
pDK213	eYFP amplification template: pYM41 backbone (Janke *et al.*, 2004) and mutation A206K	Gift from V. Sourjik
pFR29	Integration plasmid for nmt81-*sup11::ura4*$^+$	Hutzler, 2009
pFR36	Integration plasmid for *sup11*$^+$:HA*::LEU2* in pBS-*car1*$^+$:HA	Hutzler, 2009
pLW55	*sup11*$^+$:HA in pREP3-adh	This study
pLW56	*sup11*$^+$:GFP in pREP3-adh	This study
pLW65	pREP3-adh with *S. pombe act1*$^+$ promoter and HA-tag	This study
pLW78	pLW65 with *sup11*$^+$:*GFP*	This study
pLW83	*gas1*$^+$ SS:gLUC cloned in pLW65	This study
pLW86	*gas1*$^+$ without signal sequence (bp +58 to +1629) cloned in pLW83 to obtain	This study

	Gas1pSS:gLUC:Gas1p	
pLW103	*sup11*$^+$ with BamHI site after signal peptide in pLW65	This study
pLW104	*sup11*$^+$ SS:eYFP: *sup11*$^+$ without signal sequence in pLW103	This study
pLW106	*oma1*$^+$ in pLW65	This study
pLW109	*sup11*$^+$ in pLW65	This study
pLW117	*exg2*$^+$ in pLW65	This study
pLw120	*KRE9* in pENTR/D-TOPO	This study
pLW124	*sup11*$^+$:HA from pLW119 in pAG426-ccdB	This study
pLW140	*sup11*$^+$ L181N mutation in pLW65	This study
pLW141	*sup11*$^+$ P190T mutation in pLW65	This study
pLW142	*sup11*$^+$ I250N mutation in pLW65	This study
pLW143	*sup11*$^+$ with N47Q mutation in pLW65	This study
pLW144	*sup11*$^+$ with N239Q mutation in pLW65	This study
pLW147	*sup11*$^+$ SS:eGFP in pLW65	This study
pLW152	*gas2*$^+$ in CloneJET	This study
pLW153	*gas2:Dis::LEU2* in pLW152	This study

4.1.10. Strains

4.1.10.1. Strain construction

Diploid heterozygous *sup11*$^+$/*sup11*Δ (LWY1 and LWY5)

FY527/FY528 diploid wild type was used to create a *sup11*Δ (SPBC11C11.05) mutant. One copy of the *sup11*$^+$gene was deleted via deletion cassette. Homologous recombination between bp -100 to +1 of the promoter region and bp +1 to +125 of the 3'UTR of the genomic *sup11*$^+$ sequence were fused by PCR (oligoFR833 and oligo884) to the KanMX cassette of pFA6-KanMX6-P81nmt1. Positive transformands were selected on YES plates containing G418. From the positive clones replacement of the *sup11*$^+$ gene was verified by PCR using the oligopair 886 and 311. Integrants at the right locus (LWY1) were sporulated on SPO plates and used for tetrad dissection.

A heterozygous diploid *sup11*Δ strain commercial available from Bioneer (Daejeon, South Korea) was selected for sporulation competency (LWY5) and also sporulated on SPO plates for tetrad selection.

Sup11:roGFP2 (LWY12)

For genomic C-terminal tagging of *sup11*$^{+}$ with the redox sensitive roGFP2, the fluorochrome was amplified with oligos 1805/1806 (*Xho*I/*Sal*I adapter) from pRS416FLAG4-promoter-ro2-C-term (gift from Andreas Meyer, University of Bonn) and cloned via *Xho*I/*Sal*I into pLW109 to obtain pLW133. roGFP + KanMX cassette PCR fragment (3390bp) was then amplified from pLW133 with oligos 1820/1821 for genomic integration and transformed in FY527. Correct integration was verified by PCR with oligopair 311/1337 and 1806/1789 for the knock-in and 1340/1337 for the wild type allele.

nmt81-*sup11*/*exg1*Δ (LWY9), nmt81-*sup11*/*exg2*Δ (LWY10) and nmt81-*sup11*/*exg1*Δ /*exg2*Δ (LWY11)

To create double-mutants of exoglucanase *exg1*$^{+}$ and *exg2*$^{+}$ with nmt81-*sup11* and a triple-mutant the exoglucanase mutant strains LE2, LE4 and LE48 (gift from Carlos Vázquez de Aldana, University of Salamanca) were transformed with the nmt81-*sup11* recombination cassette from the pFR29 *Not*I fragment to insert the nmt81-promoter in front of *sup11*$^{+}$ (Hutzler, 2009). The obtained strains were named LWY9, LWY10 and LWY11 respectively.

nmt81-*sup11*/*gas2*Δ (LWY16)

A nmt81-*sup11/gas2*Δ double-mutant was created by transformation of a 3445bp disruption fragment released from pLW153 via *Bgl*II digestion. The nmt81-*sup11*/*gas2*Δ:*LEU2* mutant was named LWY16.

4.1.10.2. Table of strains used in this study

Bacterial strains:

strain	**genotype**	**reference**
DH5α	*F -*, λ *-, endA1, hsdR17(rK - ,mK+), supE44, thi-1, recA1, gyrA96, relA1, deoR,* Φ *80dlacZΔM15*	Hanahan, 1983
Origami	*Δ(ara-leu)7697 ΔlacX74 ΔphoA Pvu*II *phoR araD139 ahpC galE galK rpsL* F′[*lac*$^{+}$ *lacI*^{q} *pro] gor522*::Tn*10 trxB* (Kan^{R}, Str^{R}, Tet^{R})	Novagen

Yeast strains:

strain	**genotype**	**reference**
BY4741	*MATa; his3Δ1; leu2Δ0; met15Δ0; ura3Δ0;*	Euroscarf
CFY3	*MAT*a *ade2-1 his3-Δ200 leu2-3,112 trp1-Δ901 ura3-52 suc2-Δ9 pmt1*::*HIS3 pmt4*::*TRP1*	Girrbach and Strahl, 2003
FY527	h^- , *his3*-Δ1, *leu1*-32, *ura4*-Δ18, *ade6*-M216$^+$	Forsburg lab
FY528	h^+, his3-Δ1, leu1-32, *ura4*-Δ18, *ade6*-M210$^+$	Forsburg lab
FY527/FY528	h^-/h^+, *his3*-Δ1, *leu1*-32, *ura4*-Δ18, *ade6*-M216$^+$/*ade6*-M210$^+$ (diploid wild type)	Forsburg lab
SBY89	Isogenic to FY528 except *oma4::hisG*	Willer *et al.*, 2005
SBY91	Isogenic to FY528 except *oma1::hisG*	Willer *et al.*, 2005
TWY12	Isogenic to TWY11 except *oma2*$^+$/*oma2*::*his3*$^+$	Willer *et al.*, 2005
TWY16	pTW51-1 isogenic to FY527 except nmt81-*oma2*$^+$	Willer *et al.*, 2005
YMMR16	h-, *leu1*-32, *gas2*Δ::kanMX4	Gift from Carlos Vàzquez de Aldana
SP519	h-, GFP-*bgs1* his3-Δ1	Gift from Carlos Vàzquez de Aldana
SO2412	h+, Anp1-mCherry:*ura4*$^+$, *leu1*-32, *ura4*- Δ18, *ade6*-M216$^+$,	Gift from Aleksandar Vjestica
LE2	h-, *ura4*-Δ18 *exg1*Δ::KanMX4	Dueñas-Santero *et al.*, 2010
LE4	h-, *ura4*-Δ18 *exg2*Δ::KanMX4	Dueñas-Santero *et al.*, 2010
LE48	h?, *ura4*-Δ18, *exg1*Δ::KanMX2; *exg2*Δ::KanMX4	Dueñas-Santero *et al.*, 2010
JFY421	*oma1::his3*, nmt81-*oma2*+*LEU2*, nmt81-*oma4*+KanMX	Fabian, 2009
FRY11	Isogenic to FY528 except nmt81-*sup11*::*ura4*$^+$	Hutzler *et al.*, 2009
FRY12	Isogenic to FYR13 except nmt81-*sup11*::*ura4*$^+$	Hutzler *et al.*, 2009

FRY13	Isogenic to FY528 except *sup11*$^{+}$: HA*::Leu2*	Hutzler *et al.*, 2009
FRY40	Isogen zu SBY91 außer *sup11*$^{+}$:: pFR36 (pBS*sup11*$^{+}$:HA), zur Integration geschnitten mit NdeI	Hutzler *et al.*, 2009
FRY41	Isogen zu SBY89 außer *sup11*$^{+}$:: pFR36 (pBS*sup11*$^{+}$:HA), zur Integration geschnitten mit *Nde*I	Hutzler et al., 2009
FRY42	Isogen zu TWY16 außer *sup11*$^{+}$:: pFR36 (pBS*sup11*$^{+}$:HA), zur Integration geschnitten mit *Nde*I	Hutzler *et al.*, 2009
LWY1	Isogenic to FY527/FY528 except *sup11*$^{+}$/*sup11*Δ::KanMX	This study
LWY5	*leu1*-32, *ura4*-Δ18, *ade6*-M210/h90, *leu1*-32, *ura4*-Δ18, *ade6*-M210, *sup11*Δ::KanMX	Bioneer, (Daejeon, South Korea)
LWY9	Isogenic to LE2 except nmt81-*sup11::ura4*$^{+}$	This study
LWY10	Isogenic to LE4 except nmt81-*sup11::ura4*$^{+}$	This study
LWY11	Isogenic to LE48 except nmt81-*sup11::ura4*$^{+}$	This study
LWY12	Isogenic to FY527 except *sup11*$^{+}$:roGFP2::KanMX	This study
LWY16	Isotgenic to FRY11 except *gas2*Δ:*LEU2*	This study
LWY13	h?, Anp1p:mCherry:*ura4*+, *leu1-32*, *ura4*-Δ18, Sup11p:roGFP2:KanMX	This study

4.1.11. Table of oligonucleotides

Name	**Sequence**
M13fw	GTAAAACGACGGCCAGT
M13rev	CAGGAAACAGCTATGAC
311	GGCAGTGTTCCTGCGCCGGT
FR883	CAAATAAGGTGTTTCGATATACATCCCTGTTGTCAGAGCAACGATTTATATATATCGCTTACC ACTAAATTTGCAAAGTCTCTTCAAGCCGTCGAATTTA CTGTTTAGCTTGCCTCGT
884	AAAGGAAGCAGACAAAAATGCACACAGTAATATCCTAGTGTGCTAATGAAAAATCTAAATG ACATGAAAGGCTTTGGCCTTAAAAAAAATTAACAATTTA CGTTTAAACTGGATGGCG
886	GACGAACGACTCAATGTA
995	ATTTAATTAAGATTTAACAAAGCGACTATA
1257	AGAAGCGGCCGCATGAAAACCACCATGTTGATGCTAGTATTGC
1258	AGAACTCGAGGGAATATAACAACCCACGTTTGTGTTCACC

1208	CTAGGATCCCGAGATTGGTATCTATCTCAAACTAC
1209	GTTCTCGAGTTAGGAATATAACAACCCACGTT
1210	TTACTCGAGTTAATAAGAGGAAGTTTCCCATAGC
1211	CTAGGATCCTACATGTATACGTTGTATGCTAATTATG
1303	CGGGTCGACTAAGCAGCGT
1320	CAGCTTGAATGGGCTTCCATAGT
1337	CTGGCATAGCACTGTCATCACACA
1340	GCTGGACCCTTCGCTATTTCTCA
1433	ATATGCGGCCGCGGTCTTGTCTTTTGAGGGTTTT
1434	ATATCTGCAGACCTTCTCTGCCTGTAAGTGATC
1625	CTAGAAGTTCTCCTCGACAAGC
1627	ACGGATCCATTCGATTCGTCACTCCG
1628	CTAGCAGTACTGGCAAGGG
1631	ACGGATCCATGGTGAGCAAGGGCG
1632	ACGGATCCCTTGTACAGCTCGTCCATG
1673	ATATGCGGCCGCATGAGCAATCTTTTAGAAGCTG
1674	ATATCTCGAGAAATTCAGATTGCTCGTCAAAC
1679	ATATGCGGCCGCATGCGTTTACAAAGAAATTCCATC
1681	AATCGTCGACTCATACTTTTCTCATGTTGATTTTCCTTG
1710	CACCATGCGTTTACAAAGAAATTCCATC
1780	TAGCGGCCGCATGGTGAGCAAGGGCGAGGA
1781	TACTCGAGTTAAAGCTCATCAGCCTTGTACAGCTCGTCCATGCCG
1789	AACCCGGGATGAAAACCACCATGTTGATGC
1805	ATAACTCGAGATGGTGAGCAAGGGCGAGGA
1806	AATCGTCGACTTACTTGTACAGCTCGTCCATGCCG
1820	GCCTCTAAGCCTACTATAATCGCAACTC
1821	CAGACAAAAATGCACACAGTAATATCCTAGTGTGCTAATGAAAAATCTAAATGACATGAAA GGCTTTGGCCTGGATGGCGGCGTTAG
1889	CTACCGGTGTTAACCGTACAGGACC
1890	GGTCCTGTACGGTTAACACCGGTAG
1891	ATTCAAAATCGAACAGATTCTACTTTTACTG

1892	CAGTAAAAGTAGAATCTGTTCGATTTTGAAT
1893	GCCTACTATAAACGCAACTCCAACTGC
1894	GCAGTTGGAGTTGCGTTTATAGTAGGC
1907	TGGGAAGAATCTCAAACGGGAATACC
1908	GGTATTCCCGTTTGAGATTCTTCCCA
1909	GTTGTATGCTCAATATGCTAGTACGGC
1910	GCCGTACTAGCATATTGAGCATACAAC
1912	ATAGCGGCCGCAATACAAGACTGCACAAGGTTGAG
1933	ATA ATGGTCTCCTTTACCAAATTTACTTTG
1934	ATA TTATGCCTTAAGCTCACCAAC

Oligonucleotides for qPCR

Name	**Description**	**Sequence**
1159	*act1*$^+$ qPCR fw	CCAAATCCAACCGTGAGAAGATGA
1160	*act1*$^+$ qPCR rev	CACCATCACCAGAGTCCAAGACGA
1439	*ace2*$^+$ qPCR rev	GCGATCTACGCCGCCAACAC
1440	*ace2*$^+$ qPCR fw	GCTTATATTGCGGCCCTGAAGC
1637	*sup11*$^+$ qPCR fw	CGACTGTCTTTGCATCTCCAAC
1638	*sup11*$^+$ qPCR rev	TAACAACCCACGTTTGTGTTCAC
1777	*cdc18*$^+$ qPCR rev	GCTGTAATGACATCCATTTCTGG
1778	*cdc18*$^+$ qPCR fw	TTGTGTCTTCGAGATCGTTTGA

4.2. Methods

4.2.1. Growth conditions

4.2.1.1. *Escherichia coli* strains

E. coli cells were grown in LB/LB-Amp (100 μg/ml) over night in air shaker of on agar plate in incubator at constant temperature at 37°C.
Cultures for GST-fusion expression were grown and induced at 18°C.

4.2.1.2. *Saccharomyces cerevisiae* strains

S. cerevisiae strains were cultured in appropriate medium over night in air shaker or on agar plates in the incubator for several days at 30°C.
Cell density of the liquid cultures was determined photometric via optical density at 600 nm (OD_{600}).

4.2.1.3. *Schizosaccharomyces pombe* strains

S. pombe strains were cultured in appropriate medium over night in air shaker or on agar plates in the incubator for several days at 32°C.
To induce temperature sensitivity the strains were cultured at 35°C or 37°C.
Cell density of the liquid cultures was determined photometric via optical density at 600 nm (OD_{600}).

4.2.1.4. Preparation of permanent cultures

In liquid media freshly grown cultures were harvested and used for permanent cultures. Cells were resuspended in appropriate medium containing approximately 40% glycerine, shock frozen in liquid nitrogen and stored at -80°C

4.2.2. Molecular biological methods

4.2.2.1. Plasmid-DNA isolation from *E. coli*

Plasmid isolation from *E. coli* was carried out according to a method described by Holmes and Quigley (Holmes and Quigley, 1981), or by GeneJET Plasmid Miniprep Kit (Thermo Fischer).

4.2.2.2. Isolation of gDNA form *S. pombe* and *S. cerevisiae*

gDNA preparation for PCR amplifications were carried out according to the method published by Philippsen (Philippsen *et al.*, 1991).
Therefore, 40-50 OD cells were harvested, resuspended in 200 µl resuspension buffer plus 200 µl phenol: chloroform: isoamylalcohol (25:24:1) and 0.3 g glass beads. Cells were broken using the Ribolyser (3-6x for 30 sec). 200 µl ddH_2O was added and centrifuged 5 min at 3000 rpm. Top phase was collected and DNA alcohol precipitated by adding 1 ml 100% Ethanol. DNA was pelleted by centrifugation (10 min, 20000 g, 4°C) and washed once with 70% Ethanol. Pellet was then resuspended in 100 µl ddH_2O/RNase (0.1 µg/ml).

4.2.2.3. Determination of DNA concentration

DNA concentration was measured via NanoDrop.

4.2.2.4. Gel electrophoresis for nucleotide separation

DNA-fragments were separated according to (Sambrook and Russel, 2001). DNA ladders GeneRuler DNA Ladder Mix from Thermo Fischer was used as standard.

4.2.2.5. Elution of DNA-fragments form agarose gels

DNA was eluted using the GeneJET Gel Extraction Kit (Thermo Fischer) as described in the protocol.

4.2.2.6. DNA modification via restriction nucleases

Cutting DNA with restriction nucleases was carried out as described in (Sambrook and Russel, 2001). Additional instructions by the manufactor (Thermo Fischer, NEB) were followed.

4.2.2.7. Modifying DNA ends

To remove overlapping single strands to obtain blunt-ends the nucleic acids were removed by T4 DNA-Polymerase (Thermo Fischer) as described by the manufactor. Dephosporylation was achieved by treatment with alkaline phosphatase (Thermo Fischer) as described in the manual.

4.2.2.8. Ligation of DNA-fragments

Ligation of DNA-fragments was carried out according Sambrook (Sambrook and Russel, 2001). Ligation was done at room temperature for 2 h.

4.2.2.9. Polymerase chain reaction (PCR)

Amplification of specific DNA-fragments via PCR was done with Phusion High-Fidelity DNA Polymerase (Thermo Fischer) as described in the manual. PCRs form gDNA to verify knockouts were performed using DreamTaq (Thermo Fischer) according to the manufactor instructions.

4.2.2.10. RNA extraction and first strand complementary DNA (cDNA) synthesis

RNA was extracted with Quiagen RNeasy Midi Kit for transcriptome analysis. For qPCR RNA was isolated with Quiagen RNeasy Mini Kit. cDNA synthesis was done from 2 µg total RNA with RevertAid H Minus First Strand cDNA Synthese Kit according to the manufactor protocol.

4.2.2.11. Quantitative PCR (qPCR)

Each qPCR reaction contained 0.2 µg cDNA, 0.5 mM of the each specific primer in diluted 2x Maxima SYBR Green/ROX qPCR Master Mix (Fermentas). qPCR was done

with RotorGene 2000 (Corbett Research). Relative transcript amounts were compared with the ΔΔCT method (Livak and Schmittgen, 2001).

4.2.2.12. Transformation of *E. coli*

100 µl chemical competent E. coli cells were thawn on ice and 10 µl of the ligation was added and incubated for 30 min on ice. Cells were heat shocked for 75 sec at 42°C and put on ice immediately. 1 ml LB was added and transformation was shaked for 1 hour (h) at 37°C. Cells were pelleted and plated on appropriate selection plates and incubated over night at 37°C.

4.2.2.13. Chemical transformation of *S. pombe* and *S. cerevisiae*

For yeast cell transformation with plasmid DNA was carried out to the slightly modified protocol "Long protocol for fission yeast transformation" as described in (Forsburg and Rhind, 2006). The amount of transformed DNA was 1 µg for plasmids and 5 µg for PCR or liberalized vector DNA for homologous recombination. Transformation reaction was performed without DMSO and heat shock was prolonged to 15 min at 42°C.

4.2.3. Microscopic Methods

4.2.3.1. Aniline blue staining (β-1,3-glucan staining)

For aniline blue staining 1 ml cells of an exponentially growing culture were collected by centrifugation and washed 3 x with sterile ddH_2O. Cells were pelleted again and resuspended in 30 µl ddH_2O. 5 µl of cell solution was mixed with 2 µl aniline blue sock solution (0.1 mg/ml aniline blue in sterile ddH_2O) and analysed under the microscope.

4.2.3.2. Fluorescence microscopy

For Fluorescence microscopy a Leica DM IBR equipped for Nomarski optics and epifluorescence and photographed with a Leica DFC 350 FX monochrome camera. Cells were stained with aniline blue (Fluka, #95290). Time laps experiments were carried out on Nikon Total Internal Reflection Fluorescence (TIRF) on Ti inverted microscope with Nikon Perfect Focus System with an Andor Clara high-resolution sensitive black and white camera. Confocal images were taken on Perkin Elmer spinning disc confocal ERS-FRET on Nikon TE2000 inverted microscope with Hamamatsu EM-CCD camera.

4.2.3.3. Immunogold electron microscopy

Electron microscopic pictures of indirect immunogold labelling with silver enhancement was carried out by Matthias Sipiczki (Department of Genetics, University of Debrecen).

Used antibodies against β-1,3-glucan were a gift from Howard Bussey (McGill University Canada) and antibodies against β-1,6-glucan were a gift from Frans Klis (University of Amsterdam, The Netherlands).

4.2.3.4. Methanol fixation and immunofluorescence labeling

Methanol fixation of cells was done with 5 OD of logarithmically growing cultures of FY527**,** FRY13 and transformed FY527 carrying either pREP3-adh or pLW55. Harvested cells were resuspended in 1 ml methanol (-20°C) and additional 9 ml were added. Cells were incubated for 15 min at -20°C and pelleted by centrifugation at 6000 rpm for 2 min. Pellet was resuspended in 1ml PEM-buffer and washed 3 x with 1 ml of the same buffer.

Fluorescent labeling of the cells was done in 850 µl PEM-buffer with 100 µl of a 1 mg/ml stock solution of Lysing Enzymes (Sigma) and 50 µl of a 1 mg/ml stock solution Lyticase (Sigma). Cell wall digestion was monitored on microscope in 5 min intervals. When 60% of the cells were digested the samples were kept on ice. Cells were washed 3 x with PEM-buffer and permeablized for 30 sec adding 1 ml 1% Triton-X-100 in PEM-buffer. Blocking was done by incubation in 1 ml PEMBAL-buffer for 30 min at room temperature on horizontal shaker and subsequent washing with PEM-buffer for 3 x. Decoration was done either with anti-HA antibody or anti-α-tubulin antibody (gift from Carlos Vasquez de Aldana) in 30 µl of an 1:100 dilution in PEMBAL-buffer at room temperature for 16 h on shaker. After washing 3 x with PEM-buffer cells were incubated in 100 µl of 1:400 dilution of anti-mouse Alexafluor488 coupled secondary antibody for 1 h in the dark. Cells were resuspended in 100 µl PEMBAL-buffer and used for fluorescent microscopy.

4.2.3.5. FACS analysis with DAPI stained cells

For DAPI staining, *S. pombe "*ghost cells" were prepared as described in (Carlson *et al.*, 1997). 10 OD ghost cells were DAPI stained by incubation in 1 µg/ml DAPI for 10 min at room temperature in the dark. Cells were washed 3 x in distilled water and kept in the dark at 4°C. FACS measurements were performed with BD FACSAria using 405 nm laser excitation.

Nitrogen starved cells as 1C control were prepared as followed: a pre-culture was grown in EMM with low nitrogen (0.5 mg/ml NH_4Cl) to exponential phase. The culture was harvested and washed three times with EMM-N (minimal medium lacking nitrogen) and resuspended at 1.5x 10^6 cells/ml (0.1 OD) in EMM-N. The culture was grown overnight (16 h) to starvation and cells were harvested.

For 2C control cells exponentially growing culture was used. For 4C cells were harvested from exponentially growing diploids.

4.2.4. Biochemical methods

4.2.4.1. Membrane preparation from *S. pombe*

Yeast cells were grown over night to OD_{600} <1. Harvested cells (3 min at 3000 g) were washed twice with ddH2O and once with Membrane buffer. 20 OD cells were resuspended in 100 µl membrane buffer plus proteinase inhibitors (Pi) and broken up in Ribolyzer (speed 4.5, 30 sec, 3-6 x). After microscopic control of the disruption efficiency the Eppendorf cup was punctured and cells were centrifuged in another cup. Cell walls were pelleted 5 min at 3000 rpm and supernatant was collected in extra tube. Walls were washed in membrane buffer + Pi and supernatant was collected in same tube. Membranes were collected from supernatant by centrifugation at 100.000 g for 30 min. Pellet was resuspended in 100 µl same buffer and centrifuged again. Pellet then was resuspended in membrane buffer + Pi to a concentration of 0.1 OD cells/µl and shock frozen in liquid nitrogen and stored at -80°C.

4.2.4.2. Spheroblasting of *S. pombe*

Cells were grown overnight to logarithmic phase and 300 OD_{600} cells were harvested. Cells were washed 3 x with spheroblasting buffer. For spheroblasting cells were resuspended in 3 ml spheroblasting buffer + 25 µg Lysing Enzymes (Sigma, L1412) and 10 mg Lyticase (Sigma, L2524) and incubated for 3 h at 32°C. Spheroblasts were overlayed on sucrose-ficoll-cushion and centrifuged at 4°C, 3000 rcf for 15 min. The pellet with the Spheroblasts was resuspended in spheroblast lysis buffer. Cells were broken in up by using a dounce homogenizer. The homogenate was overlayed on sucrose-cushion, centrifuged at 3200 rcf for 5 min at 4°C. Microsomes were collected on top of the cushion and used for proteinase K protection assay.

4.2.4.3. Proteinase K protection assay

Microsomes were divided into Eppendorf cups. Aliquots were treated with different combinations of proteinase K (250 µg/ml), 1% (w/v) Triton-X-100 and incubated for 0-120 min on ice. Reaction was stopped by addition of 5mM PMSF and 5 mM EGTA. Microsomes were harvested in ultracentrifuge at 100.000 rcf for 30 min at 4°C, resuspended in lysis buffer (10 OD_{600}/µl) and analysed by Western blot.

4.2.4.4. SDS-PAGE

SDS-PAGE was done as described by Laemmli (Laemmli, 1970).

4.2.4.5. Western blot

Western blot was carried out according to Dunn (Dunn, 1986).

4.2.4.6. EndoH treatment

Proteins were fractionated by SDS-PAGE and transferred to nitrocellulose. Anti-HA (16B12, Babco) and anti-IgG (Sigma Aldrich) antibodies were used at 1:5.000 dilutions in TBS containing 0.05% Tween20 and 4% dry milk powder. Protein antibody complexes were visualized by detection reagent (Amersham). Deglycosylation was performed with EndoH (NEB) for 1 h at 37 °C under denaturing conditions.
For comparison of equal loading the polyclonal kin1-antibody (Cadou *et al.*, 2010) was used.

4.2.4.7. Ratiometric measurements with roGFP2

Analysis was performed as described by Braun and co-workers (Braun *et al.*, 2010). Measurements were carried out with 20 OD cells each.

4.2.4.8. Mass Spectrometry

Tandem mass spectra were extracted by OrbitrapXL. The data sets were analyzed by Mascot (version 2.2.04). Mascot was set up to search the SwissProt_2012_04 database (selected for *Schizosaccharomyces pombe*) assuming the digestion enzyme trypsin. Mascot was searched with a fragment ion mass tolerance of 0.50 Da and a parent ion tolerance of 100 PPM. Iodoacetamide derivative of cysteine was specified in Mascot as a fixed modification. Deamidation of asparagine and glutamine, oxidation of methionine and biotinylation of lysine were specified in Mascot as variable modifications.
Scaffold (version Scaffold_3.4.9, Proteome Software Inc., Portland, OR) was used to validate MS/MS based peptide and protein identifications. Peptide identifications were accepted if they could be established at greater than 95% probability as specified by the Peptide Prophet algorithm (Keller *et al.*, 2002). Protein identifications were accepted if they could be established at greater than 99% probability and contained at least 2 identified peptides.

4.2.4.9. PAS-Silver staining

Carried out as described by Dubray and Bezard (Dubray and Bezard, 1982).

4.2.4.10. Cell wall biotinylation

Protocol was followed as described by Mrsă and co-workers (Mrsă *et al.*, 1997) till the SDS extraction. Cell walls were twice SDS extracted and washed four times in the 50 mM K-phosphate buffer pH 8.0 and then twice in distilled water. Remaining cell wall proteins were divided into four equal aliquots and remaining cell wall proteins extracted by either 30 mM NaOH overnight at 4°C or by enzymatic digestion. Lysing Enzymes (Sigma, L1412) were used 1 mg per sample, or Lyticase (Sigma, L2524) 1 mg per sample (= 200U), or thermostable β-glucanase1 (G8548, Sigma Aldrich) 1 µl per

100 OD (= 2U) for 2 h at 37°C shaking. After glucanase treatment the supernatant was collected by spinning down the cell walls for 3 min at 10.000 rpm.
Electrophoresis, blotting and detection were carried out as described in (Mrsă *et al.*, 1997).

4.2.4.11. Antigen purification

GST-fusion proteins were purified using the automated purification system Profinia (Bio-Rad) and Glutathione Sepharose 4B beads according to the manufactros instructions.

4.2.4.12. Affinity purification of polyclonal antibodies raised against GST-fusion peptides of Sup11p

Antigen specific antibodies were enriched by affinity purification with the respective antigen. 100 µg protein of the purified antigens used for immunizations were separated on SDS-PAGE and blotted on Nitrocellulose membrane. GST-fusion antigens were cut from gel and used for subsequent affinity purification of the crude antisera. Membrane pieces were blocked for 30 min blocking buffer and incubated over night at 4°C with a 1:5 dilution of antisera and blocking buffer on horizontal shaker. The serum/ blocking buffer mixture was extracted by pipetting and stored at 4°C for second purification. Decorated antigens on the membrane were washed 3 x for 20 min in TBST and once in ddH_2O. Antibodies were stripped from membrane by pH shift incubating the membrane pieces in 500 µl glycine buffer pH 2.8 on ice for 2-3 min shaking. Eluate was collected in pre-cooled 2 ml Eppendorf cup containing 50 µl 1 M Tris/HCl pH 8.5 for neutralization plus 10 µl of 10% BSA solution. Purification was repeated with same antiserum/ blocking buffer mixture using 500 µl glycine buffer pH 2.2. Elution fractions were kept separately and used for Western blot decoration.

4.2.4.13. Microarray hybridization and data analysis

For Microarray analysis the Affymetrix GeneChip Yeast Genome 2.0 Array (Affymetrix) was used. RNA was prepared according to Qiagen RNeasy Midi Kit form a total of 25 OD yeast cells. Quality of RNA was confirmed by chip-based capillary electrophoresis machine (Bioanalyzer, Aligent). A 5 µg aliquot of total RNA was used as starting material for cDNA synthesis. cRNA production, and fragmentation were performed as described in the Expression Analysis Technical Manual (Affymetrix). The GeneChip Arrays were hybridized, stained, washed, and screened according to the manufacturer's protocol at the Unidad de Genómica of the Universidad Complutense de Madrid (http://www.ucm.es/info/gyp/genomica/) (Madrid, Spain).
For each strain three biological replicates were analyzed. Each one consisting of pools of three independent cultures. Compared were samples of nmt81-*sup11* under repressed and non-repressed conditions. As control for thiamine induced transcriptional changes samples of thiamine and non-thiamine treated wild types were analysed as well.

Genes were considered as differentially regulated if $P < 0.01$ and the ratio compared with the non-repressed controls was >2.0 or <0.5. Also genes regulated due to thiamine treatment were excluded from further analysis. Clustering of the affected genes into biological process or cellular compartment was done with Genecodis online tool (http://genecodis.cnb.csic.es/).

5. Results

The so far uncharacterized *Sp*Sup11p shares homologue features with the baker's yeast Kre9-family. Members *Sc*Kre9 and *Sc*Knh1 are encoding for *O*-glycoproteins, which are involved in β-1,6-glucan synthesis in baker's yeast (Dijkgraaf *et al.*, 1996; Nagahashi *et al.*, 1998).

5.1. In silico *analysis*

Detailed *in silico* analysis of the homologue proteins - *Sp*Sup11p and *Sc*Kre9/ *Sc*Knh1 - showed that these proteins share certain features. All of them contain an N-terminal signal sequence and a C-terminal, so called Kre9-domain. The highest degree of aa sequence conservation between the *Sp*Sup11p and *Sc*Kre9 proteins is found inside this domain (Fig. 5.1). A protein blast of *Sc*Kre9 and *Sp*Sup11p Kre9-domains revealed that the two regions share 29% identical and 54% similar aa. The Kre9-region contains some S/T-rich stretch between aa 198-254 (Fig. 5.1, highlighted orange (at least 29% S/T content in a window size of 21aa) and pink (43% S/T content in a window size of 21aa)) which are prone to be modified by the *O*-mannosylation machinery. Beyond their common features, *Sc*Kre9 and *Sp*Sup11p differ in at least one significant criterion: other than *Sp*Sup11p, *Sc*Kre9 is a soluble protein and most likely secreted or cell wall associated (Brown and Bussey, 1993). *Sp*Sup11p, however, is predicted to be an integral membrane protein with one to three putative transmembrane domains (TMD), depending on which prediction program is applied. TMpred (Hofmann and Stoffel, 1993) and TopPred (von Heijne, 1992; Claros and Heijne, 1994) predict three TMDs, DAS (Cserzö *et al.*, 1997) and TMHMM (Krogh *et al.*, 2001) only one TMD. The topology model suggested by SOSUI (Hirokawa *et al.*, 1998) predicts none of these TMDs. Instead, an anchorage via signal anchor sequence by non-cleavage of the N-terminal signal sequence is suggested (Fig. 5.1).

Due to the ambiguous *in silico* topology models, the correct topology of Sup11p remained to be elucidated and was experimentally characterized as described in chapter 15.1.

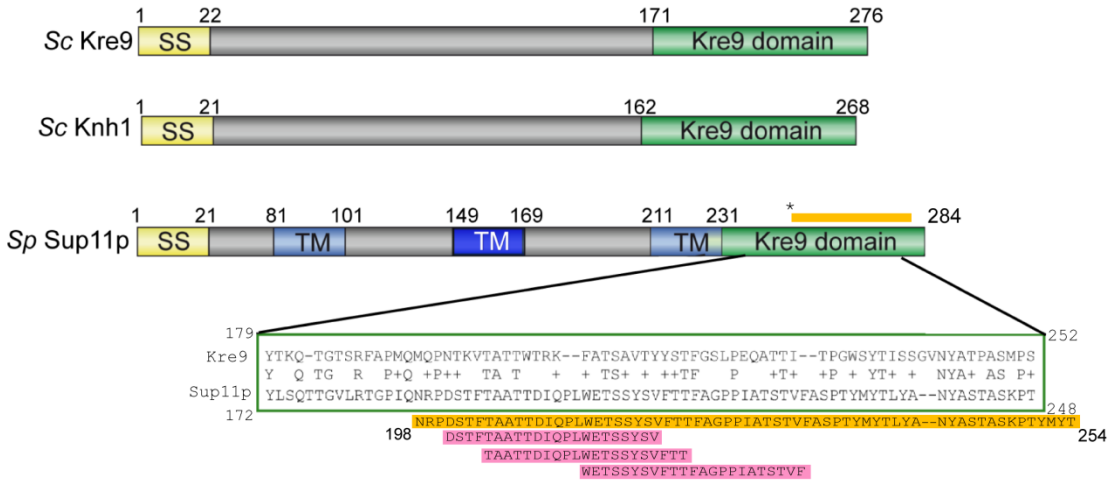

Fig. 5.1: *In silico* model of *Sc*Knh1 and *Sc*Kre9 compared to *Sp*Sup11p:
Predicted protein features of ScKnh1, *Sc*Kre9 and *Sp*Sup11p are an N-terminal signal sequence (SS) and a C-terminal so called Kre9-domain which contains the most conserved region of those two proteins. aa sequence homology of the Kre9-domain of *Sc*Kre9 and *Sp*Sup11p is depicted in the green box. The orange bar indicates S/T-rich stretch in Kre9-domain of *Sp*Sup11p (window size of 21 aa; at least 29% S/T content). The pink bars indicate S/T-rich stretches of at least 43% S/T content in a window size of 21 aa.
Primary sequence of *Sp*Sup11p suggests 1 to 3 TM spans. Most probable TMD (suggested by 4 out of 5 prediction models) is depicted in dark blue (TM). Numbers indicate aa positions of the various features.

Clustering Kre9-family proteins of various yeast organisms using the online tool ClustalW2 (Larkin *et al.*, 2007) showed that there is a high conservation of certain aa in the Kre9-domain over different species (Fig. 5.2). Particularly most of the S/T and some of the prolines are highly conserved in that aa sequence. Prolines exhibit helix breaking properties and therefore have a strong influence on the secondary structure of a protein. The conservation of specific S/T could indicate key positions for correct protein *O*-mannosylation processing inside the Kre9-domain.

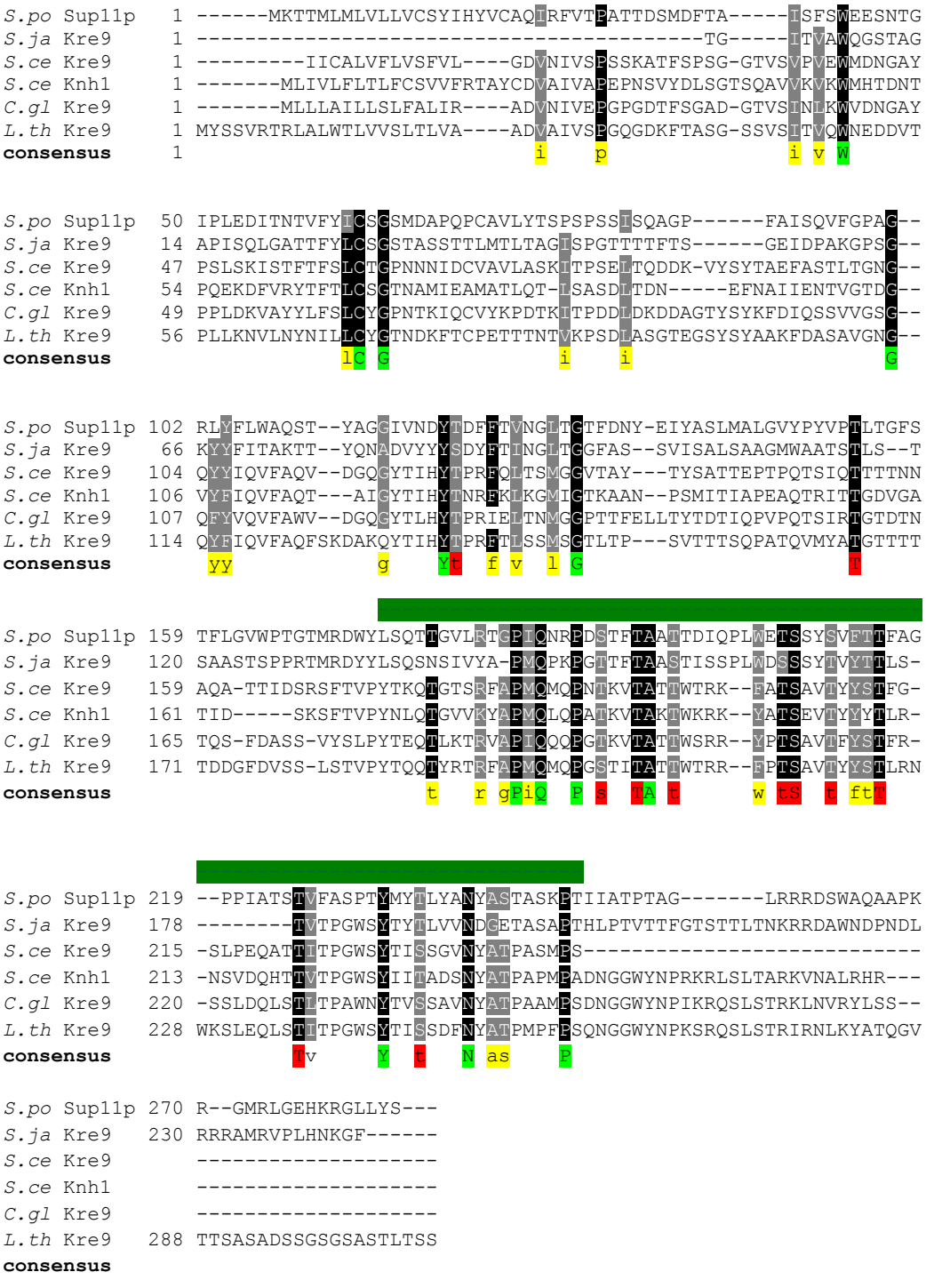

Fig. 5.2: Protein blast of Kre9-family proteins in various yeasts compared to *Sp*Sup11p:
Kre9-family proteins of various yeast species (*S. po = Schizosaccharomyces pombe, S. ja = Schizosaccharomyces japonicus, S. ce = Saccharomyces cerevisiae, C. gl = Candida glabrata, L. th = Lachancea thermotolerans*) were blasted and clustered using the online tool ClustalW2 (Larkin *et al.*, 2007). The Kre9-domain region is indicated by the dark green bar. Identical aa are indicated in green and 80% conserved aa are depicted in yellow in the consensus. Positions where either a serine or threonine is conserved are depicted in red.

5.2. The sup11$^+$ *gene is essential for cell viability.*

In order to study the role of Sup11p, a *sup11*$^+$ deletion mutant ought to be created in two different strain backgrounds (FY527/FY528 and SP286). A diploid had been created in the FY527/FY528 background in which one copy of *sup11*$^+$ gene was replaced by a KanMX4 cassette. Next, the heterozygous diploid *sup11Δ:*KanMX4/*sup11*$^+$ mutant was sporulated and tetrad analysis yielded in only 50% colony forming spores (Fig. 5.3 A). Tetrad analysis of the heterozygous *sup11Δ:*KanMX4/*sup11*$^+$ in a different strain background (SP286; diploid heterozygous *sup11Δ:*KanMX4/*sup11*$^+$ strain purchased from Bioneer, Daejeon, South Korea) gave the same result in terms of spore viability.

All of the viable colonies were tested sensitive towards Gentamycin (G418) indicating that the target gene has not been disrupted by homologous recombination in the colony forming cells. Subsequent PCR analysis demonstrated that all colony forming clones bear an intact copy of the *sup11*$^+$ gene. Microscopic analysis of the non-colony forming spores revealed that roughly 25% of them were able to actually germinate and undergo few cell divisions. However, the cells showed an aberrant roundish morphology and formed cell clumps (Fig. 5.3 B). This observation pointed towards a cell separation defect which leads to growth arrest. The terminal phenotype of the *sup11*-null mutant could not be rescued by addition of an osmotic stabilizer (1 M sorbitol) to the germination medium.

This showed that *sup11*$^+$ is an essential gene and hinted to a role of Sup11p during cell wall formation.

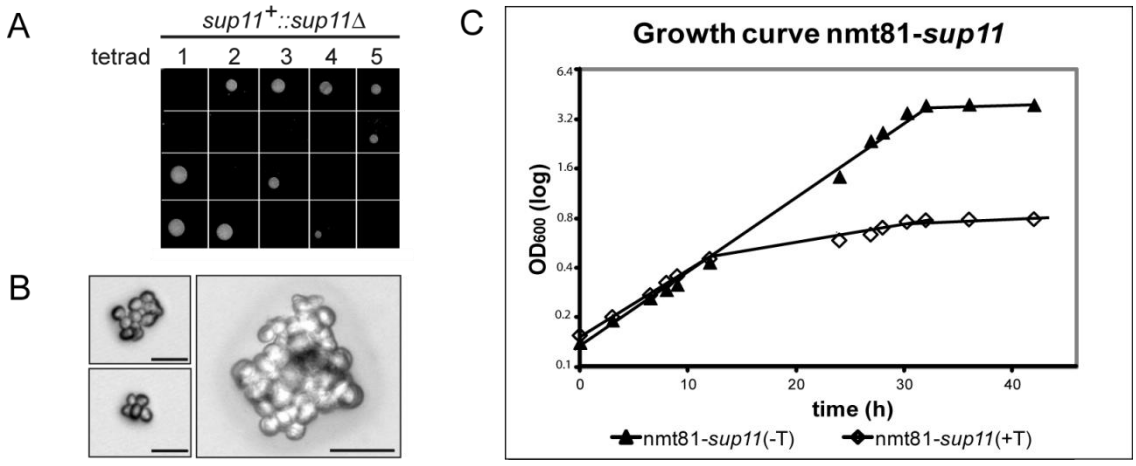

Fig. 5.3: *sup11*$^+$ is an essential gene:
(A) Tetrad dissection of five diploid heterozygous *sup11Δ:*KanMX4/*sup11*$^+$ tetrads in a FY527/FY528 background showed 50% viability. (B) Three of the non-colony forming spores underwent few division cycles before they arrest in growth and forming aberrant cell clusters. (scale bar = 20 nm) (C) A growth assay with a repressible nmt81-*sup11* mutant showed exponential growth under permissive conditions (- thiamine). Under restricted conditions (+ thiamine) the nmt81-*sup11* mutant went into growth arrest after 12 h of repression. Duplication time under permissive conditions is 195 min. In the first 12 h upon restriction the doubling time is 228 min; between 24-32 h it is 465 min and further decreasing. (n = 3)

To further test lethality of *sup11*Δ, a plasmid-shuffling experiment was performed using a vector-stabilized haploid *sup11*Δ*:*KanMX4 mutant. To create this strain, the above described heterozygous diploid *sup11Δ:*KanMX4/*sup11*$^+$ mutant (FY527/FY528 background) was transformed with a plasmid which contained an intact copy of *Spsup11*$^+$ plus *ura4*$^+$selection marker. The cells were then sporulated, and spores selected for the *ura4*$^+$ marker. Afterwards, the surviving cells were transformed with a second plasmid containing the *LEU2* gene and, either the coding sequence of *Spsup11*$^+$ under the control of a constitutive *adh1*-promoter, or the empty vector. Counter selection was performed by applying 5-fluoroorotic acid (5-FOA) treatment, which selects against the *ura4*$^+$ marker. Cells with a functional *ura4*$^+$ gene product are converting 5-FOA to 5-fluoruracil which is toxic to them (Boeke *et al.*, 1987). In order to stay viable on plates containing the drug 5-FOA, the cells need to lose the *ura4*$^+$ plasmid with the wild type *Spsup11*$^+$ copy.

This experiment revealed that only the *sup11*Δ mutant with an episomal copy of *Spsup11*$^+$ was viable, confirming that *sup11*$^+$ is essential (Fig. 5.4).

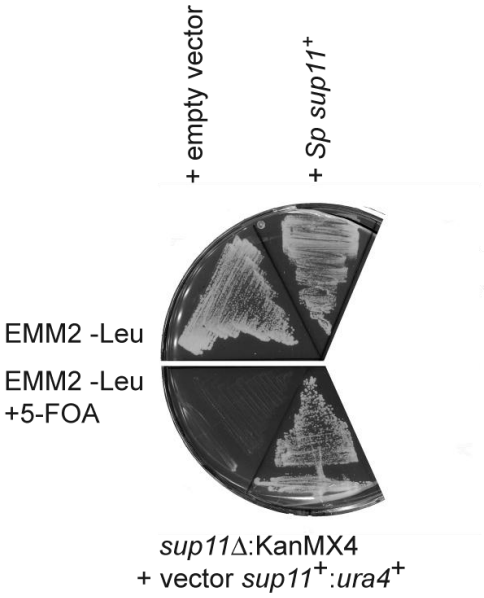

Fig. 5.4: Sup11p is essential:
The plasmid shuffling experiment was performed with plasmid-stabilized *sup11*Δ strain. The stabilizing plasmid contains the *ura4*$^+$ selection marker. Cells were transformed with an additional plasmid containing an episomal copy of *sup11*$^+$ or the empty vector with *LEU2* selection marker (upper panel). In order to survive 5-FOA selection the cells are forced to lose the stabilizing copy of *sup11*$^+$ on the *ura4*$^+$ containing vector. *sup11*Δ cells without episomal copy of *sup11*$^+$ were lethal (lower panel).

Due to lethality of a *sup11*Δ mutant, a conditional repressible nmt81-*sup11* mutant (Hutzler, 2009) was used for further characterization studies. In this mutant the *sup11*$^+$ gene is controlled by the thiamine repressible nmt81-promoter. Preliminary analysis of the nmt81-*sup11* mutant grown under restrictive conditions for 48h indicated a septum malformation phenotype (Hutzler, 2009).

This study showed that the duplication time of the nmt81-*sup11* mutant under restricted conditions (+ thiamine; 228 min), is comparable to the growth of the culture grown under permissive conditions (- thiamine; 195 min) in the first 12 hours (h). Continuous restriction of the *sup11*$^+$ gene increased duplication time and eventually causes growth arrest (duplication time 21 h 40 min between 24-42 h after restriction) while the non-restricted culture continued to grow exponentially to stationary phase (Fig. 5.3 C). However, despite arresting in growth, the nmt81-*sup11* culture stayed viable as analyzed by aniline blue staining, which is also a vital dye. That at least a fraction of the culture remained viable was showed since after ~75 h the culture started to grow again (data not shown). This might be due to some compensatory mechanism which is triggered after extended Sup11p depletion in order to rescue the growth arrest. Or it is also possible that single cells accumulated mutations in the *sup11*$^+$-regulating nmt81-promoter that restores expression of *sup11*$^+$ and allows growth.

5.3. Sup11p is required for correct septum formation

In order to analyze the essential role of Sup11p, the Sup11p deficient mutant nmt81-*sup11* was characterized in detail.

It was reported that the nmt81-pormoter has a minimal residual activity under restrictive conditions (Siam *et al.*, 2004). This allowed the expressing of at least a minimal amount of *sup11*$^{+}$ under all conditions tested. Transcript of *sup11*$^{+}$ was detected after 16 h of restriction using quantitative RT-PCR (qPCR) (Fig. 5.21 A). However, it was shown by Western blot analysis of a genomically *sup11*$^{+}$:HA tagged strain (nmt81-*sup11*:HA) that the Sup11p:HA level drops below the detection limit within 6 h after growth under restrictive conditions (Fig. 5.5 A). Moreover, an additional analysis showed that the protein levels of the nmt81-pormoter expressed Sup11p:HA was significantly lower compared to the endogenously expressed in the wild type (Fig. 5.5 A). However, microscopic analysis of the nmt81-*sup11* mutant under permissive conditions showed no visible phenotype compared to wild type (Fig. 5.6 B), indicating that the reduced level of Sup11p expressed by the permissive nmt81-promoter is sufficient to allow maintain wild type-like morphology.

Taken together, the restricted nmt81-*sup11* mutant has to be considered as a knock-down mutant. Although no Sup11p:HA was detectable under restrictive conditions, the limited nmt81-promoter activity of led to a growth arrest but allowed to culture to remain viable.

Analysis of the nmt81-*sup11* mutant demonstrated a decreased thermo-tolerance. Incubation of the nmt81-*sup11* strain at 37°C causes significant growth delay compared to the wild type (Fig. 5.5 B).

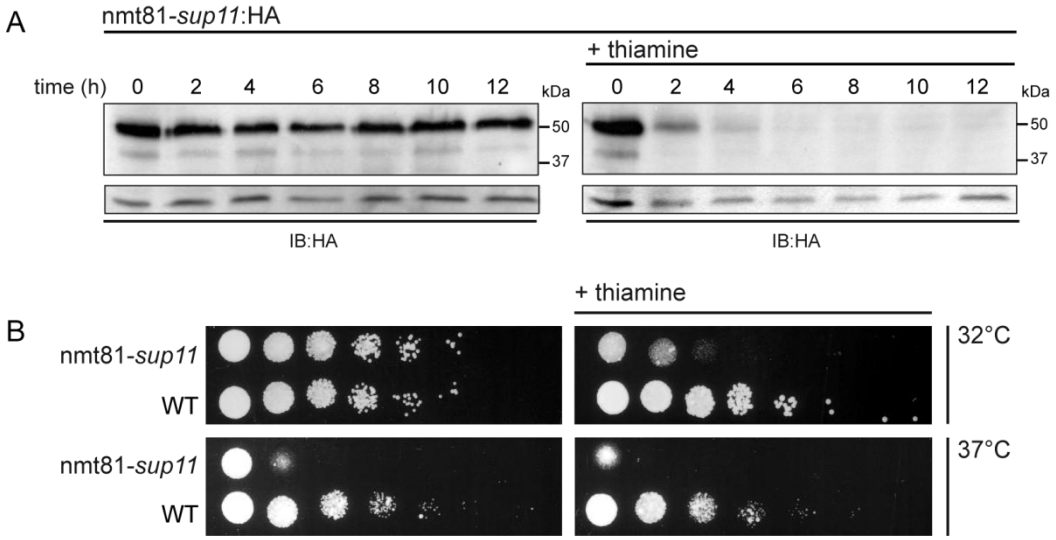

Fig. 5.5: Unnatural Sup11p levels under nmt81-promoter control leads to temperature sensitivity: (A) Western blot analysis detecting Sup11p:HA (upper panel) under permissive and restrictive (+ thiamine) conditions. Lower panel shows unspecific protein which serves as a loading control. Sup11p:HA was detected by decoration with monoclonal anti-HA antibody (1:5000) and anti-mouse IgG peroxidase conjugate (1:5000). (B) Spotting assay testing nmt81-*sup11* for temperature sensitivity demonstrated that restricted as well as permissive conditions caused growth deficiencies compared to the wild type.

Interestingly, temperature sensitivity was not only problematic for the nmt81-*sup11* mutant under restricted but also under permissive conditions under which *sup11*$^{+}$ is already depleted due to the nmt81-promoter control (see Fig. 5.11 A). Adverse effects of diminished Sup11p levels were not detectable under standard growth conditions.

Detailed phenotypic analysis of the nmt81-*sup11* mutant revealed a wild type-like morphology of the permissive mutant. Restricted nmt81-*sup11* cells were smaller in size and more roundish, pointing towards a cell wall defect (Fig. 5.6 B). Furthermore, Sup11p depletion causes the cells to form cell clusters. These cell accumulations could not be separated by sonification and a fraction of roughly 15% of the nmt81-*sup11* mutant cells were prone to cell-lysis during the separation process (Fig. 5.6 B (arrows)). These data showed that the diminished Sup11p level under permissive conditions is sufficient to prevent the morphological phenotype observed upon restriction. Moreover, microscopic examination of the restricted nmt81-*sup11* showed a defective septum and a less elongated cell shape.

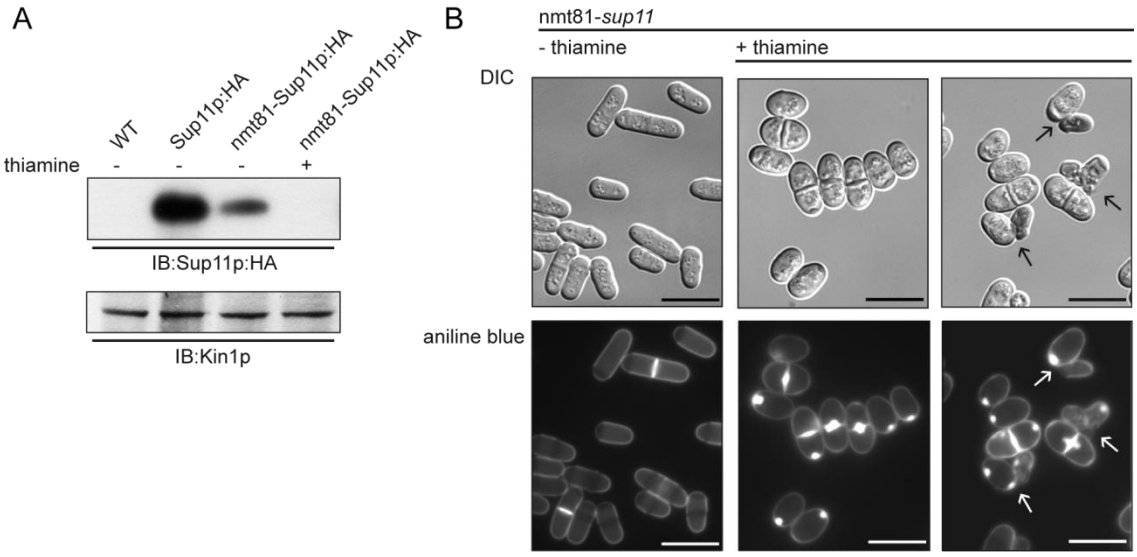

Fig. 5.6: Expression levels of Sup11p under the control of the endogenous and nmt81-promoter and morphological phenotype of nmt81-*sup11* mutant:
(A) Western blot analysis was used to compare protein levels of genomically tagged Sup11p:HA under the control of endogenous and restricted and permissive nmt81-promoter. 0.1 OD of total membrane preparations were loaded of each sample and Kin1p was analyzed as loading control. Sup11p:HA was detected by decoration with monoclonal anti-HA antibody (1:5000) and anti-mouse IgG peroxidase conjugate (1:5000). Kin1p was decorated with polyclonal anti-Kin1p antibody (1:3000) and anti-Rabbit IgG peroxidase conjugate (1:5000). (B) Microscopic analysis of the nmt81-*sup11* mutant under permissive (- thiamine) and restricted (+ thiamine; 16 h) conditions. Upper panel shows differential interference contrast (DIC) and in the lower panel the cells were stained with aniline blue and excited with ultraviolet. Aniline blue is a dye which stains the linear β-1,3-glucan of the primary septum appearing in a yellow-green color in violet light (Kippert and Lloyd, 1995). Arrows indicate pairs of cells of which at least one is dead. (scale bar = 10 µm).

Staining of linear β-1,3-glucan by aniline blue showed a severe malformation of the septum with massive accumulation of cell wall material at the center of the septum in cells lacking Sup11p (Fig. 5.7 B).

Detailed microscopic analysis revealed that these accumulations emerge in the late phase of septum assembly during septum closure. Sectional scanning through the dividing cell from top to bottom clearly showed that the depositions accumulate in the center of the septum whereas the peripheral area at the septum/ cell wall junction remains thin (Fig 5.7). This suggests that the septum material accumulation started after or during septum closure.

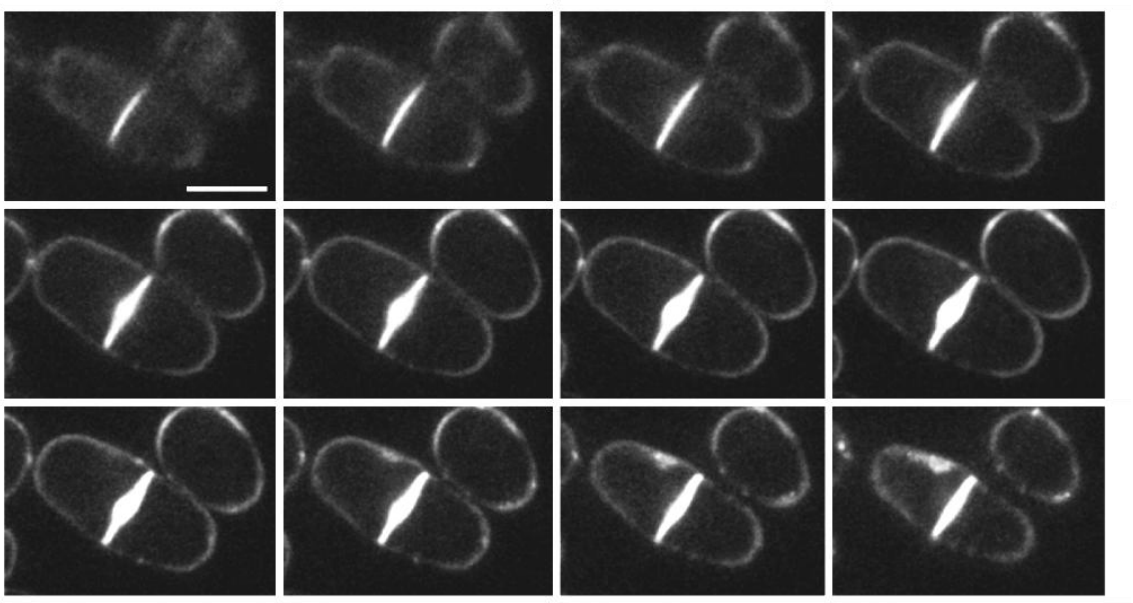

Fig. 5.7: Confocal microscopy sectioning of the septum phenotype of a restricted nmt81-*sup11* mutant:
Restricted nmt81-*sup11* cells were aniline blue stained and analysed by confocal microscopy. Septum morphology was scanned from the top to the bottom of the cell. (scale bar = 5µm)

Time laps experiments of separating nmt81-*sup11* were performed to follow cytokinesis from the onset of primary septum formation until the division into two daughter cells. Monitoring the septum formation of the restricted nmt81-*sup11* mutant showed that the assembly starts normal with a defined ring of aniline stainable primary septum. Upon septum closure more cell wall material accumulated at the septum center forming large depositions which were entirely sensitive to aniline blue staining whereas the septum periphery continued to be defined and slim (Fig. 5.8). After extended time for septum assembly and separation of approximately 90 min (~20 min in wild type) some of the cells complete cytokinesis regardless of their severe septum deformation. However, it was observed that at least one of the two arising daughter cells was likely to lyse during separation (Fig. 5.8 (arrows)). In case of one daughter cell survived the separation process the accumulated cell wall material remained at its new end (Fig. 5.8 (filled arrowhead)).

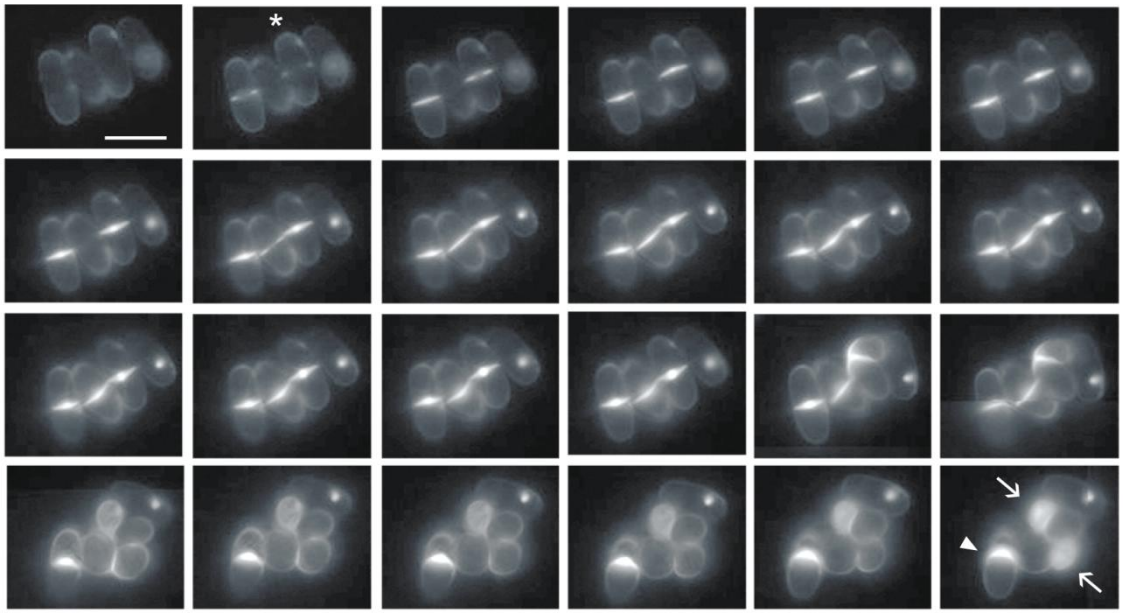

Fig. 5.8: Time lapse experiment monitoring the septum formation in restricted nmt81-*sup11* mutant:
Restricted nmt81-*sup11*cells were aniline blue stained and observed over a period of 96 min under physiological conditions. Septum formation from the actomyosin ring assembly to cell separation was monitored (following the cell indicated by asterisk). Depositions at pole are indicated by filled arrowhead. Dead cells appear stained brightly by vital dye aniline blue and indicated by arrows. Pictures were taken every 4min (scale bar = 10 µm)

Further analysis showed that gradual *sup11*$^{+}$ repression yielded in a culture with the majority of living cells having cell wall depositions at one pole. Due to repeated assembly and separation of deformed septa it would be theoretically possible that cells accumulate depositions at both poles. However, nearly none of the cells exhibited more than one pole deposition. This suggests that the depositions might contribute to the observed growth arrest (Fig. 5.8 C).

5.4. Depletion of Sup11p changes β-glucan partitioning in the septum and the lateral cell wall

Due to the severe septum deformation, it was intriguing to elucidate which kind of cell wall material builds up these massive depositions. In the wild type fission yeast, the septum is constituted of a three layered structure. The middle layer is composed of linear β-1,3-glucan which is exclusively present in the primary septum (Humbel *et al.*, 2001). To analyze the septum composition, EM images were taken of non-depleted and depleted nmt81-*sup11* mutant cells which were labeled with an antibody directed

against linear β-1,3-glucan. The indirect immunogold EM analysis revealed that the antibody labeled not only the primary septum region in the *sup11*$^{+}$ depleted cells, but interacted with the whole septum including the accumulated cell wall material (Fig. 5.9). Moreover, specific gold labeling was also observed at the lateral cell wall of nmt81-*sup11* mutant, suggesting general wall matrix alterations rather than a mere septum malformation.

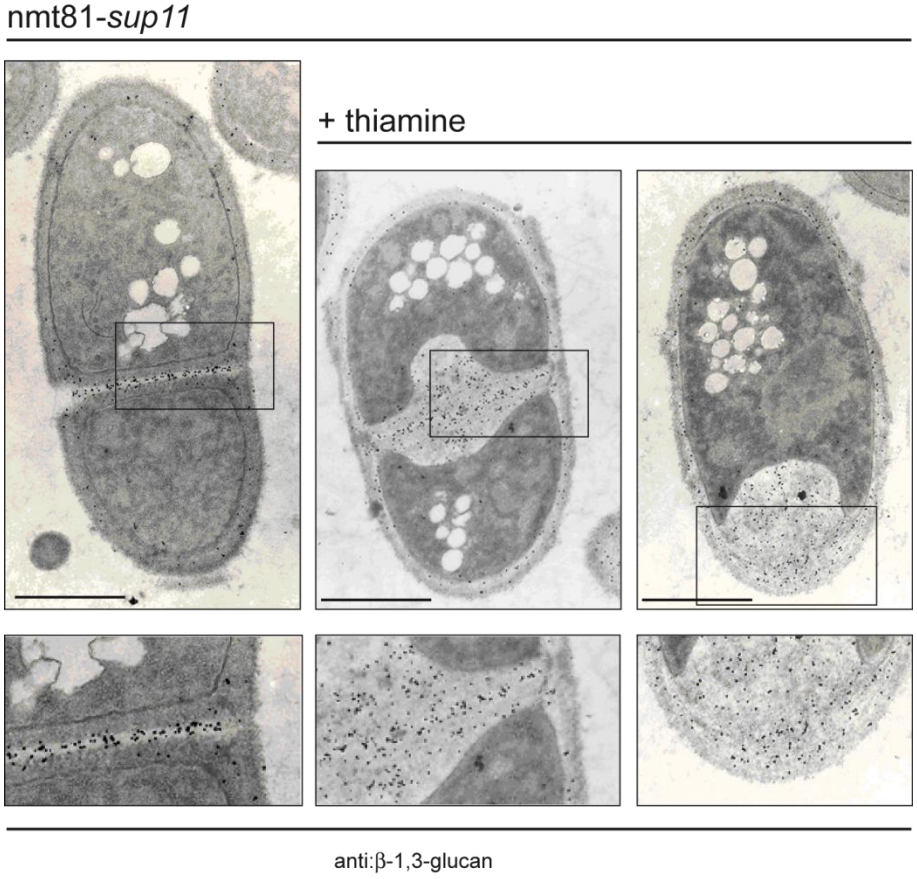

Fig. 5.9: Electron microscopic (EM) images of immunogold labeling of primary septum linear β-1,3-glucan:
Cells of the nmt81-*sup11* mutant under permissive and restricted conditions (over night) were used for indirect immunogold labeling. EM pictures were taken from cells which were decorated with gold particle coupled antibody directed against linear β-1,3-glucan. Antibody binding is depicted as black dots and condensed in the septum and pole region. EM was made by collaborating group of Matthias Sipiczki, University of Debrecen. (scale bar = 3 µm)

5.5. Variation in cell wall protein composition of the nmt81-sup11 mutant

Further cell wall abnormalities of the restricted nmt81-*sup11* strain were demonstrated by performing a biotinylation assay of cell wall proteins. For this assay cell wall

proteins were biotinylated on their free primary amides, like the N-terminus and lysine residues. The biotinylation reagent cannot cross the PM and enter the cell. Therefore, only proteins present in the extracellular space are accessible for biotin labeling. Subsequent release of the labeled cell wall proteins was done by SDS-extraction, using a buffer containing 2% SDS and 5% β-mercapthoethanol to break disulfide bonds and to release non-covalently bound proteins from the cell wall matrix. Extract analysis via Western blot revealed a striking difference between permissive and restricted nmt81-*sup11* mutant. In the SDS-extract one abundant protein of roughly 150 kDa was detected in the restricted nmt81-*sup11* mutant via Western blot (Fig. 5.10 A, filled arrowhead). This protein was hardly detectable in SDS-extracts prepared from nmt81-*sup11* mutant grown under permissive conditions. Further analysis using PAS-silver staining suggested that the prominent protein is a glycoprotein (Fig. 5.10 A, gel on the right). *N*-glycosylation of the prominent protein was demonstrated by deglycosylation with Endoglycosidase H (EndoH). EndoH is a recombinant glycosidase that cleaves oligosaccharides from *N*-linked glycoproteins and is used for removal of high mannose *N*-glycans from glycoproteins.

Applying EndoH treatment to the SDS-extracts reduces the apparent molecular weight of the prominent protein from ~150 kDa to two lower molecular weight products of ~78 and ~51 kDa (Fig. 5.10 B).

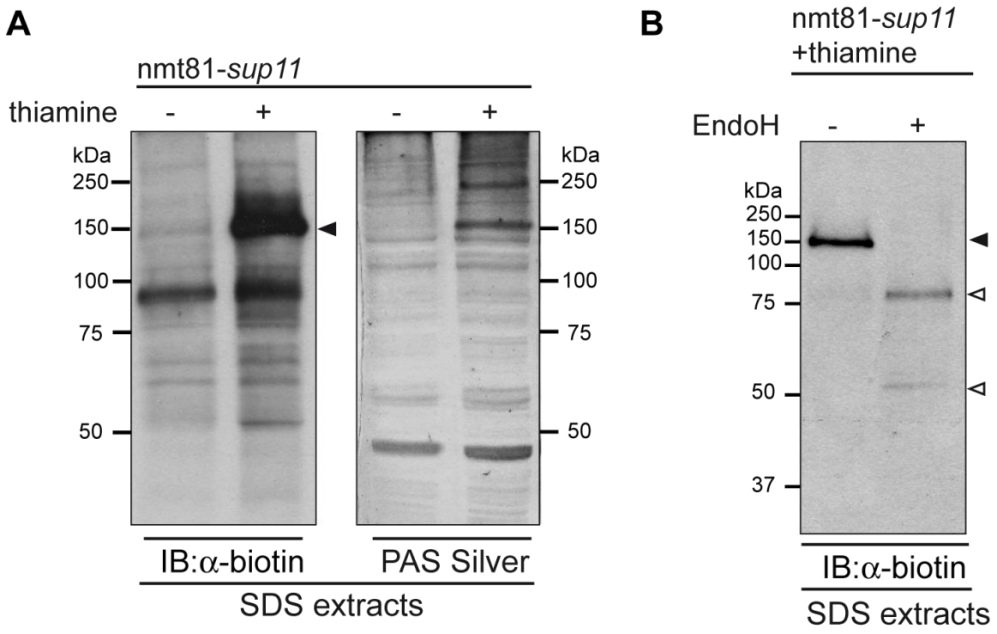

Fig. 5.10: Analysis of non-covalently bound cell wall proteins of nmt81-*sup11* mutant:
(A) Cell wall proteins of the nmt81-*sup11* under permissive and restricted conditions (16 h) were biotinylated on their primary amides. Non-covalently bound proteins were extracted via SDS. These

extracts were compared by Western blot analysis detecting biotinylated proteins with streptavidin coupled HRP (1:5000). One prominent protein of roughly 150 kDa was detected in the restricted nmt81-*sup11* mutant (filled arrowhead) which is absent under permissive conditions. A protein of this size was also stainable by PAS silver staining that specifically stains glycoproteins. (B) EndoH treatment of the SDS-extracts showed that the prominent protein (filled arrowhead) can be deglycosylated to two lower molecular weight products of about 78 and 51 kDa (blank arrowheads). Mock treated extracts served as control.

Mass spectrometry identified two candidates for the abundant proteins: Gas2p and Plb1p (Supplementary data, Table 1). Both proteins sequences contain *N*-glycosylation sites. Gas2p has 15 sequons of which five are predicted to be *N*-glycosylated (Gupta *et al.*, 2004). Without *N*-glycosylation Gas2p has a calculated molecular weight of 50.6kDa which corresponds to the smaller EndoH digestion product (Fig. 18 B). The molecular weight of Plb1p a phospholipase B homolog (14 sequons of which 4 are predicted to be used) (Gupta *et al.*, 2004), without modification is ~67 kDa which is slightly less than the larger EndoH digestion product (Fig. 17 B). However, from both proteins only Gas2p is supposed to get secreted to the cell wall since Plb1p was localized in a genome wide study to reside in the nucleus and the cytosol (Matsuyama *et al.*, 2006). For that reason Plb1p ought not be biotinylated and give no Western signal. Whether the larger digestion product is due to incomplete EndoH digestion of Gas2p or due to another glycoprotein running at 150 kDa cannot be excluded from the Western blot analysis. Therefore, Gas2p is promoted to be the real candidate.

Gas2p shows β-1,3-glucanosyl transferase activity that elongates β-1,3-glucan chains in a two-step reaction and was first described by de Medina-Redondo and co-workers (2010). Gas2p acts during septum formation. It localizes to the part of the cell wall that surrounds the septum in early stages of septum formation. After complete septum assembly, Gas2p was shown to be associated with the entire septum (de Medina-Redondo *et al.*, 2010).

To further clarify the identity of the prominent biotinylated protein of ~150 kDa a double-mutant nmt81-*sup11/gas2*Δ strain was generated and characterized. Comparison of the SDS-extracts prepared from the nmt81-*sup11* and nmt81-*sup11/gas2*Δ strains grown under permissive and restrictive conditions supported the mass spectrometry data which suggested Gas2p. No increase of a biotinylated ~150 kDa protein of was detected in the nmt81-*sup11/gas2*Δ double-mutant under restricted conditions using Western blot analysis (Fig. 5.11 B). However, the general amount of biotinylated proteins was significantly less in the nmt81-*sup11/gas2*Δ double-mutant compared to the single

nmt81-*sup11* mutant pointing towards additional cell wall alterations (Fig. 5.11 B). Western blot analysis of biotinylated SDS-extracts strongly suggested that the cell walls of both mutants differ also more generally than just in the presence or absence of Gas2p. It appeared like there are either more cell wall proteins in the nmt81-*sup11* single mutant, or that they were more easily extractable from the cell wall using SDS-extraction buffer compared to the nmt81-*sup11/gas2*Δ double-mutant (Fig. 5.11 B).

Microscopically examination and aniline blue staining of nmt81-*sup11/gas2*Δ double-mutant cells revealed that the pronounced septum deposition phenotype which was documented for the restricted nmt81-*sup11* mutant was rescued (Fig. 5.11 A). The morphology of the double-mutant was still - like for the single nmt81-*sup11* mutant - more roundish compared to wild type. Also depositions at the poles were observed in the double-mutant. However, they were less pronounced in the nmt81-*sup11/gas2*Δ than in the single nmt81-*sup11* mutant (Fig. 5.11 A) reflecting a milder phenotype in the double-mutant.

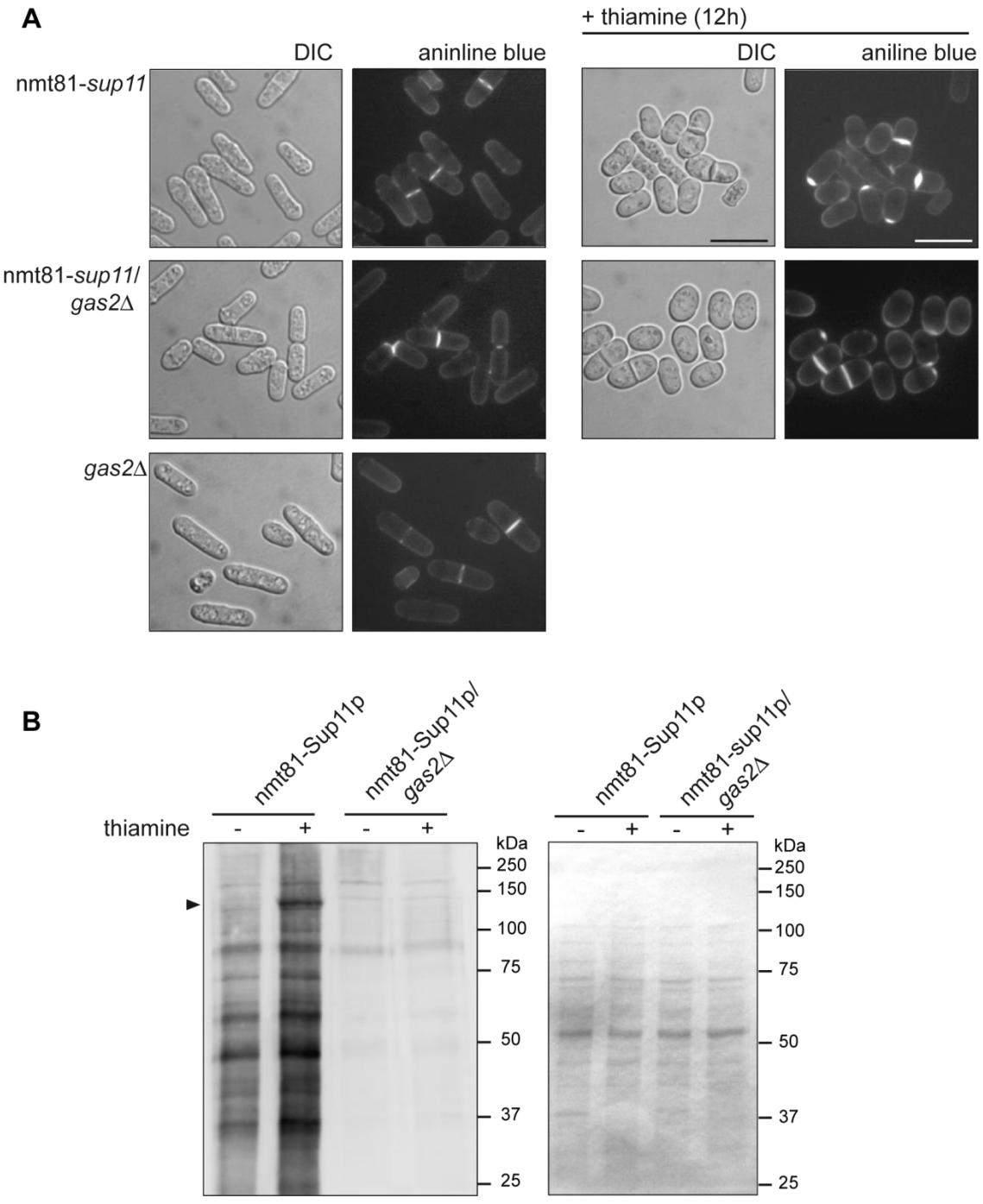

Fig. 5.11: Characterization of the nmt81-*sup11/gas2*Δ double-mutant:
(A) Microscopic analysis of *gas2*Δ, nmt81-*sup11* and nmt81-*sup11*/gas2Δ mutants using differential contrast (DIC). Primary septa were visualized by aniline blue staining. Left panel shows separating cells of exponentially growing cultures. nmt81-*sup11* and nmt81-*sup11*/*gas2*Δ mutants grown under restricted conditions (16 h) are shown in the right panel (+ thiamine). (scale bar = 10 µm) (B) Western blot analysis of biotinylated cell wall proteins obtained by SDS-extraction. Compared were extracts of nmt81-*sup11* and double-mutant nmt81-*sup11/gas2*Δ under permissive and restricted conditions (+/- thiamine). Filled arrowhead indicating Gas2p that is SDS extractable from restricted nmt81-*sup11* cell walls but not in the nmt81-*sup11/gas2*Δ double-mutant (left blot). Equal loading was demonstrated by photo of PonceauS staining (right part).

Additional phenotypic analysis of nmt81-*sup11/gas2*Δ cells revealed that the cells continued to grow exponentially upon *sup11*$^{+}$ restriction (Fig. 5.12 A). Moreover, the pronounced septum deposition of the single nmt81-*sup11* mutant was absent under restricted conditions in the double-mutant. The ratio of cells with normal septum and pole deposition remained without significant changes (Fig. 5.12 B).

Taken together these data strongly suggest that the observed septum phenotype of the restricted nmt81-*sup11* mutant is linked to Gas2p.

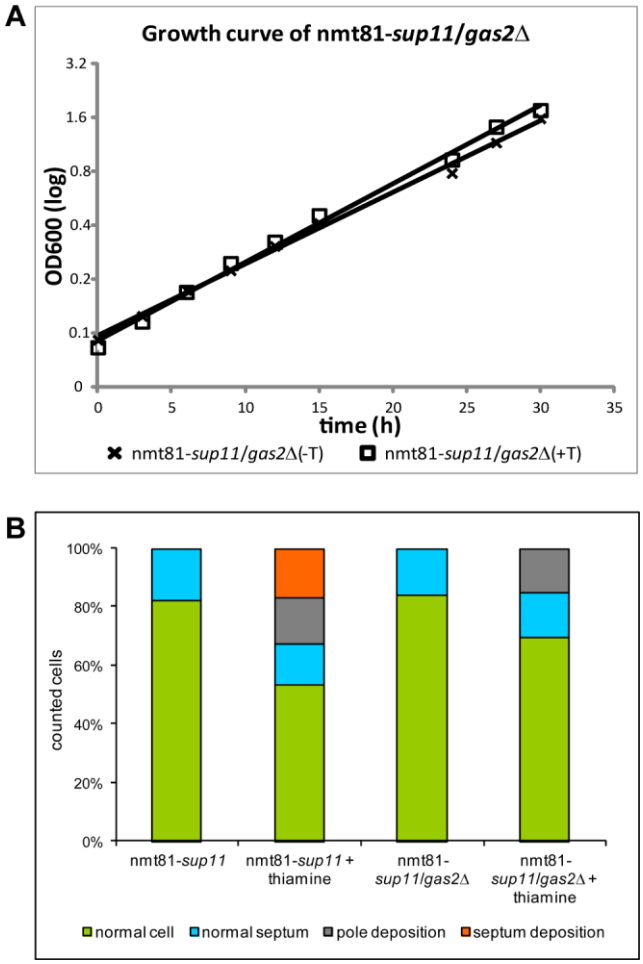

Fig. 5.12: Phenotypic characterization of the nmt81-*sup11/gas2*Δ double-mutant:
(A) Growth curve of the nmt81-*sup11/gas2*Δ double-mutant under permissive and restricted conditions. Duplication time under permissive conditions is 226 min and 206 min under restricted conditions. (n = 3). (B) Septum and pole deposition phenotype of the nmt81-*sup11* and the nmt81-*sup11/gas2*Δ mutant were quantified. Total number of counted cells: nmt81-*sup11* = 354, nmt81-*sup11* + thiamine = 260, nmt81-*sup11/gas2*Δ = 441 and nmt81-*sup11/gas2*Δ + thiamine = 428.

5.6. Sup11p is a key component of the β-1,6-glucan synthesis

Homology of *Sp*Sup11p to *Sc*Kre9 suggested that fission yeast Sup11p might also play a role for β-1,6-glucan synthesis. Although no synthase activity could be demonstrated neither for Kre9 nor any other protein of the Kre-family in *S. cerevisiae*, it was demonstrated that Kre9- and Kre5-mutants have significantly reduced β-1,6-glucan levels (Aimanianda *et al.*, 2009). Therefore, the general β-1,6-glucan content of the nmt81-*sup11* mutant was addressed.

An indirect immunogold labeling experiment with a polyclonal antibody directed against β-1,6-glucan was performed. In contrast to specific binding of the anti β-1,6-glucan antibody to the cell wall of the non-depleted mutant, only unspecific background staining was observed analyzing the depleted nmt81-*sup11* mutant (Fig. 5.13). This data demonstrated the absence of β-1,6-glucan in restricted nmt81-*sup11* mutant cell wall.

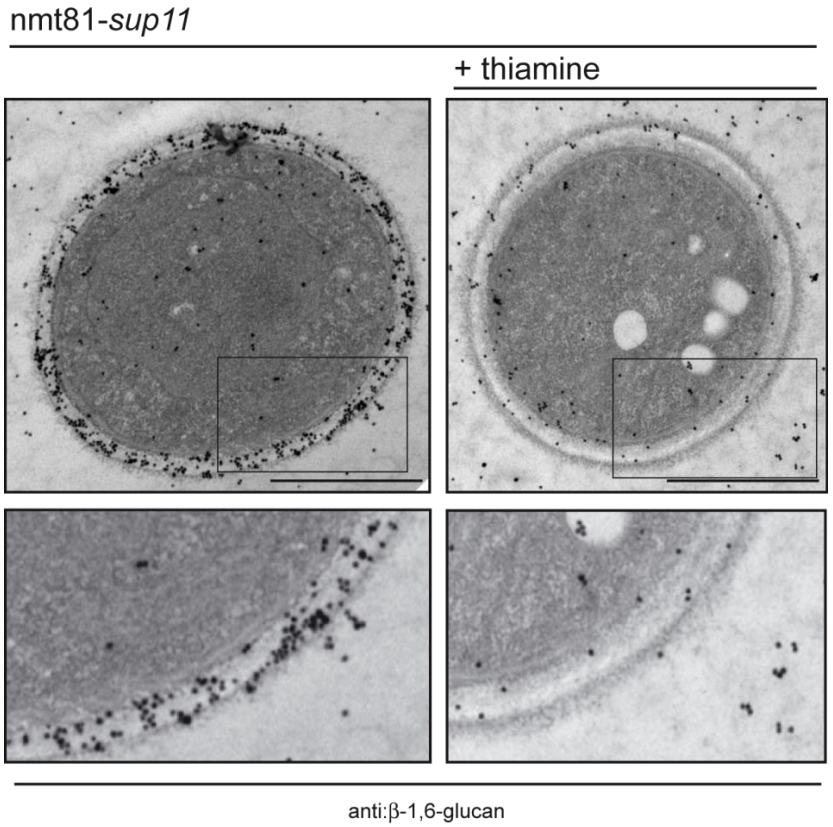

Fig. 5.13: Electron microscopic (EM) images of immunogold labeling of cell wall β-1,6-glucan: Under permissive and restricted conditions (over night) cultured nmt81-*sup11* cells were prepared for EM and decorated with gold particle coupled antibody directed against β-1,6-glucan. Antibody binding is depicted as black dots and condensed specifically at the wall matrix under permissive conditions. Restricted conditions caused only unspecific background staining. EM was made by collaborating group of Matthias Sipiczki, University of Debrecen. (scale bar = 2 µm)

5.7. sup11^{+} *interacts genetically with β-1,6-glucanase family members*

The cell wall matrix is a flexible and highly adaptable construction. Its homeostasis is depending on both, continuous synthesis and degradation of specific components. This includes also the crucial polymer linear β-1,6-glucan. Synthesis of this polysaccharide requires the interplay of several molecules and the data shown above provided evidence for Sup11p being indispensable for β-1,6-glucan formation.

Dueñas-Santero and colleagues (2010) recently described a β-1,6-glucanase family (*exg1*$^{+}$, *exg2*$^{+}$ and *exg3*$^{+}$) and demonstrated β-1,6-glucanase activity for Exg1p and Exg3p. In contrast to the other two members, Exg2p did not show such activity. Instead the authors suggest for the Exg2 protein some sensor function in controlling β-1,6-glucan homeostasis (Duenas-Santero *et al.*, 2010). Interestingly, a similar but less pronounced septum phenotype like observed for the restricted nmt81-*sup11* mutant was reported due to *exg2*$^{+}$ overexpression in wild type. In microscopic analysis, the *exg2*$^{+}$ overexpressing wild type displayed accumulations of cell wall material at the center of the septum and the new poles of the cell (Duenas-Santero *et al.*, 2010).

Here, it was investigated whether the β-1,6-glucanase family members and Sup11p show genetic interactions. First, overexpression of *exg2*$^{+}$ in the nmt81-*sup11* mutant was analyzed. Growth comparison in a spotting assay showed that *exg2*$^{+}$ overexpression improved growth of the restricted nmt81-*sup11* mutant but caused slightly delayed growth under permissive conditions (Fig. 5.14).

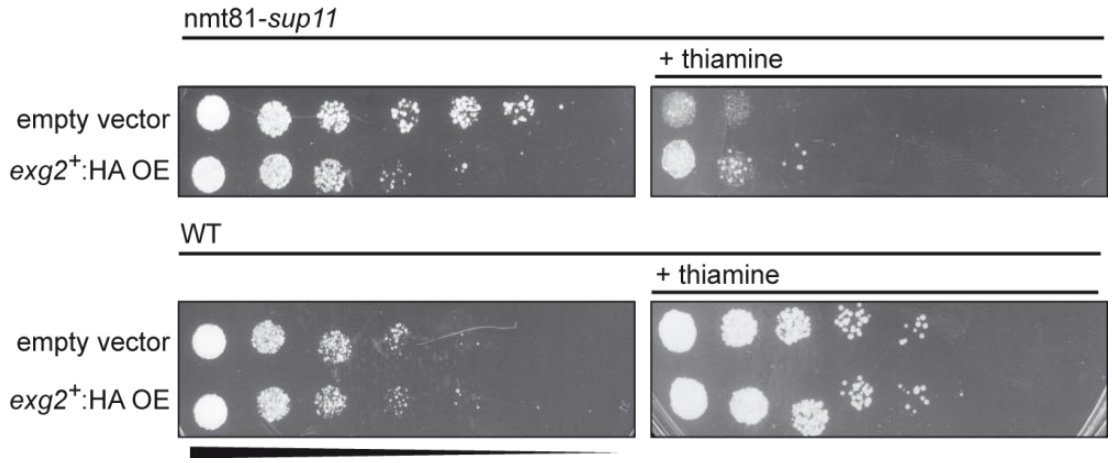

Fig. 5.14: Spotting assay with nmt81-*sup11* mutant overexpressing *exg2*$^{+}$:
Serial dilutions in (1:10) starting from 100.000 cells of permissive and restricted nmt81-*sup11* mutant cells carrying the empty vector or overexpressing *exg2*$^{+}$ from episomal copy under constitutive *act1*$^{+}$-promoter.

Restricted nmt81-*sup11* mutant cells (12 h) which were overexpressing *exg2*$^{+}$ were microscopically examined. Images that were taken with DIC illumination showed fission yeast cells with disturbed morphology (Fig. 5.15). Diverse morphology defects were observed like pear shaped cells, smaller and roundish cells and cells which are bloated in the septum region. The morphological phenotypes were even more pronounced analyzing aniline blue stained cell. Some cells overexpressing e*xg2*$^{+}$ in the restricted nmt81-*sup11* background exhibited cell wall depositions at the poles which contained linear β-1,3-glucan. Moreover, an increased amount of aniline blue stainable material was incorporated into the septum region (Fig. 5.15). In contrast to the improved growth of the *exg2*$^{+}$ overexpressing nmt81-*sup11* mutant cells, a phenotypic amplification of the individual septum phenotypes of the nmt81-*sup11* mutant and *exg2*$^{+}$ overexpressing cells was microscopically observed. The improved growth of the nmt81-*sup11* mutant *exg2*$^{+}$ overexpressing might be due to a compensatory process. A rescue mechanism might be triggered when a too many defects accumulate and a certain threshold is reached. A similar mechanism was reported for a *S. cerevisiae ccw12*Δ mutant (Hagen *et al.*, 2004).

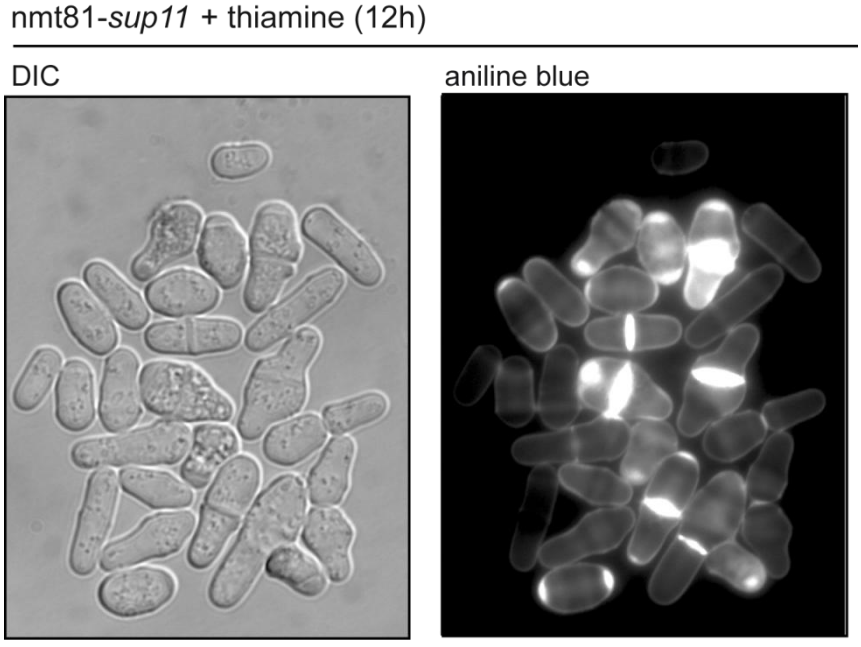

Fig. 5.15: Aniline blue staining of nmt81-*sup11* mutant overexpressing *exg2*$^{+}$:
Microscopic analysis of restricted nmt81-*sup11* mutant cells (12 h) which are overexpressing *exg2*$^{+}$. Images taken with DIC illumination show cells with disturbed morphology. The phenotype is even more pronounced analyzing cells stained with aniline blue. (scale bar = 10 µm)

To further investigate the interplay of *sup11*$^+$ and members of this exoglucanase family, double-mutants of *exg1*Δ or *exg2*Δ, with nmt81-*sup11* were created. Therefore, the endogenous *sup11*$^+$-promoter was replaced by the nmt81-promoter in the *exg1*Δ and *exg2*Δ mutants.

The diminished β-1,6-glucanase activity of an *exg1*Δ might counteract the reduced β-1,6-glucan synthesis of Sup11p depletion and may lead to milder nmt81-*sup11* cell wall/ septum phenotype. In case of Exg2p one could imagine the following scenario: Exg2p is speculated to functions as sensor to regulate β-1,6-glucan degradation, and thus an *exg2*Δ/nmt81-*sup11* double-mutant ought to exhibit also milder phenotypes than the restricted nmt81-*sup11*.

Spotting assays with the *exg1*Δ/ nmt81-*sup11* or *exg2*Δ/ nmt81-*sup11* double-mutants showed a partial rescue of the impaired growth observed for the single nmt81-*sup11* mutant (Fig. 5.16). This supported the hypothesis that reduced β-1,6-glucanase activity due to *exg1*Δ (or the disturbed Exg2p sensor function for controlled β-1,6-glucan degradation, respectively) counteracted the diminished β-1,6-glucan biogenesis of the nmt81-*sup11* mutant.

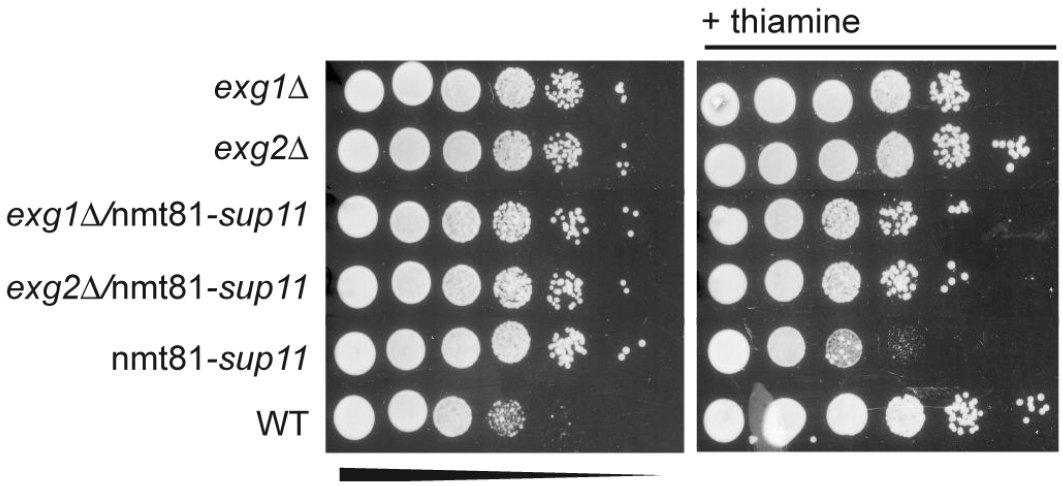

Fig. 5.16: Spotting assays comparing growth of combined exoglucanase deletion and *sup11*$^+$ depletion:
Spotting was done in serial dilution (1:10 steps) starting from 100.000 cells. Spotting assay with various combinations of exoglucanses (*exg1*$^+$, *exg2*$^+$) and nmt81-controled *sup11*$^+$ under permissive and restricted conditions compared to the wild type. Spotted plates were incubated for 3 days at 32°C.

Contrary to the milder growth phenotype of the double-mutants, microscopic phenotypic analysis revealed that their morphology was even more compromised than the restricted nmt81-*sup11* single mutant (*exg1*Δ and *exg2*Δ single mutants did not

exhibit a visible phenotype as reported by Duenas-Santero and co-workers (2010). Microscopic pictures of aniline blue stained *exg1*Δ/nmt81-*sup11* and *exg2*Δ/nmt81-*sup11* cells showed that cell wall defects accreted. Besides the typical septum depositions documented for the nmt81-*sup11* single mutant, the double-mutants were more pear and lemon shaped even under permissive conditions (Fig. 5.17). The synthetic phenotype observed under permissive conditions can be explained by an already diminished Sup11 protein level under nmt81-promoter expression (see Fig. 5.6 A).

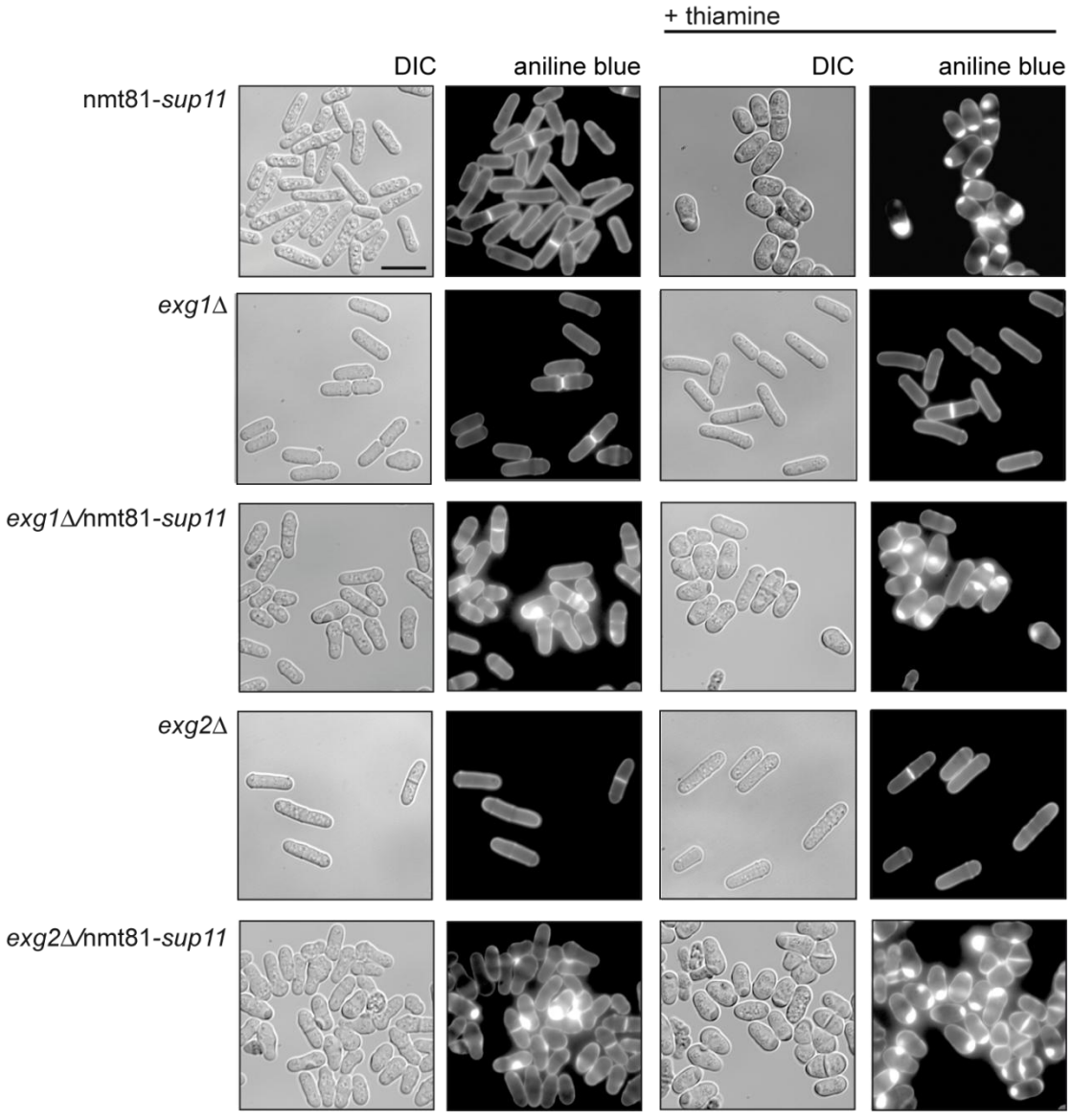

Fig. 5.17: Double mutations of exoglucanases *exg1*$^+$ or *exg2*$^+$ with nmt81-*sup11* causes severe cell wall and septum defects:
Differential contrast and fluorescent microscopy of aniline blue stained cells. Left panel shows mutants with permissive nmt81- *sup11*, right panel depicts cells under restricted conditions (16 h). Compared to the single nmt81-*sup11* mutant, the combined deletion of exoglucanases and nmt81-*sup11* accumulates cell wall and septum defects under restricted and permissive conditions. (scale bar = 10µm)

The impact of the additive cell wall damages of the double-mutants became more dramatically when the cells were exposed to elevated temperature. Challenging the double-mutants with heat stress at 37°C demonstrated a complete growth arrest in a spotting assay (Fig. 5.18).

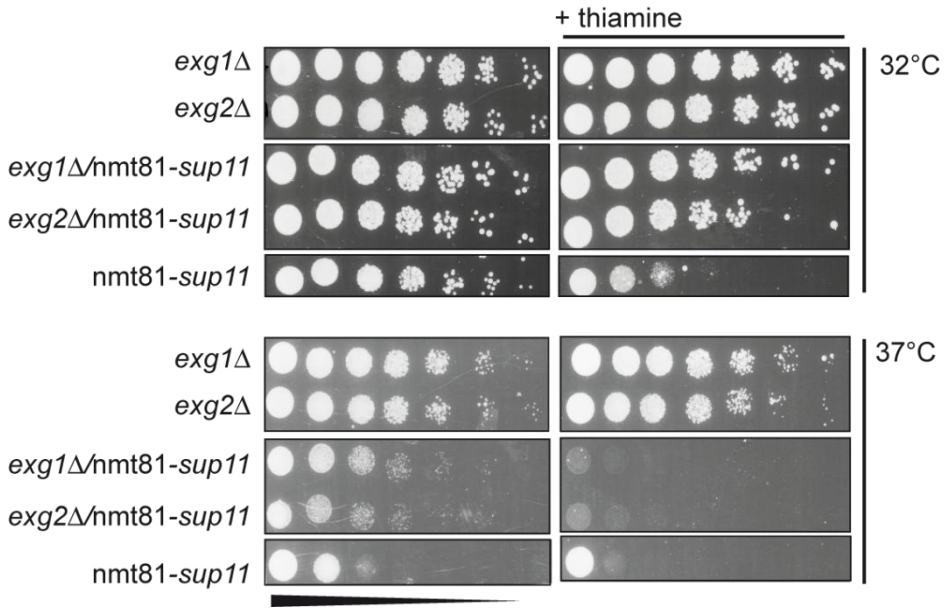

Fig. 5.18: Spotting assays comparing growth of combined exoglucanase deletion and *sup11*$^+$ depletion:
Spotting was done in serial dilution (1:10 steps) starting from 100.000 cells. Spotting assay with various combinations of exoglucanases (*exg1*$^+$, *exg2*$^+$) and nmt81-controled *sup11*$^+$ under permissive and restricted conditions compared to the wild type. Upper panel: Spotted plates were incubated for 3 days at 32°C. Lower panel: Spotting assay with selection of the same mutants testing for temperature sensitivity at 37°C.

Taken together, the microscope data and the temperature sensitive phenotype indicate that the observed effects of *sup11*$^+$/*exg1*Δ and *sup11*$^+$/*exg2*Δ are Sup11p dosage dependent. Compromised morphology and temperature sensitivity of the double-mutants were observed under permissive conditions where Sup11p levels were already diminished due to nmt81-control (see Fig. 5.6 A).

The additive morphological defects observed under the microscope indicated a genetic interaction between individual members of the β-1,6-glucanase family members and *sup11*$^+$. Despite the additional cell wall defects the double-mutants grew better than the single nmt81-*sup11* mutant. This finding is hinting towards some kind of compensatory mechanisms which is triggered when too many cell wall defects accumulate like it is described for cell wall mutants of *S. cerevisiae* (Hagen *et al.*, 2004). In case of the additional heat stress, the defects were probably too severe to be covered by that possible rescue mechanism (see Fig. 5.18).

5.8. Sup11p depletion affects oligosaccharide catabolic processes, cell wall proteins, and the septum separation pathway on transcriptional level

As shown above, Sup11p is involved in β-1,6-glucan biogenesis. Moreover, depletion of Sup11p causes morphological cell wall and septum defects and changes in the cell wall β-glucan and mannoprotein composition.

In order to better understand which regulatory events are triggered on transcriptional level upon down-regulation of *sup11*$^{+}$, a transcriptome analysis with the restricted and non-restricted nmt81- *sup11* mutant was performed.

Transcription levels of 5029 of *S. pombe* genes were analyzed in each array (Supplementary Data, Table 5). Comparison of non-repressed nmt81-*sup11* cells with cells grown in the presence of thiamine for 16h showed that 341 genes were at least 2 fold up-regulated and 68 down-regulated (statistical significance $p<0.05$) (Fig. 5.19, Supplementary Data, Table 3 and 4). The down-regulation of thiamine synthesis related genes along with the observed drop of *nmt1*$^{+}$ transcript level to 0.004% of the non-repressed level can be considered as internal controls. The almost complete loss of *nmt1*$^{+}$ transcripts demonstrated that the chosen conditions for the shut-down of the nmt81-promoter were appropriate in order to achieve best possible knock-down conditions for the nmt81-controlled *sup11*$^{+}$.

88 out of the 341 up-regulated genes were not annotated in the *S. pombe* genome database. Clustering of the respective genes according to cellular localization and biological process using the Genecodis 2.0 software (Carmona-Saez *et al.*, 2007; Nogales-Cadenas *et al.*, 2009; Tabas-Madrid *et al.*, 2012) revealed that most of the annotated up-regulated genes are involved in stress response (99 genes) (Supplementary Data, Table 2).

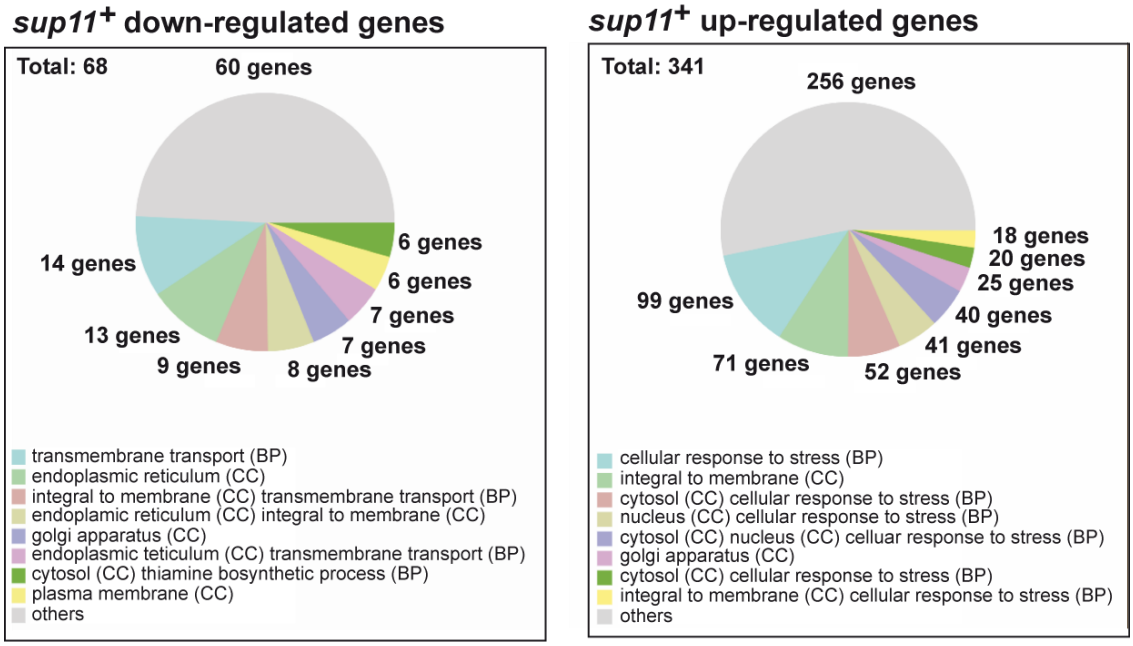

Fig. 5.19: Clustering of down- and up-regulated genes in restricted nmt81-*sup11*:
Transcriptome analysis identified 68 significantly down- and 341 significantly up-regulated genes in the restricted nmt81-*sup11* mutant. Genes were grouped in Genecodis 2.0 and clustered according to the biological process (BP) or cellular compartment (CC) as described in the figure. Single genes can be presented multiple times due to multiple annotations in BP and/or CC.

More detailed manual analysis of the up-regulated genes was done by comparison of their annotated Gene Ontology (GO) terms. The GO is a project which represents a bioinformatics cooperative. Their effort is to develop and use ontologies in order to support biologically meaningful annotation of genes and gene products in a broad spectrum of organisms (Consortium, 2008).

Analysis of the down-regulated genes showed that 10 of 68 genes were not annotated in the *S. pombe* genome database. Most of the genes with known function were annotated as membrane proteins related to TM transport (Fig. 5.19).

Analysis of the up-regulated genes according to their GO terms identified 127 genes which are annotated in “cellular response to stress” (GO term:0033554) (Supplementary data, Table 1).

Not all of the “cellular response to stress” related genes were annotated for responding to a specific stress conditions. Manual analysis of the further annotated “cellular response to stress” up-regulated genes could be categorized into oxidative stress, nitrogen starvation, and osmotic stress (Table 5.1, 5.2, and 5.3).

In the natural environment exposure to aerobic conditions and UV light can cause oxidative stress in yeast cells. But, oxide radicals are also formed during normal cell metabolism. To prevent damage by environmental oxide radicals, the fungal cell wall is a protective barrier (reviewed in Fuchs and Mylonakis, 2009). In addition, oxidative stress is sensed by the cell and subsequently counteractive measures are induced. A common fungal key defense against oxidative stress is the high osmolarity glycerol (HOG) pathway, which mediates responses to hyperosmotic shock and other stresses (reviewed in Fuchs and Mylonakis, 2009).

GO:0034599: cellular response to oxidative stress				
Regulation	**p-value**	**Systematic Name**	**Gene Name**	**Gene Product**
31.348	0.00034	SPAC5H10.02c	SPAC5H10.02c	ThiJ domain protein
25.944	0.00004	SPAC23H3.15c	SPAC23H3.15c	sequence orphan
6.400	0.00008	SPCC757.03c	SPCC757.03c	ThiJ domain protein
3.774	0.00039	SPAPB1A11.03	SPAPB1A11.03	FMN dependent dehydrogenase
3.572	0.00112	SPAC8C9.16c	SPAC8C9.16c	TLDc domain protein 1
2.963	0.00131	SPAC11D3.16c	SPAC11D3.16c	sequence orphan
2.519	0.00151	SPAC21E11.04	*ppr1*	L-azetidine-2-carboxylic acid acetyl transferase
2.366	0.00566	SPAC13F5.07c	SPAC13F5.07c	zf PARP type zinc finger protein
2.227	0.00218	SPCC191.09c	*gst1*	glutathione S-transferase Gst1
2.191	0.00027	SPAC1D4.11c	*kic1*	dual specificity protein kinase Lkh1
2.152	0.00231	SPAC18G6.09c	SPAC18G6.09c	sequence orphan
2.085	0.00877	SPBC106.02c	*srx1*	sulphiredoxin
2.042	0.00047	SPAC17G6.02c	SPAC17G6.02c	RTA1-like protein
2.037	0.00334	SPBC660.07	*ntp1*	alpha,alpha-trehalase Ntp1
2.027	0.00369	SPAC13D6.01	*pof14*	F-box protein Pof14

Table 5.1: Regulation of genes that are involved in GO:0034599 cellular response to oxidative stress upon *sup11*$^{+}$ repression:

Transcriptome analysis comparing gene expression of restricted and non-restricted nmt81-*sup11* mutant revealed eight significantly up-regulated genes (depicted in dark red) that are annotated to function in GO:0034599 cellular response to oxidative stress. The systematic names, p-values, gene names and gene products are listed in the table. Permissive expression level of selected genes equals 1.0.

GO:0071470: cellular response to osmotic stress				
Regulation	**p-value**	**Systematic Name**	**Gene Name**	**Gene Product**
4.646	0.00001	SPAC20G4.03c	*hri1*	eIF2 alpha kinase Hri1
4.322	0.00062	SPBC365.12c	*ish1*	LEA domain protein
4.295	0.00005	SPCC1183.09c	*pmp31*	plasma membrane proteolipid Pmp31
3.545	0.00273	SPCC757.07c	*cta1*	catalase
2.287	0.00012	SPCC1183.11	SPCC1183.11	MS ion channel protein 1
2.206	0.00451	SPAC31G5.09c	*spk1*	MAP kinase Spk1
2.037	0.00334	SPBC660.07	*ntp1*	alpha,alpha-trehalase Ntp1

Table 5.2: Regulation of genes that are involved in GO:0071470: cellular response to osmotic stress upon *sup11*$^{+}$ repression:

Transcriptome analysis comparing gene expression of restricted and non-restricted nmt81-*sup11* mutant revealed eight significantly up-regulated genes (depicted in dark red) that are annotated to function in GO:0034599 cellular response to oxidative stress. The systematic names, p-values, gene names and gene products are listed in the table. Permissive expression level of selected genes equals 1.0.

For the induction of mitosis and survival in high-osmolarity conditions Sty1p activity is required. Sty1p is an osmotic-stress-stimulated MAPK homolog which is activated by Wis1 MAPK kinase and inhibited by Pyp1 tyrosine phosphatase (Fig. 5.20). Subsequently, Sty1p is transcriptionally up-regulating a number of genes which are considered to be important stress responses like Gpd1p and Tps1p. It also regulates expression of Pyp2p which is a negative regulator of Sty1p (Degols *et al.*, 1996).

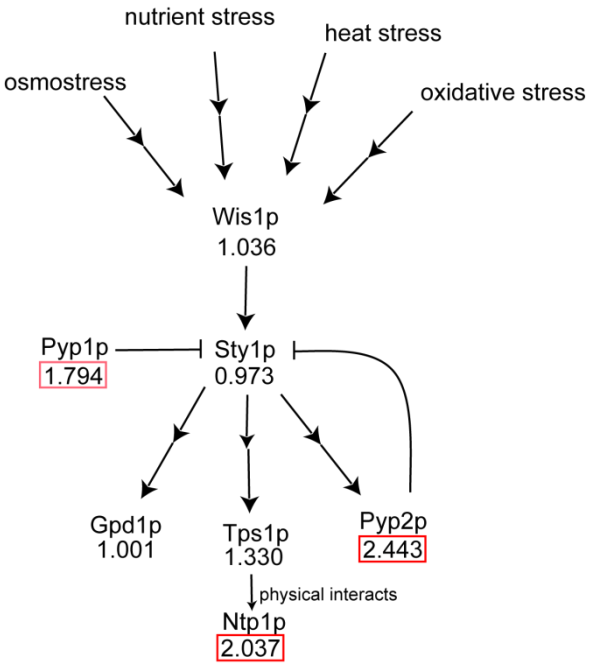

Fig. 5.20: HOG pathway in fission yeast (adapted from Degols *et al.*, 1996):
Sty1p is activated by various forms of stress by MAPK Wis1p. Sty1p is transcriptionally up-regulation a number of genes which are thought to be involved in important stress responses like Gpd1p and Tps1p. It also regulates expression of Pyp2p which is a negative regulator of Sty1p. Expression values comparing the permissive and restricted the nmt81-*sup11* mutant are shown and up-regulation is indicated by red boxes.

Transcriptome analysis showed no transcriptional regulation of Wis1p and Sty1p but regulation of genes which are controlled by Sty1p. The up-regulation of Sty1p-repressor Pyp2p indicated an elevated Sty1p activity which is compensated by higher Pyp2p levels. Moreover, a small increase of Tps1p (1.330 fold), a predicted α,α-trehalose-phosphate synthase, was observed. Tps1p and the as well up-regulated α,α-trehalase Ntp1p were demonstrated to physically interact with each other (Soto *et al.*, 2002).

Further stress responses were observed which are categorized as nutrient stresses (Table 5.3). Nutrient stress is triggered when yeasts are transferred from a nutrient-rich to a nutrient-poor conditions. However, cells used for transcriptome analysis were cultured under nutrient-rich conditions indicating a different activation than due to nutrient-poor medium.

GO:0051409: response to nitrogen starvation				
Regulation	**p-value**	**Systematic Name**	**Gene Name**	**Gene Product**
18.209	0.00009	SPAC869.02c	SPAC869.02c	nitric oxide dioxygenase (predicted)
3.731	0.00145	SPAC1F8.05	*isp3*	sequence orphan
3.708	0.00016	SPBC32C12.02	*aff1*	transcription factor Ste11
3.704	0.00116	SPAC4A8.04	*isp6*	vacuolar serine protease Isp6
3.593	0.00327	SPBC3E7.02c	*hsp16*	heat shock protein Hsp16
3.234	0.00006	SPAC2G11.13	*atg22*	autophagy associated protein Atg22 (predicted)
2.100	0.00221	SPAC589.07c	SPAC589.07c	WD repeat protein Atg18
2.032	0.00617	SPAC19B12.08	SPAC19B12.08	peptidase family C54
2.007	0.00996	SPBP8B7.24c	*atg8*	autophagy associated protein Atg8 (predicted)

Table 3.3: Regulation of genes that are involved in GO:0051409: response to nitrogen starvation upon *sup11*$^+$ repression:
Transcriptome analysis comparing gene expression of restricted and non-restricted nmt81-*sup11* mutant revealed eight significantly up-regulated genes (depicted in dark red) that are annotated to function in GO:0034599 cellular response to oxidative stress. The systematic names, p-values, gene names and gene products are listed in the table. Permissive expression level of selected genes equals 1.0.

Moreover, the cyclic adenosine monophosphate (cAMP) -pathway is also involved in nutrient sensing. Glucose and/or nitrogen depletion activates a heterotrimeric G protein and leads to the release of the Gα-GTP subunit (Gpa2p). Transciptome analysis of the restricted nmt81-*sup11* mutant revealed a significant down-regulated of Gpa2p (0.459 fold). Gpa2p activity represses the *fbp1*$^+$ gene (fructose-1,6-bisphosphatase)

which is a regulator of the gluconeogenesis. Indeed, the *fbp1*$^{+}$ gene was found to be strongly up-regulated in the restricted nmt81-*sup11* mutant (38.252 fold).

Apart from the various directly stress related responses, transcriptome data analysis revealed eight genes which were annotated in the Kyoto Encyclopedia of Genes and Genomes **(**KEGG) Pathway spo00500 (starch and sucrose metabolism, (Table 5.4). KEGG is a collection of online databases dealing with genomes and enzymatic pathways. In fission yeast, the annotated genes of this pathway are actually involved in glucan and polysaccharide metabolism including genes coding for various glucan synthases and glucanases. These findings indicated that cells with depleted Sup11p activity undergo changes in their cell wall glucan composition as many glucan modifying enzymes like Bgl2p or Meu17p are found to be significantly up-regulated in the transcriptome analysis (Table 5.4).

KEGG Pathway spo00500: glucan and polysaccharide metabolism				
Regulation	**p-value**	**Systematic Name**	**Gene Name**	**Gene Product**
4.885	0.00330	SPCC191.11	*inv1*	β-fructofuranosidase
4.847	0.00001	SPAC26H5.08c	*bgl2*	glucan 1,3-β-glucosidase
4.125	0.00089	SPBC14C8.05c	*meu17*	glucan- α -1,4-glucosidase
4.026	0.00035	SPAC22F8.05	SPAC22F8.05	α, α -trehalose-phosphate synthase (predicted)
2.528	0.00139	SPAPB24D3.10c	*agl*	α -glucosidase
2.525	0.00001	SPCC757.12	SPCC757.12	α -amylase homolog (predicted)
2.231	0.00017	SPBC19G7.05c	*bgs1*	1,3-β-glucan synthase catalytic subunit
2.037	0.00334	SPBC660.07	*ntp1*	α, α -trehalase
1.973	0.00579	SPAC23D3.14c	*aah2*	α -amylase homolog
1.766	0.00016	SPAC19B12.03	*bgs3*	1,3-β-glucan synthase subunit
1.365	0.03970	SPBC32F12.10	SPBC32F12.10	phosphoglucomutase (predicted)
1.330	0.13776	SPAC328.03	*tps1*	α, α -trehalose-phosphate synthase
1.326	0.13965	SPBC1683.07	*mal1*	α -glucosidase (predicted)
1.248	0.00005	SPCC1840.02c	*bgs4*	β-1,3-glucan synthase subunit
1.233	0.23717	SPACUNK4.16c	SPACUNK4.16c	α, α -trehalose-phosphate synthase (predicted)
1.123	0.11480	SPAC8E11.01c	SPAC8E11.01c	β-fructofuranosidase
1.172	0.08332	SPAC12B10.11	*exg2*	glucan 1,6-β-glucosidase
1.139	0.19843	SPAC25H1.09	*mde5*	α -amylase homolog
1.088	0.03917	SPAC3G6.09c	*tps2*	trehalose-phosphate synthase (predicted)
1.025	0.73324	SPCC1322.04	SPCC1322.04	UTP-glucose-1-phosphate uridylyl transferase (predicted)

0.937	0.20727	SPAC24C9.07c	*bgs2*	1,3-β-glucan synthase subunit
0.968	0.67212	SPBC16A3.13	*aah4*	α-amylase homolog
0.833	0.16003	SPAC4F8.07c	*hxk2*	hexokinase 2
0.831	0.21183	SPCC794.10	SPCC794.10	UTP-glucose-1-phosphate uridylyl transferase (predicted)
0.642	0.00758	SPAC24H6.04	*hxk1*	hexokinase 1
0.581	0.00673	SPBC1105.05	*exg1*	glucan 1,6-β-glucosidase

Table 5.4: Regulation of genes that are involved in KEGG Pathway spo00500 upon *sup11*$^+$ repression:
Transcriptome analysis comparing gene expression of restricted and non-restricted nmt81-*sup11* mutant revealed eight significantly up-regulated genes (depicted in dark red) that are annotated to function in KEGG Pathway spo00500 **(**glucan and polysaccharide metabolism). Moderately up- and down-regulated genes are depicted in light red (1.8-2.0) or light green (0.8-0.5).
The systematic names, p-values, gene names and gene products are listed in the table. Permissive expression level of selected genes equals 1.0.

Moreover, manual data analysis revealed changes in regulation of genes which were annotated in oligosaccharide catabolic process (GO:0009313) (Table 5.5). The selected genes partially overlap with the latter analyzed KEGG pathway which is controlling the glucan and polysaccharide metabolism (Table 3.4).

GO:0009313: oligosaccharide catabolic process				
Regulation	**p-value**	**Systematic Name**	**Gene Name**	**Gene Product**
15.980	0.00026	SPAC869.07c	*mel1*	α-galactosidase
4.885	0.00330	SPCC191.11	*inv1*	β-fructofuranosidase
3.544	0.00057	SPAC3C7.05c	*mug191*	α -1,6-mannanase (predicted)
3.403	0.00018	SPBC1198.07c	SPBC1198.07c	mannan endo-1,6- α -mannosidase
2.528	0.00139	SPAPB24D3.10c	*agl*	α -glucosidase
2.037	0.00334	SPBC660.07	*ntp1*	α, α -trehalase
1.326	0.13965	SPBC1683.07	*mal1*	α -glucosidase (predicted)
1.123	0.11480	SPAC8E11.01c	SPAC8E11.01c	β-fructofuranosidase
1.097	0.42720	SPAC513.05	*mns2*	alpha-mannosidase (predicted)
1.062	0.44457	SPBC530.10c	*anc1*	adenine nucleotide carrier
0.998	0.98908	SPAC30D11.01c	SPAC30D11.01c	α -glucosidase
0.891	0.10998	SPCC970.02	SPCC970.02	mannan endo-1,6-α -mannosidase
0.801	0.04537	SPBC1198.06c	SPBC1198.06c	mannan endo-1,6-α -mannosidase
0.524	0.04103	SPAC821.09	*eng1*	endo-1,3-β-glucanase
0.425	0.00470	SPAC14C4.09	*agn1*	glucan endo-1,3-α-glucosidase

Table 5.5: Regulation of genes that are involved in oligosaccharide catabolic process (GO:0009313) upon *sup11*$^+$ repression:
Transcriptome analysis comparing gene expression of restricted and non-restricted nmt81-*sup11* mutant revealed six significantly up-regulated genes (depicted in dark red) and one significantly down-regulated gene (depicted in dark green) that are annotated to function in oligosaccharide catabolic process

(GO:0009313). Moderately up- and down-regulated genes are depicted in light red (1.8-2.0) or light green (0.8-0.5).
The systematic names, p-values, gene names and gene products are listed in the table. Permissive expression level of selected genes equals 1.0.

Comparison of gene regulation in a similar GO process - the extracellular polysaccharide metabolism process (GO:0046379) - revealed also several genes which were significantly changed in their expression (Table 5.6). This GO includes some of the genes which are also annotated in the oligosaccharide catabolic process (GO:0009313), as well (see Table 5.5).

Together these data suggest that the restricted nmt81-*sup11* mutant undergoes a significant remodeling of the cell wall polysaccharides.

GO:0046379: extracellular polysaccharide metabolism process				
Regulation	**p-value**	**Systematic Name**	**Gene Name**	**Gene Product**
15.980	0.00026	SPAC869.07c	*mel1*	α -galactosidase
3.544	0.00057	SPAC3C7.05c	SPAC3C7.05c	α -1,6-mannanase (predicted)
3.403	0.00018	SPBC1198.07c	SPBC1198.07c	mannan endo-1,6- α -mannosidase
2.525	0.00001	SPCC757.12	SPCC757.12	α -amylase homolog (predicted)
1.973	0.00579	SPAC23D3.14c	*aah2*	α -amylase homolog
1.622	0.01218	SPAC11E3.13c	*gas5*	1,3-β-glucanosyl transferase (predicted)
1.185	0.01996	SPAC1527.01	*mok11*	α -1,3-glucan synthase
1.147	0.04775	SPBC646.06c	*agn2*	glucan endo-1,3- α -glucosidase
1.108	0.22122	SPCC63.02c	*aah3*	α -amylase homolog
1.055	0.55143	SPAC27E2.01	SPAC27E2.01	α -amylase homolog (predicted)
0.968	0.67212	SPBC16A3.13	*aah4*	α -amylase homolog
0.943	0.53736	SPAC27E2.07	*pvg2*	galactose residue biosynthesis protein
0.801	0.04537	SPBC1198.06c	SPBC1198.06c	mannan endo-1,6- α -mannosidase
0.730	0.10228	SPAPB1E7.04c	SPAPB1E7.04c	chitinase (predicted)
0.663	0.03646	SPAC2E1P3.05c	SPAC2E1P3.05c	fungal cellulose binding domain protein
0.647	0.02145	SPBC342.03	*gas4*	1,3-β-glucanosyltransferase (predicted)
0.524	0.04103	SPAC821.09	*eng1*	endo-1,3-β-glucanase
0.483	0.03021	SPBPB7E8.01	SPBPB7E8.01	α -amylase homolog (predicted)
0.425	0.00470	SPAC14C4.09	*agn1*	glucan endo-1,3-α -glucosidase

Table 5.7: Regulation of genes that are involved in extracellular polysaccharide metabolism process (GO:0046379) upon *sup11*$^{+}$ repression:
Transcriptome analysis comparing gene expression of restricted and non-restricted nmt81-*sup11* mutant revealed four significantly up-regulated genes (depicted in dark red) and two significantly down-regulated genes (depicted in dark green) that are annotated to function in extracellular polysaccharide metabolism

process (GO:0046379). Moderately up- and down-regulated genes are depicted in light red (1.8-2.0) or light green (0.8-0.5).
The systematic names, p-values, gene names and gene products are listed in the table. Permissive expression level of selected genes equals 1.0.

Analyzing the expression of genes annotated in localizing and function in the fungal cell wall (+septum) (GO:0009277), there were several changes revealed in the transcriptome data (Table 5.8). The data showed that Sup11p depletion must induce significant cell wall remodeling processes. The expression of many glucanases and glucan synthases present in the cell wall are up-regulated. One endo-1,3-α-glucosidase (*agn1*$^{+}$) has shown to be down-regulated. However, contrary to the up-regulated glucan synthases and glucanases in this GO which modify the cell wall, Agn1p is active during the septum separation process which will be discussed separately in this chapter.

GO:0009277: fungal-type cell wall (+septum)				
Regulation	**p-value**	**Systematic Name**	**Gene Name**	**Gene Product**
8.263	0.00179	SPBC2G2.17c	*Psu2*	β-glucosidase (predicted)
4.847	0.00001	SPAC26H5.08c	*bgl2*	glucan 1,3-beta-glucosidase
3.329	0.00049	SPBC16D10.05	*mok13*	α -1,3-glucan synthase
3.312	0.00082	SPCC569.03	SPCC569.03	cell surface glycoprotein (predicted),
3.265	0.00000	SPCC1235.01	SPCC1235.01	sequence orphan
3.202	0.00005	SPBC21B10.07	SPBC21B10.07	glycosyl hydrolase family 16
2.906	0.00043	SPCC330.04c	*mug135*	cell surface glycoprotein (predicted),
2.231	0.00017	SPBC19G7.05c	*bgs1*	1,3-β-glucan synthase catalytic subunit
1.819	0.01378	SPCC1450.09c	SPCC1450.09c	phospholipase (predicted)
1.780	0.00009	SPCC1322.10	SPCC1322.10	conserved fungal protein
1.622	0.01218	SPAC11E3.13c	*gas5*	1,3-β-glucanosyl transferase
1.594	0.01842	SPCP20C8.01c	*SPCP20C8.01c*	B13958 domain
1.546	0.00007	SPBC29A10.08	*gas2*	1,3-β-glucanosyl transferase
1.478	0.00140	SPAC19B12.02c	*gas1*	1,3-β-glucanosyl transferase
1.233	0.04216	SPBC21D10.06c	*map4*	cell agglutination protein
1.227	0.02810	SPAC26H5.11	*mud56*	spore wall assembly protein
1.160	0.01721	SPBC32H8.13c	*mok12*	α -1,3-glucan synthase
1.142	0.03712	SPAC1705.03c	*ecm33*	cell wall protein Ecm33
1.116	0.20549	SPAC1A6.04c	*plb1*	phospholipase B homolog
1.093	0.28668	SPAC27D7.04	*omt2*	4- α -hydroxytetrahydrobiopterin dehydratase (predicted)
1.043	0.62247	SPAC19G12.03	*cda1*	chitin deacetylase
1.019	0.60015	SPCC63.04	*mok14*	α -1,3-glucan synthase
0.997	0.92041	SPAC343.07	*mug28*	RNA-binding protein
0.981	0.74250	SPCC613.11c	*meu23*	cell surface glycoprotein (predicted)

0.894	0.06877	SPAC17A5.04c	*mde10*	spore wall assembly peptidase
0.822	0.08143	SPBP23A10.11c	SPBP23A10.11c	conserved fungal protein
0.768	0.15839	SPAC1002.13c	*psu1*	β-glucosidase (predicted)
0.764	0.06400	SPAC977.09c	SPAC977.09c	phospholipase (predicted)
0.730	0.10228	SPAPB1E7.04c	SPAPB1E7.04c	chitinase (predicted)
0.683	0.00006	SPBP4G3.02	*pho1*	acid phosphatase
0.614	0.00819	SPBC21H7.03c	SPBC21H7.03c	acid phosphatase (predicted)
0.425	0.00470	SPAC14C4.09	*agn1*	glucan endo-1,3-α-glucosidase
0.078	0.00001	SPBC428.03c	*pho4*	thiamine-repressible acid phosphatase

Table 5.8: Regulation of genes that are involved fungal-type cell wall (GO:0009277) upon *sup11*$^+$ repression:
Transcriptome analysis comparing gene expression of restricted and non-restricted nmt81-*sup11* mutant revealed eight significantly up-regulated genes (depicted in dark red) and two significantly down-regulated genes (depicted in dark green) that are annotated to function in fungal-type cell wall (GO:0009277). Moderately up- and down-regulated genes are depicted in light red (1.8-2.0) or light green (0.8-0.5).
The systematic names, p-values, gene names and gene products are listed in the table. Permissive expression level of selected genes equals 1.0.

Interpretation of the transcriptome data alone it is not sufficient to predict a certain cell wall alteration. However, the expression changes in many of the cell wall glucan modifying enzymes support the data by Hutzler (2009) demonstrating an enrichment of cell wall α-glucan compared to β-glucan. Also the absence of cell wall β-1,6-glucan (see Fig. 5.13) is in agreement with an severely altered cell wall composition of the restricted nmt81-*sup11* mutant.

Moreover, manual data analysis showed down-regulation of the septum separation pathway (Table 5.9) (reviewed in Sipiczki, 2007). Considering the huge cell wall material depositions at their septum center by repression of *sup11*$^+$, a defect in septum separation seems feasible. Ace2p is the key transcription factor of the septum separation pathway signal cascade. Ace2p itself is controlled by several transcription factors such as Sep1p, Plo1p or Mbx1p (Bähler, 2005; Nachman and Regev, 2009). The array showed that one key regulator of Ace2p, the Mbx1p transcription factor, is highly up-regulated. Mbx1p is known to repress the Ace2p transcription factor activity and down-regulation of Ace2p was demonstrated in the transcriptome analysis of the nmt81-*sup11* mutant. In consequence, almost all known target proteins of Ace2p which are involved in the septum separation pathway are demonstrated to be down-regulated

on the transcriptional level (Table 5.9). Several of these target proteins contain S/T-rich regions that are potential *O*-mannosylation sites for example Eng1p, Adg1p and Adg2p.

Septum separation pathway				
Regulation	**p-value**	**Systematic Name**	**Gene Name**	**Gene Product**
3.860	0.00045	SPBC19G7.06	*mbx1*	MADS-box transcription factor
1.425	0.04775	SPBC646.06c	*agn2*	glucan endo-α-1,3-glucosidase
1.248	0.00920	SPBC4C3.12	*sep1*	fork head transcription factor
1.237	0.18414	SPAC24C9.15c	*sep15*	Septin 15
1.194	0.16460	SPAC23C11.16	*plo1*	Polo kinase
1.019	0.03697	SPAPYUG7.03c	*mid2*	anillin homologue
1.001	0.79793	SPBC776.18c	*pmh1*	transcription factor TFIIH complex subunit
0.741	0.04290	SPBC3E7.12c	*cfh4*	chitin synthase regulatory factor (putative)
0.692	0.08342	SPAC4F10.11	*sep10*	septin 10
0.651	0.02491	SPAC19G12.16c	*adg2*	conserved fungal protein
0.569	0.01533	SPCC18.01c	*adg3*	β-glucosidase (predicted)
0.470	0.01053	SPAPJ760.03c	*adg1*	sequence orphan
0.414	0.01854	SPAC6G10.12c	*ace2*	transcription factor

Table 5.9: Due to *sup11*$^+$ repression up- of down-regulated genes involved in septum separation pathway:
Transcriptome analysis comparing gene expression of restricted and non-restricted nmt81-*sup11* mutant revealed a couple of genes that are function in the septum separation pathway. The systematic names and gene products are listed in the table. Significantly up-regulated genes (depicted in dark red) and significantly down-regulated genes (depicted in dark green) that are annotated to function in fungal-type cell wall. Moderately up- and down-regulated genes are depicted in light red (1.8-2.0) or light green (0.8-0.5).
The systematic names, p-values, gene names and gene products are listed in the table. Permissive expression level of selected genes equals 1.0.

The transcriptome data were further validated using qPCR. In order to clarify whether the observed down-regulation of the septum separation pathway is a direct effect upon the depletion of Sup11p or rather a secondary effect triggered by the observed cell cycle arrest, the expression level of *ace2*$^+$ and *cdc18*$^+$ were investigated at earlier restriction phases at 4 h and 10 h. *Cdc18*$^+$ is an important cell cycle regulator which was shown to be down-regulated (54% of permissive conditions) in the transcriptome analysis of cells after 16 h of repression.
In this analysis the *sup11*$^+$ and *ace2*$^+$ expression levels are stable up to 4 h of thiamine repression and their expression level then dropped significantly until 10 h of thiamine

treatment (Fig. 5.21 A, B). The similar response of *sup11*$^+$ and *ace2*$^+$ indicated a direct influence of decreased *sup11*$^+$ transcript levels on the down-regulation of *ace2*$^+$.

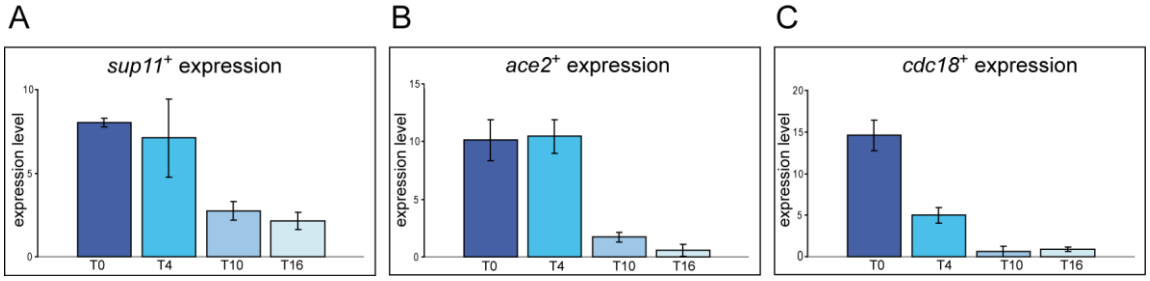

Fig. 5.21: Quantitative PCR (qPCR) of selected genes upon restriction of nmt81-*sup11* mutant: Expression level time course of *sup11*$^+$ (A), *ace2*$^+$ (B) and *cdc18*$^+$ (C) of permissive (T0) and restricted nmt81-*sup11* mutant after 4, 10, and 16 h (T4, T6 and T16). N = 3± standard deviation.

However, the transcript level of *cdc18*$^+$ decreases remarkably earlier compared to *ace2*$^+$ and *sup11*$^+$ levels (Fig. 5.21 C). After 4 h of repression the *cdc18*$^+$ transcript level was already reduced about 60% of the level under non-restricted conditions. This indicated that cell cycle arrest appears prior to inhibition of *ace2*$^+$, whose gene product controls the septum separation pathway. Considering the early response of *cdc18*$^+$ to Sup11p depletion, the down-regulation of the septum separation pathway might actually be a secondary effect caused by a previous cell cycle arrest.

Expression of *cdc18*$^+$ is crucial for entering S-phase and *cdc18*$^+$ mutants arrest in G1 having a 1C DNA content (Kelly *et al.*, 1993). It was reported that only in cells with complete loss of *cdc18*$^+$ transcripts cells arrest in G1-phase. Down-regulation of *cdc18*$^+$ rather promotes cells with 2C content because DNA synthesis cannot be completed normally (Kelly *et al.*, 1993).

In order to elucidate if the restricted nmt81-*sup11* cells enter a G1 arrest, fluorescence activated cell sorting measurements (FACS) were applied. Cell sorting of ethanol fixed cells with fluorescent stained nuclei were analysed via FACS to elucidate their DNA content which allows to draw a conclusion about their cell cycle phase. Evaluation of the different sub-populations demonstrated that the majority of cells of both - restricted and permissive - nmt81-*sup11* cultures had 2C DNA content (Fig. 5.22).

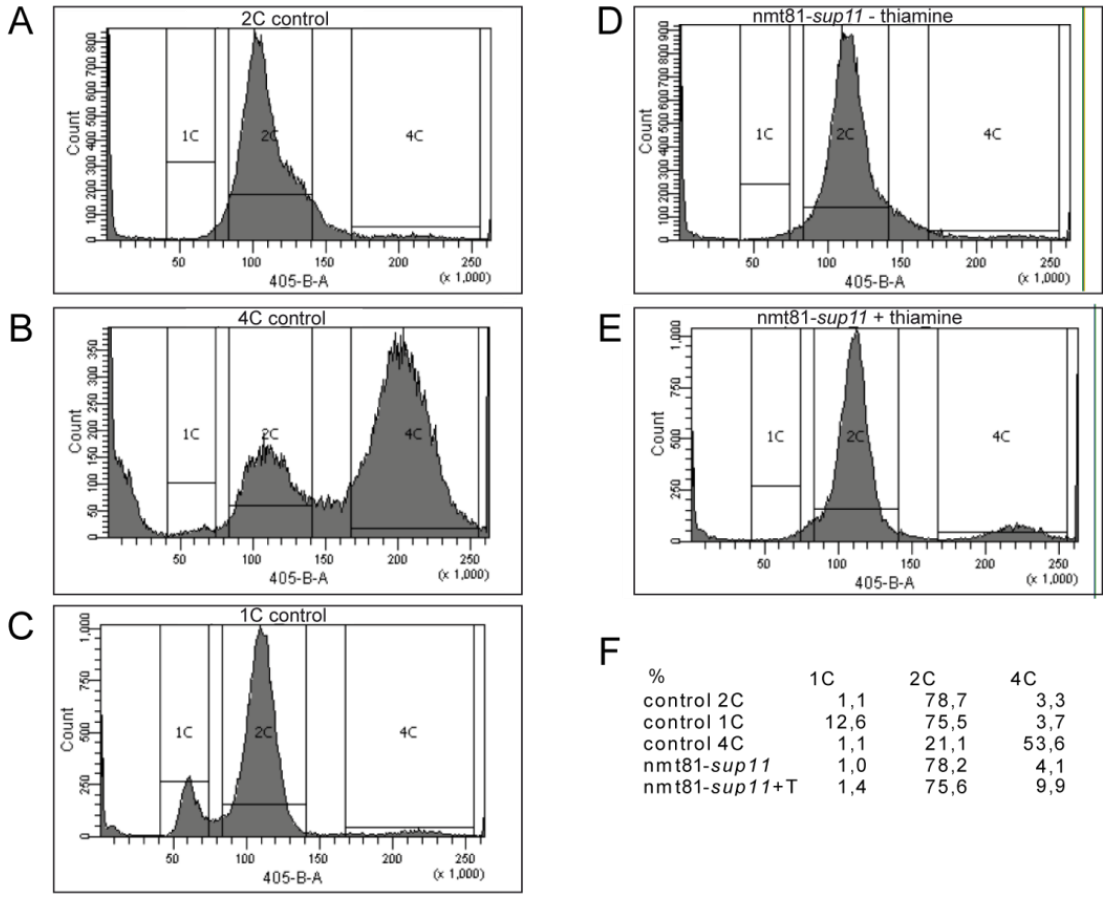

F

%	1C	2C	4C
control 2C	1,1	78,7	3,3
control 1C	12,6	75,5	3,7
control 4C	1,1	21,1	53,6
nmt81-*sup11*	1,0	78,2	4,1
nmt81-*sup11*+T	1,4	75,6	9,9

Fig. 5.22: FACS analysis of nmt81-*sup11*:
Ethanol fixed and DAPI-stained cells were analyzed for their DNA content using FACS. Gates were set as indicated by the controls for (A) 2C (haploid strain after S-phase), (B) 4C (diploid chromosome set) and (C) 1C (unreplicated haploid cells). DNA content of nmt81-*sup11* under (D) permissive and (E) restricted conditions were analyzed using these gates. (F) Percentage of cell having the respective DNA content was counted for each culture.

The data of the *cdc18*$^{+}$ qPCR time line analysis showed a significant but not complete down-regulation of the *cdc18*$^{+}$ transcript (6,7%) after 16 h grown under Sup11p depleted conditions. The observed 2C DNA content of the arrested nmt81-*sup11* mutant is likely due to *cdc18*$^{+}$ down-regulation which promotes cell cycle arrest with cell of 2C DNA content (Kelly *et al.*, 1993). Moreover, it is probable that the observed down-regulation of the septum separation pathway is a secondary effect due to cell cycle arrest, which is triggered prior. Since cells stop duplicating they ought not to need undergo intensive remodelling of the cell wall. Therefore, it appears likely that the cell wall synthesising and degrading genes are down-regulated in arrested cells. However, many of glucan modifying enzymes are significantly up-regulated in the transcriptome analysis. Considering that there are also a number of glucan modifying genes down-regulated, it appears that in the arrested cells the cell wall matrix is rather

undergoing extensive remodelling than stagnation upon *cdc18*$^{+}$ promoted cell cycle arrest.

5.9. Subcellular localization studies of Sup11p

The subcellular localization is an important protein feature which helps to narrow down possible interaction partners or even its function. *In silico* analysis showed that Sup11p is a secretory protein with ER-signal sequence (see chapter 5.1). To analyze whether *Sp*Sup11p resides in compartments of the secretory pathway or whether it is secreted, a detailed cell fractionation was performed and precipitated proteins of the growth medium were analyzed as well. The genomically Sup11p:HA version could be detected by crude cell fractionation in total cell extracts and in crude membrane fractions. No signal was obtained neither among soluble proteins nor was any detectable amount of Sup11p:HA secreted to the medium (Fig. 5.23).

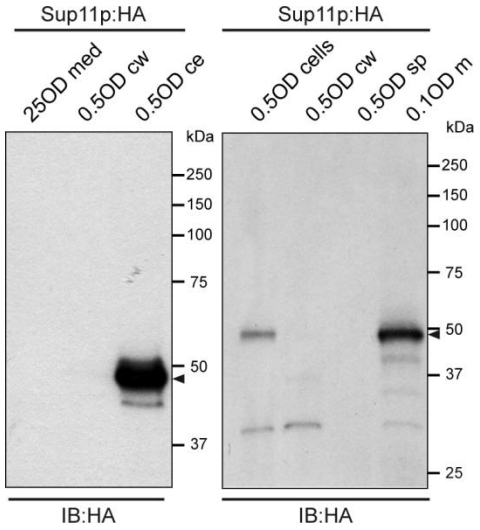

Fig. 5.23: Western blot analysis of crude cell fractionations with a genomically HA-tagged Sup11p: Western blot with extracts from genomically tagged Sup11p:HA (FRY13) and the precipitated culture medium (med). Cell lysate was separated into cell walls (cw) and remaining cell extract (ce) by low speed centrifugation (3,000 g for 2 min) (left panel). Cellular extracts were further separated into soluble proteins (sp) and total microsomes (m) by high speed centrifugation (100,000 g for 30 min). Sup11:HA indicated by filled arrowhead. Blot was decorated with monoclonal anti-HA antibody (1:5000) and anti-mouse IgG peroxidase conjugate (1:5000).

The crude cell fractionation demonstrated that Sup11p is an membrane protein residing in a secretory pathway organelle or PM and that the Sup11 protein is not secreted. However, the compartment in which Sup11p is localized still needed to be elucidated. In order to clarify its subcellular several strategies were followed.

5.9.1. C- and N-terminal tagging of Sup11p with diverse fluorochromes

The probably most widespread technique to subcellular localize a protein of interest is its fusion with a fluorophore. In the last years a broad selection of different fluorescent markers has been developed to choose from. The most frequently used fluorophore is the Green fluorescent protein (GFP) with a size of 26.9 kDa size or slightly modified versions derived from the natural form.

In order to be able to detect Sup11p by fluorescence microscopy C- and N-terminal fusions were made. But, using fluorescence detection for Sup11p localization studies turned out to be a difficult matter although various fluorochrome fusions were designed and analyzed.

Expression of a C-terminally GFP-tagged Sup11p under the control of different constitutively active promoters (pLW56 for *adh1*; pLW78 *act1*) from a 2µ plasmid yielded 60 kDa fusion proteins. Also an N-terminal reporter protein (eYFP:Sup11p) was constructed. Western blot analysis decorating with a polyclonal anti-GFP antibody (Invitrogen) showed that all reporter constructs were expressed (Fig. 5.24 A) but no fluorescence was detected when excited with fluorophore correspondent wavelength (Fig. 5.24 B).

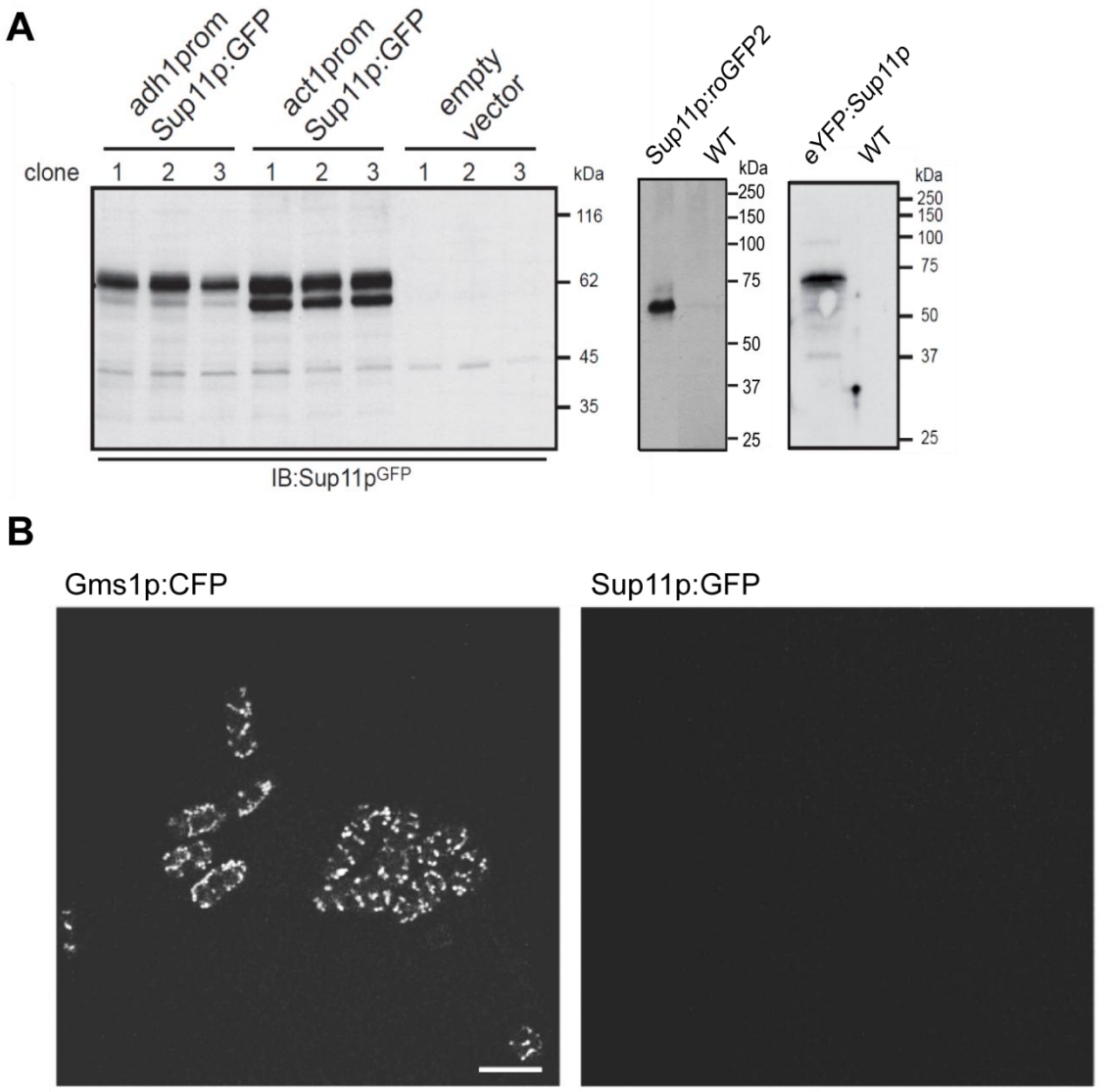

Fig. 5.24: Analysis of Sup11p C- and N-terminally tagged with various fluorochromes:
(A) Western blot to compare expression level of Sup11p:GFP under control of adh1 and act1-promoter (prom) from a vector and the empty vector control. Total membranes of 0.1 OD cells for three independent clones each were analysed. C-terminal Sup11p:roGFP and N-terminal tagged eYFP:Sup11p were analysed with different Western blots. Blots were decorated with anti-GFP (1:3000) and anti-Rabbit IgG peroxidase conjugate (1:5000).
(B) Confocal microscopy of episomal overexpression of Gms1p:CFP (Golgi marker) from pAU-gms1-CFP and cells expression Sup11p:GFP under control of *act1*-promoter from pLW78. (scale bar = 5 µm).

Amongst other fluorochromes tested a strain with genomically C-terminal tagged fusion of the redox sensitive roGFP2 to the Sup11p was created (LWY12). Western blot analysis of the Sup11p:roGFP2 fusion showed one distinct band around 60 kDa (Fig. 5.24 A).

The functionality and therefore correct localization of the genomically tagged Sup11p strains were investigated by a spotting assay. A decreased tolerance of the restricted nmt81-*sup11* mutant towards SDS was reported by Hutzler (2009) and used as indicator

for functionality of genomically tagged Sup11p versions (Fig. 5.25). The growth of LWY12 (Sup11p:roGFP2), FRY13 (Sup11p:HA), and the wild type were analyzed in presence of the anionic detergent. Functionality of both Sup11p-fusion proteins was demonstrated since the tagged strains did not exhibit a SDS-sensitive phenotype like the restricted nmt81-*sup11*. Strains expressing the native as well as tagged version of Sup11p showed no difference in growth whereas the repressed nmt81-*sup11* is susceptible towards SDS containing medium (Fig. 5.25). Since the tagged version of Sup11p:roGFP2 ought to be functional one can assume that also the subcellular localization is largely unaffected by the tag.

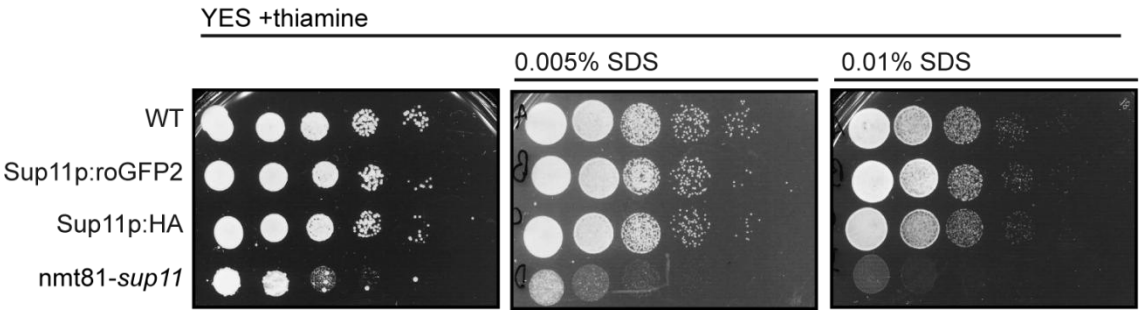

Fig. 5.25: Analyzing the sensitivity of genomically tagged Sup11p-tagged strains towards SDS: Serial dilutions in 1:10 steps starting from 100.000 cells and cultivated for 2 days at 32°C. Comparing growth of Sup11p:roGFP2 and Sup11p:HA tagged strains to the wild type on rich media plates containing none, 0.005% or 0.01% SDS. SDS sensitivity of the restricted nmt81-*sup11* mutant was demonstrated.

Microscopic analysis of the Sup11p:roGFP2-fusion gave a very weak fluorescent signal that appeared in vesicle-like spotted pattern (Fig. 5.26). The Sup11p:roGFP2 signal did not co-localize with the cis-Golgi marker Anp1p:mCherry in the double-mutant LWY13 (Fig. 5.26).

In order to clarify the subcellular localization of Sup11p other organelle markers were tagged with mCherry in the Sup11p:roGFP2 strain LWY12. The fluorescence intensity obtained by the Sup11p:roGFP2 in those strains was barely above the background and too weak for visualization in fluorescence microscopy images. However, the mCherry-tagged co-markers could be imaged and compared to the Sup11p:roGFP2 pattern of the Sup11p:roGFP2/Anp1p:mCherry strain. The Sup11p:roGFP2 pattern looked clearly different from the ER-marker and vacuole-marker (Fig. 5.26). However, the spotted fluorescence pattern of Sup11p:roGFP2 resembled the pattern of Sec31p:mCherry/ Anp1p:mCherry although there was no co-localization. This suggested a localization for Sup11p in a vesicle-like compartment in the post-ER secretory pathway (Fig. 5.26).

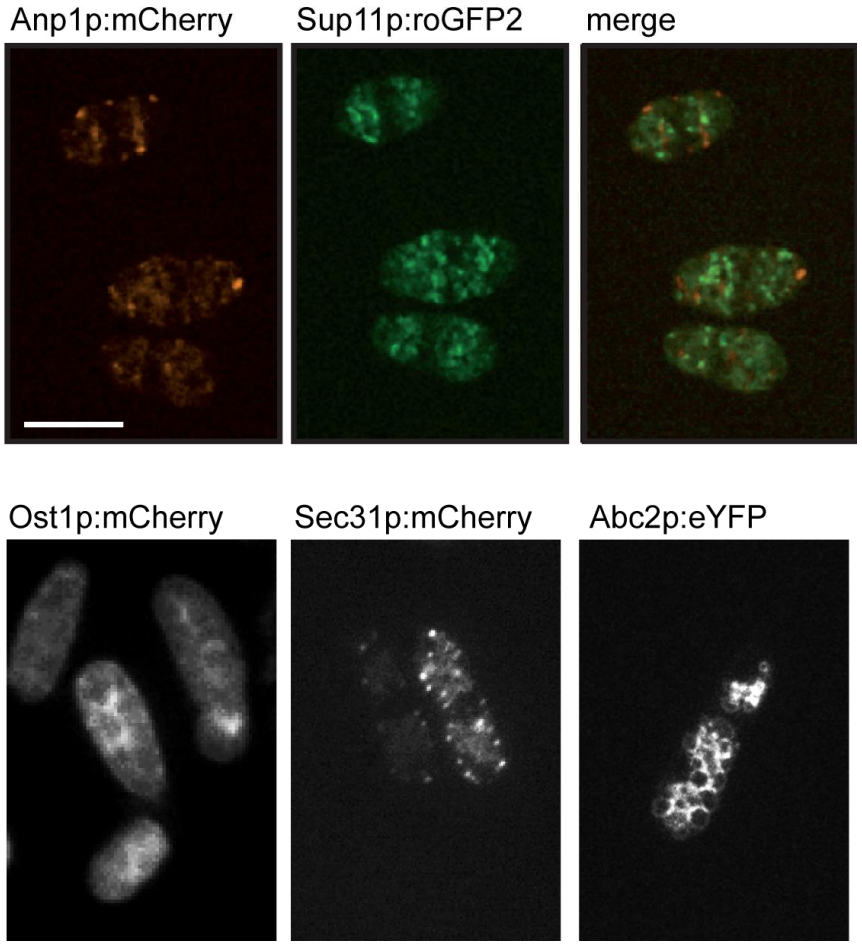

Fig. 5.26: Microscopic analysis of strain Sup11p:roGFP2/Anp1p:mCherry (LWY13) and other organelle markers for comparison:
Confocal fluorescent microscopy of a strain with genomically Sup11p:roGFP2/Anp1:mCherry tags. Independent strains with various organelle markers were for comparison of the obtained fluorescent pattern. Ost1p:mCherry was used as ER-marker, Sec31p:mCherry for detection of ER-exit sites, and Abc2p:eYFP was used as vacuole marker. (scale bar = 10 µm).

5.9.2. Subcellular localization of Sup11p using immunolabeling

Tagged proteins can be visualized for subcellular localization by decoration with a fluorochrome-labeled antibody directed against epitopes of the tag (e.g. HA- or HIS-tag). Sup11p ought to be subcellulary localized by using indirect immunofluorescence labeling of HA-tagged versions.

The functional genomically HA-tagged version of Sup11p was used for indirect immonofuorescence analysis. Due to possible low endogenous expression level of Sup11p (as indicated by analysis of the genomically tagged Sup11p:roGFP2), also a wild type strain carrying an overexpression plasmid of the HA-tagged Sup11p was analyzed.

Cell walls and membranes of methanol fixed cells were permeabilized to allow efficient immunolabeling. α-tubulin labeling served as internal technical control. Fluorescence signals were obtained with both, the genomically Sup11p:HA-tagged strain as well as the overexpressed Sup11p:HA protein (Fig. 5.27).

The strain overexpressing Sup11p:HA showed a bright fluorescence signal of an ER-like structure (Fig. 5.27). However, trapping of Sup11p:HA in the ER might likely be due to the high overexpression which might cause impaired protein folding/ processing and subsequently the unfolded/ unprocessed protein gets retained inside the ER.

In contrast, the endogenously expressed Sup11p:HA version showed a spotted, more vesicle-like pattern (Fig. 5.27). The labeling was significantly above background staining (Fig. 5.27). The observed spotted pattern of the genomically expressed Sup11p:HA is supporting a localization in the secretory pathway in an post-ER compartment.

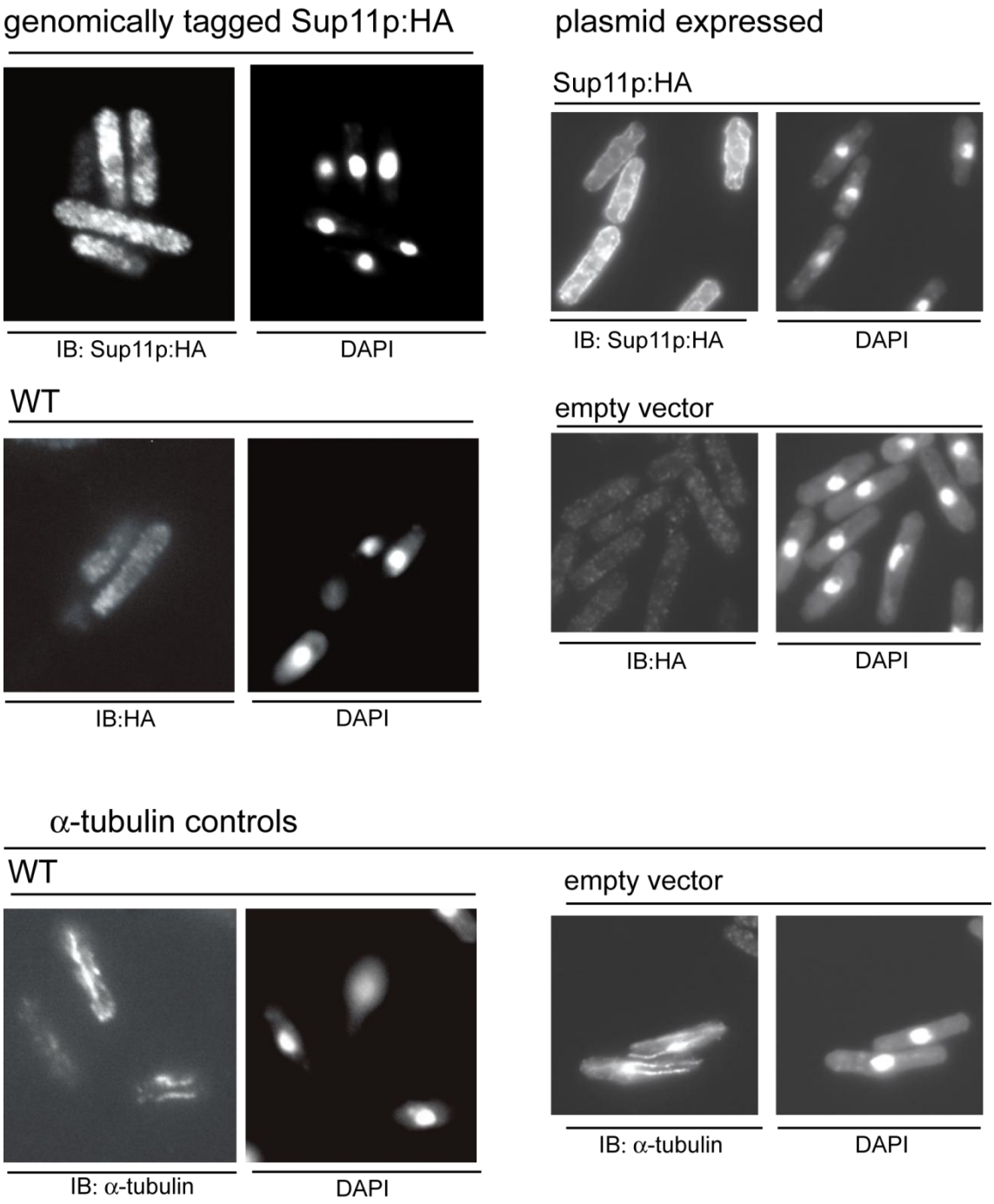

Fig. 5.27: Sub-cellular localization of Sup11p:HA by immunofluorescence labeling:
For detection of HA-tagged Sup11p, fixed and prepared cells were decorated with a monoclonal anti-HA and anti-mouse Alexafluor488 coupled secondary antibody. As technical control for the assay α-tubulin was labeled with an anti-α-tubulin antibody and detected with anti-mouse Alexafluor488 coupled antibody. The nuclei were DAPI stained. (scale bar = 10 µm).

To avoid unspecific cross reaction of the HA-tag, a polyclonal antibody against Sup11p epitopes ought to be raised. *In silico* analysis for Sup11p predicted up to three TMDs (see Fig. 5.1). Peptide sequences that were predicted to be soluble regions were used for construction of the immunization fusion-protein. Two glutathion-S-transferase (GST)

fusion proteins of soluble Sup11p domains were designed and used for rabbit immunization (Fig. 5.28). However, the serum obtained from the immunized rabbits failed to detect Sup11p and could not be used in subsequent experiments.

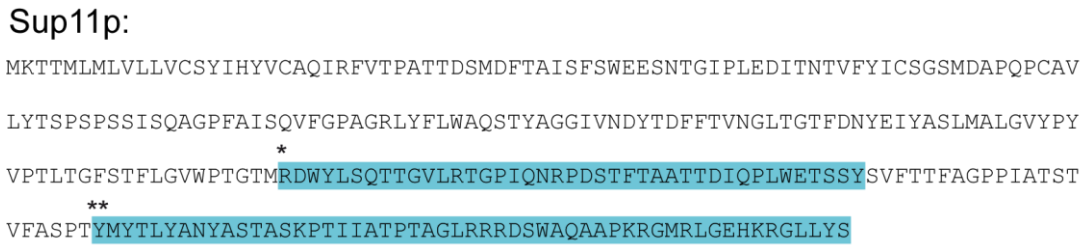

Fig. 5.28: Sup11p protein sequences chosen for antigen production and antigen purification: Selected peptide sequences of Sup11p for antigen production as GST-fusion proteins are indicated in blue (* antigen1 = pLW52 (R170-Y210) and ** antigen region 2 = pLW51 (Y232-S284)).

5.9.3. Cellular fractionation via sucrose density gradient centrifugation

A common method employed to clarify the intracellular localization of membrane proteins is by isopycnic centrifugation on a continuous sucrose density gradient. This technique enables the separation of organelles and microsomes derived from different organelles like ER, Golgi apparatus, vacuole and PM due to their accumulation in fractions of distinct densities. To obtain information about the organelle which includes Sup11p, a variety of tagged marker-proteins and Sup11p:HA were fractionated by centrifugation on a 18-60% sucrose density gradient. But density centrifugation alone was not sufficient to distinguish between Golgi apparatus and ER derived membranes. To differentiate between those two organelles it was necessary to analyse the crude membranes in two separate batches: One contained $MgCl_2$ to stabilize ribosome binding to the rough ER and another one contained EDTA to sequester $MgCl_2$ which leads to disassociation of the ribosomes from the ER (Pryme, 1986).

In this experiment different expression plasmids and tagged strains were used for organelle markers. Genomically GFP-tagged Bgs1p of strain SP519 was used for PM identification. Oma1p:HA of pLW106 was used as ER marker, Gms1p:CFP from pAU-gms1:CFP which is an UDP-galactose transporter localized to the Golgi membrane (Tabuchi *et al.*, 1997; Tanaka and Takegawa, 2001). Sup11p:HA was expressed from the plasmid pLW109. Since there was no strain expressing all of the marker proteins, each vector was transformed into the wild type yeast and strains were

cultured separately. The cells expressing the marker proteins and Sup11p:HA were mixed prior to membrane preparation.

Membranes were isolated either in presence of $MgCl_2$ or in presence of EDTA. Membrane preparations were loaded onto sucrose gradients and fractionated via centrifugation. The gradient was fractioned after centrifugation starting from the top. 14 aliquots were taken from the top (14) to bottom (1). Usually the bottom fractions 1-6 contain PM and ER derived membranes, followed by Golgi membranes (fraction ~7-9) and tonoplast fragments in the top fractions (~10-14) (Vida *et al.*, 1993; Votsmeier and Gallwitz, 2001).

Western blot analysis of the 14 fractions revealed that all tagged proteins density shifted upon EDTA treatment although only the Oma1p:HA ER-marker should shift and be retained in a more dense sucrose fraction than in the $MgCl_2$ treated gradient. But even the distribution of the Golgi-marker Gms1p:CFP and the protein of interest - Sup11p:HA - changed upon EDTA treatment (Fig. 5.29 A).

Western blot analysis of the sucrose gradients fractions containing $MgCl_2$ (Fig. 5.29 B) showed that ER-marker Oma1p:HA and the Golgi-maker Gms1p:CFP fractionated in one main peak each. The ER-marker peaked in fraction 2 and the Golgi-maker in fraction 3. The most similar co-fractionation of Sup11p:HA was obtained with the PM localized Bgs1p:GFP. Both proteins peaked twice: Bgs1p:GFP in fraction 2 and 5 and Sup11p:HA in fraction 2 and 4. The similar fractionation of Bgs1p:GFP and Sup11p:HA suggested a PM localization for Sup11p.

However, this picture changed upon fractionation in presence of EDTA (Fig. 5.29 A). Both proteins fraction showed only one peak each and the protein concentration of the two proteins spiked in very different fractions. Whereas the peak of Bgs1p:GFP significantly shifted to a lower density in fraction 5, Sup11p:HA appeared in the higher density fraction 3. This difference demonstrated that both proteins resided in different organelles. The Sup11p:HA peak did not correlate with any of the EDTA treated microsomes which allowed the conclusion that Sup11p does neither reside in ER, nor the Golgi, nor the PM. The fluorescence pattern of ER-exit sites (Sec31p:mCherry) and cis-Golgi (Anp1p:mCherry) looked different to Sup11p:roGFP2 (see Fig. 5.26). However, Sup11p contains an ER-signal sequence and thus follows the secretory pathway and immunoflourescence labelling showed a spotted vesicle-like pattern. Together these data suggest localization of Sup11p in the late Golgi or trans-Golgi network.

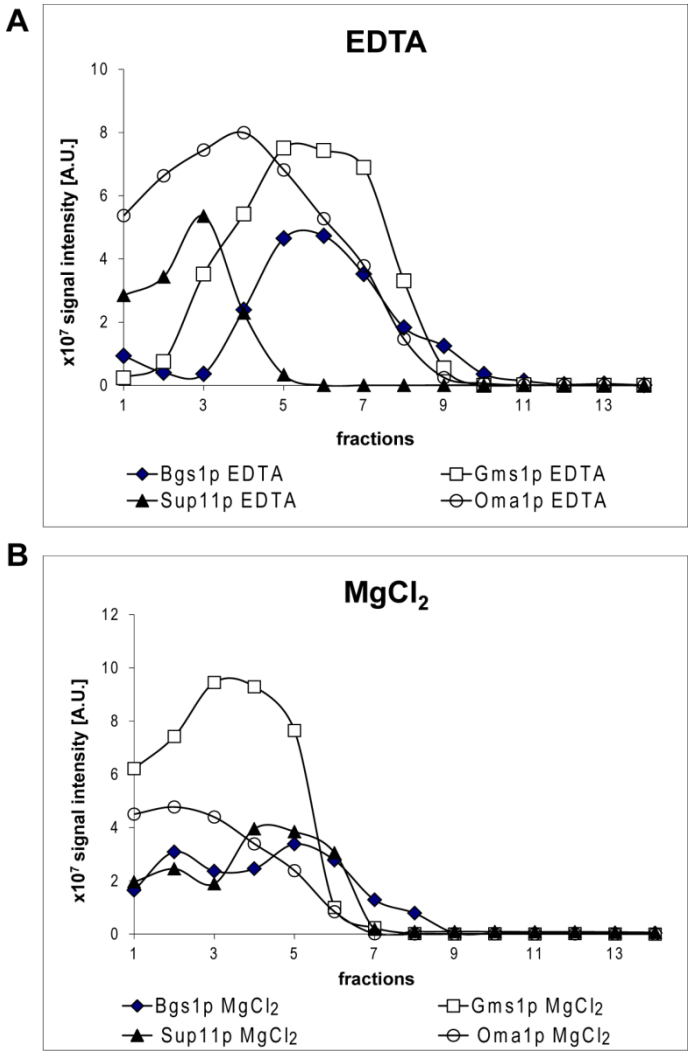

Fig. 5.29: Compartmental fragmentation by sucrose density gradient:
Differentiation between subcellular compartments by sucrose density gradient centrifugation. 14 gradient fractions were collected and analysed via Western blot. Signal intensities were quantified using the Fiji Software and illustrated in the upper diagrams. Equal samples were loaded on gradient (A) and (B) starting with the bottom fraction (1) to the top fraction (14). Membrane isolation and gradients were done in the presence of 10 mM $MgCl_2$ (A) or 5 mM EDTA (B).

5.10. Topology analysis of Sup11p showed that the protein is oriented luminal and anchored via signal anchor sequence

The topology of Sup11p is an important protein feature because it determines the compartmental orientation of the conserved C-terminal Kre9-domain. Since *in silico* prediction models are ambiguous and suggest 1 to 3 TMDs, the topology of Sup11p needs to be experimentally resolved.

The genomically tagged redox sensitive strain LWY12 (Sup11:roGFP2) which is described in chapter 5.14.1 was used as topology reporter for Sup11p. The redox sensitivity of the roGFP2 enables to distinguish whether the tag resides in a reducing (cytosol) and oxidizing (ER/ Golgi apparatus) compartment. This can be determined by excitation of the fluorophore with two distinct wavelengths and ratiometric calculation of the emitted light intensities. The calculated ratio allows deciding whether the fluorochrome is in its reduced or oxidized state and therefore facing the cytosol or luminal side of the ER/ Golgi, respectively (Meyer and Dick, 2010). Ratiometric measurements analyzing the genomically Sup11p:roGFP2 mutant (LWY12) showed that the redox sensitive C-terminal tag is indeed facing the lumen of an oxidizing compartment (Fig. 5.30 A).

In addition to that, a proteinase K protection assay revealed that not only the very C-terminus is microsome protected from protease degradation, but the whole protein is. Microsomes were prepared for this assay using a method that promotes microsome formation with right-side out orientation. Proteinase K treatment was applied to the microsomes to determine whether the investigated tag is protected inside the vesicle or digested. Analysis of the type II membrane protein Anp1p:mCherry used as a control showed a size shift of the microsome protected Anp1p:mCherry. Likewise the lower molecular weight product increased of over time. Addition of the detergent Triton-X-100 causes rapid destruction of the microsomes and thus complete digestion of Anp1p:mCherry (Fig. 5.30 B). In case of Sup11p:roGFP2 no size shift was observed over time by applying proteinase K digestion. The addition of Trition-X-100 results in complete digestion of Sup11p:roGFP2 (Fig. 5.30 B).

This showed that the full length Sup11p:roGFP2 protein is protected from proteinase K digestion inside the microsome lumen.

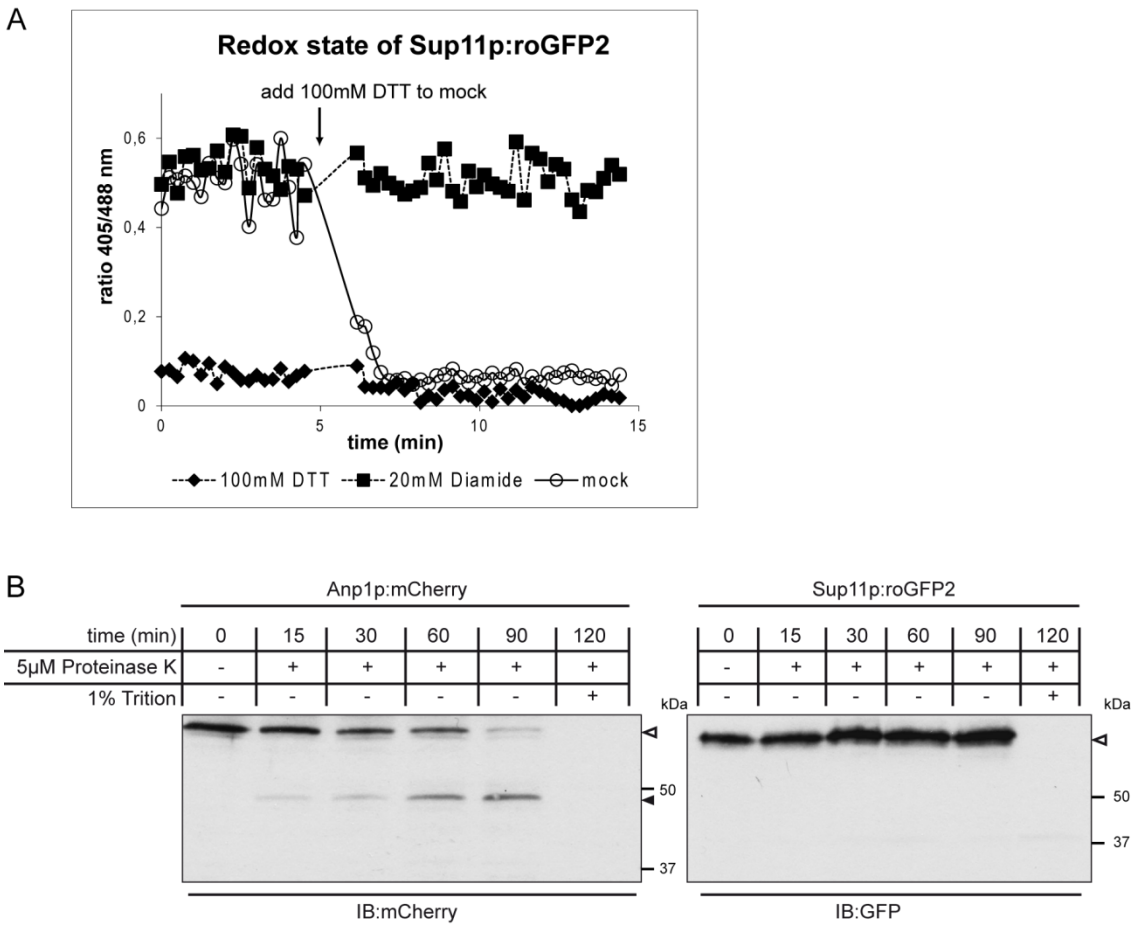

Fig. 5.30: Topology analysis of Sup11p with tagged versions:
(A) Ratiometric measurement analyzing 20 OD whole cells of Sup11p:roGFP2 (LWY12) in a 96 well plate. Emission intensities ratio by excitation of 405 and 488 nm as depicted in the diagram allows to distinguish between reduced (100 mM DTT) and oxidized (20 mM diamide) form of Sup11p:roGFP2 in the controls. To the untreaded sample (mock) 100 mM DTT was added at 5 min. (B) On the left panel proteinase K protection assay performed with 0.1 OD microsomes from Anp1p:mCherry (SO2412) and Sup11p:roGFP2 (LWY12). Full length Anp1p:mCherry (blank arrowhead) is gradually digested to a smaller, microsome protected peptide with proteinase K treatment (filled arrowhead). Addition of 1% Trition-X-100 leads to complete digestion. Performance of the proteinase K assay with Sup11p:roGFP2 showed no size shift over time (blank arrowhead) but a complete digestion upon Triton-X-100 addition. Decoration of the blot was done with anti-RFP (1:5000) and anti-Rabbit IgG peroxidase conjugate (1:5000) for Anp1p:mCherry detection. Sup11p:roGFP2 was decorated with anti-GFP (1:5000) and anti-Rabbit IgG peroxidase conjugate (1:5000).

The obtained results favor a topology for Sup11p with none of the predicted TMDs but a membrane anchorage via signal anchor sequence of the non-cleaved SS. Another possibility would be that one of the predicted TMDs is not membrane spanning but forms an amphipathic helix that dips into the lipid bilayer. *In silico* analysis using Heliquest analyzing the putative TMDs I, II and II showed that it is highly unlikely that the hydrophobic regions actually form TMDs because there is at least one proline in each of those regions which would break the α-helical structure (data not shown). The PRALINE prediction tool was used to identify peptide sequences of Sup11p which are

likely to form α-helices or β-sheets. These results suggest that only the signal sequence forms an α-helix long enough so span the lipid bilayer and therefore actually function as a TMD (Fig. 5.31 A).

The signal sequence itself is highly hydrophobic and therefore - if not cleaved - capable to anchor Sup11p by acting as signal anchor sequence.

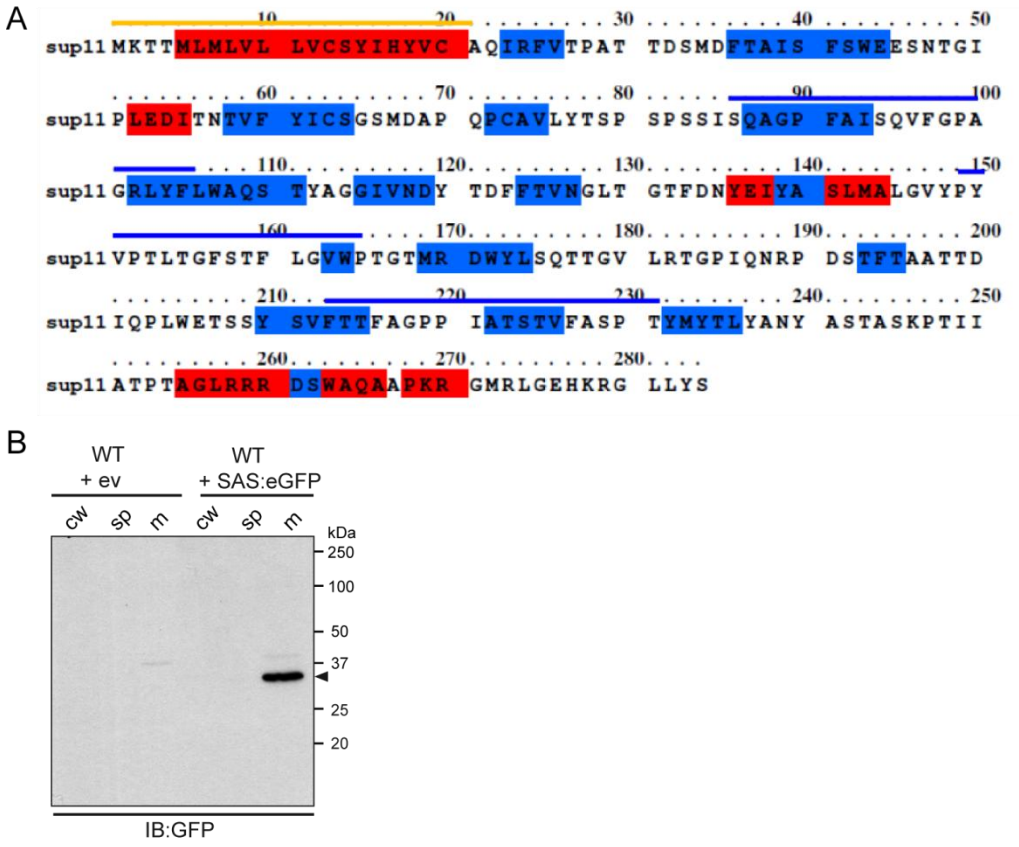

Fig. 5.31: *In silico* topology prediction of Sup11p and membrane association of truncated Sup11p:eGFP:
(A) Prediction of α-helices (red aa) or β-sheet (blue aa) forming primary sequence of Sup11p by online tool PRALINE. Bars above the protein sequence indicate signal sequence (orange) and putative TMDs (blue). (B) Western blot of a cell fraction from a wild type expressing eGFP-tagged signal anchor sequence (1-77 aa of Sup11p) (pLW147) or the empty vector (ev) (pLW65). 0.5 OD cell wall extracts (CW), 0.1 OD soluble proteins (sp) and 0.5 OD total membranes (m) were analysed. Blot was decorated with anti-GFP (1:5000) and anti-Rabbit IgG peroxidase conjugate (1:5000).

In order to analyze whether or not the N-terminal signal sequence is indeed not cleaved and thus can functions as signal anchor sequence, a truncated Sup11p version was constructed. For the reporter construct eGFP was C-terminally fused to aa 1-77 of Sup11p. This Sup11p sequence consists of the signal sequence plus 56 aa which are prior to the first predicted TMD. The reporter construct was expressed in the wild type background. Analysis of fractionated cell lysates via Western blot demonstrated

membrane association due to a signal anchor sequence since the reporter construct remained exclusively in the membrane fraction (Fig. 5.31 B).
Together, these data demonstrated that the entire Sup11p resides inside the lumen of a compartment with oxidizing environment, most likely the late Golgi apparatus or a post-Golgi compartment, and that Sup11p is membrane anchored via its signal anchor sequence.

To finally validate that Sup11p is membrane anchored via signal anchor sequence, *N*-glycosylation site scanning of Sup11p was performed. The endogenous *S. pombe* protein Sup11p is not *N*-glycosylated and does not possess a N-X-S/T sequon. In this experiment three artificial sequons were introduced by side directed mutagenesis whose usage will depend on the existence of either two TMDs plus signal anchor sequence or only the signal anchor sequence. The artificial sequons were introduced at positions L181N (I), P190N (II) and I250N (III) (Fig. 5.32 A). Sequon III was designed as positive control and ought to be modified in every of the possible topology models. In case of a signal anchor sequence anchorage of Sup11p, sequons I and II are subjects for *N*-glycosylation machinery modification. If Sup11p contains TMDs these sites are on the cytosolic side and cannot be modified (Fig. 5.32 B).
EndoH treatment with isolated membrane fractions from cells expressing the different reporter constructs showed that the artificial sequons I and II were modified but not sequon III (Fig. 5.37 C). The interpretation of the obtained results was ambiguous. On the one hand modification of *N*-glycosylation sites I (L181N) and II (P190N) supported the topology with Sup11p anchorage via signal anchor sequence. On the other hand, the artificial *N*-glycosylation site III (I250N) is located in the Kre9-domain and was designed as positive control, since experiments had shown luminal orientation of the Kre9-domain (see Fig. 5.30). However, the artificial *N*-glycosylation site III (I250N) was not modified (Fig. 5.32 C) suggesting that the artificial *N*-glycosylation site III (I250N) is somehow masked for the *N*-glycosylation machinery.

It was previously shown that *O*-glycosylation can prevent the *N*-glycosylation of sequons in S/T-rich regions (Ecker *et al.*, 2003). There are some S/T-rich stretches 198-254 inside the Kre9-domain (see Fig. 5.1) of Sup11p close to the artificial *N*-glycosylation site that makes this region prone to *O*-mannosylation.

To elucidate whether the artificial sequon III is blocked due to prior *O*-mannosylation, the construct with the artificial *N*-glycosylation III (I250N) was expressed in an *oma4*Δ background. Western blot analysis of crude membrane preparations showed an additional band to the glycosylation pattern of Sup11p:HA at 39 kDa (Fig. 5.32 D). This product was sensitive towards EndoH treatment demonstrating an additional *N*-glycosylation site usage for construct III (I250N).

In summary, the topology experiments showed that Sup11p:HA is anchored via signal anchor sequence and luminally oriented.

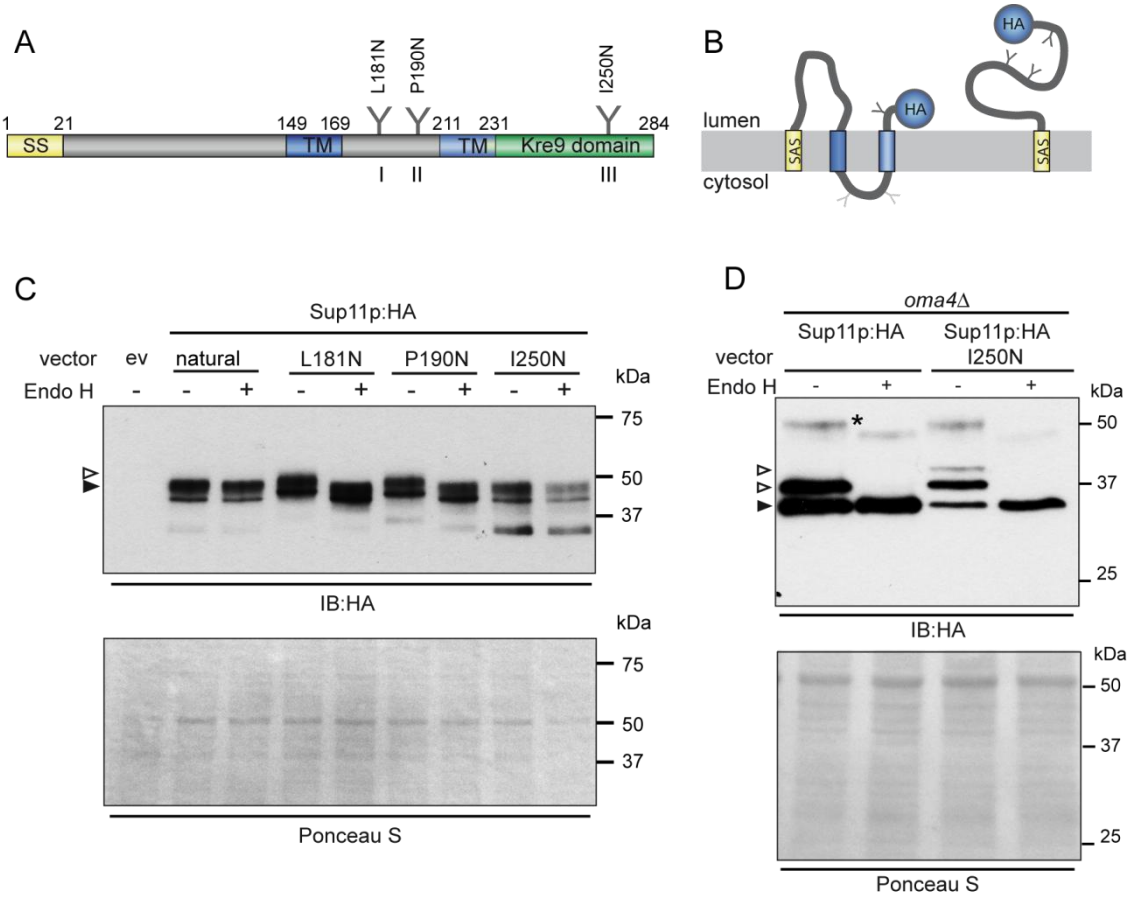

Fig. 5.32: scanning of Sup11p to solve its topology:
(A) Schematic representation of Sup11p. Positioning the sites of artificial sequons for *N*-glycosylation introduced via side directed mutagenesis are depicted as Y. Artificial site I exchanges L181N, II substitutes P190N and III exchanges I250N to gain N-X-S/T sequons in the Sup11p protein sequence. (B) Sequon usage of artificial *N*-glycosylation sites by the given topology of two TMDs (left model) or anchorage via signal anchor sequence (right model). Sides that could potentially be glycosylated assuming the depicted topology models are depicted in dark gray and non-glycosylated sequons are depicted in light gray. (C) *N*-glycosylation site usage was determined via Western blot analysis. 0.1 OD of total membranes of plasmid expressed Sup11p:HA with and without artificial *N*-glycosylation site (natural) were treated with and without EndoH before SDS-PAGE to determine *N*-glycosylation of each sequon. (D) *N*-glycosylation state of vector expressed Sup11p:HA and Sup11p:HA I250N were analysed in *oma4*Δ background. N-glycosylated versions of Sup11p are indicated by blank arrowhead and the deglycosylated versions of Sup11p:HA are indicated by filled arrowhead.
The Blots were decorated with monoclonal anti-HA antibody (1:5000) and anti-mouse IgG peroxidase conjugate (1:5000).

5.11. Sup11p:HA is a O*-mannoprotein and its expression influences the growth of* O*-mannosyl transferase mutants*

Due to its S/T-rich region, the Sup11p is likely to be substrate of the *O*-mannosylation machinery. Moreover, *sup11*$^{+}$ was identified as multi-copy suppressor of a conditional lethal nmt81-*oma2* mutant which demonstrated a connection between Sup11p and *O*-mannosylation. Preliminary analysis indicated that Sup11p:HA is modified by PMT-family members (Hutzler, 2009).

In this study, detailed Western blot analysis of total membranes isolated form genomically HA-tagged *sup11*$^{+}$ demonstrated that Sup11p:HA is *O*-mannosylated to different extent by all three members of the PMT-family (Fig. 5.33). There are also two distinct Sup11p:HA degradation products of ~28 kDa (Sup11p:HA-deg.) in some membrane preparations. The occurrence of the Sup11p:HA-deg. products was depending on the quality of membrane preparation and storage. There was also an increase of the degradation products upon repeated freeze/ thaw cycles of the membrane preparations.

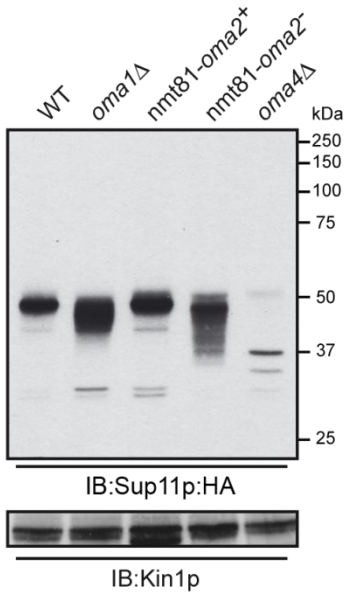

Fig. 5.33: Sup11p:HA is hypo-mannosylated in *oma*-mutants:
Western blot analysis detecting genomically tagged Sup11p:HA in WT, *oma1*Δ, *oma4*Δ and restricted or permissive nmt81-*oma2* backgrounds. 0.1 OD total membrane preparations of each sample were analyzed. Kin1p was used as loading control.

Compared to the Sup11p:HA modified by wild type and the permissive nmt81-*oma2* mutant background, the Sup11p:HA which was modified by the *oma1*Δ strain and the restricted nmt81-*oma2* mutant showed a different degree of hypo-mannosylation. The hypo-mannosylation is visible by the lower molecular weight "smear" in the lanes with both mutant membranes (Fig. 5.33). Since the nmt81-promoter cannot be repressed

completely (Siam *et al.*, 2004), there is still some residual Oma2p activity left in the nmt81-*oma2* mutant even under restricted conditions. Analysis of the glycosylation state of Sup11p:HA after restriction of the nmt81-promoter-controlled *oma2*$^{+}$ showed that a high molecular weight form of Sup11p was available for more than 12h after shut down. However, the apparent molecular weight of the major protein fraction slightly decreases by 3kDa (Fig. 5.34, filled arrow).

After 16h of *oma2*$^{+}$ restriction, increased hypo-mannosylation was visible in a low molecular weight "smear". Also increased protein degradation was observed since the total amount of Sup11p:HA diminished significantly (Fig. 5.34). However, there is a minor fraction of Sup11p:HA whose apparent molecular weight is not decreasing upon Oma2p depletion (Fig. 5.34, blank arrow) and from its low signal intensity, compared to total Sup11p:HA amounts, it resembles the Sup11p:HA+*N*+*O* which was detected in the *oma4*Δ background (see Fig 5.33). Whether or not this product is also *N*-glycosylated in the restricted nmt81-*oma2* mutant needs to be analyzed by EndoH treatment in future experiments. Nevertheless, this experiment demonstrated that depletion of Oma2p is sufficient to cause a significant hypo-mannosylation of Sup11p:HA.

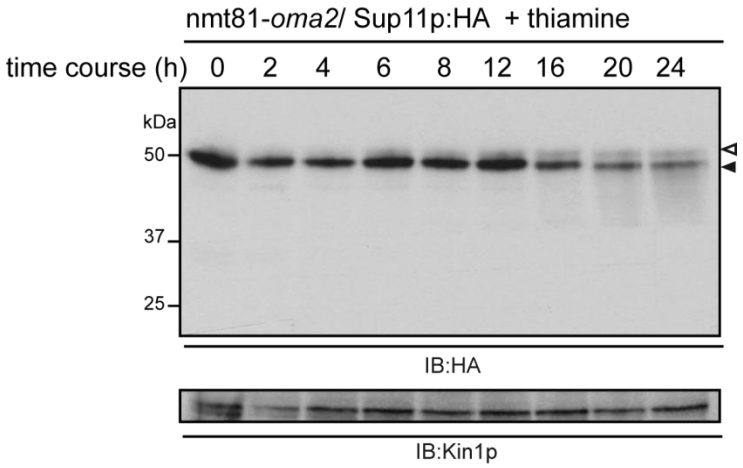

Fig. 5.34: Sup11p is hypo-mannosylated in *oma*-mutants and stability is decreased in restricted nmt81-*oma2* mutant:
(A) Western blot analysis detecting genomically tagged Sup11p:HA in WT, *oma1*Δ, *oma4*Δ and restricted or permissive nmt81-*oma2* backgrounds. 0.1 OD total membrane preparations of each sample were analyzed. Kin1p was used as loading control. (B) Protein levels of Sup11p:HA were monitored on Western blot of 0.1 OD total membranes of nmt81-*oma2*/Sup11p:HA upon restriction. Kin1p was used as loading control.
Sup11p:HA was detected by decoration with monoclonal anti-HA antibody (1:5000) and anti-mouse IgG peroxidase conjugate (1:5000). Kin1p was decorated with polyclonal anti-Kin1p antibody (1:3000) and anti-Rabbit IgG peroxidase conjugate (1:5000).

Besides the regularly modified Sup11p:HA which was detected in wild type and permissive nmt81-*oma2* mutant membranes, there was also a minor but distinct fraction of a hypo-mannosylated sub-form (hyp*O*-Sup11p:HA). Whether the hyp*O*-Sup11p:HA sub-form is also present in the *oma1*Δ and the restricted nmt81-*oma2* mutant background cannot be determined from Western blot analysis since it would be running with the "smear" of under-mannosylated Sup11p:HA (Fig. 5.5).

Although applying identical growth and membrane preparation conditions, the intensity of the hyp*O*-Sup11p:HA was varying in different experiments. However, the stability of hyp*O*-Sup11p:HA was unaffected by repeated freeze/ thaw cycles. These data suggests that hyp*O*-Sup11p:HA is rather a specific sub-population of Sup11p:HA than a degradation product.

The most significant hypo-mannosylation of Sup11p:HA was observed in an *oma4*Δ mutant (Fig. 5.5). Hardly any highly glycosylated protein of approximately 50 kDa (Sup11p:HA+*N*+*O*) is detectable in this strain background. Although the Sup11p:HA of the wild type and Sup11p:HA+*N*+*O* in the *oma4*Δ mutant share a similar apparent molecular weight, they differ regarding their glycosylation which is demonstrated in chapter 5.16.

Instead, the majority of Sup11p:HA in an *oma4*Δ mutant is present in two distinct products of roughly 36 kDa (Sup11p:HA+*N*) and 32 kDa (ngSup11p:HA). The size of ngSup11p:HA corresponds to the calculated molecular weight of the non-modified protein and can be regarded as such. The nature of Sup11p:HA+*N* is also further addressed in chapter 5.11.

There are several hypo-glycosylated/ deglycosylated versions of Sup11p:HA which will be discussed in the course of this study. To specifically address each Sup11p:HA variant, abbreviation will be given to the most common sub-forms and listed in table 5.10.

Band #	MW (kDa)	Endo H	Strain	Description	Abbreviation
1	48	-	Wild type	WT *O*-mannosylated Sup11p:HA	Sup11p:HA
2	43	-	Wild type	WT hypo *O*-mannosylated Sup11p:HA sub-form	hyp*O*-Sup11p:HA
3	28	-	*oma4*Δ	Sup11p:HA-degradation	Sup11p:HA-deg.
4	32	-	*oma4*Δ	Non-glycosylated Sup11p:HA	ngSup11p:HA
5	36	+	*oma4*Δ	*N*-glycosylated Sup11p:HA	Sup11p:HA+*N*
6	52	+	*oma4*Δ	*N*-glycosylated and *O*-glycosylated Sup11p:HA	Sup11p:HA+*N*+*O*
7	50	-	*oma4*Δ	*O*-glycosylated Sup11p:HA	Sup11p:HA- *N*+*O*

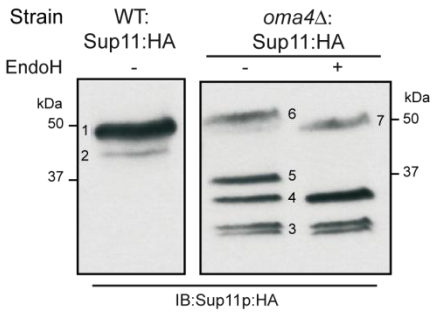

Table 5.10: Abbreviations given to specific Sup11p:HA variants detected in *O*-mannosyl transferase mutant and wild type:
Sub-forms of Sup11p:HA are shown in the Western blot on the left. Numbers indicate the Sup11p:HA sub-form found in the wild type and in an *oma4*Δ background and are listed in the above table. Correspondent molecular weight of the sub-forms plus EndoH-sensitivity are shown and the given abbreviations are listed in the table.

The following experiments were designed to answer the question whether an elevated level of Sup11p can also rescue the depletion of other *O*-mannosyl transferase genes than *oma2*$^+$ in fission yeast. Moreover, the effect of *sup11*$^+$-overexpression in the nmt81-*oma2* background was analyzed in more detail.

A spotting assay showed that the nmt81-*oma2* *sup11*$^+$-overexpressing mutant was delayed in growth compared to the empty vector control and wild type (Fig. 5.35, upper panel). The observation of impaired growth of the nmt81-*oma2* mutant due to *sup11*$^+$ overexpression indicated a contrary effect to the data obtained by Hutzler (2009) in which *sup11*$^+$ overexpression improved vitality of the nmt81-*oma2* mutant. Protein stability analysis of the protein *O*-mannosyl transferases Oma1p and Oma4p over 12 h revealed that these proteins have a long half-life. To analyze this, conditional repressible strains with HA-tagged versions of Oma1p and Oma4p (nmt81-*oma1*$^+$:HA and nmt81-*oma4*$^+$:HA) were shifted to restrictive conditions and protein stability was followed via Western blot (data not shown). These data indicated that possibly Oma2p has also a long half-life. For this reason, a spotting assay was performed using thiamine pre-treated cultures (Fig. 5.35, lower panel). Cells of the nmt81-*oma2* strain were cultured for 24 and 48 h in under restricted conditions prior to the spotting assay. The

thiamine pre-treatment demonstrated that the nmt81-*oma2* cells overexpressing *sup11*$^+$ do have an advantage compared to the control strain transformed with the empty vector when the *de novo* synthesis of Oma2p has been inhibited for more than 24 h (Fig. 5.35, lower panel). This indicated that Oma2p is - like Oma1p and Oma4p - a stable protein which needs to be degraded upon thiamine repression before the positive growth effect of *sup11*$^+$ overexpression can be observed.

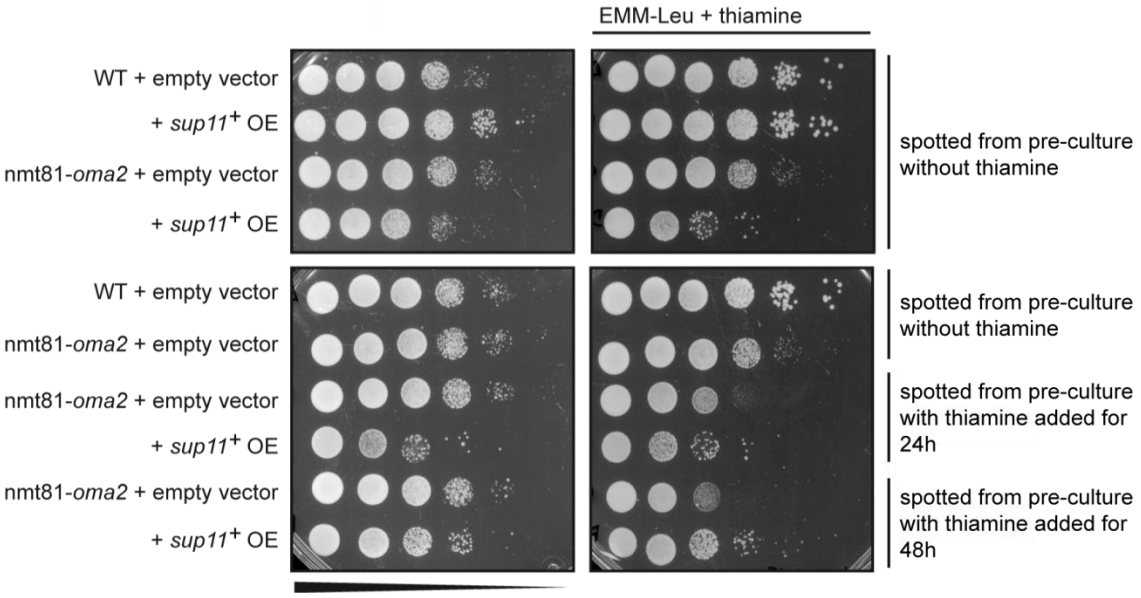

Fig. 5.35: *sup11*$^+$ overexpression influences growth of restricted nmt81-*oma2* mutant:
Pre-cultures of wild type and nmt81-*oma2* with overexpression vector of *sup11*$^+$ or empty vector were grown under permissive conditions and spotted directly on EMM plates without and with thiamine (upper panel). Plates were incubated for three days at 32°C. In the lower panel pre-cultures of nmt81-*oma2* mutant strains were grown under restricted conditions for 24 or 48 h prior to spotting on selection plates. (serial dilution 1:10 starting from 100.000 cells)

Further, the effect of *sup11*$^+$ overexpression in an *oma1*Δ and *oma4*Δ background was investigated.

Sup11p overexpression under permissive temperature caused a delayed growth of single deletion mutants of *oma1*Δ and *oma4*Δ, but not wild type indicating a Sup11p dosage dependent phenotype in the *O*-mannosyl transferase mutants (Fig. 5.36, left panel). It had been observed that deletion of *oma1*$^+$ results in a temperature sensitive phenotype (Willer *et al.*, 2005). Elevated temperature did not noticeably influence the delayed growth of the *oma4*Δ but caused lethality of the *oma1*Δ (Fig. 5.36, right panel). The lethality of the conditional lethal triple-*oma* mutant could also not be rescued by overexpression of *sup11*$^+$ (Fig. 5.37).

Together these data demonstrate that overexpression of *sup11*$^+$ exhibits a dosage dependent phenotype. Overexpression of *sup11*$^+$ had generally a negative growth effect on mutants which were deficient in protein *O*-mannosylation (*oma1*Δ, *oma4*Δ, nmt81-*oma2*) compared to wild type which showed no effect (see Fig. 5.36 and Fig. 5.35). However, if Omap2 falls below a critical threshold in the restricted nmt81-*oma2* mutant, overexpression of *sup11*$^+$ becomes beneficial and rescues lethality.

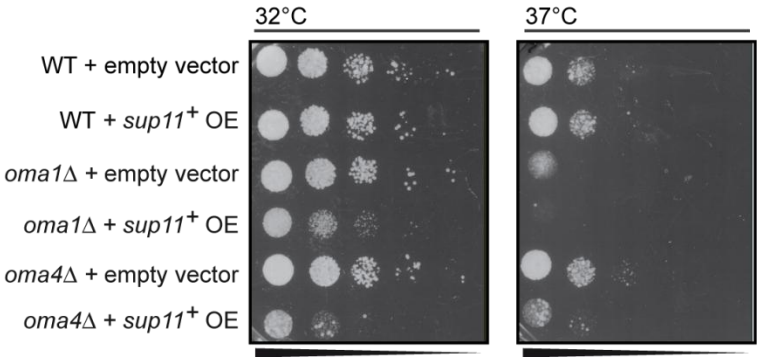

Fig. 5.36: overexpression of *sup11*$^+$ causes growth delay in *oma1*Δ and *oma4*Δ:
Spotting assay with serial dilution (1:10) starting from 100.000 cells of WT, *oma1*Δ and *oma4*Δ strains. Controls with the empty vector grew comparable under standard conditions at 32°C (left panel) and elevated temperature of 37°C (right panel).

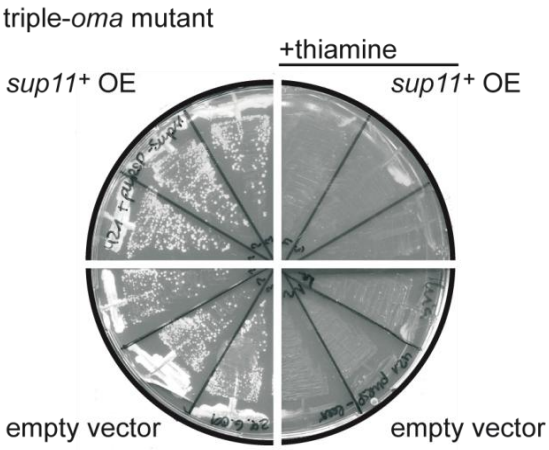

Fig. 5.37: *sup11*$^+$ over-expression does not rescue triple-*oma* mutant from lethality:
Triple-*oma* mutant with an episomal copy of *sup11*$^+$ and the empty vector on EMM plates without (left half) and with thiamine (right half). Cells were restreaked three times on each plate.

5.11. Unusual N*-glycosylation of Sup11p:HA in the* oma4*Δ mutant background*

It was shown that the artificial *N*-glycosylation site (I250N) located in a S/T-rich region can only be modified in an *oma4*Δ background but not in wild type (see Fig. 5.37 D). Thus, the experiments gave evidence that *N*- and *O*-glycosylation are also in competition to each other in *S. pombe* as it was previously demonstrated for *S. cerevisiae* (Ecker *et al.*, 2003).

The *N*-glycosylation site scanning experiments revealed that there are glycosylated Sup11p:HA versions which were actually *N*-glycosylated in the *oma4*Δ mutant background. This was shown by trimming Sup11p:HA+*N* to the a smaller Sup11p:HA product (ngSup11p:HA) that corresponds to the calculated molecular weight of the unmodified protein using EndoH digestion (Fig. 5.37 D). Nevertheless, the detected *N*-glycan of Sup11p:HA+*N* in the *oma4*Δ background was unexpected because there is no common *N*-glycosylation sequon N-X-S/T in the primary sequence of Sup11p. Interestingly, the highly glycosylated subform Sup11p:HA+*N*+*O* of the *oma4*Δ strain was also sensitive to EndoH digestion (Fig. 5.38 A). A genomic C-terminal Sup11p:ro2GFP-tag in the *oma4*Δ background did not give a fluorescent signal for subcellular localization of the hypo-mannosylated Sup11p versions (data not shown).

Because there is no common sequon in Sup11p, it was considered that an unusual *N*-glycosylation site such as N-X-C, N-X-G or N-X-V might be recognized and modified by the OST (Gavel and Heijne, 1990; Zielinska *et al.*, 2010). Indeed, a "rare" sequon N-X-G is present in the primary sequence of Sup11p at aa position 47. Another asparagine (N239) is located in the Kre9-domain (Fig. 5.38 B). The Kre9-region is the region of the highest homology among *Sp*Sup11p and *Sc*Kre9, is S/T-rich and known to be heavily *O*-mannosylated in *S. cerevisiae* (Brown and Bussy, 1993). Due to severe hypo-mannosylation of Sup11p:HA in the *oma4*Δ background the N239 might be accessible to the OST and modified.

In order to examine both potential *N*-glycosylation sites for unusual *N*-glycosylation, constructs with single aa-exchanges of N47Q or N239Q were created and constitutively expressed in the *oma4*Δ background (Fig. 5.38 B). Western blot analysis showed that *N*-glycosylation is absent in N239Q variant but is unaffected by N47Q substitution (Fig. 5.38 C). This demonstrated that in case of missing Oma4p *O*-mannosylation a N-Y-A sequon at position 239 is recognized by OST.

In wild type, the Sup11p:HA is heavily *O*-mannosylated. In case of severe hypo-mannosylation, as observed in the *oma4*Δ background, the unusual N-glycosylation site can be modified since it is not masked by *O*-mannosylation.

An interesting observation on Western blot indicated, that the unusual *N*-glycosylation might affect stability of Sup11p:HA. The obtained signals of the N239Q variant were

about ten times less intense than with the variants which could be *N*-glycosylated in the *oma4*Δ background (Fig. 5.38 C).

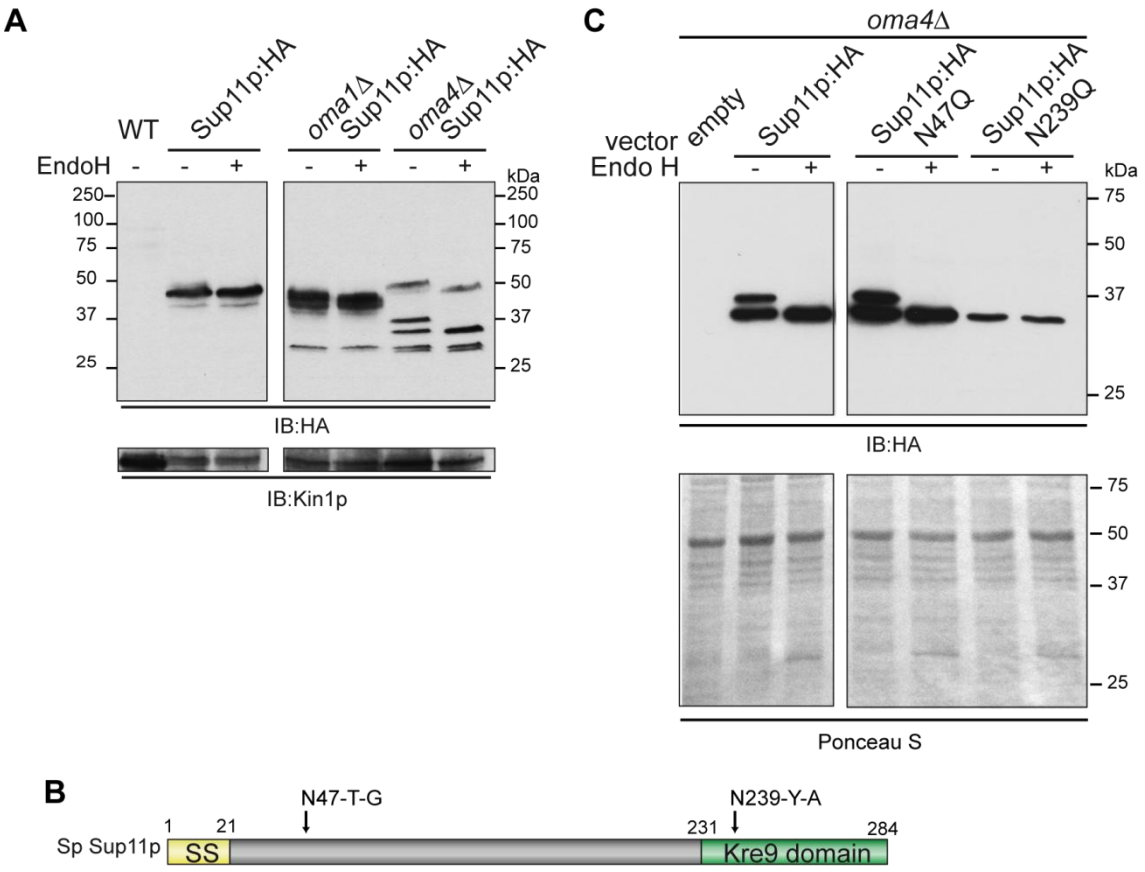

Fig. 5.38: scanning and mutation of Sup11p identified unusual sequon usage in *oma4*Δ strain background:
(A) Western blot with total membranes of genomically HA-tagged Sup11 in WT, *oma1*Δ and *oma4*Δ background. 0.1 OD equivalents of total membrane preparations were EndoH or mock treated. *N*-glycosylation of Sup11p:HA was detected only in *oma4*Δ background, indicated by filled arrowheads. Unmodified version of Sup11p:HA indicated by blank arrowhead. Kin1p, PM associated protein, was used as loading control. (B) Putative alternative sequons of Sup11p that might be modified in the *oma4*Δ background were mutated by exchange of N47Q or N239Q. (C) 0.1 OD total membranes were EndoH treated and analyzed by Western blot. Thereby the unusual sequon of Sup11p that is used in the *oma4*Δ strain was identified (N239). PonceauS staining of the membrane is shown as loading control.
Sup11p:HA was detected by decoration with monoclonal anti-HA antibody (1:5000) and anti-mouse IgG peroxidase conjugate (1:5000). Kin1p was decorated with polyclonal anti-Kin1p antibody (1:3000) and anti-Rabbit IgG peroxidase conjugate (1:5000).

The signal intensities of the Sup11p:HA expression pattern in *oma*-mutants (see Fig. 5.33) indicated that *O*-mannosylation positively influences stability of the protein. In order to analyze this, protein stability of Sup11p:HA was followed after block of protein biosynthesis in the *oma4*Δ background using a cycloheximide chase experiment. Quantification of Western blot signals intensities brought evidence that the glycosylation state of Sup11p:HA contributes to protein stability (Fig. 5.39 A). The

signals of the hypo-mannosylated Sup11p:HA+*N* and the ngSup11p:HA were clearly fainting faster upon cycloheximide treatment than the high molecular weight sub-form Sup11p:HA+*N*+*O* and the wild type Sup11p:HA (Fig. 5.39 B). In fact, the Sup11p:HA+*N*+*O* in the *oma4*Δ background was observed to be extremely stable, even more than wild type the Sup11p:HA (Fig. 5.39 B). Comparing protein stability of subforms Sup11p:HA+*N* and ngSup11p:HA, it could be demonstrated that *N*-glycosylation prolonged the half-time.

The cycloheximide chase experiments revealed that protein glycosylation positively influences the Sup11p:HA stability and that these kind of modifications can significantly prolong the half-life of Sup11p:HA variants.

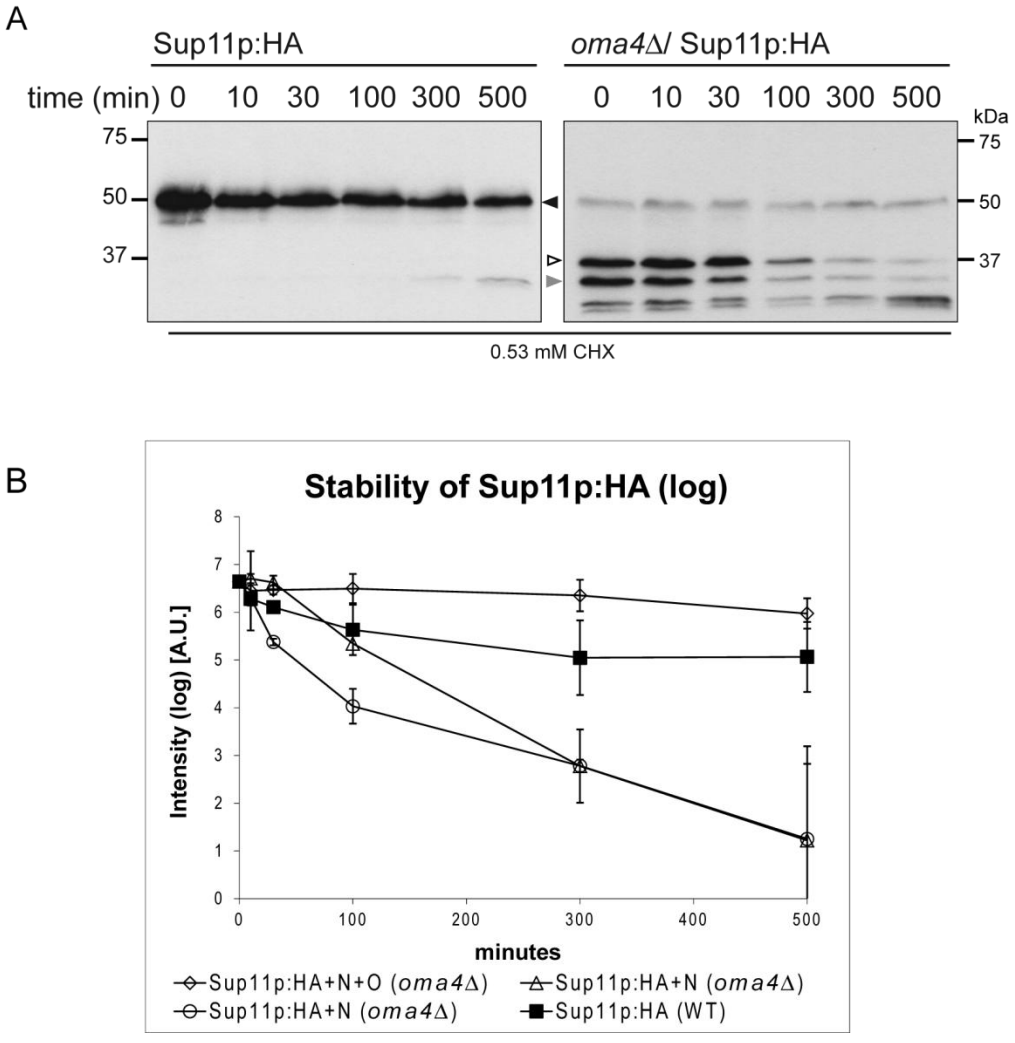

Fig. 5.39: Stability of Sup11p:HA is depending on the glycosylation state of the protein:
(A) Western blot detecting genomically tagged Sup11p:HA in the wild type and the *oma4*Δ background upon cycloheximide (CHX) addition. 0.1 OD total membranes of several time points after CHX treatment were collected and loaded on SDS-PAGE. Sup11p:HA modified in wild type is indicated by filled black arrowhead. Sup11p:HA+*N* is indicated by blank arrowhead, non-glycosylated ngSup11p:HA by gray arrowhead and highly modified Sup11p:HA+*N*+*O* is indicated by filled brown arrowhead.

Sup11p:HA was detected by decoration with monoclonal anti-HA antibody (1:5000) and anti-mouse IgG peroxidase conjugate (1:5000). (B) Diagram illustrating the signal intensities over time due to CHX treatment obtained by Western blot. (Quantification of signal intensities was done with the Fiji program)

Taken together, these data demonstrate that *O*-mannosylation of essential Sup11p affects stability and/or protein folding. Sup11p exhibited the highest degree of hypo-mannosylation in an *oma4*Δ background. Yet, this mutant was viable which suggested that even the *oma4*Δ hypo-mannosylated Sup11p has some residual activity.

Since the restricted nmt81-*oma2* mutant is lethal, the hypo-mannosylation in this strain background might reduce Sup11p activity below a critical threshold. Besides, it is likely that the restricted nmt81-*oma2* mutant accumulated too many defects caused by protein hypo-mannosylation - including under-mannosylated Sup11p related defects - which in consequence caused lethality. However, due to overexpression elevated levels of *sup11*$^{+}$ were able to compensate for the reduced activity of the hypo-mannosylated Sup11p to re-cross the defect threshold and restore viability. This possibly is the mechanism which allows *sup11*$^{+}$ to act as a multicopy-suppressor for the restricted nmt81-*oma2* mutant.

Furthermore, overexpression of *sup11*$^{+}$ was not beneficial for the growth of an *oma1*Δ or *oma4*Δ mutant, whereas the wild type remained unaffected (see Fig. 5.36). This indicated that an elevated level of Sup11p in mutants of the PMT-family is generally of disadvantage.

*5.12. Characterization of a triple-*oma *mutant*

A vital connection between protein *O*-mannosylation and Sup11p was indicated since lethality of a restricted nmt81-*oma2* mutant could be restored by *sup11*$^{+}$ overexpression. Moreover, this study showed that Sup11p is modified by all *O*-mannosyl transferases and that overexpression of Sup11p has a generally effects growth in PMT-family mutants.

To answer the question whether an elevated level of Sup11p can also rescue the simultaneous depletion of all three *O*-mannosyl transferase genes in *S. pombe*, a conditional lethal triple-*oma* mutant was created (Fabian, 2009). In this mutant the *oma1*$^{+}$ gene is disrupted by a *his3*$^{+}$ cassette and *oma2*$^{+}$ and *oma4*$^{+}$ are under the control of the conditional repressible nmt81-promoter. Transcriptional shut-down of the nmt81-controlled *oma2*$^{+}$ and *oma4*$^{+}$ was demonstrated via Northern blot analysis for the single mutants which were used to create the triple-*oma* mutant (Fabian, 2009).

However, a transcriptome analysis performed in this study of the triple-*oma* mutant after 16 h of repression showed that the there is still a significant amount of transcript present. The transcript level of *oma2*$^{+}$ was still at 39% and of *oma4*$^{+}$ even at 47% compared to the non-restricted level. In the triple-*oma* mutant the *oma1*$^{+}$ is not deleted but disrupted and thus the non-functional disruption-transcript was detected by the array. The expression level of the disrupted transcript was shown to be more than fourfold (4.207) up-regulated under restricted conditions compared permissive conditions (Table 5.11). Sup11p was not significantly regulated on transcriptional level (0.942 fold). However, a high p-value of 0.5172 indicated that the response of *sup11*+ differed a lot in the three biological replicates used for the transcriptome analysis.

Protein *O*-mannosyl transferases				
Regulation	**p-value**	**Systematic Name**	**Gene Name**	**Gene Product**
4.207	0.0000	SPAC22A12.07c	*oma1*	protein O-mannosyl transferase Oma1
0.473	0.0001	SPBC16C6.09	*oma4*	protein O-mannosyl transferase Oma4
0.389	0.0000	SPAPB1E7.09	*oma2*	protein O-mannosyl transferase Oma2

Table 5.11: Up- of down-regulated protein *O*-mannosyl transferase genes in the triple-*oma* mutant: Regulation of *O*-mannosyl transferase genes as shown in the transcriptome analysis comparing the expression of restricted and non-restricted triple-*oma* mutant. *oma2*$^{+}$ and *oma4*$^{+}$ are under the control of the nmt81-promoter and *oma1*$^{+}$ is disrupted.
The systematic names and gene products are listed in the table. Significantly up-regulated genes (depicted in dark red) and significantly down-regulated genes (depicted in dark green) that are annotated to function in fungal-type cell wall.
The systematic names, p-values, gene names and gene products are listed in the table. Permissive expression level of selected genes equals 1.0.

For detailed morphological characterization of the triple-*oma* mutant, cells were grown under permissive conditions to exponential phase prior to restriction. Under permissive condition the culture exhibited a comparable growth rate like the wild type (data not shown).

Upon repression, the observed phenotype was documented in more detail than in previous studies in 3 h intervals. Oma1p and Oma4p have been shown to be highly stable, showing no significant degradation over 12 h in a shut-down experiment (data not shown). Therefore, the first morphological changes of the restricted triple-*oma* mutant could be followed earliest 6 h after shut-down (equates approximately 2 cell divisions). The observed initial defects were of moderate nature. 5% of the cells tent to assemble multiple septa and built up chains of four to five cells (Fig. 5.40). It was observed that these cell clusters can fall apart when given additional time to complete

the separation process (Fig. 5.40, filled arrowheads). In the subsequent hours of repression cells with multiple septa disappeared completely from the culture. Instead, the triple-*oma* mutant cells were prone to accumulate extra cell wall material which could cover approximately up to one fifth of the total cell volume. The incorporated wall material was stainable with aniline blue indicating a significant incorporation of linear β-1,3-glucan to the cell wall. These depositions were preferentially located to the cell poles but were also found in the septum region. It also needs to be mentioned, that dead cell often appeared in pairs, like they deceased during or right after completion of the septum separation process (Fig. 5.40, double asterisk).

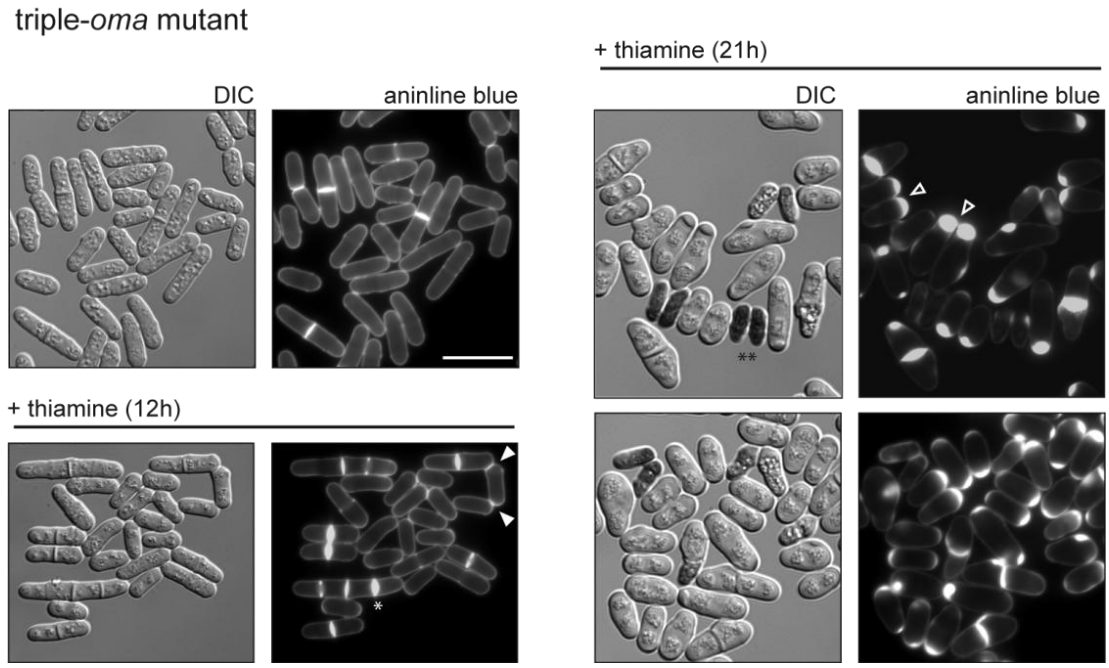

Fig. 5.40: Microscopic analysis of triple-*oma* mutant:
Under permissive conditions the triple-*oma* mutant (*oma1*:Dis/nmt81-*oma2*/nmt81-*oma4*) exhibits no visible phenotype neither in differential contrast (DIC) nor with aniline blue staining (upper left panel). Upon restriction of *oma2*$^{+}$ and *oma4*$^{+}$ for 12 h (lower left panel) a minor fraction of the culture exhibits multi-septed cells (asterisk) which are able to complete separation after prolonged time (filled arrowheads). After 21 h of repression the triple-*oma* mutant suffers sever cell wall accumulations at the poles (blank arrowheads). Cells also lose their rod like shape and look swollen at their septum region. Dead cells tent to appear in pairs (double asterisk).

Quantification of the phenotype showed that the non-repressed triple-*oma* mutant behaves similarly to wild type. Roughly 20% of cells showed one septum and 80% single cells were counted in an exponentially growing culture. However, depletion of all three *oma*$^{+}$-genes caused severe malformations of the cells. Over time it was observed that the initial multiple septum phenotype only appears between 6 to 12 h repression and then suddenly the percentage of cells with deposition rises drastically. After

inhibiting the *de novo* synthesis of *O*-mannosyl transferases for more than 21 h, all cells in the culture contained cell wall depositions (more than 80%) and/or are deceased (approximately 15%) (Fig. 5.41).

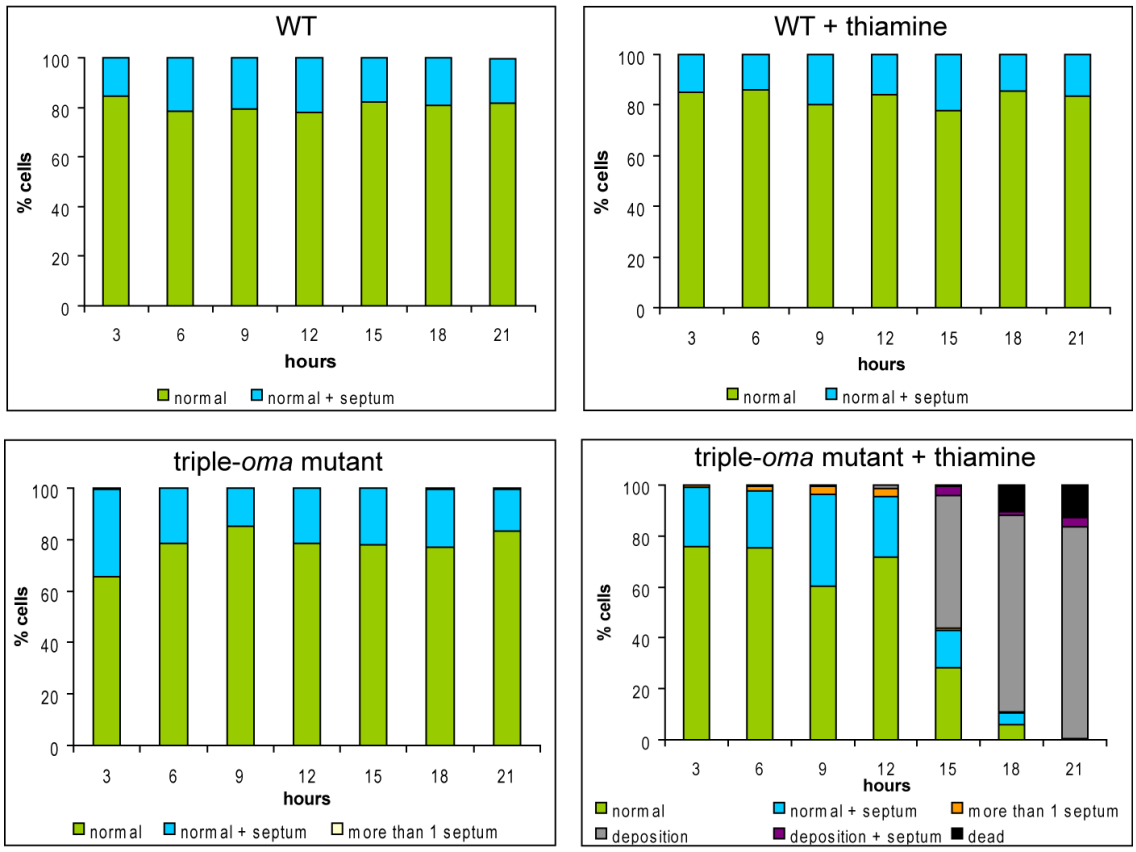

Fig. 5.41: Quantification of triple-*oma* mutant phenotypes:
Phenotypic evaluation over 21h of the triple-*oma* mutant compared to the wild type with and without addition of thiamine to the medium. Aniline blue stained cells were analyzed under microscope and distinguished between aberrancies cell walls and septa.
n = 796 for WT, n = 631 for WT + thiamine, n = 569 for triple-*oma* mutant, n = 861 for triple-*oma* mutant + thiamine.

6. Discussion

The major goal of this thesis was to characterize the *sup11*$^+$ gene product that was identified in a multicopy-suppressor screen to rescue *S. pombe oma2* knock-down cells from lethality (Hutzler, 2009). This study showed that Sup11p is an essential gene with a key functions in β-1,6-glucan biosynthesis and correct septum assembly. Moreover, it was demonstrated that depletion of Sup11p led to induction of stress responses connected to cell wall stress and an abnormal cell wall glucan composition. Sup11p itself is membrane anchored via SAS and localized inside the lumen of a post-Golgi compartment. In addition, it was shown that in an *oma4Δ* background the Sup11p can receive a *N*-linked glycosylation at an unusual N-Y-A *N*-glycosylation site inside the conserved Kre9-domain at aa position 239. Furthermore, it was demonstrated that stability of Sup11p is depending on its glycosylation.

6.1. Sup11p is an essential gene

This detailed study demonstrated that the fission yeast *sup11*$^+$ is an essential gene. Its product shows some homology to members of the *S. cerevisiae* Kre9-family (Kre9 and Knh1) based on *in silico* analysis (see Fig. 5.1) with the highest homology in their Kre9-domains. A function of the Kre9-domain has not been described yet, neither in *S. cerevisiae* nor *S. pombe*. However, a not further characterized role in β-1,6-glucan synthesis was demonstrated for the *S. cerevisiae* Kre9-family members (Brown and Bussey, 1993).

In this work was demonstrated that fission yeast Sup11p is crucial for spore viability and germination. Still, roughly 25% of the non-colony forming *sup11*Δ:KanMX/*sup11*$^+$ spores were able to undergo limited cell divisions. In those cells, the cell separation process seemed to be severely impaired. They exhibited a roundish morphology and the cells were forming clusters (see Fig. 5.3 B). This observation indicated that the amount of Sup11p, which was inherited from the mother cell, enables some of the daughter cells to germinate and undergo few cell divisions. However, cells without a functional copy of *sup11*$^+$ were unable to establish viable colonies.

In a genome wide profiling of *S. cerevisiae* genes was reported that *KRE9* is an essential gene in the S288C background (Giaever *et al.*, 2002). However, in the initial *ScKRE9* characterization using the strain backgrounds SEY6210 and TA405, *kre9*Δ mutants

were viable (Brown and Bussey, 1993). EM analysis of the viable *kre9*Δ mutants revealed that the cells had an altered cell wall ultrastructure. It appeared that the cell wall lost the outer mannoprotein layer which is usually observed in wild type cells (Brown and Bussey, 1993). Moreover, it was reported that *kre9*Δ mutants were hypersensitive towards Zymolyase treatment (Brown and Bussey, 1993) supporting the crucial role for Kre9 in correct cell wall formation of *S. cerevisiae*. The *ScKRE9* homologue gene *ScKNH1* was shown to function as multicopy-suppressor of a *kre9*Δ null mutant by suppressing the growth defect phenotype and conferring K1 killer toxin sensitivity (Dijkgraaf *et al.*, 1996). Possibly the functional homologue *ScKNH1* can fill in for loss of Kre9 in the viable *kre9*Δ strain backgrounds. There is no such compensatory mechanism between Kre9-family members in *S. pombe*, since *sup11*$^{+}$ is only homologue. Thus, the deletion of *sup11*$^{+}$ is lethal.

6.2. Sup11p is involved in cell wall formation and crucial for β-1,6-glucan synthesis

6.2.1. Fission yeast cell wall integrity depends on Sup11p

The fungal cell wall is the main defense from environmental hazards. The fission yeast morphology and cell wall integrity is depending on a sound cell wall protein- and polysaccharide network. The unobstructed interplay of all cell wall components provides cell wall matrix rigidity and thereby maintaining its morphology and function (Latgé, 2007). Mutants with an altered cell wall often exhibit defects upon treatment with cell wall stressing agents like caffeine, calcofluor white, congo red, SDS or treatment with Zymolyase (β-1,3-glucanase). Moreover, cell wall mutants likely are impaired when exposed to environmental stress conditions for example elevated temperature or osmotic challenge (reviewed in Klis *et al.*, 2002).

This study revealed increased temperature sensitivity of the nmt81-*sup11* mutant under restricted conditions. In *S. cerevisiae*, a known response to thermal stress is the accumulation of cytosolic trehalose in order to protect proteins from heat denaturation (Neves and François, 1992). Amongst other genes, elevated expression level (4.026 fold) of a predicted α,α -trehalose-phosphate synthase (SPAC22F8.05) were identified in the restricted nmt81-*sup11*. This data indicated that trehalose levels might

be increased as a stress response in the restricted nmt81-*sup11* mutant. However, this needs to be elucidated in the future by metabolomics analysis.

Moreover, it is reported that cell wall stress conditions like elevated temperature activate certain stress responses in *S. cerevisiae.* Heat stress responses have been extensively studied in baker's yeast (Gasch *et al.*, 2000; Causton *et al.*, 2001). Amongst other responses, the cell wall integrity (CWI) pathway can be induced upon stresses like heat or osmotic changes (Kamada *et al.*, 1995; Madrid *et al.*, 2006). The CWI pathway is conserved among fungi and its key cascade is the Pkc1-activated mitogen-activated protein (MAP) kinase cascade which in the end promotes for example the expression of cell wall synthesizing genes like *FKS1*/ *FKS2,* subunits for β-1,3-glucan synthesis (reviewed in Levin, 2005; reviewed in Fuchs and Mylonakis, 2009).

Similarly, it was shown for both fission yeast CWI MAPK genes $pck1^{+}$ and $pck2^{+}$ to genetically interact with $bgs1^{+}$ (Arellano *et al.*, 1999), the *S. pombe* homologue of *Sc*Fks1. Moreover, heat stress CWI-activated kinases Mkh1p, Pek1p, and Pmk1p localize in the cell division area (Madrid *et al.*, 2006). It is speculated that active Pmk1p might interact with glucan synthases which are responsible for the building of the primary or secondary septa (e.g., Bgs1p) (Madrid *et al.*, 2006). Indeed, analysis of the restricted nmt81-*sup11* mutant revealed that several glucan modifying enzymes were changed in their expression in order to compensate CWI defects. For example, Bgs1p which is responsible for establishing the primary septum and which is also active during polarized growth (Liu *et al.*, 1999; Cortés *et al.*, 2002) was up-regulated in the restricted nmt81-*sup11* mutant.

However, previous studies in *S. cerevisiae* indicated that the CWI signaling pathway is not sensing the temperature change directly. It is postulated that Pkc1 activation is rather a secondary response effect caused by high temperature exposure (Kamada *et al.*, 1995). For *S. cerevisiae PMT*-mutants it was demonstrated that the CWI is impaired due to failed signaling by the Pkc1-activating sensors which are normally highly *O*-mannosylated in wild type (Lommel *et al.*, 2004).

In the restricted nmt81-*sup11* mutant there was no change in the expression of enzymes involved in the CWI signaling. Though, activation of the CWI pathway not necessarily implies up-regulation of the involved MAPKs on transcriptional level since their regulation is due to phosphorylation or dephosphorylation rather than on their gene expression. Activation of the CWI is more likely to be observed by analyzing changes

in its target genes like *bgs1*$^{+}$. There were also expression changes of fungal-type cell wall proteins including cell wall glucan modifying enzymes (e.g. Bgl2p, Mok13p) and cell surface glycoproteins (e.g., Mug135p) indicating that there is a general remodeling of the nmt81-*sup11* mutant cell wall matrix.

The fact that Sup11p depletion negatively affects cell wall integrity was further supported by the increased sensitivity of the nmt81-*sup11* knock-down mutant towards cell wall stressing agent SDS (Hutzler, 2009). This strong anionic detergent interferes with the integrity of the PM. It was also reported that the presence of SDS causes more trouble to cell wall mutants than to the wild type with a rigid cell wall matrix (Shimizu *et al.*, 1994; Igual *et al.*, 1996). Furthermore, nmt81-*sup11* mutants showed an increased resistance towards gradual Zymolyase treatment compared to the wild type cells (Hutzler, 2009), indicating that Sup11p depletion promotes an abnormal distribution of β-1,3-glucan.

6.2.2. Sup11p is needed for β-1,6-glucan synthesis

This study revealed that the cell wall β-1,6-glucan is not detectable in the restricted nmt81-*sup11* mutant (see Fig. 5.13). It is likely that the absence of the β-1,6-glucan caused the decrease in β-glucan to α-glucan ratio as observed in the preliminary cell wall analysis by Hutzler (2009). In agreement to these data, the α-1,3-glucan synthase gene *mok13*$^{+}$ was identified to be up-regulated (3.329 fold) in the restricted nmt81-*sup11* mutant.

Data presented in this study demonstrated that Sup11p is a key component for β-1,6-glucan synthesis like it had been shown for the *S. cerevisiae* homolog Kre9 - along with other members of the Kre-family (Brown *et al.*, 1993). Even though the members involved in *S. cerevisiae* β-1,6-glucan synthesis have been identified a long time ago, it is still uncertain which enzyme actually catalyzes the formation of β-1,6-glucan polymers of that are smaller than 350 glucose residues (Shahinian and Bussey, 2000; Lesage and Bussey, 2006).

In addition, contribution of Sup11p in the β-1,6-glucan synthesis was supported by genetic interactions with two members of the *S. pombe* glycoside hydrolase family 5 (GH5) - Exg1p and Exg2p. These genes were initially identified and

characterized by Duenas-Santero and co-workers (2010). They demonstrated endo-β-1,6-glucanase activity against β-1,6-glucans for Exg1p and Exg3p, but they detected no such activity for Exg2p. *exg1*$^{+}$ showed a periodic expression pattern during the cell cycle with an expression peak during the separation process. However, the proteins of the GH5 family did not appear to perform an essential role in cell wall organization since deletion of *exg*$^{+}$-genes exhibited no apparent growth phenotype and no altered cell wall composition (Duenas-Santero *et al.*, 2010). Solely overexpression of *exg2*$^{+}$ led to a visible phenotype with accumulation of septum material in the septum center and poles. The phenotype observed closely resembles the septum malformation of the restricted nmt81-*sup11* mutant. This septum deposition phenotype in the septum center has never been observed by any other cell wall mutant and is exclusively documented for the restricted nmt81-*sup11* mutant and for overexpression of *exg2*$^{+}$ in wild type. Moreover, it was shown that the *exg2*$^{+}$ overexpression alters the cell wall composition by accumulation of increased amounts of α- and β-glucans (α-glucan increased from 11.5% to 19.4%; β-glucan 17.9% to 25.2%) (Duenas-Santero *et al.*, 2010). However, despite being a member of the GH5 family, there is no direct evidence for β-1,6-glucanase activity for Exg2p. This indicates that strains with *exg2*$^{+}$ overexpression lack the ability to properly coordinate glucan polymer synthesis. The authors speculate that not specified glucan synthases produce an excess of cell wall material under above mentioned conditions (Duenas-Santero *et al.*, 2010).

Phenotypic analysis of *exg2*$^{+}$ overexpression in a nmt81-*sup11* background showed additive morphological defects (see Fig. 5.15) which were more severe than in the single mutant and the wild type overexpressing *exg2*$^{+}$. This is in agreement with the model that Exg2p coordinates β-1,6-glucan degradation and thus elevated Exg2p levels promote enhanced glucanases activity. In combination with the diminished β-1,6-glucan level of the restricted nmt81-*sup11* mutant the observed cell wall defect phenotype is more pronounced (see Fig. 5.15).

Comparing the growth of the nmt81-*sup11* mutant (restricted and permissive conditions) and wild type under *exg2*$^{+}$ overexpression, revealed that elevated Exg2p levels caused delayed growth of the nmt81-*sup11* mutant already under permissive conditions. However, under restricted conditions a minor growth improvement of the mutant compared to the empty vector was observed (see Fig. 5.16), suggesting that

elevated *exg2*$^{+}$ support nmt81-*sup11* vitality. Microscopic phenotype analysis revealed additive cell wall and septum malformation due to overexpression of *exg2*$^{+}$ in the nmt81-*sup11* mutant. The observation that the cells accumulate additional morphological defects but show improved growth indicated that some kind of compensatory mechanism is triggered in the *exg2*$^{+}$ overexpressing nmt81-*sup11* mutant. Wild type growth remained unaffected by *exg2*$^{+}$ overexpression indicating that no compensatory mechanism is triggered in this background.

Additional genetic interactions of *sup11*$^{+}$ and GH5-family members were demonstrated by analyzing double the mutants nmt81-*sup11/exg1*Δ and nmt81-*sup11/exg2*Δ. Comparing the growth phenotype in a spotting assay revealed that the double-mutants grew noticeably better under *sup11*$^{+}$-restricting conditions than the single nmt81-*sup11* mutant. This indicated, that the due to deletion of *exg1*Δ or *exg2*Δ reduced β-1,6-glucanase activity was beneficial to restore the β-1,6-glucan homeostasis in a Sup11p depleted background. However, similar to the *exg2*$^{+}$ overexpression in the nmt81-*sup11* mutant the double-mutants showed additive morphological defects in microscopic analysis.
These findings indicated an activation of a compensatory process. A rescue mechanism might be triggered when too many cell wall defects accumulate and a certain threshold is reached. A similar mechanism was reported for a *S. cerevisiae ccw12*Δ mutant (Hagen *et al.*, 2004). It is postulated that the combined deletion of cell wall relevant genes accumulates minor defects which are in combination severe enough to trigger rescue mechanisms and consequently stabilizes the cell wall. A compensatory process of similar nature might be activated in the *exg1*Δ, *exg2*Δ and *exg2*$^{+}$ overexpression in the nmt81-*sup11* background which is not triggered in the single mutants. A mechanism like that could explain the rescued growth phenotype of the multiple mutants in the spotting assay which is almost comparable to wild type.

Taken together, data shown in this study illustrate that Sup11p depletion caused changes in the cell wall glucan composition with absence of β-1,6-glucan. In consequence of the altered cell wall composition, stress responses were triggered and transcriptional regulation of cell wall glucan modeling enzymes is induced in order to maintain a functional cell wall.

6.3. Sup11p is crucial for correct septum formation

This study demonstrates that Sup11p depletion causes septum malformation with massive accumulations of cell wall material at the septum center and mainly one pole. These depositions were sensitive to aniline blue staining demonstrating that they contained linear β-1,3-glucan. Thus, the distribution of this polysaccharide was no longer restricted to the usually defined primary septum but present in the entire septum. It appeared that there was generally more linear β-1,3-glucan in the mutant cell wall under restricted than under permissive conditions. However, these data remain to be investigated in more detail on statistical level (analyzing more immunogold labeled cells of independent experiments) in order to make a clear statement about the linear β-1,3-glucan distribution in the nmt81-*sup11* mutant cell wall. Due to a limited availability of images this was not possible so far.

It was shown that the start of the septum formation was comparable to the wild type until the septum was closed (see Fig. 5.8). The depositions started to accumulate in the restricted nmt81-*sup11* mutant after the septum had already been closed. This pointed to problems occurring upon septum closure and the beginning of the septum separation. Indeed, the septum separation process was prolonged in the restricted nmt81-*sup11* mutant (~90 min) compared to the wild type (~20 min). After extended time, also cells carrying massive septum depositions were able to finish the separation process. However, one of the two daughter cells was likely to lyse during the separation. It was observed that the surviving cell carries a major fraction of the deposition material at its new end in from of a pole deposition indicating a defective septum splitting.

The so far discussed results lead to the question: Why is the restricted nmt81-*sup11* mutant accumulating such massive amounts of linear β-1,3-glucan at the septum center? Besides linear β-1,3-glucan, another essential cell wall polysaccharide, β-1,6-glucan, might likely play a crucial role in the septum malformation. β-1,6-glucan is responsible to interconnect various wall matrix components (Kollár *et al.*, 1997). In addition, it was shown that there usually is an increased density of β-1,6-glucan present at the very tips of the closing septum (Humbel *et al.*, 2001). Localized at the tip of the growing septum, the β-1,6-glucan could possibly be necessary to link certain proteins which might assist or monitor the septum assembly. Hence, absence of β-1,6-glucan as observed in the

depleted nmt81-*sup11* mutant might be the cause of the septum phenotype with huge linear β-1,3-glucan accumulations in the septum center.
Another possibility was provided by transcriptional analysis (see Table. 5.4) which revealed an elevated level of *bgs1*$^{+}$ (2.231 fold), the catalytic subunit of the β-1,3-glucan synthase that was demonstrated to be crucial for liner β-1,3-glucan synthesis of the primary septum (Cortés *et al.*, 2007).

Moreover, key role in the formation of the septum depositions was indicated for the β-1,3-glucanosyl transferase Gas2p. Gas2p is a member of the GH72 family which displays glucanosyl transferase activity and is involved in linear β-1,3-glucan remodeling (de Medina-Redondo *et al.*, 2010). Gas2p localizes during septum formation as a ring at the cell wall/ septum junction and stays inside the cell wall that surrounds the septum. Only after septum assembly was completed, Gas2p was associated with the entire septum (de Medina-Redondo *et al.*, 2010).
This study identified a high abundance of Gas2p in SDS-extracts of the restricted nmt81-*sup11* mutant. Analyzing SDS-extracts of a nmt81-*sup11*/*gas2*Δ double-mutant demonstrated that the protein was no longer detectable.

From the high levels of Gas2p in SDS-extracts of a nmt81-*sup11* mutant one can conclude either that (1) there is in general more Gas2p in the cell wall, that (2) the present Gas2p is extractable more easily from the mutant wall matrix using a method to solubilize non-covalently bound and disulfide-bridge linked cell wall proteins, or (3) labeling is less efficient.
Possibility (1) is favored by a transcriptional increased *gas2*$^{+}$ level in the restricted nmt81-*sup11* mutant. Although it was a rather mild increase on expression level (1.546 fold) the very small p-value of 0.00007 indicated that the observed up-regulation was indeed significant. Therefore the remarkable overrepresentation of Gas2p in the SDS-extracts may be connected to elevated expression and subsequent enhanced protein-biosynthesis. This favors the model, that the elevated Gas2p extraction from the mutant cell wall is based on changes of the overall Gas2 protein level.
Model (2) suggests an enhanced Gas2p-extractability from the cell wall matrix. Changes in the cell wall glucan composition might be the reason why the solubility of Gas2p is increased in the restricted nmt81-*sup11*. The transcriptional regulation of

many glucan synthases and glucanases in the restricted nmt81-*sup11* mutant (see Table 6.1) and the absence of β-1,6-glucan (see Fig. 5.13) indicated a general alteration of the cell wall. These data are in agreement with the altered cell wall composition which was demonstrated by preliminary characterization (Hutzler, 2009). Therefore, the well documented alterations of the cell wall glucan composition may cause the observed increased extractability of Gas2p in the restricted nmt81-*sup11* mutant.

Possibility (3) suggesting a less efficient protein labeling in the restricted nmt81-*sup11* mutant is rather unlikely. Even though the cell wall matrix shows a different composition in the polysaccharides, the small biotin-labeling reagent will not be affected in its mobility. Also different concentrations of the biotin label were tested to guarantee an excess of the reagent for efficient labeling of all cell wall proteins (data not shown).

Taken together, the high abundance of Gas2p in SDS-extracts of restricted nmt81-*sup11* cell wall is a combinatory effect of elevated Gas2p levels in the cell wall due to up-regulated transcription and an enhanced solubility caused by an altered cell wall polysaccharide composition.

The fact that Gas2p plays a role in the formation of the septum depositions was validated by the restricted nmt81-*sup11*/*gas2*Δ double-mutant, which showed no such malformed septa. Due to this knowledge one can assume that an elevated level of Gas2p at the site of septum assembly together with the elevated *bgs1*$^{+}$ expression level is responsible for the linear β-1,3-glucan deposition of the nmt81-*sup11* mutant septum. More β-1,3-glucan than needed for regular septum formation is produced by the overexpressed Bgs1p. Gas2p, located at the cell wall/ septum junction, might remodel and incorporate the overproduction of that polysaccharide. Consequently, the excess of β-1,3-glucan is visible in the depositions that accumulate at the septum center of the restricted nmt81-*sup11* mutant. The elevated amounts of Gas2p in the mutant might be a compensatory process of the restricted nmt81-*sup11* mutant.

The absence of Gas2p in a nmt81-*sup11*/*gas2*Δ double-mutant revealed that the observed septum depositions of the single nmt81-*sup11* mutant were related to Gas2p. The depositions in the septum center were absent and exponential growth could be restored. Moreover, Gas2p overrepresentation in the nmt81-*sup11* single mutant was eliminated in the nmt81-*sup11*/*gas2*Δ double-mutant.

Taken together, these data demonstrate that the observed nmt81-*sup11* septum deposition phenotype is caused by elevated levels of Gas2p in the mutant cell wall. For further characterization of the interplay between Sup11p and Gas2p, a transcriptome analysis of the nmt81-*sup11/gas2*Δ double-mutant might be useful.

Besides a defective septum assembly, the restricted nmt81-*sup11* mutant exhibited another phenotype in the division process itself. Microscopic observations revealed that restricted mutant cells were more likely to lyse during the separation process than the permissive mutant (see Fig. 5.6 B). It appeared that the two daughter cells were rather torn apart than splitted in a controlled manner. Regardless of the malformed septa some cells still managed to separate into two daughter cells after extended separation time (see Fig. 5.8). However, after successful division the septum deposition leftovers remained as cell wall clumps at the new end pole. Time laps analysis demonstrated that the cells had issues to degrade the primary septum regularly which is probably due to malfunction of the cell-separation ring. During cytokinesis, this ring is usually located at the junction region of septum and cell wall and contains endo-β-1,3-glucanase Eng1p, 1,3-α-glucanase Agn1p and the chitinase homologue Cfh4p (Martín-Cuadrado *et al.*, 2003; Alonso-Nunez *et al.*, 2005). These genes are members of the septum separation pathway in fission yeast and periodically expressed in the cell cycle during the separation process. In this study, genes involved in the septum separation pathway were shown to be transcriptionally down-regulated in the restricted nmt81-*sup11* mutant (see Table 5.9). The reason for the increased amount of lysed cells during cytokinesis might due to defective processing of the malformed septa due to down-regulation of the cell-separation ring enzymes.

However, the observed down-regulation of these periodically expressed septum separation genes might be a secondary effect due to a slowed down cell cycle. Expression of the cell cycle regulator *cdc18*$^{+}$ already dropped significantly in the nmt81-*sup11* mutant after 4h restriction (see Fig. 5.21) and as a result, the cells went into growth arrest (see Fig. 5.3 C). Thus, septum separation genes were no longer required and expressed since there were no more septa established which were needed to be degraded.

6.4. Membrane protein Sup11p resides inside the late Golgi or post-Golgi vesicles

This work demonstrated that the Sup11 protein resides in a compartment of the secretory pathway (see Fig. 5.30 A). Further was shown that Sup11p is membrane anchored via its ER-signal sequence which is not cleaved during maturation. In this study, several approaches were used to narrow down the subcellular localization of Sup11p.

Localization of Kre-family proteins seems to be a difficult matter. In *S. cerevisiae* Kre-family genes have been studies for decades including their subcellular localization. Fission yeast Sup11p is the homologue of the *S. cerevisiae* Kre9-family members. Most gene products of the Kre-family were suggested to be scattered across the secretory pathway (reviewed in Shahinian and Bussey, 2000 and Klis *et al.*, 2002). *Sc*Kre9 was only localized by its overexpression where it was found to be secreted to the medium. It was not possible to visualize *Sc*Kre9 expressed under its endogenous promoter in a global localization study of a genomically GPF-tagged budding yeast proteome. (Huh *et al.*, 2003). Thus the actual localization of *Sc*Kre9 is still under debate. Moreover, there are several studies which address the subcellular localization for Kre6. Initial studies using a fluorescent tag indicated that the Kre6 protein resides in the Golgi apparatus (Li *et al.*, 2002). However, recent results indicated that the majority of Kre6 locates to the ER and secretory vesicle-like compartments and the PM (Kurita *et al.*, 2011). In their experiments they used a HA-tagged version for indirect immunolableing and a polyclonal antibody. Concerning the difficulties to subcellular localize other Kre-family proteins it seems indispensable to use various approaches to ensure correct interpretation of their subcellular localization like it was done in this study.

Isopycmic centrifugation on a sucrose gradient allowed excluding ER, the PM, and the Gms1p-resident Golgi apparatus as possible compartment for Sup11p localization (see Fig. 5.29). In addition, immunoflourescence labelling of the genomically tagged Sup11p:HA showed a spotted vesicle-like pattern which was clearly distinct from the ER (see Fig. 5.27).

A C-terminal roGFP2-tag gave a fluorescent signal, although the obtained fluorescence was very weak and hardly detectable by applying microscope analysis to single cells (see Fig 5.26). Functionality of the Sup11p:roGFP2 fusion protein was verified (see Fig. 5.25). Comparison between the fluorescence pattern of Sup11p:roGFP2 and the

organelle markers showed, that the Sup11p:roGFP2 distribution looked clearly different from the ER-marker and vacuole-marker (Fig. 5.26). The most similarities were observed between the pattern of Sup11p:roGFP2 and the dot like ER-exit site Sec31p:mCherry and the spotted Anp1p:mCherry of the cis-Golgi apparatus.
In a genome wide localization study in *S. pombe* 4431 proteins were tagged on their genomically tagged on their C-terminus or the tagged version was overexpressed from plasmid (Matsuyama *et al.*, 2006). In that screen the fluorescent pattern of a eYFP-tagged Sup11p is reported to show similarities to the ER and Golgi apparatus (Matsuyama *et al.*, 2006). However, the experiment gave no clear result about the Sup11p localization.
Together the data obtained in experiments of this study suggest localization for Sup11p in vesicles of post ER secretory pathway or the late Golgi/ trans-Golgi network.

Topology predictions of Sup11p were ambiguous showing different results in diverse *in silico* models. In order to elucidate the true topology of Sup11p, the roGFP2-tagged strain was used by taking advantage of its redox sensitive properties. Ratiometric measurements revealed that the tagged C-terminus of Sup11p resides in the lumen of an oxidizing compartment (e.g. Golgi, ER (latter was excluded)) (see Fig. 5.30). Again, the obtained fluorescence was very weak but specificity of the measured roGFP2 signal was guaranteed by applied controls.
In addition, it was shown that Sup11p is not a multi spanning TMD protein as predicted by several models (see Fig 5.32). Instead, Sup11p is actually membrane anchored by its uncleaved signal sequence which functions as signal anchor sequence (see Fig. 5.31 B).
Taken together, Sup11p is membrane anchored via its non-cleaved signal sequence. In addition, this study gave evidence that there is no further TMD and that the full length Sup11 protein - including the Kre9-domain - resides in the lumen of an oxidizing compartment.

6.5. Sup11p stability profits from glycosylation

Sup11p is a secretory protein that localizes in vesicles of post ER secretory pathway or the late Golgi/ trans-Golgi network (see Fig. 5.31). Both features allow that Sup11p is modified by the *O*-mannosylation-machinery. Indeed, extensive *O*-mannosylation of

Sup11p was demonstrated by analyzing the glycosylation level of the HA-tagged protein in PMT-family mutants (see Fig. 5.33).
The molecular weight of Sup11p:HA is decreased in all three *oma*-mutants indicating a hypo-mannosylation. Taken into account that the nmt81-*oma2* is only a knock-down mutant, the observed hypo-mannosylation would probably be even more prominent in an *oma2*$^{+}$-null mutant. Since *oma2*Δ is lethal (Willer *et al.*, 2005) it was not possible to analyze the Sup11p glycosylation state in that specific background.
The most striking observed Sup11p hypo-mannosylation was in the *oma4*Δ mutant background indicating that this protein is mainly *O*-mannosylated by Oma4p (see Fig. 5.33). *S. cerevisiae* Kre9 is only modified by the Pmt1/Pmt2 complex but unaffected in a *pmt3*Δ or *pmt4*Δ background (Gentzsch and Tanner, 1997). This indicated a different substrate specificity of the *O*-mannosylation machinery complexes for the two homologue proteins.

In this study, evidence was provided that protein stability of Sup11p is depending on its glycosylation state. An *oma2*$^{+}$-shut down experiment demonstrated that the amount of hypo-mannosylated Sup11p:HA increased after 12 h of *oma2*$^{+}$ restriction, indicated by a smear of apparent lower molecular weight (see Fig. 5.34). In addition, hypo-mannosylation of Sup11p seemed to destabilize the protein since the total signal intensity of tagged protein decreased rapidly after 12 h of *oma2*$^{+}$ restriction. However, the data were obtained in a steady state experiment and the stability of a hypo-mannosylated Sup11p needed to be experimentally investigated by inhibition of protein-biosynthesis.
Due to the significant hypo-mannosylation of Sup11p which was documented in the *oma4*Δ background (see Fig. 5.33) the influence of glycosylation on Sup11p:HA stability was analyzed using an *oma4*Δ background in comparisons to the wild type. There were three versions of Sup11p:HA present in an *oma4*Δ mutant: two lower molecular weight products of 32 kDa (ngSup11p:HA) and 36 kDa (Sup11p:HA+*N*), and one high molecular weight product of 52 kDa (Sup11p:HA+*N*+*O*). It was demonstrated that the Sup11p:HA+*N*+*O* version is significantly more stable than the less glycosylated Sup11p:HA+*N* and ngSup11p:HA variants (see Fig. 5.39). Comparison between the latter two showed that the product which is glycosylated least (ngSup11p:HA), exhibited the shortest half-life.

These data clearly suggested, that glycosylation positively influence and increase stability of Sup11p:HA. It was reported that glycosylation improved solubility of folding intermediates which supports proper protein folding and protection from ER-associated degradation (Lis and Sharon, 1993; Xu *et al.*, 2013).

Moreover, it is likely that the ngSup11p:HA in the *oma4*Δ background did not exit the ER. Hypo-mannosylation of the ngSup11p:HA impaired correct protein folding and only fully folded proteins are packed into vesicles and transported from the ER to the Golgi apparatus (reviewed in Ellgaard *et al.*, 1999). After prolonged time in the ER and the processing of the ER-quality control system, the hypo-mannosylated and unfolded ngSup11p:HA sub-form most likely got subject of the ER-associated degradation (Xu *et al.*, 2013).

In addition, evidence was brought that in an *oma4*Δ background a fraction of Sup11p:HA is *N*-glycosylated at an unusual N-Y-A sequon at aa position 239 to the Sup11p:HA+*N* sub-form. Typically the attachment of *N*-linked glycans occurs at the peptide sequence N-X-S/T where X can be any aa except proline (Marshall, 1972; Bause and Legler, 1981). There are reports of very few *N*-glycosylation events at alternative sequons, so called “rare sequons”. Evidence was given that the S/T at the +2 position after the asparagine can be substituted by a cysteine (0.5%) or glycine (0.2%) (Gavel and Heijne, 1990). For example there is a N-A-C sequon in the heavy chain of protein C from bovine plasma reported (Stenflo and Fernlund, 1982). There are also reports of glycosylated sequons with glycine, valine and alanine at the +2 position (Zielinska *et al.*, 2010; Lizak *et al.*, 2011). However, these unusual sequons appear in very low abundance (Lizak *et al.*, 2011). Analysis of the X-ray structure of a bacterial OST in complex with an acceptor peptide gave insight about the positioning of the sequon and the catalytic subunit (Lizak *et al.*, 2011). The authors report that glycine, valine and alanine at the +2 position are small enough to be accommodated in the binding pocket of the bacterial OST and therefore allow *N*-glycosylation of the unusual sequon (Lizak *et al.*, 2011).

The unusual *N*-glycosylation site of Sup11p:HA could only be modified in an *oma4*Δ background. Thus, it is very likely that the *N*-glycosylation site was masked by *O*-mannosylation in the wild type. Indeed, the unusual sequon resides in a S/T-rich stretch (aa 198-254, see Fig. 5.1) of the Kre9-domain which was demonstrated to be

prone to *O*-mannosylation in *S. cerevisiae* (Brown and Bussey, 1993). Interestingly, the N329 is highly conserved across various yeast species (see Fig. 5.2) indicating functional importance.

Since the unusual *N*-glycosylation site was only used in an *oma4*Δ background provided another example for the reported competition between *N*- and *O*-glycosylation in *S. cerevisiae* (Ecker *et al.*, 2003). For *Sc*Ccw5 it was demonstrated that an internal sequon cannot be *N*-glycosylated in the wild type background but only in a *pmt4*Δ mutant (Ecker *et al.*, 2003). Similar to the unusual sequon found in *Sp*Sup11p, the *Sc*Ccw5 sequon was located in a S/T-rich region which was usually modified by *Sc*Pmt4.

The alternative *N*-glycosylation of the ngSup11p:HA in the *oma4*Δ mutant might be beneficial for protein stability since it might prolong the time for proper folding. Nonnative proteins and correctly folded proteins with *N*-linked glycans undergo trimming of glucose residues in the ER lumen. Unfolded proteins are recognized by the ER-quality control system and subject of the calnexin calreticulin cycle which are part of the ER-quality control. The lectins of the calnexin calreticulin cycle transiently bind to oligosaccharides containing a terminal glucose residue of non-native proteins where they exhibit chaperone activity (reviewed in Helenius and Aebi, 2004). It is possible that due to the calnexin calreticulin cycle, the *N*-glycosylated Sup11p:HA+*N* resided in the ER for an elongated time to assist proper protein folding. It had been shown, that glycoproteins which were not able fold to their mature conformations during an appropriate time window became target for the ER-associated degradation (reviewed in Helenius and Aebi, 2004). In agreement to this, this study showed that the Sup11p:HA signal with mutation in the unusual sequon is roughly ten times weaker than in the version with intact N-Y-A sequon at aa position 239 (see Fig. 5.38 C).

In addition, it is likely that the unusual *N*-glycosylation of Sup11p:HA+*N* assists proper maturation since *N*-glycans are bulky hydrophilic polymers which increase protein solubility (Tams *et al.*, 1999). *N*-glycans can also contribute to a higher stability against proteolysis by affecting the intramolecular energy partition of the folded proteins. It was shown, that the thermodynamic stabilization is depending on the position and degree of glycosylation but only very weakly on the size of the glycans (Shental-Bechor and

Levy, 2008). Indeed, it was demonstrated that the Sup11p:HA+*N* had a longer half-life than the ngSup11p:HA (see Fig. 5.39).
Together these data indicated that protein-glycosylation Sup11p:HA in this S/T-rich region has a major influence on the protein stability. Thereby, not the kind protein-glycosylation of is mainly important for Sup11p:HA stability but rather that the protein receives any glyco-modification at all in this S/T-rich region (aa 198-254) in order to assist proper folding.

Furthermore, there was a minor fraction of apparently Sup11p:HA+*N*+*O* present in the *oma4*Δ mutant. In this specific background the 52 kDa product was both, *N*-glycosylated and *O*-mannoslylated. The complete Sup11p:HA+*N*+*O* fraction was sensitive towards EndoH treatment demonstrating that the *N*-glycosylation site is used prior to *O*-mannosylation because the unusual sequon would be masked otherwise. The Sup11p:HA+*N*+*O* size shift due to EndoH treatment was rather small with 3 kDa demonstrating that the core *N*-oligosaccharide got not extensively modified. This supported the assumption that both sub-forms, Sup11p:HA+*N* and Sup11p:HA+*N*+*O*, did not exit the ER since extensive *N*-glycan elongation takes place in the Golgi apparatus (reviewed in Helenius and Aebi, 2004).

The observed Sup11p:HA+*N*+*O* sub-form in the *oma4*Δ background might be a product of inappropriate protein *O*-mannosylation like it has been described for misfolded proteins in *S. cerevisiae*. Prolonged ER residence of misfolded proteins allowed a progressive *O*-mannosylation of exposed acceptor sites (Harty *et al.*, 2001; Xu *et al.*, 2013). It was shown that a mutant form of a α-factor precursor got highly *O*-mannosylated by Pmt2p and that the *O*-mannosylated protein was not degraded (Harty *et al.*, 2001). The authors suggested that there is a time window during which misfolded proteins can be removed from the ER (reviewed in Helenius and Aebi, 2004). After that, unfolded proteins receive unusual modifications which can interfere with their removal (Harty *et al.*, 2001).
A similar mechanism for *S. pombe* Sup11p:HA is supported by the fact that Sup11p:HA+*N*+*O* is even more stable than the wild type modified Sup11p:HA (see Fig. 5.39). Sup11p:HA+*N*+*O* accumulates in the ER due to inappropriate

O-mannosylation. In addition, the fact that the *N*-glycan of Sup11p:HA+*N*+*O* received no extensive elongation supported that the protein is actually retained in the ER lumen.

6.6. Alterations caused by Sup11p depletion on transcriptional level

Initial analysis of the restricted nmt81-*sup11* mutant showed severe phenotypes like septum malformation (see Fig. 5.6 B) and the absence of β-1,6-glucan (see Fig. 5.13). In order to gain an advanced understanding about the pathways which were triggered by repression of the *sup11*$^+$ gene, a transcriptome analysis was performed to shed some light on these processes. 341 genes were identified to be significantly up-regulated and 68 down-regulated (Supplementary Table 3 and 4).

Among the 68 down-regulated genes, four genes were associated to thiamine biosynthesis and thus excluded from analysis. However, *sup11*$^+$ transcript level was reduced to only roughly 20% compared to the expression level under permissive conditions. The reason for the rather weak depletion of Sup11p under restrictive conditions needs to be elucidated yet. Nevertheless, the severe morphological defects as documented in the microscopic images and in cell wall analysis became manifest already with 20% of *sup11*$^+$ transcript left.

Clustering of significantly up- or down-regulated genes revealed that 99 of the 341 up-regulated genes were related to stress response. Among those, more detailed annotated genes could be further categorized into oxidative stress, nitrogen starvation, and osmotic stress (see Table 5.1, 5.2, and 5.3).

A common defense mechanism against oxidative stress is the activation of the HOG pathway, which also mediates responses to hyperosmotic shock and other stresses (reviewed in Fuchs and Mylonakis, 2009).

Transcriptional up-regulation of the HOG pathway target genes was revealed by transcriptome analysis (see Fig 5.20). However, the expressions of HOG activated MAPK Wis1p and Sty1p showed no change since their regulation is via phosphorylation or dephosphorylation rather than adapting their gene expression. The up-regulation of Sty1p-repressor Pyp2p phosphatase indicated an elevated Sty1p activity which is counteracted by increased Pyp2p levels. One target gene of Sty1p was also up-regulated in the restricted nmt81-*sup11* mutant. A minor increase of Tps1p

(1.330 fold), a predicted α,α-trehalose-phosphate synthase, was observed. Tps1p and the also up-regulated Ntp1p were demonstrated to physically interact with each other (Soto *et al.*, 2002). Npt1p is a α,α-trehalase which is involved in two of the observed stress responses: osmotic (GO:0071470) and oxidative stress (GO:0034599) (see Table 5.1 and 5.2). The data suggested that Npt1p and Tps1p were induced by the HOG-pathway and recruited for remodeling the Sup11p depleted mutant cell wall.

Furthermore, nutrient stress responses are triggered in the restricted nmt81-*sup11* mutant (see Table 5.3). The availability of nutrients influences cellular functions such as cell growth and cell cycle.

The target of rapamycin (TOR) -signaling cascade senses the availability of nitrogen sources to regulate gene expression. Usually these pathways are activated when yeasts are transferred from a nutrient-rich to a nutrient-poor conditions. However, cells used for the transcriptome analysis were cultured in nutrient-rich conditions at all times indicating a different activation mechanism.

Under nutrient-poor conditions, TOR-signaling is inhibited by nitrogen starvation and subsequently activates the CWI pathway (reviewed in Fuchs and Mylonakis, 2009). A prominent target up-regulated gene of the CWI response in *S. cerevisiae* is the β-1,3-glucan synthase Fks1 (reviewed in Fuchs and Mylonakis, 2009). *bgs1*$^{+}$ is the homologue of *S. cerevisiae fks1* encoding for a β-1,3-glucan synthase in *S. pombe*, which was demonstrated to be up-regulated in the restricted nmt81-*sup11* mutant (see Table. 5.4). Thus, the observed up-regulation of Bgs1p might be in response of the nitrogen starvation activated CWI pathway or directly induced by malfunction of the septum formation.

In addition to the TOR-signaling, the cAMP - pathway is also involved in nutrient sensing. Glucose and/or nitrogen depletion activates the heteromeric G protein Gpa2p. Gpa2p induces the cAMP signal which activates protein kinase A (PKA) to express the transcription of genes involved in gluconeogenesis and sexual development (reviewed in Davey, 1998). The pathways downstream of the PKA are stimulated to different extents by the nutrient depletion signals: nitrogen starvation promotes sexual development and glucose depletion stimulates gluconeogenesis (reviewed in Davey, 1998).

Nitrogen starvation activated cAMP-pathway which leads to production of the Ste11p transcription factor and consequent expression of *mei2*$^{+}$. Ste11p is the key transcription factor for sexual development and cells lacking Ste11p are sterile (reviewed in Davey, 1998). However, Ste11p showed only minor changes (1.376 fold) in the expression of the restricted nmt81-*sup11* mutant and in consequence also *mei2*$^{+}$ showed no up-regulation (0.900 fold) in the transcriptome analysis.

Moreover, it was shown that the restricted nmt81-*sup11* have a 2C DNA content. This indicated that the responses related to nitrogen starvation are secondary effects by nutrient sensing via the cAMP-pathway. Nitrogen starvation promotes cell cycle arrest with 1C DNA content and at least a sub-population of 1C cells should be detectable in the FACS analysis (see Fig. 5.22). Since there is no such population it is unlikely that the restricted nmt81-*sup11* culture is challenged with nitrogen starvation.

Upon glucose starvation, the activity of Gpa2p is down-regulated to promote gluconeogenesis. Gpa2p activity represses the expression of *fbp1*$^{+}$ gene which is a positive regulator of the gluconeogenesis. Transcriptome analysis of the restricted nmt81-*sup11* mutant revealed a significant down-regulation of Gpa2p (0.459 fold). Hence, the expression of the *fbp1*$^{+}$ gene got strongly activated (38.252 fold). Moreover, the gene encoding for the external invertase *inv1*$^{+}$ was significantly up-regulated (4.885 fold) indicating that glucose is limited inside the cells.

Taken together, the data suggested that the Gpa2p activated cAMP pathway rather responded to glucose starvation than to nitrogen depletion in the restricted nmt81-*sup11* mutant. Moreover, a strong need for additional glucose is indicated by up-regulation of *inv1*$^{+}$ and *fbp1*$^{+}$ which are both involved in providing glucose. That glucose becomes a limiting factor in the restricted nmt81-*sup11* mutant seems likely since the huge linear β-1,3-glucan containing depositions at the septum and pole are built of carbohydrates. Glucose and UDP-glucose respectively, are needed as substrate for Bgs1p mediated linear β-1,3-glucan synthesis. The chains of this polysaccharide were subsequently remodeled to the central septum depositions by Gas2p. Considering the massive amounts of incorporated cell wall glucan, it is obvious that the cells need a huge glucose pool for polysaccharide synthesis which ought to be provided by elevated activity of *fbp1*$^{+}$ and *inv1*$^{+}$.

Apart from the directly stress related responses, eight of the up-regulated genes were annotated to be involved in KEGG pathway spo00500 which is controlling the glucan and polysaccharide metabolism. This hinted to alterations in the general cell wall metabolism. Manual analysis of GO pathways "oligosaccharide catabolic process", "extracellular polysaccharide metabolism process" and "fungal-type cell wall" suggested that the restricted nmt81-*sup11* mutant undergoes a major remodeling of the cell wall polysaccharides. Small p-values validate the significance of the observed regulation.

Since there were glucanases as well as synthases regulated in the transcriptome (Table 6.1 and 6.2), it was not possible to certainly predict an alteration to a specific cell wall polysaccharide.

Polysaccharide degrading				
Regulation	**p-value**	**Systematic Name**	**Gene Name**	**Gene Product**
15.980	0.00026	SPAC869.07c	*mel1*	α-galactosidase
8.263	0.00179	SPBC2G2.17c	SPBC2G2.17c	β-glucosidase Psu2 (predicted)
4.847	0.00001	SPAC26H5.08c	*bgl2*	β-1,3-glucosidase Bgl2
4.125	0.00089	SPBC14C8.05c	*meu17*	α-1,4-glucosidase
3.544	0.00057	SPAC3C7.05c	SPAC3C7.05c	α -1,6-mannanase (predicted)
3.403	0.00018	SPBC1198.07c	SPBC1198.07c	endo-α-1,6-mannosidase (predicted)
2.528	0.00139	SPAPB24D3.10c	*agl*	α-glucosidase Agl1
2.525	0.00001	SPCC757.12	SPCC757.12	α-amylase homolog (predicted)
2.037	0.00334	SPBC660.07	*ntp1*	α,α-trehalase Ntp1
1.973	0.00579	SPAC23D3.14c	*aah2*	α-amylase homolog Aah2
0.581	0.00673	SPBC1105.05	*exg1*	β-1,6-glucosidase
0.483	0.03021	SPBPB7E8.01	SPBPB7E8.01	α-amylase homolog (predicted)
0.425	0.00470	SPAC14C4.09	*agn1*	endo-α-1,3-glucosidase Agn1

Table 6.1: Polysaccharide degrading enzymes which are regulated in the restricted nmt81-*sup11* mutant:
Transcriptome analysis comparing gene expression of restricted and non-restricted nmt81-*sup11* mutant revealed significantly regulated genes encoding for glucanases (dark red and dark green). Moderately up-and down-regulated genes are depicted in light red (1.8-2.0) or light green (0.8-0.5).
The systematic names, p-values, gene names and gene products are listed in the table. Permissive expression level of selected genes equals 1.0.

Polysaccharide synthesizing				
Regulation	**p-value**	**Systematic Name**	**Gene Name**	**Gene Product**
4.026	0.00035	SPAC22F8.05	SPAC22F8.05	α,α-trehalose-phosphate synthase (predicted)
3.329	0.00049	SPBC16D10.05	*mok13*	α-1,3-glucan synthase Mok13
2.231	0.00017	SPBC19G7.05c	*bgs1*	β-1,3-glucan synthase catalytic subunit Bgs1
1.766	0.00016	SPAC19B12.03	*bgs3*	β -1,3-glucan synthase subunit Bgs3

Table 6.2: Polysaccharide synthesizing enzymes which are up-regulated in the restricted nmt81-*sup11* mutant:
Transcriptome analysis comparing gene expression of restricted and non-restricted nmt81-*sup11* mutant revealed significantly regulated genes encoding for glucan synthases (dark red). The moderately up-regulated gene is depicted in light red (1.8-2.0).
The systematic names, p-values, gene names and gene products are listed in the table. Permissive expression level of selected genes equals 1.0.

Polysaccharide transferase activity				
Regulation	**p-value**	**Systematic Name**	**Gene Name**	**Gene Product**
1.622	0.01218	SPAC11E3.13c	*gas5*	β-1,3-glucanosyl transferase (predicted)
1.546	0.00007	SPBC29A10.08	*gas2*	β-1,3-glucanosyl transferase (predicted)
1.478	0.00140	SPAC19B12.02c	*gas1*	β-1,3-glucanosyl transferase

Table 6.3: Regulation of enzymes with polysaccharide transferase activity:
Transcriptome analysis comparing gene expression of restricted and non-restricted nmt81-*sup11* mutant revealed moderately regulation of genes encoding for polysaccharide transferases Gas5p, Gas2p, and Gas1p.
The systematic names, p-values, gene names and gene products are listed in the table. Permissive expression level of selected genes equals 1.0.

On the one Hand, α-glucosidase Agl1p is up-regulated (2.528 fold) indicating a promotion of α-glucan degradation. On the other Hand, α-1,3-glucan synthase Mok13p was found to be up-regulated (3.329 fold, see Table 6.1) counteracting the increased degradation.

Interestingly, also *meu17*$^{+}$, encoding for a α-1,4-glucosidase, is up-regulated. During synthesis of the mature cell wall α-1,3-glucan polysaccharide, insertion of some α-1,4-glucan residues is required. These α-1,4-glucan residues later reside in the center of the full length glucan. The elevated *meu17*$^{+}$ levels in the restricted nmt81-*sup11* mutant may suggest that the full length α-glucan is degraded into shorter α-glucan chains for cell wall remodeling reasons.

However, the observed down-regulation of endo-α-1,3-glucosidase Agn1p must be considered in a different context since this glucosidase participates in the controlled

degradation of the division septum. Thus, this glucosidase must be linked to the general down-regulation of the septum separation pathway.

There were also β-glucan glucosidases (Bgl2p, Psu2p, Exg1p) as well as β-glucan synthases (Bgs1p and Bgs3p) identified to be transcriptional regulated in the restricted nmt81-*sup11* mutant (see Table 6.1). As response to the diminished amount of cell wall β-1,6-glucan in a Sup11p depleted mutant (see Fig. 5.13), the levels of the β-1,6-glucanase *exg1*$^+$ were decreased to preserve the remaining β-1,6-glucan. Furthermore, *bgs1*$^+$, which is crucial for primary septum synthesis (Cortés *et al.*, 2007), was identified to be up-regulated in the restricted nmt81-*sup11* mutant. An increased Bgs1p activity in combination the increased *gas2*$^+$ transcription (Table 6.2 and 6.3) may be responsible for the observed septum phenotype of the restricted nmt81-*sup11* mutant as discussed in chapter 6.3.

Overall, chemical cell wall analysis demonstrated an elevated α-glucan to β-glucan ratio in the restricted nmt81-*sup11* mutant compared the cell wall with endogenous *sup11*$^+$ expression (Hutzler, 2009). This altered ratio might be either due to increased α-glucan level or decreased β-glucans or a combination of both compared to the wild type cell wall. However, β-1,6-glucan was absent in the Sup11p depleted mutant (see Fig. 5.13) contributing to the decreased β-glucan ratio in the mutant (Hutzler, 2009). In addition, loss β-1,6-glucan probably has a major impact on the cell all structure due to its role in covalent linkage of GPI-anchored proteins. Many of those proteins are involved in cell wall organization. For example β-1,3-glucanosyl transferase Gas1p was demonstrated to be transglycosylated to the β-1,6-glucan network via the remnant of a cleaved GPI-anchor (de Groot *et al.*, 2007). Impaired cell wall binding of this and other transglycosylated proteins might likely interfere with the regular cell wall constitution.

Transcriptome analysis demonstrated that both, cell wall α- and β-glucans, need to undergo remodeling processes by various enzymes. This is in agreement with the up-regulation *fbp1*$^+$ and subsequent activation of gluconeogenesis in order to provide the substrate for synthesis of new cell wall glucans.

Apart from the already discussed *bgs1*$^+$ and *agn1*$^+$, there were more up- or down-regulated genes in the repressed nmt81-*sup11* mutant which were implicated in septum assembly and separation (see Table 5.9). For example *ace2*$^+$ - the key

transcription factor of the septum separation pathway - and several down-stream Ace2p-regulated genes exhibited significant expression changes in the transcriptome data.

Expression analysis obtained in four hour intervals supported *ace2*$^+$ down-regulation and showed that its transcript level was already considerably affected after 10 h of repression. However, the transcriptome data also revealed a significant drop in the *cdc18*$^+$ mRNA level, a gene encoding for a crucial cell cycle checkpoint factor for the G1/S-transition. Therefore, it was necessary to consider that the observed growth arrest of the restricted nmt81-*sup11* mutant might be caused by a triggered cell cycle checkpoint due to Cdc18p depletion. Indeed, *cdc18*$^+$ was already strongly affected after 4h of repression; that is 6h earlier than the *ace2*$^+$ response (see Fig. 5.21).

Deletion of the *cdc18*$^+$ prevents the entry into S-phase resulting in the appearance of cells with less than a 1C DNA content (Kelly *et al.*, 1993). However, there was some inconsistency concerning the DNA content of the examined temperature sensitive *cdc18*-K46 and *cdc18*Δ null arrested cells. Deletion of the *cdc18*$^+$ prevented the entry into S-phase resulting in the appearance of cells with less than a 1C DNA content. In contrast, down-regulation of *cdc18*$^+$ in a temperature sensitive strain caused arrested cells with 2C DNA content. The authors argued that temperature sensitive alleles are leaky and the temperature sensitive *cdc18*-K46 mutant is partially functional at the restrictive temperature. DNA synthesis is not completed normally and cells arrest with 2C content in this mutant (Kelly *et al.*, 1993). Thus, the observed growth arrest of the restricted nmt81-*sup11* mutant with 2C DNA content is in agreement with the 5% residual *cdc18*$^+$ transcript level.

This study showed that restriction of the nmt81-*sup11* mutant led to a rapid *cdc18*$^+$ decline. The significant drop of the *cdc18*$^+$ expression level subsequently induced a cell cycle arrest with 2C DNA content (see Fig. 5.3 C and 5.22). Interpretation of these data led to the conclusion that the observed down-regulation of the septum separation pathway was some secondary effect due to a prior triggered cell cycle arrest. Thus, the cells stopped to duplicate and in consequence no further expression of septum separation genes was required as indicated in the transcriptome data showing a down-regulation of genes involved in the septum separation pathway.

Taken together the characterization data of the restricted nmt81-*sup11* mutant leads to the following model:

The post-Golgi localized Sup11p is indispensable for correct septum formation and β-1,6-glucan synthesis. β-1,6-glucan is crucial for covalent linkage of transglysosylated GPI-anchor proteins to the cell wall matrix which are often involved in cell wall glucan modifications. Thus, loss of this kind of β-glucan will also interfere with the cell wall protein (e.g. increased Gas2p in SDS-extracts) and glucan organization (e.g. altered β- to α-glucan ratio, absence of β-1,6-glucan, β-1,3-glucan septum depositions).

Depletion of this protein causes a rapid decline of cell cycle regulator *cdc18*$^{+}$ which in consequence induces a cell cycle arrest. Moreover, the loss of Sup11p activity leads to huge accumulations of linear β-1,3-glucan containing cell wall material in the septum center. After prolonged separation time the cells manage to split the malformed septum. The decrease of *cdc18*$^{+}$ transcript and thus slowed down cell cycle might likely be related to the elongated separation process. Also the down-regulation of the septum separation pathway is related to the slowed down cell cycle. However, the separation process itself is impaired since one of the two daughter cells is likely to lyse during cytokinesis and the surviving cell bears the septum deposition at its new end.

In addition, the cell wall and septum glucan composition is severely altered in the restricted nmt81-*sup11* mutant. A significant decrease of the β- to α-glucan ratio was demonstrated (Hutzler, 2009) and β-1,6-glucan is absent in the cell wall. These cell wall alterations trigger several stress responses like CWI-pathway, osmotic- and oxidative stress responses. In consequence, there are significant cell wall remodelling processes indicated by strong regulation of several glucan synthesising/modifying enzymes in order to counteract cell wall defects.

Moreover, the division septum is also affected by Sup11p depletion. The primary septum linear β-1,3-glucan synthesising Bgs1p is increased in its expression. In order to synthesize these huge amount of linear β-1,3-glucan, which are accumulated in the septum center, the glucose-substrate must not be limited. To provide sufficient amounts of glucose inside the cell, the expression of *fbp1*$^{+}$ for gluconeobiogenesis is significantly increased. Restriction of the nmt81-*sup11* mutant also triggers elevated levels of septum β-1,3-glucan remodelling Gas2p in the cell wall. These elevated Gas2p levels are not essential for survival of the nmt81-*sup11* mutant since the deletion of *gas2*$^{+}$ in the restricted nmt81-*sup11* mutant was vital. Moreover, the synthetic deletion could even

rescue the septum deposition phenotype and the cell cycle arrest. This demonstrated that Gas2p is responsible for the accumulation of the septum material.

6.7. Function of Sup11p as suppressor of O*-mannosylation mutants*

As illustrated, glycosylated proteins fulfill several functions in the cell wall. For example they act as sensors or remodel the polysaccharides of the wall or septum (Heinisch et al., 1999; Rodicio and Heinisch, 2010). In order to gain an improved and comprehensive understanding about the processes and functions which are dependent on protein *O*-mannosylation the conditionally lethal triple-*oma* mutant (Fabian, 2009) was analyzed in more detail. It was described that the *S. cerevisiae* PMT-family members mannosylate specific protein substrates and therefore the consequences of a completely blocked protein *O*-mannosylation needed to be elucidated (Gentzsch and Tanner, 1997).

A transcriptome analysis carried out after 16 h restriction of the triple-*oma* knock-down mutant revealed that the transcriptional levels of *oma2*$^+$ and *oma4*$^+$ were only decreased to 39% and 47%, respectively (see Table 5.11). These two values indicated that the shut-down of the nmt81-promotor in this strain is rather very weak. Apparently, the Oma2p and Oma4p depleted cells try to compensate the diminished levels of both *O*-mannosyl transferases via transcriptional up-regulation of non-functional *oma1*:Dis. The expression level of the disrupted transcript was shown to be more than fourfold (4.207) up-regulated under restricted conditions compared permissive conditions. Similar compensatory mechanisms have been reported for *S. cerevisiae pmt*-mutants in which decreased amounts of *O*-mannosyl glycans can trigger an up-regulation of other PMT-family members (Girrbach and Strahl, 2003). Moreover, it is likely that a comparable mechanism up-regulates *oma1*$^+$ and *oma4*$^+$ transcription in the restricted nmt81-*oma2* mutant. *O*-mannoprotein Sup11p is processed by more Oma1p and Oma4p, however, the residual activity remains below a critical threshold. Overexpression of *sup11*$^+$ in the multicopy-suppressor screen elevated the Sup11p level. Even though Sup11p is still hypo-mannosylated and possibly less active, the elevated protein level compensates for the diminished activity and thus restores viability of the restricted nmt81-*oma2* mutant.

Furthermore, preliminary analysis suggested a cell wall defect of the triple-*oma* mutant since they lost their characteristic rod like shape and became more roundish and pear shaped 28 h after repression (Fabian, 2009). Similar morphological changes were already reported for the single *oma1*Δ and *oma4*Δ mutants (Willer *et al.*, 2005).
The transcriptome analysis of the triple-*oma* mutant revealed 439 up-regulated and 239 down-regulated genes in the restricted (see Supplementary Data, Table 4). For *S. cerevisiae* it had been shown that block of *O*-mannosyl transferase activity using an inhibitor triggered specific stress responses like the CWI and unfolded protein response/ER-associated degradation (Arroyo *et al.*, 2011). However, no certain stress response like the CWI could be shown to be activated in the fission yeast triple-*oma* mutant. The set of regulated genes in the restricted nmt81-*sup11* mutant was quite similar to the regulated genes in the triple-*oma* mutant. A lot of genes whose products are involved in glucan and polysaccharide metabolism as well as the septum separation pathway were changed in expression (see Supplementary Data, Table 4). This indicated that the absence of β-1,6-glucan due to Sup11p depletion triggered similar rescue mechanisms like the general depletion of protein *O*-mannosyl transferase activity.

Phenotype characterization shown in this work revealed that the initial morphological changes were appearing 12 h after depletion of all three *oma*$^+$-genes. A minor fraction of cells built multiple septa but still managed to complete cytokinesis successfully after a prolonged time. A transcriptome analysis of a 16 h restricted triple-*oma* mutant revealed that *cdc18*$^+$ (50% of permissive level) and *ace2*$^+$ gene is almost completely down-regulated (7.5% of permissive level). An *ace2*Δ mutant is viable and exhibits a similar phenotype with chain forming, multisepted cells (Alonso-Nunez *et al.*, 2005). In a later stage of *oma*-repression the multiple septa phenotype disappeared completely and cells accumulated cell wall matrix depositions at the poles and the septum instead. The additional septum material seemed to be more evenly distributed compared to the centric depositions of the nmt81-*sup11* mutant. The additional cell wall depositions enlarged with time and after 21 h under restricted conditions almost the complete culture exhibited the above described wall defects. At this time 13% of all cells in the culture were already dead (see Fig. 5.41).
Severe malformations and the terminal lethal phenotype demonstrated that protein *O*-mannosylatation is a vital modification and that diminished Oma2p and Oma4p

activity in combination with Oma1p deletion is not sufficient to maintain viability. On transcriptional level the triple-*oma* mutant and the restricted nmt81-*sup11* mutant exhibited similar gene responses (data not shown). Phenotype analysis showed similar morphological wall defects in PMT-family mutants and *sup11*$^{+}$. Comparison of the observed malformations indicated strong cell wall and septum defects. Both mutants showed linear β-1,3-glucan containing depositions at the pole region and massive cell wall incorporations at the septum. However, the septum phenotypes differed and were distinct for each mutant. In contrast to the depositions in the septum center observed in the restricted nmt81-*sup11* mutant, the incorporated septum material was more evenly distributed over the entire septum in the triple-*oma* mutant. In addition, the pole depositions were more pronounced in the triple-*oma* mutant. In these cells the incorporated cell wall material could account for more than 50% of the total cell volume whereas the depositions in the restricted nmt81-*sup11* mutant were rather moderate (~5% of total cell volume).

The similarities of the triple-*oma* and nmt81-*sup11* mutant in transcriptome and phenotype analysis do not necessarily imply that these gene products are directly functionally linked. It rather indicates that their contribution to the cell wall and septum rigidity is of equal importance. Perhaps these defects are linked in both mutants to negative effects on covalently β-1,6-glucan-GPI-anchored wall proteins.

A hypothesis for linking *sup11*$^{+}$ overexpression to the rescue of the restricted nmt81-*oma2* mutant is by their contribution cell wall integrity. Some glycosylated proteins are attached to a GPI-anchor. A genome wide screen identified 33 of such *S. pombe* proteins (De Groot *et al.,* 2003). Due to *sup11*$^{+}$ overexpression in the multicopy-suppressor screen the β-1,6-glucan content may be elevated and thus the hypo-mannosylated GPI-proteins might be more efficiently transglycosylated to the wall matrix, thereby stabilizing the cell wall.

The hypo-mannoslyted proteins in *S. cerevisiae pmt*-mutants activate the ER-quality control system and thus promote degradation (Arroyo *et al.,* 2011). The portion of hypo-mannosylated GPI-proteins, which passes the ER-quality control, are released to the extracellular space but their decreased solubility might interfere with the transglycosylation efficiency to the wall matrix β-1,6-glucan. Moreover, the phenotype of the triple-*oma* mutant also resembles the described morphology of mutants which are

defective in GPI-anchor biosynthesis. Those mutants are incapable to interconnect the GPI-anchor of *O*-mannosylated proteins with the β-1,6-glucan of the wall matrix (Yada *et al.*, 2001).

However, the reasons for impaired transglycosylation of GPI-anchored proteins in the nmt81-*sup11* mutant are of different nature. Although the *O*-mannoproteins are correctly modified in the restricted nmt81-*sup11* mutant, the GPI-anchor cannot be transglycosylated efficiently to the β-1,6-glucan because this polysaccharide is vastly missing.

Another likely hypothesis why *sup11*$^+$ can act as multicopy-suppressor for the restricted nmt81-*oma2* mutant is because essential Sup11p itself is an *O*-mannoprotein. In contrast to the restricted nmt81-*oma2* knock-down mutant, overexpression of *sup11*$^+$ failed to rescue the *oma2*Δ and triple-*oma* mutant from lethality. This indicates that an elevated level of Sup11p can only complement for a decrease in Oma2p but not for a complete loss. The residual *oma2*$^+$ expression in the nmt81-*oma2* mutant might be negligible compared to endogenous levels but sufficient enough to allow the rescue due to *sup11*$^+$ overexpression. Moreover, the residual Oma2p activity is probably supported by up-regulation of Oma1p and Oma4p as indicated in the response of the triple-*oma* mutant.

sup11$^+$ overexpression in the *oma1*Δ, *oma4*Δ and permissive nmt81-*oma2* mutant caused impaired growth (see Fig. 5.35 and 5.36). However, growth of the wild type was unaffected by elevated Sup11p levels. Overexpression of the *O*-mannoprotein in PMT-family mutants probably caused an overload of the already impaired *O*-mannosylation machinery and the ER-quality control system which in consequence lead to impaired growth.

Compensatory up-regulation of the *oma1*$^+$ and *oma4*$^+$ *O*-mannosyl transferase genes upon restriction of the nmt81-*oma2* mutant could explain multicopy-suppressor function of *sup11*$^+$. Since Sup11p was shown to be mainly modified by Oma4p, up-regulated Oma4p levels might assists proper Sup11p processing in the restricted nmt81-*oma2* and thus relieves the overloaded ER and ensure sufficient proper folded/ modified Sup11p levels.

That Sup11p is mainly modified by Oma4p is probably the reason why overexpression in the *oma4*Δ mutant shows the most severe growth defect compared to *oma1*Δ and

nmt81-*oma2* (see Fig. 5.35 and 5.36). However, this model remains to be further investigated in future experiments.

So far, it is not clear which effect is responsible for Sup11p multicopy-suppressor property. Most likely it is a combinatory effect and possibly another - yet unknown - mechanism. However, this study presents the first example of an essential *O*-mannoprotein, whose hypo-mannosylation leads to lethality. Further experiments have to be performed to finally elucidate the linkage between Sup11p and protein *O*-mannosylation.

7. References

Aimanianda, V., C. Clavaud, C. Simenel, T. Fontaine, M. Delepierre and J.-P. Latgé (2009). "Cell Wall beta-(1,6)-Glucan of *Saccharomyces cerevisiae*: Structural Characterization and *in situ* Synthesis." *Journal of Biological Chemistry* **284**(20): 13401-13412.

Alonso-Nunez, M. L., H. An, A. B. Martín-Cuadrado, S. Mehta, C. Petit, M. Sipiczki, . . . C. R. Vázquez de Aldana (2005). "Ace2p Controls the Expression of Genes Required for Cell Separation in *Schizosaccharomyces pombe*." *Molecular Biology of the Cell* **16**(4): 2003-2017.

Altschul, S. F., T. L. Madden, A. A. Schäffer, J. Zhang, Z. Zhang, W. Miller and D. J. Lipman (1997). "Gapped BLAST and PSI-BLAST: a new generation of protein database search programs." *Nucleic Acids Research* **25**(17): 3389-3402.

Arellano, M., A. Duran and P. Perez (1996). "Rhol GTPase activates the (1-3)beta-D-glucan synthase and is involved in *Schizosaccharomyces pombe* morphogenesis." *The EMBO Journal* **15**(17): 4584-4591.

Arellano, M., M. H. Valdivieso, T. M. Calonge, P. M. Coll, A. Duran and P. Perez (1999). "*Schizosaccharomyces pombe* protein kinase C homologues, pck1p and pck2p, are targets of rho1p and rho2p and differentially regulate cell integrity." *Journal of cell science* **112**(20): 3569-3578.

Arroyo, J., J. Hutzler, C. Bermejo, E. Ragni, J. García-Cantalejo, P. Botías, . . . S. Strahl (2011). "Functional and genomic analyses of blocked protein *O*-mannosylation in baker's yeast." *Molecular Microbiology* **79**(6): 1529-1546.

Bähler, J. (2005). "A Transcriptional Pathway for Cell Separation in Fission Yeast." *Cell Cycle* **4**(1): 39-41.

Bähler, J. and J. R. Pringle (1998). "Pom1p, a fission yeast protein kinase that provides positional information for both polarized growth and cytokinesis." *Genes & Development* **12**(9): 1356-1370.

Bause, E. and G. Legler (1981). "The role of the hydroxy amino acid in the triplet sequence Asn-Xaa-Thr(Ser) for the *N*-glycosylation step during glycoprotein biosynthesis." *Biochem. J.* **195**(3): 639–644.

Bertani, G. (1951). "Studies on lysogenisis I.: The Mode of Phage Liberation by Lysogenic Escherichia coli." *Journal of Bacteriology* **62**(3): 293-300.

Boeke, J. D., J. Trueheart, G. Natsoulis and G. R. Fink (1987). 5-Fluoroorotic acid as a selective agent in yeast molecular genetics. Methods in Enzymology. L. G. Ray Wu, Academic Press. **Volume 154:** 164-175.

Boone, C., S. S. Sommer, A. Hensel and H. Bussey (1990). "Yeast KRE genes provide evidence for a pathway of cell wall beta-glucan assembly." *The Journal of Cell Biology* **110**(5): 1833-1843.

Braun, N. A., B. Morgan, T. P. Dick and B. Schwappach (2010). "The yeast CLC protein counteracts vesicular acidification during iron starvation." *Journal of Cell Science* **123**(13): 2342-2350.

Brown, J. L. and H. Bussey (1993). "The yeast *KRE9* gene encodes an *O*-glycoprotein involved in cell surface beta-glucan assembly." *Molecular and Cellular Biology* **13**(10): 6346-6356.

Brown, J. L., Z. Kossaczka, B. Jiang and H. Bussey (1993). "A mutational analysis of killer toxin resistance in *Saccharomyces cerevisiae* identifies new genes involved in cell wall (1-6)-beta-glucan synthesis." *Genetics* **133**(4): 837-849.

Bush, D. A., M. Horisberger, I. Horman and P. Wursch (1974). "The Wall Structure of *Schizosaccharomyces pombe*." *Journal of General Microbiology* **81**(1): 199-206.

Bussey, H. (1991). "K1 killer toxin, a pore-forming protein from yeast." *Molecular Microbiology* **5**(10): 2339-2343.

Cadou, A., A. Couturier, C. Le Goff, T. Soto, I. Miklos, M. Sipiczki, . . . X. Le Goff (2010). "Kin1 is a plasma membrane-associated kinase that regulates the cell surface in fission yeast." *Molecular Microbiology* **77**(5): 1186-1202.

Carlson, C. R., B. Grallert, R. Bernander, T. Stokke and E. Boye (1997). "Measurement of nuclear DNA content in fission yeast by flow cytometry." *Yeast* **13**(14): 1329-1335.

Carmona-Saez, P., M. Chagoyen, F. Tirado, J. Carazo and A. Pascual-Montano (2007). "GENECODIS: a web-based tool for finding significant concurrent annotations in gene lists." *Genome Biology* **8**(1): R3.

Causton, H. C., B. Ren, S. S. Koh, C. T. Harbison, E. Kanin, E. G. Jennings, . . . R. A. Young (2001). "Remodeling of Yeast Genome Expression in Response to Environmental Changes." *Molecular Biology of the Cell* **12**(2): 323-337.

Chappell, T. G., M. A. Hajibagheri, K. Ayscough, M. Pierce and G. Warren (1994). "Localization of an alpha-1,2-galactosyl transferase activity to the Golgi apparatus of *Schizosaccharomyces pombe*." *Molecular Biology of the Cell* **5**(5): 519-528.

Claros, M. G. and G. v. Heijne (1994). "TopPred II: an improved software for membrane protein structure predictions." *Computer applications in the biosciences : CABIOS* **10**(6): 685-686.

Colussi, P. A., C. H. Taron, J. C. Mack and P. Orlean (1997). "Human and Saccharomyces cerevisiae dolichol phosphate mannose synthases represent two classes of the enzyme, but both function in *Schizosaccharomyces pombe*." *Proceedings of the National Academy of Sciences* **94**(15): 7873-7878.

Consortium, T. G. O. (2008). "The Gene Ontology project in 2008." *Nucleic Acids Research* **36**(suppl 1): D440-D444.

Cortés, J. C. G., E. Carnero, J. Ishiguro, Y. Sánchez, A. Durán and J. C. Ribas (2005). "The novel fission yeast (1,3)beta-D-glucan synthase catalytic subunit Bgs4p is essential during both cytokinesis and polarized growth." *Journal of Cell Science* **118**(1): 157-174.

Cortés, J. C. G., J. Ishiguro, A. Durán and J. C. Ribas (2002). "Localization of the (1,3)β-D-glucan synthase catalytic subunit homologue Bgs1p/Cps1p from fission yeast suggests that it is involved in septation, polarized growth, mating, spore wall formation and spore germination." *Journal of Cell Science* **115**(21): 4081-4096.

Cortés, J. C. G., M. Konomi, I. M. Martins, J. Muñoz, M. B. Moreno, M. Osumi, . . . J. C. Ribas (2007). "The (1,3)β-d-glucan synthase subunit Bgs1p is responsible for the fission yeast primary septum formation." *Molecular Microbiology* **65**(1): 201-217.

Cortés, J. C. G., M. Sato, J. Munoz, M. B. Moreno, J. A. Clemente-Ramos, M. Ramos, . . . J. C. Ribas (2012). "Fission yeast Ags1 confers the essential septum strength needed for safe gradual cell abscission." *The Journal of Cell Biology* **198**(4): 637-656.

Cserzö, M., E. Wallin, I. Simon, G. von Heijne and A. Elofsson (1997). "Prediction of transmembrane alpha-helices in prokaryotic membrane proteins: the dense alignment surface method." *Protein Engineering* **10**(6): 673-676.

Davey, J. (1998). "Fusion of a fission yeast." *Yeast* **14**(16): 1529-1566.

De Groot, P. W. J., K. J. Hellingwerf and F. M. Klis (2003). "Genome-wide identification of fungal GPI proteins." *Yeast* **20**(9): 781-796.

De Groot, P. W. J., A. F. Ram and F. M. Klis (2005). "Features and functions of covalently linked proteins in fungal cell walls." *Fungal Genetics and Biology* **42**(8): 657-675.

de Groot, P. W. J., Q. Y. Yin, M. Weig, G. J. Sosinska, F. M. Klis and C. G. de Koster (2007). "Mass spectrometric identification of covalently bound cell wall proteins from the fission yeast *Schizosaccharomyces pombe*." *Yeast* **24**(4): 267-278.

de Medina-Redondo, M., Y. Arnáiz-Pita, C. Clavaud, T. Fontaine, F. del Rey, J. P. Latgé and C. R. Vázquez de Aldana (2010). "β(1,3)-Glucanosyl-Transferase Activity Is Essential for Cell Wall Integrity and Viability of *Schizosaccharomyces pombe*." *PLoS ONE* **5**(11): e14046.

De Medina-Redondo, M., Y. Arnáiz-Pita, T. Fontaine, F. Del Rey, J. P. Latgé and C. R. V. De Aldana (2008). "The β-1,3-glucanosyltransferase gas4p is essential for ascospore wall maturation and spore viability in *Schizosaccharomyces pombe*." *Molecular Microbiology* **68**(5): 1283-1299.

de Nobel, H. and P. N. Lipke (1994). "Is there a role for GPIs in yeast cell-wall assembly?" *Trends in Cell Biology* **4**(2): 42-45.

Degols, G., K. Shiozaki and P. Russell (1996). "Activation and regulation of the Spc1 stress-activated protein kinase in *Schizosaccharomyces pombe*." *Molecular and cellular biology* **16**(6): 2870-2877.

Dekker, N., D. Speijer, C. H. Grun, M. van den Berg, A. de Haan and F. Hochstenbach (2004). "Role of the beta-Glucanase Agn1p in Fission-Yeast Cell Separation." *Molecular Biology of the Cell* **15**(8): 3903-3914.

Dijkgraaf, G. J. P., J. L. Brown and H. Bussey (1996). "The KNH1 gene of *Saccharomyces cerevisiae* is a functional homolog of KRE9." *Yeast* **12**(7): 683-692.

Dubray, G. and G. Bezard (1982). "A highly sensitive periodic acid-silver stain for 1,2-diol groups of glycoproteins and polysaccharides in polyacrylamide gels." *Analytical biochemistry* **119**(2): 325-329.

Duenas-Santero, E., A. B. Martín-Cuadrado, T. Fontaine, J.-P. Latgé, F. del Rey and C. Vázquez de Aldana (2010). "Characterization of Glycoside Hydrolase Family 5 Proteins in *Schizosaccharomyces pombe*." *Eukaryotic Cell* **9**(11): 1650-1660.

Dunn, S. D. (1986). "Effects of the modification of transfer buffer composition and the renaturation of proteins in gels on the recognition of proteins on western blots by monoclonal antibodies." *Analytical biochemistry* **157**(1): 144-153.

Ecker, M., V. Mrsa, I. Hagen, R. Deutzmann, S. Strahl and W. Tanner (2003). "*O*-mannosylation precedes and potentially controls the *N*-glycosylation of a yeast cell wall glycoprotein." *EMBO reports* **4**(6): 628-632.

Ellgaard, L., M. Molinari and A. Helenius (1999). "Setting the Standards: Quality Control in the Secretory Pathway." *Science* **286**(5446): 1882-1888.

Fabian, J. (2009). Funktionelle Charakterisierung der Protein *O*-Mannosylierung der Spalthefe. HIP - Cell Chemistry. Heidelberg, Karls-Rupprecht-University.

Ferguson, M. A., S. W. Homans, R. A. Dwek and T. W. Rademacher (1988). "Glycosyl-phosphatidylinositol moiety that anchors Trypanosoma brucei variant surface glycoprotein to the membrane." *Science* **239**(4841): 753-759.

Forsburg, S. L. (1993). "Comparison of *Schizosaccharomyces pombe* expression systems." *Nucleic Acids Research* **21**(12): 2955-2956.

Forsburg, S. L. and N. Rhind (2006). "Basic methods for fission yeast." *Yeast* **23**(3): 173-183.

Frank, C. G., S. Sanyal, J. S. Rush, C. J. Waechter and A. K. Menon (2008). "Does Rft1 flip an N-glycan lipid precursor?" *Nature* **454**(7204): E3-E4.

Frieman, M. B. and B. P. Cormack (2003). "The ω-site sequence of glycosylphosphatidylinositol-anchored proteins in *Saccharomyces cerevisiae can* determine distribution between the membrane and the cell wall." *Molecular Microbiology* **50**(3): 883-896.

Fuchs, B. B. and E. Mylonakis (2009). "Our paths might cross: the role of the fungal cell wall integrity pathway in stress response and cross talk with other stress response pathways." *Eukaryotic cell* **8**(11): 1616-1625.

García, I., D. Jiménez, V. Martín, A. Durán and Y. Sánchez (2005). "The alpha-glucanase Agn1p is required for cell separation in *Schizosaccharomyces pombe*." *Biol. Cell* **97**(7): 569-576.

Gasch, A. P., P. T. Spellman, C. M. Kao, O. Carmel-Harel, M. B. Eisen, G. Storz, . . . P. O. Brown (2000). "Genomic Expression Programs in the Response of Yeast Cells to Environmental Changes." *Molecular Biology of the Cell* **11**(12): 4241-4257.

Gauthier, N. P., L. J. Jensen, R. Wernersson, S. r. Brunak and T. S. Jensen (2010). "Cyclebase.org: version 2.0, an updated comprehensive, multi-species repository of cell cycle experiments and derived analysis results." *Nucleic Acids Research* **38**(suppl 1): D699-D702.

Gauthier, N. P., M. E. Larsen, R. Wernersson, U. de Lichtenberg, L. J. Jensen, S. r. Brunak and T. S. t. Jensen (2008). "Cyclebase.org - a comprehensive multi-organism online database of cell-cycle experiments." *Nucleic Acids Research* **36**(suppl 1): D854-D859.

Gavel, Y. and G. v. Heijne (1990). "Sequence differences between glycosylated and non-glycosylated Asn-X-Thr/Ser acceptor sites: implications for protein engineering." *Protein Engineering* **3**(5): 433-442.

Gemmill, T. R. and R. B. Trimble (1999). "*Schizosaccharomyces pombe* produces novel Gal0–2Man1–3 *O*-linked oligosaccharides." *Glycobiology* **9**(5): 507-515.

Gentzsch, M. and W. Tanner (1997). "Protein *O*-glycosylation in yeast: protein-specific mannosyltransferases." *Glycobiology* **7**(4): 481-486.

Georgopapadakou, N. H. and J. S. Tkacz (1995). "The fungal cell wall as a drug target." *Trends in Microbiology* **3**(3): 98-104.

Georgopapadakou, N. H. and T. J. Walsh (1996). "Antifungal agents: chemotherapeutic targets and immunologic strategies." *Antimicrobial Agents and Chemotherapy* **40**(2): 279-291.

Giaever, G., A. M. Chu, L. Ni, C. Connelly, L. Riles, S. Veronneau, . . . M. Johnston (2002). "Functional profiling of the Saccharomyces cerevisiae genome." *Nature* **418**(6896): 387-391.

Girrbach, V. and S. Strahl (2003). "Members of the Evolutionarily Conserved PMT Family of ProteinO-Mannosyltransferases Form Distinct Protein Complexes among Themselves." *Journal of Biological Chemistry* **278**(14): 12554-12562.

Gonzalez, M., P. W. de Groot, F. M. Klis and P. N. Lipke (2009). "Glycoconjugate structure and function in fungal cell walls." *Microbial Glycobiology: Structures, Relevance, and Applications*: 169-183.

Gonzalez, M., P. N. Lipke and R. Ovalle (2009). Chapter 15 GPI Proteins in Biogenesis and Structure of Yeast Cell Walls. The Enzymes. P. O. T. K. Anant K. Menon and T. Fuyuhiko, Academic Press. **Volume 26:** 321-356.

Goto, M. (2007). "Protein *O*-Glycosylation in Fungi: Diverse Structures and Multiple Functions." *Bioscience, Biotechnology, and Biochemistry* **71**(6): 1415-1427.

Grün, C. H., F. Hochstenbach, B. M. Humbel, A. J. Verkleij, J. H. Sietsma, F. M. Klis, . . . J. F. G. Vliegenthart (2005). "The structure of cell wall α-glucan from fission yeast." *Glycobiology* **15**(3): 245-257.

Gupta, R., E. Jung and S. Brunak (2004). "Prediction of *N*-glycosylation sites in human proteins." *In preparation*.

Hagen, I., M. Ecker, A. Lagorce, J. M. Francois, S. Sestak, R. Rachel, . . . S. Strahl (2004). "Sed1p and Srl1p are required to compensate for cell wall instability in Saccharomyces cerevisiae mutants defective in multiple GPI-anchored mannoproteins." *Molecular Microbiology* **52**(5): 1413-1425.

Hanahan, D. (1983). "Studies on transformation of *Escherichia coli* with plasmids." *Journal of molecular Biology* **166**(4): 557-580.

Harty, C., S. Strahl and K. Römisch (2001). "*O*-Mannosylation Protects Mutant Alpha-Factor Precursor from Endoplasmic Reticulum-associated Degradation." *Molecular Biology of the Cell* **12**(4): 1093-1101.

Helenius, A. and M. Aebi (2004). "Roles of N-Linked Glycans in the Endoplasmic Reticulim." *Annual Review of Biochemistry* **73**: 1019-1049.

Herscovics, A. and P. Orlean (1993). "Glycoprotein biosynthesis in yeast." *The FASEB Journal* **7**(6): 540-550.

Hirokawa, T., S. Boon-Chieng and S. Mitaku (1998). "SOSUI: classification and secondary structure prediction system for membrane proteins." *Bioinformatics* **14**(4): 378-379.

Hirschberg, C. and M. Snider (1987). "Topography of glycosylation in the rough endoplasmic reticulum and Golgi apparatus." *Annual Review of Biochemistry* **56**: 63-87.

Hochstenbach, F., F. M. Klis, H. van den Ende, E. van Donselaar, P. J. Peters and R. D. Klausner (1998). "Identification of a putative alpha-glucan synthase essential for cell wall construction and morphogenesis in fission yeast." *Proceedings of the National Academy of Sciences* **95**(16): 9161-9166.

Hofmann, K. and W. Stoffel (1993). "TMbase - A database of membrane spanning proteins segments." *Biol. Chem. Hoppe-Seyler* **374**(166).

Holmes, D. S. and M. Quigley (1981). "A rapid boiling method for the preparation of bacterial plasmids." *Analytical biochemistry* **114**(1): 193-197.

Horisberger, M. and M. Rouvet-Vauthey (1985). "Cell wall architecture of the fission yeastSchizosaccharomyces pombe." *Experientia* **41**(6): 748-750.

Howard, A. and S. R. Pelc (1953). "Synthesis of Desoxyribonuclein Acid in Normal and Irradiated Cells and its Relation to Chromosome Breakage." *Heredity* **6**(261).

Huh, W.-K., J. V. Falvo, L. C. Gerke, A. S. Carroll, R. W. Howson, J. S. Weissman and E. K. O'Shea (2003). "Global analysis of protein localization in budding yeast." *Nature* **425**(6959): 686-691.

Humbel, B. M., M. Konomi, T. Takagi, N. Kamasawa, S. A. Ishijima and M. Osumi (2001). "In situ localization of β-glucans in the cell wall of *Schizosaccharomyces pombe*." *Yeast* **18**(5): 433-444.

Hutzler, F. (2009). Der Einfluss der Glykosylierung auf Zellwandintegrität und weitere vitale Prozesse in den Modellorganismen *Schizosaccharomyces pombe* und *Saccharomyces cerevisiae*. COS. Heidelberg, Karls-Rupprecht-University.

Igual, J. C., A. L. Johnson and L. H. Johnston (1996). "Coordinated regulation of gene expression by the cell cycle transcription factor Swi4 and the protein kinase C MAP kinase pathway for yeast cell integrity." *EMBO J* **15**(18): 5001–5013.

Ikeda, Y., T. Ohashi, N. Tanaka and K. Takegawa (2009). "Identification and characterization of a gene required for α1,2-mannose extension in the O-linked glycan synthesis pathway in Schizosaccharomyces pombe." *FEMS Yeast Research* **9**(1): 115-125.

Ishiguro, J., A. Saitou, A. Durán and J. C. Ribas (1997). "*cps1*$^{+}$, a *Schizosaccharomyces pombe* gene homolog of *Saccharomyces cerevisiae FKS* genes whose mutation confers

hypersensitivity to cyclosporin A and papulacandin B." *Journal of Bacteriology* **179**(24): 7653-7662.

Iwaki, T., A. Hosomi, S. Tokudomi, Y. Kusunoki, Y. Fujita, Y. Giga-Hama, . . . K. Takegawa (2006). "Vacuolar protein sorting receptor in *Schizosaccharomyces pombe*." *Microbiology* **152**(5): 1523-1532.

Janke, C., M. M. Magiera, N. Rathfelder, C. Taxis, S. Reber, H. Maekawa, . . . M. Knop (2004). "A versatile toolbox for PCR-based tagging of yeast genes: new fluorescent proteins, more markers and promoter substitution cassettes." *Yeast* **21**(11): 947-962.

Johnson, B. F., B. Y. Yoo and G. B. Calleja (1973). "Cell Division in Yeasts: Movement of Organelles Associated with Cell Plate Growth of *Schizosaccharomyces pombe*." *Journal of Bacteriology* **115**(1): 358-366.

Kaelin, W. G., W. Krek, W. R. Sellers, J. A. DeCaprio, F. Ajchenbaum, C. S. Fuchs, . . . E. K. Flemington (1992). "Expression cloning of a cDNA encoding a retinoblastoma-binding protein with E2F-like properties." *Cell* **70**(2): 351-364.

Kainuma, M., N. Ishida, T. Yoko-o, S. Yoshioka, M. Takeuchi, M. Kawakita and Y. Jigami (1999). "Coexpression of alpha-1,2 galactosyltransferase and UDP-galactose transporter efficiently galactosylates *N*- and *O*-glycans in *Saccharomyces cerevisiae*." *Glycobiology* **9**(2): 133-141.

Kamada, Y., U. S. Jung, J. Piotrowski and D. E. Levin (1995). "The protein kinase C-activated MAP kinase pathway of *Saccharomyces cerevisiae* mediates a novel aspect of the heat shock response." *Genes & Development* **9**(13): 1559-1571.

Katayama, S., D. Hirata, M. Arellano, P. Pérez and T. Toda (1999). "Fission Yeast α-Glucan Synthase Mok1 Requires the Actin Cytoskeleton to Localize the Sites of Growth and Plays an Essential Role in Cell Morphogenesis Downstream of Protein Kinase C Function." *The Journal of Cell Biology* **144**(6): 1173-1186.

Keller, A., A. I. Nesvizhskii, E. Kolker and R. Aebersold (2002). "Empirical Statistical Model To Estimate the Accuracy of Peptide Identifications Made by MS/MS and Database Search." *Analytical Chemistry* **74**(20): 5383-5392.

Kelly, T. J., G. S. Martin, S. L. Forsburg, R. J. Stephen, A. Russo and P. Nurse (1993). "The fission yeast *cdc18*$^{+}$ gene product couples S phase to START and mitosis." *Cell* **74**(2): 371-382.

Kippert, F. and D. Lloyd (1995). "The aniline blue fluorochrome specifically stains the septum of both live and fixed *Schizosaccharomyces pombe* cells." *FEMS Microbiology Letters* **132**(3): 215-219.

Kitayama, C., A. Sugimoto and M. Yamamoto (1997). "Type II Myosin Heavy Chain Encoded by the myo2 Gene Composes the Contractile Ring during Cytokinesis in *Schizosaccharomyces pombe*." *The Journal of Cell Biology* **137**(6): 1309-1319.

Klis, F. M., A. Boorsma and P. W. J. De Groot (2006). "Cell wall construction in *Saccharomyces cerevisiae*." *Yeast* **23**(3): 185-202.

Klis, F. M., P. Mol, K. Hellingwerf and S. Brul (2002). "Dynamics of cell wall structure in *Saccharomyces cerevisiae*." *FEMS Microbiology Reviews* **26**(3): 239-256.

Kollár, R., B. B. Reinhold, E. Petrákoá, H. J. C. Yeh, G. Ashwell, J. Drgonová, . . . E. Cabib (1997). "Architecture of the Yeast Cell Wall." *Journal of Biological Chemistry* **272**(28): 17762-17775.

Konomi, M., K. Fujimoto, T. Toda and M. Osumi (2003). "Characterization and behaviour of α-glucan synthase in *Schizosaccharomyces pombe* as revealed by electron microscopy." *Yeast* **20**(5): 427-438.

Kopecká, M., G. H. Fleet and H. J. Phaff (1995). "Ultrastructure of the Cell Wall of *Schizosaccharomyces pombe* Following Treatment with Various Glucanases." *Journal of Structural Biology* **114**(2): 140-152.

Kopecká, M., H. J. Phaff and G. H. Fleet (1974). "Demonstration of a Fibrillar Component in the Cell Wall of the Yeast *Sacchormyces cerevisiae* and its Chemical Nature." *The Journal of Cell Biology* **62**(1): 66-76.

Kornfeld, R. and S. Kornfeld (1985). "Assembly of Asparagine-Linked Oligosaccharides." *Annual Review of Biochemistry* **54**(1): 631-664.

Krogh, A., B. Larsson, G. von Heijne and E. L. L. Sonnhammer (2001). "Predicting transmembrane protein topology with a hidden markov model: application to complete genomes." *Journal of Molecular Biology* **305**(3): 567-580.

Kukuruzinskai, M. A., M. L. E. Berghi and B. J. Jacksoni (1987). "Protein Glycosylation in Yeast." *Annual Reviews* **56**: 915-944.

Kurita, T., Y. Noda, T. Takagi, M. Osumi and K. Yoda (2011). "Kre6 Protein Essential for Yeast Cell Wall beta-1,6-Glucan Synthesis Accumulates at Sites of Polarized Growth." *Journal of Biological Chemistry* **286**(9): 7429-7438.

Laemmli, U. K. (1970). "Cleavage of structural proteins during the assembly of the head of bacteriophage T4." *Nature* **227**: 680-685.

Larkin, M. A., G. Blackshields, N. P. Brown, R. Chenna, P. A. McGettigan, H. McWilliam, . . . D. G. Higgins (2007). "Clustal W and Clustal X version 2.0." *Bioinformatics* **23**(21): 2947-2948.

Latgé, J.-P. (2007). "The cell wall: a carbohydrate armour for the fungal cell." *Molecular Microbiology* **66**(2): 279-290.

Le Goff, X., A. Woollard and V. Simanis (1999). "Analysis of the cps1 gene provides evidence for a septation checkpoint in *Schizosaccharomyces pombe*." *Molecular and General Genetics MGG* **262**(1): 163-172.

Lehle, L., S. Strahl and W. Tanner (2006). "Protein Glycosylation, Conserved from Yeast to Man: A Model Organism Helps Elucidate Congenital Human Diseases." *Angewandte Chemie International Edition* **45**(41): 6802-6818.

Lesage, G. and H. Bussey (2006). "Cell Wall Assembly in *Saccharomyces cerevisiae*." *Microbiology and Molecular Biology Reviews* **70**(2): 317-343.

Levin, D. E. (2005). "Cell Wall Integrity Signaling in *Saccharomyces cerevisiae*." *Microbiology and Molecular Biology Reviews* **69**(2): 262-291.

Levinson, J. N., S. Shahinian, A.-M. Sdicu, D. C. Tessier and H. Bussey (2002). "Functional, comparative and cell biological analysis of Saccharomyces cerevisiae Kre5p." *Yeast* **19**(14): 1243-1259.

Li, H., N. Pagé and H. Bussey (2002). "Actin patch assembly proteins Las17p and Sla1p restrict cell wall growth to daughter cells and interact with cis-Golgi protein Kre6p." *Yeast* **19**(13): 1097-1112.

Lis, H. and N. Sharon (1993). "Protein glycosylation." *European Journal of Biochemistry* **218**(1): 1-27.

Liu, J., X. Tang, H. Wang and M. Balasubramanian (2000). "Bgs2p, a 1,3-Î²-glucan synthase subunit, is essential for maturation of ascospore wall in *Schizosaccharomyces pombe*." *FEBS Letters* **478**(1â€“2): 105-108.

Liu, J., X. Tang, H. Wang, S. Oliferenko and M. K. Balasubramanian (2002). "The Localization of the Integral Membrane Protein Cps1p to the Cell Division Site is Dependent on the Actomyosin Ring and the Septation-Inducing Network in *Schizosaccharomyces pombe*." *Molecular Biology of the Cell* **13**(3): 989-1000.

Liu, J., H. Wang, D. McCollum and M. K. Balasubramanian (1999). "Drc1p/Cps1p, a 1,3-beta-Glucan Synthase Subunit, Is Essential for Division Septum Assembly in *Schizosaccharomyces pombe*." *Genetics* **153**(3): 1193-1203.

Livak, K. J. and T. D. Schmittgen (2001). "Analysis of Relative Gene Expression Data Using Real-Time Quantitative PCR and the 2-delta delta CT Method." *Methods* **25**(4): 402-408.

Lizak, C., S. Gerber, S. Numao, M. Aebi and K. P. Locher (2011). "X-ray structure of a bacterial oligosaccharyltransferase." *Nature* **474**(7351): 350-355.

Lommel, M., M. Bagnat and S. Strahl (2004). "Aberrant Processing of the WSC Family and Mid2p Cell Surface Sensors Results in Cell Death of *Saccharomyces cerevisiae O*-Mannosylation Mutants." *Molecular and Cellular Biology* **24**(1): 46-57.

Lommel, M. and S. Strahl (2009). "Protein *O*-mannosylation: Conserved from bacteria to humans." *Glycobiology* **19**(8): 816-828.

Lu, C. F., R. C. Montijn, J. L. Brown, F. Klis, J. Kurjan, H. Bussey and P. N. Lipke (1995). "Glycosyl phosphatidylinositol-dependent cross-linking of alpha-agglutinin and beta 1,6-glucan in the *Saccharomyces cerevisiae* cell wall." *The Journal of Cell Biology* **128**(3): 333-340.

Lussier, M., A. M. Sdicu and H. Bussey (1999). "The KTR and MNN1 mannosyltransferase families of *Saccharomyces cerevisiae*." *Biochimica et Biophysica Acta* **1426**(2): 323-334.

Madrid, M., T. Soto, H. K. Khong, A. Franco, J. Vicente, P. Pérez, . . . J. Cansado (2006). "Stress-induced Response, Localization, and Regulation of the Pmk1 Cell Integrity Pathway in *Schizosaccharomyces pombe*." *Journal of Biological Chemistry* **281**(4): 2033-2043.

Magliani, W., S. Conti, M. Gerloni, D. Bertolotti and L. Polonelli (1997). "Yeast killer systems." *Clinical Microbiology Reviews* **10**(3): 369-400.

Magnelli, P. E., J. F. Cipollo and P. W. Robbins (2005). "A glucanase-driven fractionation allows redefinition of *Schizosaccharomyces pombe* cell wall composition and structure: assignment of diglucan." *Analytical biochemistry* **336**(2): 202-212.

Manners, D. J. and M. T. Meyer (1977). "The molecular structures of some glucans from the cell walls of *Schizosaccharomyces pombe*." *Carbohydrate Research* **57**(0): 189-203.

Marshall, R. D. (1972). "Glycoproteins." *Annual Review of Biochemistry* **41**(1): 673-702.

Martín-Cuadrado, A. B., E. Duenás, M. Sipiczki, C. R. V. de Aldana and F. del Rey (2003). "The endo-β-1,3-glucanase eng1p is required for dissolution of the primary septum during cell separation in *Schizosaccharomyces pombe*." *Journal of Cell Science* **116**(9): 1689-1698.

Martín, V., B. García, E. Carnero, A. Durán and Y. Sánchez (2003). "Bgs3p, a Putative 1,3-β-Glucan Synthase Subunit, Is Required for Cell Wall Assembly in *Schizosaccharomyces pombe*." *Eukaryotic Cell* **2**(1): 159-169.

Martín, V., J. C. Ribas, E. Carnero, A. Durán and Y. Sánchez (2000). "*bgs2*$^{+}$, a sporulation-specific glucan synthase homologue is required for proper ascospore wall maturation in fission yeast." *Molecular Microbiology* **38**(2): 308-321.

Matsuyama, A., R. Arai, Y. Yashiroda, A. Shirai, A. Kamata, S. Sekido, . . . M. Yoshida (2006). "ORFeome cloning and global analysis of protein localization in the fission yeast *Schizosaccharomyces pombe*." *Nat Biotech* **24**(7): 841-847.

Meaden, P., K. Hill, J. Wagner, D. Slipetz, S. S. Sommer and H. Bussey (1990). "The yeast KRE5 gene encodes a probable endoplasmic reticulum protein required for (1-6)-beta-D-glucan synthesis and normal cell growth." *Molecular and Cellular Biology* **10**(6): 3013-3019.

Meyer, A. J. and T. P. Dick (2010). "Fluorescent Protein-Based Redox Probes." *Antioxidants & Redox Signaling.* **13**(5): 621-650.

Michelsen, B. K. (1995). "Transformation of Escherichia coli increases 260-fold upon inactivation of T4 DNA ligase." *Analytical biochemistry* **225**(1): 172-174.

Mitchison, J. M. and J. Creanor (1971). "Further measurements of DNA synthesis and enzyme potential during cell cycle of fission yeast *Schizosaccharomyces pombe*." *Experimental Cell Research* **69**(1): 244-247.

Montijn, R. C., E. Vink, W. H. MÃ¼ller, A. J. Verkleij, H. Van Den Ende, B. Henrissat and F. M. Klis (1999). "Localization of Synthesis of beta-1,6-Glucan in *Saccharomyces cerevisiae*." *Journal of Bacteriology* **181**(24): 7414-7420.

Moreno, S., A. Klar and P. Nurse (1991). "Molecular genetics analysis of fission yeast *Schizosaccharomyces pombe*." *Methods Enzymology* **194**: 795-823.

Moseley, J. B., A. Mayeux, A. Paoletti and P. Nurse (2009). "A spatial gradient coordinates cell size and mitotic entry in fission yeast." *Nature* **459**(7248): 857-860.

Mrsă, V., T. Seidl, M. Gentzsch and W. Tanner (1997). "Specific Labelling of Cell Wall Proteins by Biotinylation. Identification of Four Covalently Linked *O*-mannosylated Proteins of *Saccharomyces cerevisiae*." *Yeast* **13**(12): 1145-1154.

Murray, A. (1994). "Cell cycle checkpoints." *Current Opinion in Cell Biology* **6**(6): 872-876.

Nachman, I. and A. Regev (2009). "BRNI: Modular analysis of transcriptional regulatory programs." *BMC Bioinformatics* **10**(1): 155.

Nagahashi, S., M. Lussier and H. Bussey (1998). "Isolation of Candida glabrata Homologs of the Saccharomyces cerevisiae KRE9 and KNH1Genes and Their Involvement in Cell Wall beta-1,6-Glucan Synthesis." *Journal of Bacteriology* **180**(19): 5020-5029.

Nakamata, K., T. Kurita, M. S. A. Bhuiyan, K. Sato, Y. Noda and K. Yoda (2007). "KEG1/YFR042w Encodes a Novel Kre6-binding Endoplasmic Reticulum Membrane Protein Responsible for beta-1,6-Glucan Synthesis in *Saccharomyces cerevisiae*." *Journal of Biological Chemistry* **282**(47): 34315-34324.

Neves, M. J. and J. François (1992). "On the mechanism by which a heat shock induces trehalose accumulation in *Saccharomyces cerevisiae*." *Biochem J.* **288(**(3): 859-864.

Nogales-Cadenas, R., P. Carmona-Saez, M. Vazquez, C. Vicente, X. Yang, F. Tirado, . . . A. Pascual-Montano (2009). "GeneCodis: interpreting gene lists through enrichment analysis and integration of diverse biological information." *Nucleic Acids Research* **37**(suppl 2): W317-W322.

Novak, B., A. Csikasz-Nagy, B. Gyorffy, K. Chen and J. J. Tyson (1998). "Mathematical model of the fission yeast cell cycle with checkpoint controls at the G1/S, G2/M and metaphase/anaphase transitions." *Biophysical Chemistry* **72**(1-2): 185-200.

Ohashi, T., K. Fujiyama and K. Takegawa (2012). "Identification of Novel alpha-1,3-Galactosyltransferase and Elimination of alpha-Galactose-containing Glycans by Disruption of Multiple alpha-Galactosyltransferase Genes in *Schizosaccharomyces pombe*." *Journal of Biological Chemistry* **287**(46): 38866-38875.

Ohashi, T., S.-i. Nakakita, W. Sumiyoshi, N. Yamada, Y. Ikeda, N. Tanaka and K. Takegawa (2010). "Structural analysis of alpha-1,3-linked galactose-containing oligosaccharides in *Schizosaccharomyces pombe* mutants harboring single and multiple alpha-galactosyltransferase genes disruptions." *Glycobiology* **21**(3): 340-351.

Ohkura, H., I. M. Hagan and D. M. Glover (1995). "The conserved *Schizosaccharomyces pombe* kinase plo1, required to form a bipolar spindle, the actin ring, and septum, can drive septum formation in G1 and G2 cells." *Genes & Development* **9**(9): 1059-1073.

Parent, S. A., J. B. Nielsen, N. Morin, G. Chrebet, N. Ramadan, A. M. Dahl, . . . F. Foor (1993). "Calcineurin-dependent growth of an FK506- and CsA-hypersensitive mutant of *Saccharomyces cerevisiae*." *Journal of General Microbiology* **139**(12): 2973-2984.

Philippsen, P., A. Stotz and C. Scherf (1991). "DNA of *Saccharomyces cerevisiae*." *Methods in Enzymology* **194**: 169-182.

Pollard, T. D. and J.-Q. Wu (2010). "Understanding cytokinesis: lessons from fission yeast." *Nat Rev Mol Cell Biol* **11**(2): 149-155.

Proctor, Stephen A., N. Minc, A. Boudaoud and F. Chang (2012). "Contributions of Turgor Pressure, the Contractile Ring, and Septum Assembly to Forces in Cytokinesis in Fission Yeast." *Current Biology* **22**(17): 1601-1608.

Pryme, I. F. (1986). "The importance of salt concentration during nitrogen cavitation of MPC-11 cells for the isolation of heavy rough endoplasmic reticulum membranes." ***Biochem Int*** **13**(2): 287-293.

Roemer, T., S. Delaney and H. Bussey (1993). "SKN1 and KRE6 define a pair of functional homologs encoding putative membrane proteins involved in beta-glucan synthesis." *Molecular and Cellular Biology* **13**(7): 4039-4048.

Roemer, T., G. Paravicini, M. A. Payton and H. Bussey (1994). "Characterization of the yeast (1,6)-beta-glucan biosynthetic components, Kre6p and Skn1p, and genetic interactions between the PKC1 pathway and extracellular matrix assembly." *The Journal of Cell Biology* **127**(2): 567-579.

Sambrook, J. A. R. and D. W. Russel (2001). Molecular Cloning: A Laboratory Manual. New York, Cold Spring Harbor Laboratory Press.

Shahinian, S. and H. Bussey (2000). "β-1,6-Glucan synthesis in *Saccharomyces cerevisiae*." *Molecular Microbiology* **35**(3): 477-489.

Sharma, C. B., P. Babczinski, L. Lehle and W. Tanner (1974). "The Role of Dolicholmonophosphate in Glycoprotein Biosynthesis in *Saccharomyces cerevisiae*." *European Journal of Biochemistry* **46**(1): 35-41.

Shematek, E. M., J. A. Braatz and E. Cabib (1980). "Biosynthesis of the yeast cell wall. I. Preparation and properties of beta-(1-3)glucan synthetase." *Journal of Biological Chemistry* **255**(3): 888-894.

Shental-Bechor, D. and Y. Levy (2008). "Effect of glycosylation on protein folding: A close look at thermodynamic stabilization." *Proceedings of the National Academy of Sciences* **105**(24): 8256-8261.

Shimizu, J., K. Yoda and M. Yamasaki (1994). "The hypo-osmolarity-sensitive phenotype of the Saccharomyces cerevisiae hpo2 mutant is due to a mutation in PKC1, which regulates expression of beta-glucanase." *Molecular and General Genetics MGG* **242**(6): 641-648.

Siam, R., W. P. Dolan and S. L. Forsburg (2004). "Choosing and using *Schizosaccharomyces pombe* plasmids." *Methods* **33**(3): 189-198.

Sipiczki, M. (2007). "Splitting of the fission yeast septum." *FEMS Yeast Research* **7**(6): 761-770.

Sipiczki, M. and A. Bozsik (2000). "The use of morphomutants to investigate septum formation and cell separation in *Schizosaccharomyces pombe*." *Archives of Microbiology* **174**(6): 386-392.

Sipiczki, M., B. Grallert and I. Miklos (1993). "Mycelial and syncytial growth in Schizosaccharomyces pombe induced by novel septation mutations." *Journal of Cell Science* **104**(2): 485-493.

Sohrmann, M., C. Fankhauser, C. Brodbeck and V. Simanis (1996). "The dmf1/mid1 gene is essential for correct positioning of the division septum in fission yeast." *Genes & Development* **10**(21): 2707-2719.

Solá, R. J. and K. Griebenow (2009). "Effects of glycosylation on the stability of protein pharmaceuticals." *Journal of Pharmaceutical Sciences* **98**(4): 1223-1245.

Soto, T., A. Franco, S. Padmanabhan, J. Vicente-Soler, J. Cansado and M. Gacto (2002). "Molecular interaction of neutral trehalase with other enzymes of trehalose metabolism in the fission yeast *Schizosaccharomyces pombe*." *European Journal of Biochemistry* **269**(15): 3847-3855.

Stenflo, J. and P. Fernlund (1982). "Amino acid sequence of the heavy chain of bovine protein C." *Journal of Biological Chemistry* **257**(20): 12180-12190.

Strahl-Bolsinger, S., M. Gentzsch and W. Tanner (1999). "Protein *O*-mannosylation." *Biochimica et Biophysica Acta (BBA) - General Subjects* **1426**(2): 297-307.

Sugawara, T., M. Sato, T. Takagi, T. Kamasaki, N. Ohno and M. Osumi (2003). "In situ localization of cell wall alpha-1,3-glucan in the fission yeast *Schizosaccharomyces pombe*." *Journal of Electron Microscopy* **52**(2): 237-242.

Tabas-Madrid, D., R. Nogales-Cadenas and A. Pascual-Montano (2012). "GeneCodis3: a non-redundant and modular enrichment analysis tool for functional genomics." *Nucleic Acids Research* **40**(W1): W478-W483.

Tabuchi, M., N. Tanaka, S. Iwahara and K. Takegawa (1997). "The *Schizosaccharomyces pombe gms1*$^{+}$ Gene Encodes an UDP-Galactose Transporter Homologue Required for Protein Galactosylation." *Biochemical and Biophysical Research Communications* **232**(1): 121-125.

Tams, J. W., J. Vind and K. G. Welinder (1999). "Adapting protein solubility by glycosylation.: *N*-Glycosylation mutants of Coprinus cinereus peroxidase in salt and organic solutions." *Biochimica et Biophysica Acta (BBA) - Protein Structure and Molecular Enzymology* **1432**(2): 214-221.

Tanaka, N. and K. Takegawa (2001). "Functional characterization of Gms1p/UDP-galactose transporter in *Schizosaccharomyces pombe*." *Yeast* **18**(8): 745-757.

Tran, P. T., L. Marsh, V. Doye, S. Inoué and F. Chang (2001). "A Mechanism for Nuclear Positioning in Fission Yeast Based on Microtubule Pushing." *The Journal of Cell Biology* **153**(2): 397-412.

Tyson, J. J., A. Csikasz-Nagy and B. Novak (2002). "The dynamics of cell cycle regulation." *BioEssays* **24**(12): 1095-1109.

Van Der Vaart, J. M., R. te Biesebeke, J. W. Chapman, F. M. Klis and C. T. Verrips (1996). "The beta-glucan containing side-chain of cell wall proteins of *Saccharomyces cerevisiae* is bound to the glycan core of the GPI moiety." *FEMS Microbiology Letters* **145**(3): 401-407.

Vida, T. A., G. Huyer and S. D. Emr (1993). "Yeast vacuolar proenzymes are sorted in the late Golgi complex and transported to the vacuole via a prevacuolar endosome-like compartment." *The Journal of Cell Biology* **121**(6): 1245-1256.

von Heijne, G. (1992). "Membrane protein structure prediction: Hydrophobicity analysis and the positive-inside rule." *Journal of Molecular Biology* **225**(2): 487-494.

Votsmeier, C. and D. Gallwitz (2001). "An acidic sequence of a putative yeast Golgi membrane protein binds COPII and facilitates ER export." *EMBO J* **20**(23): 6742-6750.

Wickner, R. B. (1986). "Double-Stranded RNA Replication in Yeast: The Killer System." *Annual Review of Biochemistry* **55**(1): 373-395.

Willer, T. (2003). Protein *O*-Mannosylierung konserviert von der Hefe bis zum Menschen: Untersuchungen zur Bedeutung der Protein *O*-Mannosyltransferasen in der Spalthefe und in Säugern. HIP. Heidelberg, Karls-Rupprecht-University.

Willer, T., M. Brandl, M. Sipiczki and S. Strahl (2005). "Protein *O*-mannosylation is crucial for cell wall integrity, septation and viability in fission yeast." *Molecular Microbiology* **57**(1): 156-170.

Wu, J.-Q., V. Sirotkin, D. R. Kovar, M. Lord, C. C. Beltzner, J. R. Kuhn and T. D. Pollard (2006). "Assembly of the cytokinetic contractile ring from a broad band of nodes in fission yeast." *The Journal of Cell Biology* **174**(3): 391-402.

Xu, C., S. Wang, G. Thibault and D. T. W. Ng (2013). "Futile Protein Folding Cycles in the ER Are Terminated by the Unfolded Protein *O*-Mannosylation Pathway." *Science* **340**(6135): 978-981.

Yada, T., R. Sugiura, A. Kita, Y. Itoh, Y. Lu, Y. Hong, . . . T. Kuno (2001). "Its8, a Fission Yeast Homolog of Mcd4 and Pig-n, Is Involved in GPI Anchor Synthesis and Shares an Essential Function with Calcineurin in Cytokinesis." *Journal of Biological Chemistry* **276**(17): 13579-13586.

Yoko-o, T., S. K. Roy and Y. Jigami (1998). "Differences in in vivo acceptor specificity of two galactosyltransferases, the *gmh3*$^{+}$ and *gma12*$^{+}$ gene products from *Schizosaccharomyces pombe*." *European Journal of Biochemistry* **257**(3): 630-637.

Zielinska, D. F., F. Gnad, J. R. Wisniewski and M. Mann (2010). "Precision Mapping of an In Vivo *N*-Glycoproteome Reveals Rigid Topological and Sequence Constraints." *Cell* **141**(5): 897-907.

8. Supplementary Data

Supplementary table 1:
Mass spectrometry results of the biotinylated cell wall proteins of the restricted nmt81-*sup11* mutant.

Displaying: Number of Unique Peptides					
#	Identified Proteins (27)	Accession Number	Molecular Weight	# of fragments detected in run 1	# of fragments detected in run 2
1	Isoleucine-tRNA ligase	SYIC_SCHPO	123 kDa	12	11
2	Putative coatomer subunit alpha OS	COPA_SCHPO	136 kDa	20	4
3	Carbamoyl-phosphate synthase arginine-specific large chain	CARB_SCHPO	127 kDa	12	6
4	Pyruvate carboxylase	PYC_SCHPO	131 kDa	14	2
5	Elongation factor 3	EF3_SCHPO	116 kDa	7	4
6	Lysophospholipase 1	PLB1_SCHPO	67 kDa	3	2
7	Putative alpha,alpha-trehalose-phosphate synthase	TPSX_SCHPO	107 kDa	7	2
8	1,3-beta-glucanosyltransferase gas2	GAS2_SCHPO	51 kDa	4	1
9	Probable DNA-directed RNA polymerase I subunit RPA2	RPA2_SCHPO	132 kDa	4	1
10	Tetratricopeptide repeat protein 1	TPR1_SCHPO	119 kDa	5	0
11	DNA-directed RNA polymerase II subunit RPB2	RPB2_SCHPO	138 kDa	4	0
12	Ubiquitin carboxyl-terminal hydrolase 21	UBP21_SCHPO	131 kDa	2	0
13	5'-3' exoribonuclease 2	XRN2_SCHPO	112 kDa	3	3
14	Pumilio domain-containing protein	YN8E_SCHPO	114 kDa	1	2
15	Probable nucleoporin	NG06_SCHPO	148 kDa	4	1
16	Uncharacterized protein	YKH3_SCHPO	136 kDa	2	1
17	Probable phosphoribosylformylglycinamidine synthase	PUR4_SCHPO	145 kDa	4	0
18	Cation-transporting ATPase 4	ATC4_SCHPO	136 kDa	3	1
19	Plasma membrane ATPase 1	PMA1_SCHPO	100 kDa	3	1
20	Vesicle-associated membrane protein-associated protein	YH75_SCHPO	41 kDa	2	1
21	Heat shock protein 70 homolog	YAM6_SCHPO	95 kDa	2	1
22	Protein transport protein sec31	SEC31_SCHPO	133 kDa	3	0
23	KH domain-containing protein	YJVE_SCHPO	141 kDa	3	0
24	Elongation factor 2	EF2_SCHPO	93 kDa	2	1
25	Probable ubiquitin carboxyl-terminal hydrolase 5	UBP5_SCHPO	129 kDa	2	1
26	Cell cycle control protein cwf11	CWF11_SCHPO	148 kDa	2	1
27	Glyceraldehyde-3-phosphate dehydrogenase 1	G3P1_SCHPO	36 kDa	2	0

Supplementary data table 2:
Up-regulated genes annotated with GO:0033554: cellular response to stress (biological process)

Regulation	p-value	Systematic Name	Gene Name	Gene Product
64.118	0.00069	SPAC869.09	SPAC869.09	conserved fungal protein
38.252	0.00002	SPBC1198.14c	fbp1	fructose-1,6-bisphosphatase
31.348	0.00034	SPAC5H10.02c	SPAC5H10.02c	ThiJ domain protein
31.062	0.00004	SPAC22H10.13	zym1	metallothionein
31.060	0.00001	SPBC16E9.16c	SPBC16E9.16c	sequence orphan
25.944	0.00004	SPAC23H3.15c	SPAC23H3.15c	sequence orphan
22.039	0.00015	SPAC3G6.07	SPAC3G6.07	sequence orphan
19.860	0.00320	SPAC22G7.11c	SPAC22G7.11c	conserved fungal protein
18.805	0.00051	SPCC338.18	SPCC338.18	sequence orphan
18.209	0.00009	SPAC869.02c	SPAC869.02c	nitric oxide dioxygenase (predicted)
16.907	0.00116	SPCC1739.08c	SPCC1739.08c	short chain dehydrogenase
14.409	0.00065	SPAC11D3.01c	SPAC11D3.01c	conserved fungal protein
14.285	0.00034	SPBPB2B2.12c	SPBPB2B2.12c	UDP-glucose 4-epimerase
14.204	0.00005	SPAC15E1.02c	SPAC15E1.02c	DUF1761 family protein
13.795	0.00109	SPBC1289.14	SPBC1289.14	adducin
13.609	0.00056	SPBC56F2.06	SPBC56F2.06	sequence orphan
11.843	0.00004	SPBC24C6.09c	SPBC24C6.09c	phosphoketolase (predicted)
11.387	0.00011	SPAC32A11.02c	SPAC32A11.02c	conserved fungal protein
10.973	0.00004	SPAC23C11.06c	SPAC23C11.06c	hydrolase (inferred from context)
10.303	0.00027	SPBC839.06	cta3	P-type ATPase, calcium transporting Cta3
10.025	0.00274	SPBC3H7.08c	SPBC3H7.08c	conserved fungal protein
9.642	0.00007	SPCC16A11.15c	SPCC16A11.15c	sequence orphan
9.100	0.00021	SPCPB1C11.02	SPCPB1C11.02	amino acid permease, unknown 16
8.715	0.00034	SPAC139.05	SPAC139.05	succinate-semialdehyde dehydrogenase (predicted)
8.000	0.00069	SPAC4H3.03c	SPAC4H3.03c	glucan 1,4-alpha-glucosidase (predicted)
7.126	0.00005	SPAC16A10.01	SPAC16A10.01	DUF1212 family protein
6.807	0.00019	SPCC1393.12	SPCC1393.12	sequence orphan
6.607	0.00054	SPACUNK4.17	SPACUNK4.17	NAD binding dehydrogenase family protein
6.539	0.00006	SPAC57A7.05	SPAC57A7.05	conserved protein (fungal and plant)
6.400	0.00008	SPCC757.03c	SPCC757.03c	ThiJ domain protein
5.983	0.00013	SPBC119.03	SPBC119.03	S-adenosylmethionine-dependent methyl transferase (predicted)
5.852	0.00059	SPAC22A12.17c	SPAC22A12.17c	short chain dehydrogenase (predicted)
5.539	0.00044	SPAC2C4.17c	SPAC2C4.17c	MS ion channel protein 2
5.191	0.00078	SPAPJ691.02	SPAPJ691.02	yippee-like protein
5.028	0.00014	SPAC637.03	SPAC637.03	conserved fungal protein
4.889	0.00051	SPCC417.05c	cfh2	chitin synthase regulatory factor (putative)
4.646	0.00001	SPAC20G4.03c	hri1	eIF2 alpha kinase Hri1

4.626	0.00695	SPAC1F8.01	ght3	hexose transporter Ght3
4.564	0.00599	SPAC13F5.03c	SPAC13F5.03c	glycerol dehydrogenase (Phlippen, Stevens, Wolf, Zimmermann manuscript in preparation)
4.446	0.00028	SPAC513.02	SPAC513.02	phosphoglycerate mutase family
4.412	0.00170	SPAC167.06c	SPAC167.06c	sequence orphan
4.400	0.00170	SPAC14C4.01c	SPAC14C4.01c	DUF1770 family protein
4.322	0.00062	SPBC365.12c	ish1	LEA domain protein
4.295	0.00005	SPCC1183.09c	pmp31	plasma membrane proteolipid Pmp31
4.289	0.00040	SPBC1773.05c	tms1	hexitol dehydrogenase (predicted)
4.284	0.00428	SPBP4H10.10	SPBP4H10.10	rhomboid family protease
4.274	0.00068	SPAC3A11.10c	SPAC3A11.10c	dipeptidyl aminopeptidase (predicted)
4.219	0.00083	SPBC725.03	SPBC725.03	conserved fungal protein
4.026	0.00089	SPAC22F8.05	SPAC22F8.05	alpha,alpha-trehalose-phosphate synthase (predicted)
3.985	0.00050	SPCC4G3.03	SPCC4G3.03	WD repeat protein
3.885	0.01477	SPAC977.13c	---	---
3.854	0.00029	SPBC428.10	SPBC428.10	sequence orphan
3.841	0.00026	SPAC17G8.13c	mst2	histone acetyl transferase Mst2
3.774	0.00039	SPAPB1A11.03	SPAPB1A11.03	FMN dependent dehydrogenase
3.731	0.00145	SPAC1F8.05	isp3	sequence orphan
3.708	0.00016	SPBC32C12.02	aff1	transcription factor Ste11
3.704	0.00116	SPAC4A8.04	isp6	vacuolar serine protease Isp6
3.694	0.00037	SPBC725.10	SPBC725.10	tspO homolog
3.630	0.00318	SPAC26F1.14c	aif1	apoptosis-inducing factor homolog Aif1
3.593	0.00327	SPBC3E7.02c	hsp16	heat shock protein Hsp16
3.590	0.00026	SPAC4H3.04c	SPAC4H3.04c	UPF0103 family
3.572	0.00112	SPAC8C9.16c	SPAC8C9.16c	TLDc domain protein 1
3.545	0.00273	SPCC757.07c	cta1	catalase
3.544	0.00091	SPAC3C7.05c	SPAC3C7.05c	alpha-1,6-mannanase (predicted)
3.542	0.00035	SPCC191.01	SPCC191.01	sequence orphan
3.529	0.00112	SPAC19G12.09	SPAC19G12.09	NADH/NADPH dependent indole-3-acetaldehyde reductase AKR3C2
3.460	0.00021	SPAC3C7.13c	SPAC3C7.13c	glucose-6-phosphate 1-dehydrogenase (predicted)
3.403	0.00039	SPCC338.12	SPCC338.12	protease inhibitor (predicted)
3.366	0.00342	SPAC27E2.05	cdc1	DNA polymerase delta small subunit
3.297	0.00034	SPAC4D7.02c	SPAC4D7.02c	glycerophosphoryl diester phosphodiesterase (predicted)
3.293	0.00110	SPCP31B10.06	SPCP31B10.06	C2 domain protein (predicted)
3.265	0.00000	SPCC1235.01	SPCC1235.01	sequence orphan
3.234	0.00006	SPAC2G11.13	atg22	autophagy associated protein (predicted)
3.206	0.00078	SPBC23G7.11	SPBC23G7.11	DNA-3-methyladenine glycosidase (predicted)
3.203	0.00003	SPBC660.06	SPBC660.06	conserved fungal protein
3.177	0.00005	SPCC1020.10	oca2	serine/threonine protein kinase (predicted)

3.129	0.00078	SPAC688.04c	gst3	glutathione S-transferase
3.098	0.00005	SPBC1271.03c	SPBC1271.03c	phosphoprotein phosphatase
3.070	0.00014	SPAC513.06c	SPAC513.06c	dihydrodiol dehydrogenase (predicted)
2.995	0.00028	SPCC1450.13c	SPCC1450.13c	riboflavin synthase
2.963	0.00131	SPAC11D3.16c	SPAC11D3.16c	sequence orphan
2.954	0.00014	SPCC16A11.01	SPCC16A11.01	conserved fungal protein
2.890	0.00408	SPBC1105.14	rsv2	transcription factor Rsv2
2.764	0.00427	SPAC1687.14c	SPAC1687.14c	EF hand family protein, unknown role
2.761	0.00141	SPBC16A3.02c	SPBC16A3.02c	mitochondrial peptidase (predicted)
2.746	0.00382	SPBC1683.08	ght4	hexose transporter Ght4
2.743	0.00349	SPAC29A4.17c	SPAC29A4.17c	FUN14 family protein
2.704	0.00003	SPAC2E1P3.01	SPAC2E1P3.01	zinc binding dehydrogenase
2.694	0.00042	SPAC1B3.06c	SPAC1B3.06c	UbiE family methyl transferase (predicted)
2.659	0.00005	SPCC330.03c	SPCC330.03c	NADPH-hemoprotein reductase
2.565	0.00011	SPAC26F1.04c	etr1	enoyl-[acyl-carrier protein] reductase
2.554	0.00041	SPAC1687.07	SPAC1687.07	conserved fungal protein
2.519	0.00151	SPAC21E11.04	ppr1	L-azetidine-2-carboxylic acid acetyl transferase
2.517	0.00073	SPAC20G4.02c	fus1	formin Fus1
2.443	0.00525	SPAC19D5.01	pyp2	tyrosine phosphatase Pyp2
2.366	0.00566	SPAC13F5.07c	SPAC13F5.07c	previusly annotated as dubious, may not be protein coding
2.334	0.08091	SPBC1683.09c	frp1	ferric-chelate reductase Frp1
2.316	0.00172	SPBC1683.06c	SPBC1683.06c	uridine ribohydrolase (predicted)
2.313	0.00549	SPCC24B10.14c	nej1	xrcc4 like factor
2.312	0.00413	SPAC31G5.18c	SPAC31G5.18c	ubiquitin family, human C1ORF55 related
2.295	0.00204	SPAC27D7.09c	SPAC27D7.09c	S. pombe specific But2 family protein
2.295	0.00086	SPCC576.17c	SPCC576.17c	membrane transporter
2.287	0.00012	SPCC1183.11	SPCC1183.11	MS ion channel protein 1
2.251	0.00176	SPAC15A10.05c	SPAC15A10.05c	YjeF family protein
2.248	0.01070	SPAC11D3.09	SPAC11D3.09	agmatinase (predicted)
2.237	0.00371	SPBC1348.12	---	---
2.227	0.00218	SPCC191.09c	gst1	glutathione S-transferase Gst1
2.221	0.00293	SPBC1604.01	SPBC1604.01	sulfatase modifying factor 1 related
2.220	0.00188	SPCC4F11.04c	SPCC4F11.04c	mannosyl transferase complex subunit (predicted)
2.212	0.00098	SPAC8E11.03c	dmc1	RecA family ATPase Dmc1
2.206	0.00451	SPAC31G5.09c	spk1	MAP kinase Spk1
2.193	0.01578	SPAC343.12	rds1	conserved fungal protein
2.191	0.00027	SPAC1D4.11c	kic1	dual specificity protein kinase Lkh1
2.187	0.00131	SPAC1687.22c	puf3	RNA-binding protein Puf3 (predicted)
2.164	0.00055	SPAC8C9.03	cgs1	cAMP-dependent protein kinase regulatory subunit
2.152	0.00231	SPAC18G6.09c	SPAC18G6.09c	sequence orphan
2.126	0.00473	SPBC3B8.10c	SPBC3B8.10c	NLI interacting factor family

2.100	0.00221	SPAC589.07c	SPAC589.07c	WD repeat protein Atg18
2.093	0.00131	SPBC25B2.03	SPBC25B2.03	zf-C3HC4 type zinc finger
2.085	0.00877	SPBC106.02c	srx1	sulphiredoxin
2,081	0.00209	SPAC343.06c	SPAC343.06c	scramblase
2,067	0.00362	SPAC4G8.10	gos1	SNARE Gos1
2.062	0.01716	SPCC1450.01c	---	---
2.044	0.01027	SPAC22G7.08	ppk8	serine/threonine protein kinase (predicted)
2.042	0.00047	SPAC17G6.02c	SPAC17G6.02c	RTA1-like protein
2.037	0.00334	SPBC660.07	ntp1	alpha,alpha-trehalase Ntp1
2.037	0.00866	SPAC458.04c	SPAC458.04c	sequence orphan
2.034	0.00411	SPCC1223.03c	gut2	glycerol-3-phosphate dehydrogenase Gut2
2.032	0.00617	SPAC19B12.08	SPAC19B12.08	peptidase family C54
2.027	0.00369	SPAC13D6.01	pof14	F-box protein Pof14
2.007	0.00996	SPBP8B7.24c	atg8	autophagy associated protein Atg8 (predicted)
2.005	0.00182	SPCC1020.05	SPCC1020.05	phosphoprotein phosphatase (predicted)

Supplementary data table 3:
Up-regulated genes in restricted nmt81-*sup11* mutant.

Regulation	p-value	Systematic Name	Gene Name	Gene Product
159.737	0.00000	SPBPB21E7.04c	SPBPB21E7.04c	S-adenosylmethionine-dependent methyl transferase (predicted)
111.813	0.00002	SPCC737.04	SPCC737.04	S. pombe specific UPF0300 family protein 6
85.219	0.00069	SPAC4F10.17	SPAC4F10.17	conserved fungal protein
71.741	0.00002	SPBPB21E7.01c	SPBPB8B6.07c	enolase (predicted)
64.118	0.00098	SPAC869.09	SPAC869.09	conserved fungal protein
38.252	0.00002	SPBC1198.14c	fbp1	fructose-1,6-bisphosphatase Fbp1
37.250	0.00049	SPAC29A4.12c	SPAC29A4.12c	sequence orphan
31.348	0.00034	SPAC5H10.02c	SPAC5H10.02c	ThiJ domain protein
31.062	0.00004	SPAC22H10.13	zym1	metallothionein
31.060	0.00001	SPBC16E9.16c	SPBC16E9.16c	sequence orphan
29.266	0.00004	SPBCPT2R1.02	SPBCPT2R1.02	sequence orphan
25.944	0.00015	SPAC23H3.15c	SPAC23H3.15c	sequence orphan
25.254	0.00023	SPBPB21E7.02c	---	---
23.798	0.00320	SPBPB2B2.18	SPBPB2B2.18	dubious
22.039	0.00051	SPAC3G6.07	SPAC3G6.07	sequence orphan
21.246	0.00009	SPCPB16A4.06c	SPCPB16A4.06c	sequence orphan
21.084	0.00009	SPBC359.06	SPBC359.06	adducin
19.860	0.00083	SPAC22G7.11c	SPAC22G7.11c	conserved fungal protein
19.506	0.00002	SPBP4G3.03	SPBP4G3.03	PI31 proteasome regulator related
18.805	0.00024	SPCC338.18	SPCC338.18	sequence orphan
18.230	0.00065	SPAC6B12.03c	SPAC6B12.03c	HbrB family protein

18.209	0.00009	SPAC869.02c	SPAC869.02c	nitric oxide dioxygenase (predicted)
17340	0.00545	SPAC977.15	SPAC977.15	dienelactone hydrolase family
16.907	0.00116	SPCC1739.08c	SPCC1739.08c	short chain dehydrogenase
16.515	0.00024	SPAC3G9.11c	SPAC3G9.11c	pyruvate decarboxylase (predicted)
16.037	0.00003	SPAC15A10.10	mde6	Muskelin homolog
15.980	0.00026	SPAC869.07c	mel1	alpha-galactosidase
14.409	0.00065	SPAC11D3.01c	SPAC11D3.01c	conserved fungal protein
14.285	0.00034	SPBPB2B2.12c	SPBPB2B2.12c	UDP-glucose 4-epimerase
14.204	0.00005	SPAC15E1.02c	SPAC15E1.02c	DUF1761 family protein
13.795	0.00109	SPBC1289.14	SPBC1289.14	adducin
13.706	0.00002	SPAC212.02	SPAC212.02	sequence orphan
13.609	0.00056	SPBC56F2.06	SPBC56F2.06	sequence orphan
12.736	0.00012	SPBC1198.01	SPBC1198.01	glutathione-dependent formaldehyde dehydrogenase (predicted)
11.843	0.00004	SPBC24C6.09c	SPBC24C6.09c	phosphoketolase (predicted)
11.411	0.00315	SPAC750.04c	SPAC750.04c	dubious
11.387	0.00011	SPAC32A11.02c	SPAC32A11.02c	conserved fungal protein
11.321	0.00022	SPBC83.19c	SPBC83.19c	sequence orphan
10.973	0.00004	SPAC23C11.06c	SPAC23C11.06c	hydrolase (inferred from context)
10.776	0.00048	SPCC757.02c	SPCC757.02c	epimarase (predicted)
10.303	0.00027	SPBC839.06	cta3	P-type ATPase, calcium transporting Cta3
10.174	0.00274	SPAC977.04	SPAC977.04	membrane transporter /
10.025	0.00089	SPBC3H7.08c	SPBC3H7.08c	conserved fungal protein
9.642	0.00007	SPCC16A11.15c	SPCC16A11.15c	sequence orphan
9.538	0.00088	SPAC186.07c	SPAC186.07c	hydroxyacid dehydrogenase (predicted)
9.479	0.00090	SPCC794.01c	SPCC794.01c	glucose-6-phosphate 1-dehydrogenase (predicted)
9.304	0.00012	SPAC750.01	SPAC977.14c	aldo/keto reductase, unknown biological role
9.100	0.00021	SPCPB1C11.02	SPCPB1C11.02	amino acid permease, unknown 16
9.019	0.01809	SPAC977.16c	dak2	dihydroxyacetone kinase Dak2
8.733	0.00006	SPAC25G10.04c	rec10	meiotic recombination protein Rec10
8.715	0.00034	SPAC139.05	SPAC139.05	succinate-semialdehyde dehydrogenase (predicted)
8.300	0.00029	SPBC19F8.06c	meu22	amino acid permease, unknown 11
8.263	0.00179	SPBC2G2.17c	SPBC2G2.17c	beta-glucosidase Psu2 (predicted)
8.178	0.03738	SPAC869.06c	SPAC869.06c	cation binding protein (predicted)
8.000	0.00069	SPAC4H3.03c	SPAC4H3.03c	glucan 1,4-alpha-glucosidase (predicted)
7.851	0.00915	SPCC320.07c	mde7	RNA-binding protein Mde7
7.126	0.00005	SPAC16A10.01	SPAC16A10.01	DUF1212 family protein
7.057	0.00019	SPAC1002.20	SPAC1002.20	sequence orphan
6.930	0.00133	SPCC794.02	SPCC794.02	wtf element Wtf5
6.807	0.00013	SPCC1393.12	SPCC1393.12	sequence orphan
6.806	0.00171	SPCC1259.14c	meu27	S. pombe specific UPF0300 family protein 5
6.713	0.00054	SPBPB21E7.06	---	---
6.708	0.00006	SPBC19C7.04c	SPBC19C7.04c	conserved fungal protein

6.607	0.00058	SPACUNK4.17	SPACUNK4.17	NAD binding dehydrogenase family protein
6.539	0.00005	SPAC57A7.05	SPAC57A7.05	conserved protein (fungal and plant)
6.508	0.00216	SPAC222.15	meu13	Tat binding protein 1(TBP-1)-interacting protein (TBPIP) homolog (predicted)
6.400	0.00008	SPCC757.03c	SPCC757.03c	ThiJ domain protein
6.247	0.00064	SPCC1235.13	ght6	hexose transporter Ght6
6.184	0.00311	SPAC869.08	pcm2	protein-L-isoaspartate O-methyl transferase (predicted)
5.983	0.00013	SPBC119.03	SPBC119.03	S-adenosylmethionine-dependent methyl transferase (predicted)
5.977	0.00498	SPAC4H3.08	SPAC4H3.08	short chain dehydrogenase (predicted)
5.947	0.00035	SPCC1906.04	wtf20	wtf element Wtf20
5.852	0.00059	SPAC22A12.17c	SPAC22A12.17c	short chain dehydrogenase (predicted)
5.774	0.00249	SPAPB24D3.07c	SPAPB24D3.07c	sequence orphan
5.539	0.00044	SPAC2C4.17c	SPAC2C4.17c	MS ion channel protein 2
5.383	0.00342	SPAC1002.19	urg1	GTP cyclohydrolase (predicted)
5.319	0.01814	SPAC2H10.01	SPAC2H10.01	transcription factor
5.290	0.00017	SPBC660.09	SPBC660.09	sequence orphan
5.247	0.00106	SPCC4F11.05	SPCC4F11.05	dubious
5.222	0.00638	SPBC947.05c	SPBC947.05c	ferric-chelate reductase (predicted)
5.191	0.00078	SPAPJ691.02	SPAPJ691.02	yippee-like protein
5.084	0.00038	SPAC1093.06c	dhc1	dynein heavy chain
5.028	0.00014	SPAC637.03	SPAC637.03	conserved fungal protein
4.997	0.00060	SPAC22G7.07c	SPAC22G7.07c	mRNA (N6-adenosine)-methyl transferase (predicted)
4.895	0.00191	SPCC1906.04	wtf20	wtf element Wtf20
4.889	0.00051	SPCC417.05c	cfh2	chitin synthase regulatory factor (putative) Chr2
4.885	0.00330	SPCC191.11	inv1	beta-fructofuranosidase
4.847	0.00001	SPAC26H5.08c	bgl2	glucan 1,3-beta-glucosidase Bgl2
4.706	0.00842	SPBC1706.02c	wtf10	wtf element Wtf10
4.646	0.00001	SPAC20G4.03c	hri1	eIF2 alpha kinase Hri1
4.626	0.00695	SPAC1F8.01	ght3	hexose transporter Ght3
4.564	0.00599	SPAC13F5.03c	SPAC13F5.03c	glycerol dehydrogenase (Phlippen, Stevens, Wolf, Zimmermann manuscript in preparation)
4.481	0.00028	SPCC1906.04	wtf20	wtf element Wtf20
4.451	0.00003	SPBC119.05c	SPBC119.05c	Wiskott-Aldrich syndrome homolog binding protein Lsb1 (predicted)
4.446	0.00128	SPAC513.02	SPAC513.02	phosphoglycerate mutase family
4.412	0.00170	SPAC167.06c	SPAC167.06c	sequence orphan
4.400	0.00170	SPAC14C4.01c	SPAC14C4.01c	DUF1770 family protein
4.381	0.00066	SPCC576.01c	SPCPB1C11.04c	sulfonate dioxygenase (predicted)
4.330	0.00093	SPBC119.04	mei3	meiosis inducing protein Mei3
4.322	0.00062	SPBC365.12c	ish1	LEA domain protein
4.305	0.00008	SPAC4G8.13c	prz1	transcription factor Prz1

4.295	0.00005	SPCC1183.09c	pmp31	plasma membrane proteolipid Pmp31
4.289	0.00040	SPBC1773.05c	tms1	hexitol dehydrogenase (predicted)
4.284	0.00428	SPBP4H10.10	SPBP4H10.10	rhomboid family protease
4.274	0.00068	SPAC3A11.10c	SPAC3A11.10c	dipeptidyl aminopeptidase (predicted)
4.235	0.58073	SPAC977.05c	SPAC977.05c	conserved fungal protein
4.219	0.00083	SPBC725.03	SPBC725.03	conserved fungal protein
4.175	0.00025	SPAC1039.07c	SPAC1039.07c	2,2-dialkylglycine decarboxylase (predicted)
4.132	0.00108	SPAC32A11.01	SPAC32A11.01	conserved fungal protein
4.126	0.00360	SPBC1685.05	SPBC1685.05	serine protease (predicted)
4.125	0.00089	SPBC14C8.05c	meu17	glucan-alpha-1,4-glucosidase
4.077	0.00057	SPAC20H4.11c	rho5	Rho family GTPase Rho5
4.026	0.00035	SPAC22F8.05	SPAC22F8.05	alpha,alpha-trehalose-phosphate synthase (predicted)
3.985	0.00050	SPCC4G3.03	SPCC4G3.03	WD repeat protein
3.914	0.00002	SPAC15A10.09c	SPAC15A10.09c	conserved fungal protein
3.885	0.01477	SPAC977.13c	---	---
3.860	0.00045	SPBC19G7.06	mbx1	MADS-box transcription factor Mbx1
3.854	0.00029	SPBC428.10	SPBC428.10	sequence orphan
3.853	0.00064	SPCC417.06c	mug27	serine/threonine protein kinase Ppk35
3.841	0.00026	SPAC17G8.13c	mst2	histone acetyl transferase Mst2
3.816	0.00172	SPAC186.04c	---	---
3.803	0.00009	SPAPB2B4.04c	SPAPB2B4.04c	P-type ATPase, calcium transporting Pmc1
3.787	0.00015	SPCC737.03c	SPCC737.03c	conserved eukaryotic protein
3.782	0.00039	SPAC824.02	SPAC824.02	GPI inositol deacylase
3.774	0.00153	SPAPB1A11.03	SPAPB1A11.03	FMN dependent dehydrogenase
3.731	0.00145	SPAC1F8.05	isp3	sequence orphan
3.708	0.00016	SPBC32C12.02	aff1	transcription factor Ste11
3.704	0.00116	SPAC4A8.04	isp6	vacuolar serine protease Isp6
3.694	0.00037	SPBC725.10	SPBC725.10	tspO homolog
3.644	0.00230	SPCC70.04c	SPCC70.04c	sequence orphan
3.630	0.00318	SPAC26F1.14c	aif1	apoptosis-inducing factor homolog Aif1
3.601	0.00169	SPBC15D4.02	SPBC15D4.02	transcription factor
3.593	0.00327	SPBC3E7.02c	hsp16	heat shock protein Hsp16
3.590	0.00026	SPAC4H3.04c	SPAC4H3.04c	UPF0103 family
3.572	0.00112	SPAC8C9.16c	SPAC8C9.16c	TLDc domain protein 1
3.545	0.00273	SPCC757.07c	cta1	catalase
3.544	0.00057	SPAC3C7.05c	SPAC3C7.05c	alpha-1,6-mannanase (predicted)
3.542	0.00091	SPCC191.01	SPCC191.01	sequence orphan
3.529	0.00035	SPAC19G12.09	SPAC19G12.09	NADH/NADPH dependent indole-3-acetaldehyde reductase AKR3C2
3.496	0.00204	SPBC1683.01	SPBC1683.01	inorganic phosphate transporter (predicted)
3.494	0.00001	SPAC2F3.01	SPAC2F3.01	mannosyltransferase complex subunit
3.468	0.00018	SPBC15C4.06c	SPBC15C4.06c	ubiquitin-protein ligase E3 (predicted)
3.460	0.00021	SPAC3C7.13c	SPAC3C7.13c	glucose-6-phosphate 1-dehydrogenase (predicted)

3.454	0.00452	SPCC794.02	SPCC794.02	wtf element Wtf5
3.403	0.00039	SPCC338.12	SPCC338.12	protease inhibitor (predicted)
3.403	0.00018	SPBC1198.07c	SPBC1198.07c	mannan endo-1,6-alpha-mannosidase (predicted)
3395	0.00003	SPAC18B11.03c	SPAC18B11.03c	N-acetyl transferase (predicted)
3.376	0.00023	SPAC630.05	gyp7	GTPase activating protein Gyp7 (predicted)
3.366	0.00016	SPAC27E2.05	cdc1	DNA polymerase delta small subunit Cdc1
3.352	0.00342	SPCC576.16c	---	---
3.334	0.00034	SPBC646.17c	SPBP35G2.01c	dynein intermediate chain Dic1
3.329	0.00049	SPBC16D10.05	mok13	alpha-1,3-glucan synthase Mok13
3.328	0.00863	SPAC186.06	SPAC186.06	human MAWBP homolog
3.312	0.00082	SPCC569.03	SPCC569.03	DUF1773 family protein 4
3.297	0.00059	SPAC4D7.02c	SPAC4D7.02c	glycerophosphoryl diester phosphodiesterase (predicted)
3.293	0.00110	SPCP31B10.06	SPCP31B10.06	C2 domain protein Tcb3 (predicted)
3.287	0.00951	SPAC1A6.11	SPAC1A6.11	dubious
3.265	0.00000	SPCC1235.01	SPCC1235.01	sequence orphan
3.239	0.00069	SPAC4G9.07	SPAC4G9.07	S. pombe specific UPF0300 family protein 2
3.234	0.00006	SPAC2G11.13	atg22	autophagy associated protein Atg22 (predicted)
3.233	0.00001	SPAC13C5.05c	SPAC13C5.05c	N-acetylglucosamine-phosphate mutase (predicted)
3.206	0.00078	SPBC23G7.11	SPBC23G7.11	DNA-3-methyladenine glycosidase Mag2 (predicted)
3.203	0.00003	SPBC660.06	SPBC660.06	conserved fungal protein
3.202	0.00005	SPBC21B10.07	SPBC21B10.07	glycosyl hydrolase family 16
3.177	0.00081	SPCC1020.10	oca2	serine/threonine protein kinase Oca2 (predicted)
3.162	0.00116	SPBC23E6.03c	nta1	protein N-terminal amidase Nta1 (predicted)
3.160	0.00060	SPCC4B3.02c	SPCC4B3.02c	Golgi transport protein Got1 (predicted)
3.145	0.00005	SPACUNK12.02c	cmk1	calcium/calmodulin-dependent protein kinase Cmk1
3.129	0.00078	SPAC688.04c	gst3	glutathione S-transferase
3.103	0.01196	SPAC212.06c	tlh1 /// tlh2	RecQ type DNA helicase /// RecQ type DNA helicase Tlh1
3.098	0.00005	SPBC1271.03c	SPBC1271.03c	phosphoprotein phosphatase
3.095	0.00004	SPAC144.10c	gwt1	pig-W
3.076	0.02227	SPAC977.17	SPAC977.17	MIP water channel
3.070	0.00014	SPAC513.06c	SPAC513.06c	dihydrodiol dehydrogenase (predicted)
3.036	0.00259	SPCC548.02c	---	---
3.004	0.00698	SPBC4.01	SPBC4.01	sequence orphan
2.995	0.00028	SPCC1450.13c	SPCC1450.13c	riboflavin synthase
2.970	0.00003	SPBC19C7.12c	SPBC19C7.12c	alpha-1,2-mannosyltransferase
2.963	0.00131	SPAC11D3.16c	SPAC11D3.16c	sequence orphan
2.954	0.00014	SPCC16A11.01	SPCC16A11.01	conserved fungal protein
2.934	0.00861	SPCC285.06c	---	---

2.921	0.01224	SPCC1840.12	SPCC1840.12	OPT oligopeptide transporter family
2.906	0.00043	SPCC330.04c	SPCC330.04c	DUF1773 family protein 3
2.903	0.00124	SPAC23G3.07c	snf30	SWI/SNF complex subunit Snf30
2.890	0.00408	SPBC1105.14	rsv2	transcription factor Rsv2
2.866	0.00062	SPAC19A8.05c	vps27	sorting receptor for ubiquitinated membrane proteins (ISS)
2.863	0.00011	SPAC186.05c	SPAC186.05c	human TMEM165 homolog
2.859	0.00019	SPAC5D6.04	SPAC5D6.04	auxin family
2.847	0.00192	SPAC1006.01	psp3	serine protease Psp3 (predicted)
2.769	0.00048	SPBC19F8.07	crk1	cyclin-dependent kinase activating kinase Crk1
2.769	0.00389	SPBC1773.03c	SPBC1773.03c	aminotransferase class-III (predicted)
2.764	0.00427	SPAC1687.14c	SPAC1687.14c	EF hand family protein, unknown role
2.761	0.00141	SPBC16A3.02c	SPBC16A3.02c	mitochondrial peptidase (predicted)
2.756	0.00063	SPAC14C4.07	SPAC14C4.07	membrane transporter
2.756	0.00247	SPAC630.04c	SPAC630.04c	sequence orphan
2.746	0.00382	SPBC1683.08	ght4	hexose transporter Ght4
2.743	0.00349	SPAC29A4.17c	SPAC29A4.17c	FUN14 family protein
2.733	0.00059	SPAC23G3.02c	sib1	ferrichrome synthetase Sib1
2.733	0.00159	SPAC17H9.06c	SPAC17H9.06c	conserved fungal protein
2.704	0.00003	SPAC2E1P3.01	SPAC2E1P3.01	zinc binding dehydrogenase
2.694	0.00042	SPAC1B3.06c	SPAC1B3.06c	UbiE family methyl transferase (predicted)
2.692	0.00025	SPAC27F1.05c	SPAC27F1.05c	4-aminobutyrate transaminase
2.672	0.00074	SPBC18H10.05	SPBC18H10.05	WD repeat protein Wdr44 family, WD repeat protein
2.659	0.00005	SPCC330.03c	SPCC330.03c	NADPH-hemoprotein reductase
2.658	0.00011	SPAC18B11.04	ncs1	related to neuronal calcium sensor Ncs1
2.644	0.01297	SPAPB1A10.14	SPAPB1A10.14	F-box protein, unnamed
2.641	0.04100	SPAC13G7.02c	ssa1	heat shock protein Ssa1
2.615	0.01922	SPCPJ732.03	meu15	sequence orphan
2.613	0.00124	SPBC800.14c	SPBC800.14c	DUF1772 family protein
2.606	0.00031	SPAPB8E5.04c	SPAPB8E5.04c	phosphatidylglycerol/phosphatidylinositol transfer protein (predicted)
2.574	0.00060	SPCP20C8.03	SPCC569.03	DUF1773 family protein 4
2.565	0.00221	SPAC26F1.04c	etr1	enoyl-[acyl-carrier protein] reductase
2.557	0.00008	SPBC3H7.06c	pof9	F-box protein Paf9
2.554	0.00041	SPAC1687.07	SPAC1687.07	conserved fungal protein
2.528	0.00139	SPAPB24D3.10c	agl	alpha-glucosidase Agl1
2.525	0.00001	SPCC757.12	SPCC757.12	alpha-amylase homolog (predicted)
2.519	0.00151	SPAC21E11.04	ppr1	L-azetidine-2-carboxylic acid acetyl transferase
2.517	0.00073	SPAC20G4.02c	fus1	formin Fus1
2.517	0.00266	SPAC9E9.15	SPAC9E9.15	CIA30 family protein
2.511	0.00079	SPAC23H3.04	SPAC23H3.04	conserved fungal protein
2.501	0.01100	SPAC2E12.05	---	---
2.496	0.11439	SPAC1F7.06	SPAC1F7.06	ThiJ domain protein

2.494	0.00922	SPBC216.02	mcp5	cortical anchoring factor for dynein Mcp5/Num1
2.484	0.00081	SPAC11H11.04	mam2	pheromone p-factor receptor (
2.483	0.01283	SPAC977.03	SPAC750.03c	methyl transferase (predicted)
2.480	0.00101	SPCC663.03	pmd1	leptomycin efflux transporter Pmd1
2.479	0.06756	SPAPB8E5.10	SPAPB8E5.10	sequence orphan
2.443	0.00010	SPAC25B8.10	SPAC25B8.10	trans-aconitate 3-methyl transferase (predicted)
2.443	0.00525	SPAC19D5.01	pyp2	tyrosine phosphatase Pyp2
2.432	0.00086	SPBC3H7.13	SPBC3H7.13	FHA domain protein Far10 (predicted)
2.428	0.02772	SPCC548.07c	ght1	hexose transporter Ght1
2.427	0.00482	SPAC13C5.04	SPAC13C5.04	glutamine amidotransferase (predicted)
2.412	0.00005	SPAC13A11.04c	ubp8	ubiquitin C-terminal hydrolase Ubp8
2.401	0.00676	SPCC1393.07c	SPCC1393.07c	sequence orphan
2.400	0.00025	SPBP35G2.13c	swc2	chromatin remodeling complex subunit Swc2 (predicted)
2.397	0.00036	SPBP22H7.03	SPBP22H7.03	sequence orphan
2.389	0.00680	SPAC688.03c	SPAC688.03c	human AMMECR1 homolog
2.373	0.00494	SPAC11E3.09	pyp3	protein-tyrosine phosphatase Pyp3
2.366	0.00566	SPAC13F5.07c	SPAC13F5.07c	previusly annotated as dubious, may not be protein coding
2.363	0.00325	SPBC146.02	SPBC146.02	sequence orphan
2.359	0.00421	SPCC63.13	SPCC63.13	DNAJ domain protein
2.357	0.00010	SPAPB1A10.08	SPAPB1A10.08	sequence orphan
2.350	0.00848	SPBC887.16	SPBC887.16	dubious
2.347	0.00059	SPBC19C2.06c	SPBC19C2.06c	sequence orphan
2.343	0.00257	SPBC1347.03	meu14	sporulation protein Meu14
2.341	0.00861	SPBC19C2.05	pat1	serine/threonine protein kinase Ran1
2.334	0.08091	SPBC1683.09c	frp1	ferric-chelate reductase Frp1
2.331	0.00917	SPAC1002.17c	SPAC1002.17c	uracil phosphoribosyltransferase (predicted)
2.316	0.00172	SPBC1683.06c	SPBC1683.06c	uridine ribohydrolase (predicted)
2.313	0.00549	SPCC24B10.14c	nej1	xrcc4 like factor
2.312	0.00413	SPAC31G5.18c	SPAC31G5.18c	ubiquitin family, human C1ORF55 related
2.309	0.00045	SPAC1B3.10c	SPAC1B3.10c	SEL1 repeat protein, unknown biological role
2.307	0.00491	SPAC17A2.07c	SPAC17A2.07c	sequence orphan
2.300	0.00613	SPBC29A10.02	mrb1	meiotic RNA-binding protein 1
2.295	0.00204	SPAC27D7.09c	SPAC27D7.09c	S. pombe specific But2 family protein
2.295	0.00086	SPCC576.17c	SPCC576.17c	membrane transporter
2.291	0.00939	SPAPB8E5.05	mfm1	M-factor precursor Mfm1
2.290	0.00375	SPCC622.21	wtf12	wtf element Wtf12
2.288	0.00105	SPCC1235.12c	mug146	meiotically upregulated gene Mug46
2.287	0.00012	SPCC1183.11	SPCC1183.11	MS ion channel protein 1
2.284	0.00072	SPAC27D7.09c	SPAC27D7.09c	S. pombe specific But2 family protein
2.281	0.01796	SPCC1183.10	wtf10	wtf element Wtf10

2.278	0.00044	SPAC22E12.09c	krp	kexin
2.253	0.00074	SPBPJ4664.03	mfm3	M-factor precursor Mfm3
2.251	0.00176	SPAC15A10.05c	SPAC15A10.05c	YjeF family protein
2.248	0.01070	SPAC11D3.09	SPAC11D3.09	agmatinase (predicted)
2.237	0.00371	SPBC1348.12	---	---
2.231	0.00017	SPBC19G7.05c	bgs1	1,3-beta-glucan synthase catalytic subunit Bgs1
2.227	0.00218	SPCC191.09c	gst1	glutathione S-transferase Gst1
2.221	0.00293	SPBC1604.01	SPBC1604.01	sulfatase modifying factor 1 related
2.220	0.00188	SPCC4F11.04c	SPCC4F11.04c	mannosyltransferase complex subunit (predicted)
2.216	0.00001	SPCC1322.09	SPCC1322.09	conserved fungal protein
2.212	0.00098	SPAC8E11.03c	dmc1	RecA family ATPase Dmc1
2.211	0.01211	SPCC584.16c	SPCC584.16c	sequence orphan
2.206	0.00451	SPAC31G5.09c	spk1	MAP kinase Spk1
2.193	0.01578	SPAC343.12	rds1	conserved fungal protein
2.191	0.00027	SPAC1D4.11c	kic1	dual specificity protein kinase Lkh1
2.187	0.00131	SPAC1687.22c	puf3	RNA-binding protein Puf3 (predicted)
2.182	0.00055	SPBC24C6.06	gpa1	G-protein alpha subunit
2.178	0.00255	SPAC5D6.10c	SPAC5D6.10c	sequence orphan
2.177	0.00006	SPAC9G1.10c	SPAC9G1.10c	inositol polyphosphate phosphatase (predicted)
2.164	0.00231	SPAC8C9.03	cgs1	cAMP-dependent protein kinase regulatory subunit Cgs1
2.153	0.00019	SPAC821.13c	SPAC821.13c	P-type ATPase
2.152	0.00473	SPAC18G6.09c	SPAC18G6.09c	sequence orphan
2.143	0.00094	SPAC1556.06b	meu1 /// meu2	sequence orphan /// sequence orphan
2.143	0.01249	SPBC83.12	SPBC83.12	sequence orphan
2.137	0.00165	SPAC23C11.08	php3	CCAAT-binding factor complex subunit Php3
2.126	0.00221	SPBC3B8.10c	SPBC3B8.10c	NLI interacting factor family
2.125	0.00058	SPBC3B8.07c	dsd1	dihydroceramide delta-4 desaturase
2.123	0.00090	SPBC19C7.05	SPBC19C7.05	cell wall organization protein (predicted)
2.121	0.00095	SPBC947.06c	SPBC947.06c	spermidine family transporter (predicted)
2.110	0.00131	SPBC609.03	SPBC609.03	WD repeat protein, human IQWD1 family
2.107	0.19879	SPCC1795.06	map2	P-factor
2.104	0.01058	SPBC1778.04	spo6	Spo4-Spo6 kinase complex regulatory subunit Spo6
2.101	0.00877	SPCC548.03c	wtf13	wtf element Wtf13
2.100	0.00301	SPAC589.07c	SPAC589.07c	WD repeat protein Atg18
2.099	0.00252	SPAC6F12.03c	fsv1	SNARE Fsv1
2.098	0.00778	SPBC36B7.05c	SPBC36B7.05c	phosphatidylinositol(3)-phosphate binding protein (predicted)
2.095	0.04634	SPAC212.07c	---	---
2.093	0.00072	SPBC25B2.03	SPBC25B2.03	zf-C3HC4 type zinc finger
2.093	0.00126	SPBC1709.01	chs2	chitin synthase homolog Chs2
2.085	0.00164	SPBC106.02c	srx1	sulphiredoxin

2.085	0.00158	SPAC24H6.13	SPAC24H6.13	DUF221 family protein
2.082	0.00484	SPAC6B12.08	SPAC6B12.08	DNAJ domain protein Jjj family
2.081	0.00209	SPAC343.06c	SPAC343.06c	scramblase
2.078	0.00014	SPAC26H5.09c	SPAC26H5.09c	GFO/IDH/MocA family oxidoreductase
2.077	0.00062	SPCC1020.13c	SPCC1020.13c	phospholipase (predicted)
2.074	0.00046	SPCC320.14	SPCC320.14	threo-3-hydroxyaspartate ammonia-lyase (predicted)
2.072	0.01110	SPCC70.10	SPCC70.10	sequence orphan
2.067	0.00362	SPAC4G8.10	gos1	SNARE Gos1
2.063	0.00601	SPCC970.11c	wtf9	wtf element, Wtf2, pseudo
2.062	0.01716	SPCC1450.01c	---	---
2.062	0.00230	SPAC1002.12c	SPAC1002.12c	succinate-semialdehyde dehydrogenase (predicted)
2.061	0.00073	SPAC1687.08	SPAC1687.08	sequence orphan
2.053	0.12514	SPAPB1A11.02	SPAPB1A11.02	esterase/lipase (predicted)
2.050	0.00064	SPAC6F6.12	SPAC6F6.12	autophagy associated protein Atg24
2.046	0.03136	SPAC750.05c	SPAC750.05c	S. pombe specific 5Tm protein family
2.044	0.01027	SPAC22G7.08	ppk8	serine/threonine protein kinase Ppk8 (predicted)
2.042	0.00140	SPAC17G6.02c	SPAC17G6.02c	RTA1-like protein
2.041	0.02659	SPCC285.07c	wtf13 /// wtf18	wtf element Wtf13 /// wtf element Wtf18
2.041	0.00108	SPAC1751.01c	gti1	gluconate transporter inducer Gti1
2.037	0.00334	SPBC660.07	ntp1	alpha,alpha-trehalase Ntp1
2.037	0.00866	SPAC458.04c	SPAC458.04c	sequence orphan
2.037	0.00047	SPAC227.06	SPAC227.06	Rab GTPase binding (predicted)
2.034	0.00411	SPCC1223.03c	gut2	glycerol-3-phosphate dehydrogenase Gut2
2.032	0.00617	SPAC19B12.08	SPAC19B12.08	peptidase family C54
2.028	0.00007	SPAPB18E9.04c	SPAPB18E9.04c	sequence orphan
2.027	0.00369	SPAC13D6.01	pof14	F-box protein Pof14
2.027	0.00330	SPAC23E2.03c	ste7	meiotic suppressor protein Ste7
2.026	0.00022	SPAC16E8.16	SPAC16E8.16	transcription factor TFIIB
2.026	0.00080	SPBC11G11.01	fis1	mitochondrial fission protein Fis1 (predicted)
2.023	0.00196	SPCC11E10.09c	SPCC11E10.09c	alpha-amylase homolog (predicted)
2.023	0.00002	SPBC354.09c	SPBC354.09c	Tre1 family protein (predicted)
2.021	0.00155	SPCC1281.08	SPCC1281.08	wtf element Wtf11
2.017	0.00313	SPAC1834.09	SPAC1834.09	conserved fungal protein
2.016	0.01729	SPAC17G6.05c	SPAC17G6.05c	Rhophilin-2 homolog
2.007	0.00996	SPBP8B7.24c	atg8	autophagy associated protein Atg8 (predicted)
2.005	0.00182	SPCC1020.05	SPCC1020.05	phosphoprotein phosphatase (predicted)
2.003	0.00002	SPCC584.15c	SPCC584.15c	arrestin/PY protein 2
2.001	0.00272	SPAC1B2.05	mcm5	MCM complex subunit Mcm5
2.001	0.04087	SPBC32H8.07	git5	heterotrimeric G protein beta subunit Git5

Supplementary data table 4:
Down-regulated genes in restricted nmt81-*sup11* mutant. Sup11p is highlighted in light orange.

Regulation	p-value	Systematic Name	Gene Name	Gene Product
0.496	0.00263	SPAC56F8.10	met5	methylenetetrahydrofolate reductase Met9
0.491	0.00816	SPBPB2B2.04	---	---
0.491	0.00129	SPBC26H8.03	cho2	phosphatidylethanolamine N-methyl transferase Cho2
0.483	0.03021	SPBPB7E8.01	SPBPB7E8.01	sequence orphan
0.480	0.00096	SPBC1105.04c	abp1	CENP-B homolog
0.479	0.01227	SPCC285.17	spp27	RNA polymerase I upstream activation factor complex subunit Spp27
0.477	0.00104	SPBC428.11	SPBC428.11	homocysteine synthase
0.476	0.00222	SPCC330.05c	---	---
0.474	0.00226	SPCC330.05c	---	---
0.473	0.00011	SPCC1529.01	SPCC1529.01	membrane transporter
0.470	0.01053	SPAPJ760.03c	adg1	sequence orphan
0.468	0.00119	SPCC330.05c	ura4	orotidine 5'-phosphate decarboxylase Ura4 (PMID 2834100)
0.465	0.01901	SPAC26F1.05	SPAC26F1.05	sequence orphan
0.461	0.01869	SPAC1B3.03c	cyp5	cyclophilin family peptidyl-prolyl cis-trans isomerase Wis2
0.459	0.00317	SPAC23H3.13c	gpa2	heterotrimeric G protein alpha-2 subunit Gpa2
0.458	0.00087	SPBC8E4.01c	SPBP4G3.01	inorganic phosphate transporter (predicted)
0.451	0.00598	SPBP16F5.08c	SPBP16F5.08c	flavin dependent monooxygenase (predicted)
0.448	0.01181	SPAC31G5.08	ups	uroporphyrinogen-III synthase Ups1
0.448	0.00612	SPBPB2B2.01	SPBPB2B2.01	amino acid permease, unknown 12
0.444	0.00018	SPBC119.11c	hcs	double-strand-specific ribonuclease Pac1
0.441	0.01629	SPBC215.07c	SPBC215.07c	PWWP domain protein
0.425	0.00470	SPAC14C4.09	agn1	glucan endo-1,3-alpha-glucosidase Agn1
0.423	0.00229	SPCPB1C11.01	amt1	ammonium transporter Amt1
0.415	0.00101	SPAC57A10.06	SPAC57A10.06	sequence orphan
0.414	0.01854	SPAC6G10.12c	ace2	transcription factor Ace2
0.414	0.00307	SPAC31G5.14	gcv1	glycine decarboxylase T subunit
0.414	0.01700	SPAC17H9.19c	cdt2	WD repeat protein Cdt2
0.411	0.00087	SPCC330.05c	---	---
0.401	0.00150	SPCC645.14c	sti1	chaperone activator Sti1 (predicted)
0.398	0.00307	SPAC11D3.06	SPAC11D3.06	MatE family transporter
0.386	0.01468	SPAC5D6.09c	SPAC5D6.09c	acetate transporter (predicted)
0.384	0.00271	SPAC869.10c	SPAC869.10c	proline specific permease (predicted)
0.371	0.00143	SPBC1861.02	abp2	ARS binding protein Abp2
0.370	0.00002	SPBP8B7.30c	thi5	transcription factor Thi5
0.353	0.00105	SPAC13G6.06c	SPAC13G6.06c	glycine cleavage complex subunit P

0.351	0.03213	SPBPB10D8.02c	SPBPB10D8.02c	arylsulfatase (predicted)
0.334	0.00021	SPCPB1C11.03	SPCPB1C11.03	cysteine transporter (predicted)
0.329	0.00235	SPBC13A2.03	SPBC13A2.03	phosphatidate cytidylyltransferase
0.323	0.00013	SPAC1002.16c	SPAC1002.16c	nicotinic acid plasma membrane transporter (predicted)
0.314	0.00022	SPAC110.01	ppk1	serine/threonine protein kinase Ppk1 (predicted)
0.310	0.00624	SPAC750.07c	SPAC750.07c	S. pombe specific GPI anchored protein family 1
0.307	0.00156	SPAC29B12.10c	SPAC29B12.10c	OPT oligopeptide transporter family
0.264	0.00684	SPBC3H7.07c	SPBC3H7.07c	phosphoserine phosphatase (predicted)
0.258	0.00241	SPBC947.04	SPBC947.04	DIPSY family
0.217	0.00038	SPCC18B5.05c	SPCC18B5.05c	phosphomethylpyrimidine kinase (predicted)
0.215	0.00030	SPBC11C11.05	SPBC11C11.05	KRE9 family cell wall biosynthesis protein (predicted) = Sup11p
0.168	0.00009	SPCC162.02c	SPCC162.02c	AMP-binding dehydrogenase (predicted)
0.167	0.00312	SPBPB10D8.01	SPBPB10D8.01	cysteine transporter (predicted)
0.154	0.00001	SPCC31H12.06	SPCC31H12.06	sequence orphan
0.136	0.02587	SPCC417.12	SPCC417.12	carboxylesterase-lipase family (predicted)
0.120	0.00013	SPCC794.03	SPCC794.03	amino acid permease, unknown 13
0.119	0.00007	SPCC162.03	SPCC162.03	short chain dehydrogenase (predicted)
0.109	0.00008	SPBC1604.04	SPBC1604.04	thiamine pyrophosphate transporter
0.108	0.00001	SPAC23H4.10c	thi4	thiamine-phosphate dipyrophosphorylase/ hydroxyethylthiazole kinase
0.089	0.00000	SPAC9.10	SPAC9.10	amino acid permease, unknown 2
0.087	0.00001	SPBC530.07c	SPBC530.07c	TENA/THI domain
0.078	0.00001	SPBC428.03c	pho4	thiamine-repressible acid phosphatase Pho4
0.068	0.00006	SPBC26H8.01	nmt2	thiazole biosynthetic enzyme
0.051	0.00001	SPBP8B7.18c	SPBP8B7.18c	phosphomethylpyrimidine kinase
0.042	0.00007	SPBPB2B2.08	SPBPB2B2.08	conserved fungal protein
0.039	0.00001	SPBPB2B2.05	SPBPB2B2.05	GMP synthase [glutamine-hydrolyzing] (predicted)
0.033	0.00000	SPAC17A2.01	bsu1	high-affinity import carrier for pyridoxine, pyridoxal, and pyridoxamine Bsu1
0.008	0.00003	SPBPB2B2.06c	SPBPB2B2.06c	phosphoprotein phosphatase (predicted)
0.004	0.00001	SPCC1223.02	nmt1	no message in thiamine Nmt1

9. Acknowledgements

Zum Ende dieser Arbeit möchte ich mich bei allen bedanken, die mich während meiner Doktorarbeit tatkräftig unterstützt haben und somit zu deren Gelingen beigetragen haben:

Prof. Dr. Sabine Strahl danke ich für die intensive Unterstützung bei der Betreuung und Erstellung dieser Arbeit. Vielen Dank auch für die unzähligen Anregungen und Hilfestellungen, auf die ich jederzeit zählen konnte.
Auch möchte ich mich bei Prof. Dr. Thomas Söllner bedanken, dass er das Zweitgutachten für diese Arbeit übernommen hat.
Bei meinen Kooperationspartnern möchte ich mich ebenfalls bedanken: Prof. Matthias Sipiczki von der Universität Debrecen in Ungarn für die elektronenmikorskopischen Analysen. Ausserdem danke ich Dr. Thomas Ruppert und seiner Arbeitsgruppe, für die Durchführung der massenspektrometrischen Analysen meiner Arbeit.

Für die Unterstützung bei der Laborarbeit und für das tolle Arbeitsklima danke ich der gesamten derzeitigen AG Strahl und auch aller ausgeschiedenen Mitglieder.
Besonderer Dank gilt dabei Dr. Mark Lommel, der mich insbesondere am Anfang meiner Promotion intensiv betreut hat. Meinen Kollegen und Doktoranden-Mitstreitern Martin Loibl, Patrick Winterhalter, Markus Bartels, Ewa Zatorska, Lina Fleig, Alexander Schneiders, Nina Sadeh, Anke Metschies und Dr. Michael Büttner danke ich für die gute Atmosphäre und die gegenseitige Unterstützung. Nicht zu vergessen Andrea Schott, Claudia Müller und Enrico Ragni.
Ganz besonderer Dank gilt natürlich meinem „ältesten“ Kollegen und Freund Dr. Gernot Poschet. Auf seine seelisch-moralische Unterstützung konnte ich jederzeit bauen und auch für die großzügige Papierspende danke ich ihm :). Ebenso möchte ich mich bei der „Mittagsrunde“ Gernot Poschet, Anja Bausewein, Britta Kupfer und Claudia Müller für die entspannenden Unterhaltungen danken.
Ebenso möchte ich mich bei meinen „Mitläufern“ Patrick und Andi für die kurzweiligen und -atmigen ;) Gespräche beim joggen bedanken.

Abschließend möchte ich mich ganz herzlich Bedanken bei meinen lieben Eltern, meinem Bruder, Onkel Roland und Tante Birgit und natürlich auch allen anderen aus der Familie, die mich fortwährend Unterstützt haben.

Vermutlich hab ich den Einen oder Anderen vergessen namentlich zu erwähnen, der/ die es noch verdient hätte. Falls das so sein sollte, entschuldige ich mich in aller Form und bitte ich um ein wenig Nachsicht. Ich danke euch im Stillen ;)

Ich erkläre hiermit, dass ich die vorgelegte Dissertation selbst verfasst und mich dabei keiner anderen als der von mir ausdrücklich bezeichneten Quellen und Hilfen bedient habe.

Ich erkläre hiermit, dass ich an keiner anderen Stelle ein Prüfungsverfahren beantragt bzw. die Dissertation in dieser oder anderer Form bereits anderweitig als Prüfungsarbeit verwendet oder einer anderen Fakultät als Dissertation vorgelegt habe.

Heidelberg, 28.08.2013